

Physicochemical stability and effector function of IgG4-Fc: impact of photo-induced chemical
modification and glycosylation

By

Copyright 2019

Huan Kang

Submitted to the graduate degree program in Pharmaceutical Chemistry and the Graduate
Faculty of the University of Kansas in partial fulfillment of the requirements for the degree of
Doctor of Philosophy

Chairperson Christian Schöneich

Teruna J. Siahaan

John F. Stobaugh

Thomas J. Tobert

Robert C. Dunn

Date Defended: July 9, 2019

The Dissertation Committee for Huan Kang certifies that this is the approved version of the
following dissertation:

Physicochemical stability and effector function of IgG4-Fc: impact of photo-induced chemical
modification and glycosylation

Chairperson Christian Schöneich

Date Approved: July 9, 2019

Abstract

Immunoglobulin gamma monoclonal antibodies are glycoproteins that have emerged as powerful and promising protein therapeutics. During the process of production, storage and transportation, exposure to ambient light is inevitable, which can cause protein physical and chemical degradation. For mechanistic studies of photo-degradation, we have exposed IgG4-Fc to UV light. The photoirradiation of IgG4-Fc with monochromatic UVC light at $\lambda = 254$ nm and UVB light with $\lambda_{\text{max}} = 305$ nm in air-saturated solutions revealed multiple photo-products originating from tyrosine side chain fragmentation at Tyr³⁰⁰, Tyr³⁷³ and Tyr⁴³⁶. Tyr side chain fragmentation yielded either Gly or various backbone cleavage products, including glyoxal amide derivatives. A mechanism is proposed involving intermediate Tyr radical cation formation, either through direct light absorption of Tyr or through electron transfer to an initial Trp radical cation, followed by elimination of quinone methide. In previous studies we discovered that the exposure of IgG4-Fc and IgG1 to UV light resulted in the side chain cleavage of specific Tyr and Trp residues, converting these amino acids into a series of products, including Gly (Haywood et al. *Mol. Pharm.* **2013**, *10*, 1146-1150; Kang et al. *Mol. Pharm.* **2019**, *16*, 258-272). In order to evaluate the physico-chemical consequences of such photochemical transformations, we prepared a series of IgG4-Fc mutants, in which Trp and Tyr residues were mutated to Gly, i.e., Y300G, Y373G, Y436G, W381G, and W381A for biophysical studies. Among these mutants, Y373G displayed significantly lower melting temperatures compared to wild-type IgG4-Fc, as analyzed by differential scanning calorimetry and fluorescence spectroscopy, indicating a decrease of thermal stability of both the C_H2 and C_H3 domains. In contrast, W381G and W381A showed no thermal transitions, indicating

a significant loss of overall thermal stability. Both, W381A and Y300G IgG4-Fc displayed ca. 10-fold reduction of binding affinity to Fc γ R11A as compared to wild-type IgG4-Fc. Interestingly, W381A and W381G IgG4-Fc did not only contain N-linked glycans but also high levels of O-mannose (> 60%) at Ser³⁷⁵. Furthermore, a series of well-defined N-glycosylated IgG4-Fc variants were utilized as model to investigate the effect of glycan structure on the physico-chemical properties (conformational stability and photostability) and interaction with Fc γ R11A. The size of glycans at Asn²⁹⁷ affects the yields of light-induced Tyr side chain fragmentation products, where the yields decreased in the following order: N297Q > GlcNAc₁ > Man₅ > HM. These yields correlate with the thermal stability of the glycoforms. The presence of HM and Man₅ reveals increased affinity for Fc γ R11A by at least 14.7-fold, as compared to GlcNAc₁ IgG4-Fc. N297Q does not present a detectable affinity to Fc γ R11A.

Acknowledgements

First, I would like to express my gratitude and forever appreciation to my advisor, Christian Schöneich, for providing me with unsurpassed guidance, mentorship, and words of wisdom. He has helped me succeed despite of my failures, limitations and challenges. I am grateful to him for his breadth of knowledge enlightening me through my graduate work, for his support of my industry internship, and for giving me the opportunities to present in multiple scientific conferences. His mentorship has developed me into a scientist to think critically, independently, and creatively to solve problems.

I would like to thank my excellent dissertation committee members: Chrisitan Schöneich, Teruna Siahaan, John Stobaugh, Thomas Tolbert, and Robert Dunn. Thank you for attending my review meetings and my defense. Your critiques and suggestions assisted me in interpreting the experimental results from different perspectives and training me with a deep desire to question the data. My special thanks go to the readers of my dissertation, Christian, Teruna and Thomas, for their invaluable expertise, comments and insights.

I would like to thank the group members of the Schöneich's group: Olivier Mozziconacci, Björn-Hendrik Peters, Rupesh Bommana, Yi Yang, Asha Hewarathna, Indira Prajapati, Hasitha Rathnayaka, and Natalia Subelzu, for making the laboratory an enjoyable place to work. I would like to thank my collaborators that made significant contributions to my projects: Thomas Tolbert for contributions in multiple projects of my dissertation, Ishan Shah and Solomon Okbazghi for protein expression and purification, Derek White for the binding studies and providing us with receptors, Russell Middaugh for his comments and insights in biophysical characterization,

Nicholas Larson for his significant contributions to multiple projects of my dissertation, Yangjie Wei for biophysical analysis, David Weis and Yuqi Shi for HX MS analysis.

All the research I have completed would not have been possible without our funding sources. I would like to thank the support by a Graduate Fellowship from the Genentech Foundation.

Last and foremost, I would like to dedicate this dissertation to my family and friends. I would not be able to reach this point without the love and support of my family and friends.

Table of contents

Chapter 1. Photostability, effector function, and glycosylation of mAbs.....	1
1.1. IgG4 as therapeutics.....	2
1.2. Structures of IgG4.....	3
1.3. The importance of Fc fragment in IgGs	3
1.4. Effector function of IgG4	4
1.5. Photostability	5
1.5.1. Photochemistry of Tyr	6
1.5.2. Photochemistry of Trp.....	9
1.5.3. Consequences of photo-induced chemical modifications of mAbs	11
1.5.4. Mitigation strategies to protect from light.....	11
1.6. Glycosylation and its role in effector function and physicochemical properties of mAbs	12
1.7. Aim and outline of the dissertation.....	14
1.7.1. Dissertation outline	14
1.8. References.....	15
Chapter 2. Photo-induced tyrosine side chain fragmentation in IgG4-Fc: mechanisms and solvent isotope effects.....	24
2.1. INTRODUCTION	25
2.2. EXPERIMENTAL SECTION	30
2.2.1. Materials.	30
2.2.2. Production of WT IgG4-Fc.	30
2.2.3. Purification of high mannose (HM) IgG4-Fc.	32
2.2.4. Cloning, expression and purification of N297Q-IgG4-Fc, H435R/Y436F-IgG4-Fc and W381F-IgG4-Fc.....	33
2.2.5. Characterization of WT, W381F, and H435R/Y436F IgG4-Fc by intact protein LC-MS analysis.	34
2.2.6. Sodium dodecyl sulfate - polyacrylamide gel electrophoresis (SDS-PAGE).....	35
2.2.7. Peptide mapping with GluC.....	36
2.2.8. HPLC-MS/MS analysis.....	37
2.3. RESULTS.....	39

2.3.1. WT IgG4-Fc production and initial characterization.....	39
2.3.2. Photoirradiation of WT HM IgG4-Fc and N297Q IgG4-Fc.....	41
2.3.3. Quantification of the photodegradation products.....	50
2.3.4. Conformational effects on photo-product formation.....	51
2.3.5. Solvent isotope effects (SIE).....	54
2.3.6. Comparison of WT HM and W381F HM IgG4-Fc.....	56
2.3.7. Comparison of WT HM and H435R/Y436F HM IgG4-Fc.....	58
2.3.8. Photo-irradiation of N-acetyl-tyrosine (N-Ac-Tyr) in the presence of oxidized glutathione (GSSG).....	60
2.4. DISCUSSION.....	63
2.4.1. Tyr side chain fragmentation mechanism.....	63
2.4.2. Effect of IgG4-Fc conformation on Tyr side chain cleavage.....	64
2.5. CONCLUSION.....	68
2.6. Acknowledgements.....	68
2.7. REFERENCES.....	69
Chapter 3. Photo-induced Trp and Tyr side chain cleavage in IgG4-Fc: impact on physicochemical stability and receptor binding, and effect of N- and O-glycosylation on product formation.....	99
3.1. Introduction.....	100
3.2. Materials.....	106
3.2.1. Cloning of WT, W381A, S375A, S375A/W381A, Y300G, Y373G, Y436G, and W381G.....	107
3.2.2. Expression of IgG4-Fc.....	108
3.2.3. Purification of IgG4-Fc using affinity chromatography.....	109
3.2.4. PNGase F digestion of WT, S375A, W381A, S375A/W381A IgG4-Fc.....	110
3.2.5. Characterization of WT, S375A, W381A, S375A/W381A, Y300G, Y373G, and Y436G IgG4-Fc by LC-MS analysis of intact proteins.....	110
3.2.6. Characterization of IgG4-Fc with sodium dodecyl sulfate-polyacrylamide gel electrophoresis (SDS-PAGE).....	111
3.2.7. Peptide mapping with GluC and Trypsin/LysC.....	112
3.2.8. HPLC-MS/MS.....	113
3.2.9. Differential scanning calorimetry (DSC).....	113

3.2.10. Intrinsic fluorescence.	114
3.2.11. FTIR analysis.	115
3.2.12. Hydrogen Exchange (HX) -Mass spectrometry analysis of WT and W381A IgG4-Fc.	115
3.2.13. Deuteration controls.	116
3.2.14. Photoirradiation of glycosylated and deglycosylated WT, S375A, W381A and S375A/W381A IgG4-Fc.....	117
3.2.15. Binding assays of WT, Y300G, Y373G, Y436G and W381A IgG4-Fc.	117
3.3. Results.	119
3.3.1 Characterization of Y300G, Y373G, and Y436G IgG4-Fc.	120
3.3.2 Initial characterization of WT, S375A, W381A, S375A/W381A, WT_degly, S375A_degly, W381A_degly, and S375A/W381A_degly IgG4-Fc by MS and SDS-PAGE.	122
3.3.3. HPLC-MS/MS analysis of O-mannosylation at Ser375 in W381A IgG4-Fc.	123
3.3.4. Thermal stability of WT, S375A, W381A, S375A/W381A, WT_degly, S375A_degly, W381A_degly, and S375A/W381A_degly IgG4-Fc.	126
3.3.5. Tertiary structure of WT, S375A, W381A, S375A/W381A, WT_degly, S375A_degly, W381A_degly, and S375A/W381A_degly IgG4-Fc.	128
3.3.6. Secondary structure of WT, S375A, W381A, S375A/W381A, WT_degly, S375A_degly, W381A_degly, and S375A/W381A_degly IgG4-Fc.	130
3.3.7. Backbone flexibility of WT and W381A IgG4-Fc examined by HX-MS.	132
3.3.8. Photo-degradation of WT, S375A, W381A, S375A/W381A, WT_degly, S375A_degly, W381A_degly, and S375A/W381A_degly IgG4-Fc.	133
3.3.9. Binding of WT, Y300G, Y373G, Y436G, and W381A IgG4-Fc to FcγRIIIA.	144
3.4. Discussion.	150
3.4.1. The impact of photo-induced conversion of Tyr to Gly on the conformational stability of IgG4-Fc.	151
3.4.2. Thermal stability of WT, S375A, W381A, and S375A/W381A IgG4-Fc.	151
3.4.3. The impact of photo-induced conversion of Trp and Tyr on binding kinetics and equilibria with FcγRIIIA.	154
3.4.4. O-glycosylation at Ser ³⁷⁵ in W381A and W381G IgG4-Fc.	156
3.4.5. Photostability of WT, S375A, W381A, and S375A/W381A IgG4-Fc.	157
3.5. Conclusions.....	158

3.6. Acknowledgements	159
3.7. Associated content	159
3.8. References.....	161
Chapter 4. Effects of glycan structure on the physicochemical stability, photostability, and receptor binding of IgG4-Fc	189
Chapter 5. The reaction of acetonitrile with N-terminal Cys of IgG4-Fc.....	235
5.1 Introduction.....	236
5.2 Experimental section.....	237
5.2.1 Materials.	237
5.2.2 Reaction of acetonitrile with intact WT IgG4-Fc under reducing conditions.	238
5.2.3 Reaction of 4-cyano-1-butyne (HCCCH ₂ CH ₂ CN) and intact N297Q IgG4-Fc under reducing conditions.....	238
5.2.4 HPLC-MS of intact IgG4-Fc.....	238
5.2.5 Peptide mapping of IgG4-Fc.	239
5.2.6 HPLC-MS/MS.	239
5.3 Results.	240
5.3.1 Identification of an N-terminal peptide derivative resulting from reaction with acetonitrile.....	240
5.3.2 Characterization of reaction of intact IgG4-Fc with acetonitrile: identification of reaction intermediates, products and effect of incubation time	242
5.3.3 Characterization of the reaction of IgG4-Fc with 4-cyano-1-butyne.....	244
5.4 Discussion.....	246
5.4.1 Proposed mechanism of N-terminal Cys of IgG4-Fc with acetonitrile.....	246
5.5 References.....	248
Chapter 6. The role of ultrafiltration device bias hydrolysis products during peptide map	249
6.1 Introduction.....	250
6.2 Materials and Methods	251
6.2.1 Materials.	251
6.2.2 Peptide mapping of IgG4-Fc.	251
6.2.3 HPLC-MS analysis.	252
6.3 Results	252

6.3.1 Identification of hydrolysis products.....	252
6.3.2 The origin of oxygen in hydrolysis products.....	255
6.3.3 The effects of the usage of Amicon filter on the quantity of products.....	257
6.4 Discussion.....	259
6.5 References.....	263
Chapter 7. Conclusions and future perspectives.....	266
7.1 Summary and conclusions.....	267
7.2 Future directions.....	269
7.3 References.....	270

Chapter 1. Photostability, effector function, and glycosylation of mAbs

1.1. IgG4 as therapeutics

Monoclonal antibodies (mAbs), primarily immunoglobulin Gs (IgGs), have evolved as effective therapeutics, owing to their target specificity and long serum half-life¹. IgGs are composed of four subclasses, including IgG1, 2, 3, and 4, named in order of decreasing abundance in serum. The four IgG subtypes differ in their constant region, particularly upper hinge region and C_H2 domain². Among the four subclasses, IgG1, 2, and 4 have been developed into therapeutics. IgG3 is rarely used due to its shorter half-life and bioprocessing issues associated with IgG3's long hinge region³. Since the first antibody approved in 1986, approximately 80 mAb-based therapeutics have been marketed in the USA and the EU (data collected at the end of 2018)^{4, 5}. IgG4 is utilized in more than 10 mAbs (including IgG4-based Fc-fusion protein)^{4, 5}. So far, IgG4 has been utilized for several indications, e.g., migraine prevention, HIV infection, allergy and cancers⁵. The IgG4 subclass is preferably selected when the recruitment of host effector functions is undesired or unnecessary. For example, IgG4-based mAbs developed for targeting programmed cell death protein 1 (PD1) are utilized to block the binding between PD1 on patients' immune cells and the ligand for PD1 on tumor cells⁶, referred to as immune-check point therapy. Such therapy does not require the deletion of patients' immune cells. A similar example is the development of an IgG4-based ibalizumab targeting CD4 on immune cells, approved for HIV infection⁵. IgG4 is an important 'blocking antibody' in immune-checkpoint therapy, HIV infection, and allergy.

1.2. Structures of IgG4

IgG4 is a dimer composed of two heavy chains and two light chains, connected by inter-chain disulfide bonds in the hinge region⁷. The light chain is composed of one variable domain (V_L) and one constant domain (C_L), while the heavy chain is composed of one variable domain (V_H) and three constant domains (C_{H1} , C_{H2} , and C_{H3})². The IgG4 structure can also be divided into two fragments: the antigen-binding fragment (Fab, including V_L , C_L , V_H , and C_{H1} domains) and the crystallizable fragment (Fc, including C_{H2} and C_{H3} domains). IgG4 reveals several unique properties as compared to other subclasses. First, it is capable to form hinge isomers (e.g., intra-chain disulfides and inter-chain disulfides) due to the presence of the sequence CPS²²⁸C (instead of the equivalent sequence CPP²²⁸C in IgG1²; Eu numbering⁸). Second, it reveals relatively weak hydrophobic interactions between the C_{H3} domains due to the presence of Arg⁴⁰⁹ (instead of an equivalent Lys⁴⁰⁹ in IgG1). Based on these properties, wild type IgG4 can undergo half-molecule exchange, and predominantly exists as a monovalent bispecific antibody in vivo^{9, 10}.

1.3. The importance of Fc fragment in IgGs

The importance of the Fc fragment in an IgG can be rationalized in various factors. First, it is critical in extending IgG serum half-life through binding to the neonatal Fc receptor (FcRn), rescuing it from lysosomal degradation¹¹. Second, it contributes to elicit antibody dependent cell cytotoxicity (ADCC) and complement-dependent cytotoxicity (CDC) through binding to cell surface Fc γ receptors (Fc γ Rs) and complement protein 1 q (C1q), respectively. The binding

affinity to FcγRs and C1q is significant for IgG biological functions¹². Third, the Fc fragment eases the purification of IgGs from cell media due to its high affinity to protein G/A columns at neutral pH, and reduced binding affinity at acidic pH. Fourth, previous biophysical analysis indicates that the Fc domain folds independently, and improves solubility and stability of the partner molecule in vivo and in vitro¹³. So far, approximately twenty Fc-fusion proteins and peptides have been approved by regulatory authorities¹⁴. Fc-fusion proteins have been developed for autoimmune diseases and enzyme replacement therapy¹⁵.

1.4. Effector function of IgG4

Antibodies present two important functions: (i) antigen-binding functions through binding to specific antigens with their Fab region, and (ii) effector functions through binding to complement proteins and FcγRs with their Fc region¹⁶. IgG1 and IgG3 typically trigger effector functions, while IgG2 and IgG4 induce more subtle ones. IgG4 presents no binding affinity to C1q, resulting in a lack of CDC activity². For ADCC responses, IgG4 displays low affinity to activating receptor, FcγRIIIA, while comparatively high affinity to inhibiting FcγRs (e.g., FcγR IIB and IIC). This prevents IgG4 excessive host effector functions against targeting antigen. Hence IgG4 has been utilized as a “blocking antibody”².

There are three types of FcγR: FcγRI, FcγRII (IIA, IIB and IIC), and FcγRIII (IIIA and IIIB). Among these, FcγRIIB and IIC are inhibitory receptors, and all others are activating receptors¹⁷. FcγRIIIA is the only activating Fc receptor present on natural killer cells and essential in eliciting

ADCC. The interaction between the Fc-domain and FcγRIIIA involves carbohydrate-carbohydrate interactions, and is sensitive to the glycosylated state of the Fc fragment and FcγRIIIA¹⁸.

1.5. Photostability

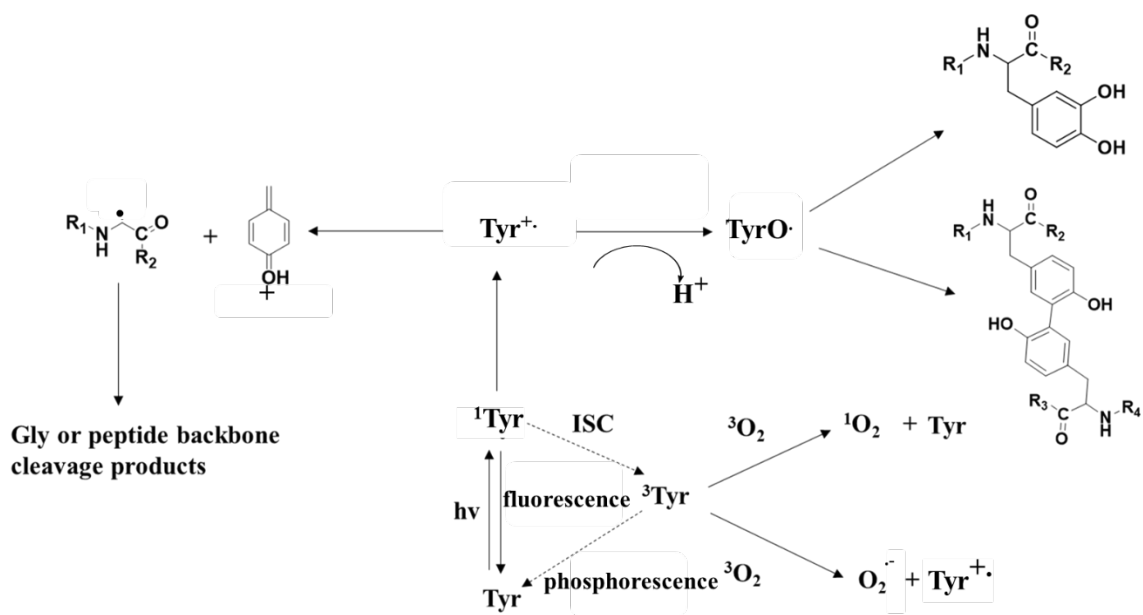
Light exposure is inevitable during the stages of pharmaceutical processing¹⁹ from upstream production, downstream purification, visual inspection, storage, transportation to administration to patients²⁰. The light conditions can be categorized into ultraviolet (UV) and visible-light exposure. Three types of UV radiation include UVA (315-400 nm), UVB (280-315nm) and UVC (100-280 nm), where UVA accounts for ca. 95% of the UV radiation reaching the Earth's surface, while UVB and UVC are primarily absorbed by the ozone layer and the atmosphere²¹. UVB and UVC exposure can be encountered during purification and analysis steps. For instance, chromatography analysis commonly uses UV (214 nm, 254 nm or 280 nm) absorbance for analytical detection²². Under these conditions, photo-sensitive amino acids, e.g., Trp, Tyr, Phe, Cys, and cystine can directly absorb light²³, which induce photochemical degradation. Such mechanisms will be discussed in sections **1.5.1** and **1.5.2**, summarizing the photochemistry of Tyr and Trp, respectively. Visible light exposure, on the other hand, is difficult to avoid. The small-scale production of proteins using clear glass bioreactors can potentially result in the exposure to ambient light. Visual inspection for visible particles in parenteral leads to light exposure. The usage of prefilled syringes and IV bags for medication administration can increase the risk of light exposure. Ambient light sources (e.g., cool white fluorescence light and LED white lamp) emit

primarily visible light (400 nm-800 nm)^{24, 25}. Both UV and visible light sources can negatively impact protein stability^{24, 26}, although the mechanisms of protein degradation can be different. Therefore, the International Conference for Harmonization guideline on photostability (ICH Q1B) suggests the exposure of a combination of a minimum of 200 Whr/m² of UVA (320 nm-400 nm) and 1.2 million lux hours of visible light (400-800 nm) at room temperature to cover the potential light exposure conditions²⁷.

1.5.1. Photochemistry of Tyr

The photochemistry of Tyr is summarized in Scheme 1^{28, 29}. Ground state Tyr directly absorbs light at wavelengths below 290 nm with an absorption maximum at ca. 275 nm³⁰. Upon absorption, ground state Tyr is excited to its singlet state ¹Tyr, which is highly reactive³¹. ¹Tyr undergoes several degradation pathways³². First, it can fluoresce back to ground state Tyr. Second, ¹Tyr undergoes intersystem crossing (ICS) forming triplet ³Tyr. ³Tyr reacts with ³O₂, generating reactive oxygen species (ROS), such as ¹O₂ and/or O₂⁻, and in parallel, yielding Tyr and Tyr radical cation (Tyr^{+•}), respectively. Third, ¹Tyr can undergo photoionization yielding Tyr^{+•} and a solvated electron (e⁻_{aq}). The Tyr^{+•} radical cation can potentially eliminate its side chain, yielding carbon-center glyceryl radical³³. Alternatively, the Tyr^{+•} radical cation can deprotonate and yield the tyrosyl radical (TyrO[•]). The addition of ³O₂³⁴, peroxy radical (ROO[•])³⁵ and hydroxyl radicals (RO[•])³⁶ on TyrO[•] subsequently yields dihydroxyphenylalanine (DOPA). On the other hand, TyrO[•] can dimerize and yield dityrosine (Di-Tyr). DOPA reveals a mass addition of 16 Da compared to native Tyr, which can be detected by HPLC-MS. Recently, a fluorogenic derivatization protocol of DOPA with 4-

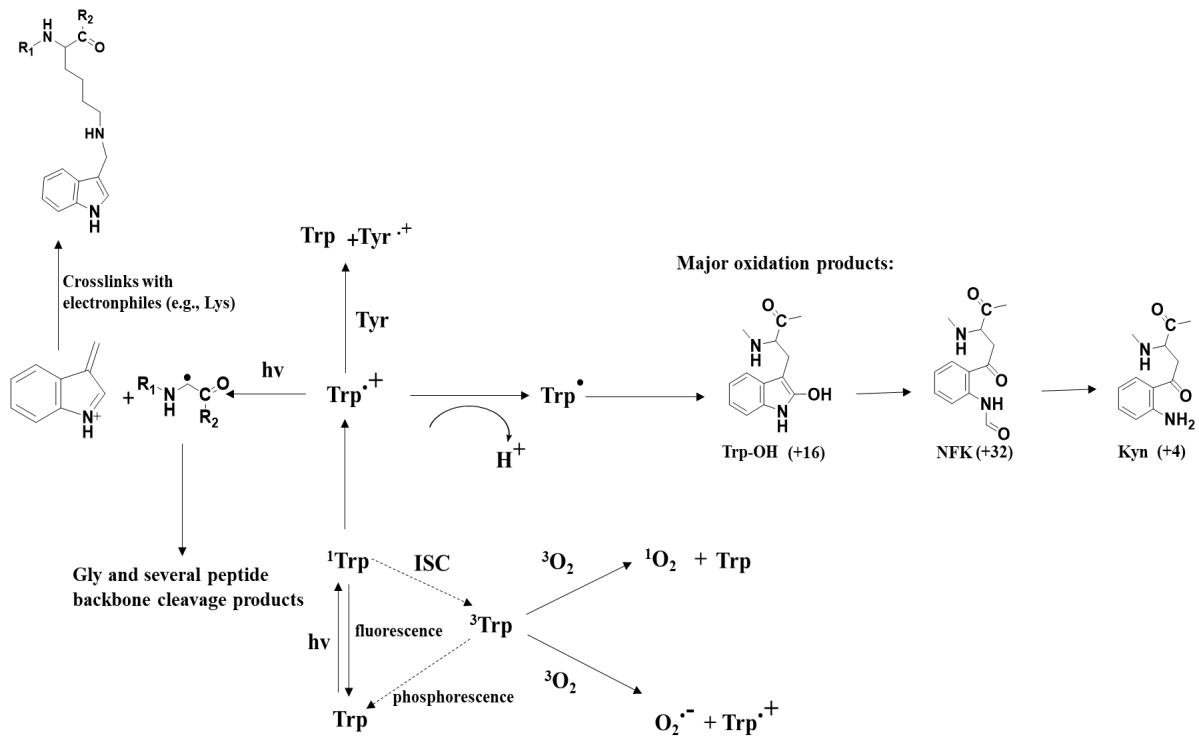
amino methyl benzenesulfonic acid (ABS) was reported to be a potential fast screening approach³⁵, considering the fact that HPLC-MS/MS analysis requires method development, which can be time-consuming. Di-Tyr has been extensively studied in biological sample and recognized as an important biomarker of oxidative stress³⁷⁻³⁹; however to our knowledge is rarely reported in mAbs. The formation of Di-Tyr depends on the proximity of two Tyr, the solvent accessibility of Tyr, and the higher order structure of proteins⁴⁰. Analytical methods for the detection and quantification of Di-Tyr have been reviewed⁴¹, including fluorescence spectroscopy³⁷ (e.g., excitation at 284 nm and/or 315 nm, emission at 420 nm), immuno-histochemical detection and HPLC-MS/MS, etc⁴¹.



Scheme 1. Photochemistry of Tyr and generation of potential degradation products.

1.5.2. Photochemistry of Trp

Trp represents the strongest UV chromophore in proteins, predominantly absorbing light below 310 nm (the maxima absorption at 280 nm). The photochemistry of Trp is summarized in Scheme 2, revealing similar pathways as Tyr. Common oxidation products of Trp such as hydroxytryptophan (OH-Trp), N-formylkynurine (NFK), and kynurenine (Kyn) were observed during the UV exposure of mAbs (e.g., at 254 nm) and near UV-visible light at 300-700 nm⁴². These products need to be carefully characterized and controlled. It was reported that Kyn is associated with the color-change in an IgG1⁴². In addition, the absorption of these Trp oxidation products shifts to a longer wavelength, and results in additional susceptibility of proteins to photo-degradation⁴³. Various studies have reported novel Trp degradation products in mAbs upon exposure to UV irradiation. These products include the conversion of Trp³⁰⁹ and Trp³⁷⁷ into Gly/Gly hydroperoxide in an IgG1⁴⁴. The resultant Trp side chain (3-methyleneindolenine, e.g., 3-MEI) crosslinks with an adjacent nucleophilic Lys residue⁴⁵. In addition, Trp plays important roles in electron transfer with Tyr, resulting in Tyr radical cation⁴⁶⁻⁴⁹.



Scheme 2. Photochemistry of Trp and generation of potential degradation products.

1.5.3. Consequences of photo-induced chemical modifications of mAbs

Photo-induced modifications of mAbs potentially result in alterations of the primary, secondary, tertiary and quaternary structures. The perturbed structures can subsequently lead to unfolding of the hydrophobic region, resulting in additional oxidation. For example, the C_H2 domain of a photo-stressed IgG1 was considerably destabilized⁵⁷. In addition, the aggregation hotspot (segment 247-256) in the heavy chain of an IgG1 revealed increased flexibility after irradiation with UVA light for 72 hr⁵⁸. In the above two cases, Met sulfoxide (MetSO) at Met²⁵² and Met⁴²⁸ were proven to be the major products. Moreover, photo-induced chemical instability of mAbs can contribute to charge heterogeneity^{50, 59}, discoloration (e.g., oxidation of His^{51, 60} or Trp^{42, 61}), immunogenicity⁶², reduced affinity to protein A, FcRn, and FcγRs⁶³, and loss of binding to antigen⁴⁷.

1.5.4. Mitigation strategies to protect from light

The majority of marketed therapeutic antibodies contains the warning label “protect from light” due to the intrinsic susceptibility of protein drugs to light. From the pharmaceutical development perspective, mitigation strategies can be designed such as applications of primary and secondary packaging containers (e.g., cardboard boxes)⁶¹, installation of safe lights (e.g., exclusion of the potential damaging wavelengths) during manufacturing and storage²⁵, and addition of excipients (e.g., Met or N-acetyl- tryptophan as free radical or oxygen scavengers)^{64, 65}. Mallela et al., reported that the addition of Met mitigates the photo-oxidation of an IgG1⁵⁷. Stroop et al., reported that light prevention, pH modification, and oxygen depletion are effective migration strategies for His buffer-mediated photo-degradation of a monoclonal antibody⁵¹. Hence, in order to select a proper mitigation strategy, the photo-degradation pathway needs to be fully understood.

1.6. Glycosylation and its role in effector function and physicochemical properties of mAbs

Glycosylation is a heterogeneous post-translational modification (PTM) composed of two types, N- and O-linked ones. N-glycosylation has been extensively studied in IgGs. All IgG subclasses contain N-glycans at Asn²⁹⁷ in the C_H2 domain. Crystal structures reveal that Asn²⁹⁷ glycans are shielded and occupy the inner space between the C_H2 domains, maintaining the optimal ‘open’ conformation of the Fc domain⁶⁶. In contrast, biophysical characterization with size exclusion chromatography indicates that the hydrodynamic radius of non-glycosylated IgGs is slightly larger than that of glycosylated ones⁶⁷. Such discrepancy of observation indicates the potential different states of IgGs in crystal structures and in solution. The presence and the unique forms of Asn²⁹⁷ glycans are essential in preserving IgGs conformations, enhancing their binding to FcγRs, and maintaining long serum half-life^{15, 68, 69}. In addition, N-glycans are present in approximately 20% of Fab regions in human IgG. These N-glycans can positively and negatively affect their binding to antigens^{70, 71}. The glycoforms in the Fab regions contain high galactose, sialic acid, and high mannose as compared to the Fc region⁷², suggesting the increased exposure and accessibility of Fab regions for cellular glycosylation enzymes. N-glycans in the Fab regions are resistant to PNGase F treatment, and require the treatment with endoglycosidase F for release of the Fab glycans^{73, 74}. Moreover, N-glycans are reported to be present in Fab variable regions in some therapeutic mAbs (e.g., Cetuximab)^{73, 75}. The selection of expression host cells for such mAbs needs to be carefully considered, since Fab regions preferably present elongated glycoforms.

Atypical N-glycans at Asn in a C_H1 domain of human antibodies were observed in non-consensus sequences at a quantity of 0.5-2.0%⁷⁶. O-linked glycosylation in IgGs is not as common, but has been characterized in the hinge region of human serum-derived IgG3⁷⁷, or in the complementarity-determining regions (CDRs) of recombinant mAbs (rMAb), e.g., O-fucosylation^{78, 79} and O-glucosylation (~10%) at Ser in an IgG1, or O-mannosylation in an IgG2⁸⁰.

Table 1 summarizes the previously characterized N-glycosylation in IgGs, and their potential role for the pharmacokinetic (PK) profile, referred to as clearance; for the pharmacodynamic (PD) profile, referred to as ADCC; and for the physicochemical profile of mAbs, referred to as “other effect”^{15, 81, 82}. Generally, Asn²⁹⁷ glycans impact IgG half-life⁸³ via the presence of specific carbohydrate patterns. For example, terminal mannose, GlcNAc, and galactose correlate with a faster removal of antibodies from the circulation, due to their binding to glycan receptors (e.g., the mannose and the asialoglycoprotein receptors)¹⁵. Asn²⁹⁷ glycans play an essential role in the binding to FcγRIIIA, attributed to carbohydrate-carbohydrate interactions⁸⁴. The binding between therapeutic mAbs and FcγRIIIA is strongly associated with mechanisms of action for cancer therapy and autoimmunity. The role of individual glycan structure in binding to FcγRIIIA is summarized in Table 1. It has to be noted that heterogeneous glycoforms can be caused by culture media components⁸⁵, host cell lines⁸⁶, and protein primary sequences, etc⁸⁷. The glycoforms of therapeutic mAbs, which potentially lead to increased clearance, low ADCC, and reduced thermal stability⁷⁸, belong to important critical quality attributes (CQAs). These glycoforms need to be controlled within strict limits (Table 1). Studies regarding the impact of different glycans on the

safety, quality and efficacy profiles of IgGs can help guide process optimization studies to ensure the antibody is being produced with appropriate and consistent glycosylation^{88, 89}.

1.7. Aim and outline of the dissertation

As outlined in the introduction, photo-induced chemical modifications and glycosylation potentially introduce heterogeneity in mAb-based therapeutics. A thorough characterization of these modifications will help fill in the gap to understand their impact on the quality and efficacy of mAb therapeutics. The goal of this dissertation was to utilize IgG4-Fc as the model system to investigate the undiscovered photo-induced chemical modifications and post-translational modifications (e.g., glycosylation) induced microheterogeneity, and their correlation with physicochemical stability and receptor binding.

1.7.1. Dissertation outline

Chapter 2 investigates photo-induced Tyr side chain fragmentation in IgG4-Fc upon exposure to UVB and UVC irradiation with respect to mechanisms and solvent isotope effects

Chapter 3 studies the impact of photo-induced Trp and Tyr side chain fragmentation of IgG4-Fc on its physicochemical stability, receptor binding, and the effects of N- and O-linked glycosylation on product formation

Chapter 4 explores effect of glycan structure on the physicochemical stability and receptor binding of IgG4-Fc

Chapter 5 reports a reaction between acetonitrile and N-terminal Cys of IgG4-Fc, which leads to

the formation of a cyclic product

Chapter 6 investigates the role of Amicon filter bias a hydrolysis reaction during sample preparation

Chapter 7 summarizes our findings and conclusions of this dissertation and suggestions for future research directions

1.8. References

1. Ecker, D. M.; Jones, S. D.; Levine, H. L., The therapeutic monoclonal antibody market. *MAbs* **2015**, *7* (1), 9-14.
2. Vidarsson, G.; Dekkers, G.; Rispens, T., IgG subclasses and allotypes: from structure to effector functions. *Front Immunol* **2014**, *5*, 520.
3. Brezski, R. J.; Georgiou, G., Immunoglobulin isotype knowledge and application to Fc engineering. *Curr Opin Immunol* **2016**, *40*, 62-9.
4. Kaplon, H.; Reichert, J. M., Antibodies to watch in 2018. *MAbs* **2018**, *10* (2), 183-203.
5. Kaplon, H.; Reichert, J. M., Antibodies to watch in 2019. *MAbs* **2019**, *11* (2), 219-238.
6. Scapin, G.; Yang, X.; Prosser, W. W.; McCoy, M.; Reichert, P.; Johnston, J. M.; Kashi, R. S.; Strickland, C., Structure of full-length human anti-PD1 therapeutic IgG4 antibody pembrolizumab. *Nat Struct Mol Biol* **2015**, *22* (12), 953-8.
7. Fekete, S.; Guillarme, D.; Sandra, P.; Sandra, K., Chromatographic, Electrophoretic, and Mass Spectrometric Methods for the Analytical Characterization of Protein Biopharmaceuticals. *Anal Chem* **2016**, *88* (1), 480-507.
8. Sandrine Béranger, C. M.-J. Fatena Bellahcene and Marie-Paule Lefranc Correspondence between the IMGT unique numbering for C-DOMAIN, the IMGT exon numbering, the Eu and Kabat numberings: Human IGHG. http://www.imgt.org/IMGTScientificChart/Numbering/Hu_IGHGnber.html.
9. van der Neut Kolfshoten, M.; Schuurman, J.; Losen, M.; Bleeker, W. K.; Martinez-Martinez, P.; Vermeulen, E.; den Bleker, T. H.; Wiegman, L.; Vink, T.; Aarden, L. A.; De Baets, M. H.; van de Winkel, J. G.; Aalberse, R. C.; Parren, P. W., Anti-inflammatory activity of human IgG4 antibodies by dynamic Fab arm exchange. *Science* **2007**, *317* (5844), 1554-7.
10. Rispens, T.; Davies, A. M.; Ooijevaar-de Heer, P.; Absalah, S.; Bende, O.; Sutton, B. J.; Vidarsson, G.; Aalberse, R. C., Dynamics of inter-heavy chain interactions in human immunoglobulin G (IgG) subclasses studied by kinetic Fab arm exchange. *J Biol Chem* **2014**,

- 289 (9), 6098-109.
11. Beck, A.; Reichert, J. M., Therapeutic Fc-fusion proteins and peptides as successful alternatives to antibodies. *MAbs* **2011**, *3* (5), 415-6.
 12. Gaboriaud, C.; Juanhuix, J.; Gruez, A.; Lacroix, M.; Darnault, C.; Pignol, D.; Verger, D.; Fontecilla-Camps, J. C.; Arlaud, G. J., The crystal structure of the globular head of complement protein C1q provides a basis for its versatile recognition properties. *J Biol Chem* **2003**, *278* (47), 46974-82.
 13. Czajkowsky, D. M.; Hu, J.; Shao, Z.; Pleass, R. J., Fc-fusion proteins: new developments and future perspectives. *EMBO Mol Med* **2012**, *4* (10), 1015-28.
 14. Lagasse, H. A.; Alexaki, A.; Simhadri, V. L.; Katagiri, N. H.; Jankowski, W.; Sauna, Z. E.; Kimchi-Sarfaty, C., Recent advances in (therapeutic protein) drug development. *F1000Res* **2017**, *6*, 113.
 15. Liu, L., Antibody glycosylation and its impact on the pharmacokinetics and pharmacodynamics of monoclonal antibodies and Fc-fusion proteins. *J Pharm Sci* **2015**, *104* (6), 1866-1884.
 16. Newsome, B. W.; Ernstoff, M. S., The clinical pharmacology of therapeutic monoclonal antibodies in the treatment of malignancy; have the magic bullets arrived? *Br J Clin Pharmacol* **2008**, *66* (1), 6-19.
 17. Mellor, J. D.; Brown, M. P.; Irving, H. R.; Zalcborg, J. R.; Dobrovic, A., A critical review of the role of Fc gamma receptor polymorphisms in the response to monoclonal antibodies in cancer. *J Hematol Oncol* **2013**, *6*, 1.
 18. Wang, X.; Mathieu, M.; Brezski, R. J., IgG Fc engineering to modulate antibody effector functions. *Protein Cell* **2018**, *9* (1), 63-73.
 19. Tamizi, E.; Jouyban, A., Forced degradation studies of biopharmaceuticals: Selection of stress conditions. *Eur J Pharm Biopharm* **2016**, *98*, 26-46.
 20. Chan, C. P., Forced degradation studies: current trends and future perspectives for protein-based therapeutics. *Expert Rev Proteomics* **2016**, *13* (7), 651-8.
 21. Pattison, D. I.; Rahmanto, A. S.; Davies, M. J., Photo-oxidation of proteins. *Photochem Photobiol Sci* **2012**, *11* (1), 38-53.
 22. Shukla, A. A.; Thommes, J., Recent advances in large-scale production of monoclonal antibodies and related proteins. *Trends Biotechnol* **2010**, *28* (5), 253-61.
 23. Martin, S. R.; Bayley, P. M., Absorption and circular dichroism spectroscopy. *Methods Mol Biol* **2002**, *173*, 43-55.
 24. Sreedhara, A.; Yin, J.; Joyce, M.; Lau, K.; Weckslar, A. T.; Deperalta, G.; Yi, L.; John Wang, Y.; Kabakoff, B.; Kishore, R. S., Effect of ambient light on IgG1 monoclonal antibodies during drug product processing and development. *Eur J Pharm Biopharm* **2016**, *100*, 38-46.
 25. Du, C.; Barnett, G.; Borwankar, A.; Lewandowski, A.; Singh, N.; Ghose, S.; Borys, M.; Li, Z. J., Protection of therapeutic antibodies from visible light induced degradation: Use safe light in manufacturing and storage. *Eur J Pharm Biopharm* **2018**, *127*, 37-43.

26. Mozziconacci, O.; Kerwin, B. A.; Schöneich, C., Exposure of a monoclonal antibody, IgG1, to UV-light leads to protein dithiohemiacetal and thioether cross-links: a role for thiy radicals? *Chem Res Toxicol* **2010**, *23* (8), 1310-2.
27. Baertschi, S. W.; Alsante, K. M.; Tonnesen, H. H., A critical assessment of the ICH guideline on photostability testing of new drug substances and products (Q1B): Recommendation for revision. *J Pharm Sci* **2010**, *99* (7), 2934-40.
28. Jain, R.; Freund, H. G.; Budzinsky, E.; Sharma, M., Radiation-induced formation of 3,4-dihydroxyphenylalanine in tyrosine-containing peptides and proteins as a function of X-irradiation dose. *Bioconjug Chem* **1997**, *8* (2), 173-8.
29. Fletcher, G. L.; Okada, S., Radiation-induced formation of dihydroxyphenylalanine from tyrosine and tyrosine-containing peptides in aqueous solution. *Radiat Res* **1961**, *15*, 349-54.
30. Kerwin, B. A.; Remmele, R. L., Jr., Protect from light: photodegradation and protein biologics. *J Pharm Sci* **2007**, *96* (6), 1468-79.
31. Hasselmann, C.; Laustriat, G., [Photochemistry of aromatic amino acids in solution. I. DL-phenylalanine, DL-tyrosine and L-dopa]. *Photochem Photobiol* **1973**, *17* (5), 275-94.
32. Bent, D. V.; Hayon, E., Excited state chemistry of aromatic amino acids and related peptides. I. Tyrosine. *J Am Chem Soc* **1975**, *97* (10), 2599-2606.
33. Kang, H.; Tolbert, T. J.; Schöneich, C., Photoinduced Tyrosine Side Chain Fragmentation in IgG4-Fc: Mechanisms and Solvent Isotope Effects. *Mol Pharm* **2019**, *16* (1), 258-272.
34. Dalsgaard, T. K.; Nielsen, J. H.; Brown, B. E.; Stadler, N.; Davies, M. J., Dityrosine, 3,4-dihydroxyphenylalanine (DOPA), and radical formation from tyrosine residues on milk proteins with globular and flexible structures as a result of riboflavin-mediated photo-oxidation. *J Agric Food Chem* **2011**, *59* (14), 7939-47.
35. Bommana, R.; Mozziconacci, O.; John Wang, Y.; Schöneich, C., An Efficient and Rapid Method to Monitor the Oxidative Degradation of Protein Pharmaceuticals: Probing Tyrosine Oxidation with Fluorogenic Derivatization. *Pharm Res* **2017**, *34* (7), 1428-1443.
36. Fu, S.; Dean, R.; Southan, M.; Truscott, R., The hydroxyl radical in lens nuclear cataractogenesis. *J Biol Chem* **1998**, *273* (44), 28603-9.
37. Scheidegger, D.; Pecora, R. P.; Radici, P. M.; Kivatinitz, S. C., Protein oxidative changes in whole and skim milk after ultraviolet or fluorescent light exposure. *J Dairy Sci* **2010**, *93* (11), 5101-9.
38. Annibal, A.; Colombo, G.; Milzani, A.; Dalle-Donne, I.; Fedorova, M.; Hoffmann, R., Identification of dityrosine cross-linked sites in oxidized human serum albumin. *J Chromatogr B Analyt Technol Biomed Life Sci* **2016**, *1019*, 147-55.
39. Balasubramanian, D.; Kanwar, R., Molecular pathology of dityrosine cross-links in proteins: structural and functional analysis of four proteins. *Mol Cell Biochem* **2002**, *234-235* (1-2), 27-38.
40. Petruk, A. A.; Bartesaghi, S.; Trujillo, M.; Estrin, D. A.; Murgida, D.; Kalyanaraman, B.; Marti, M. A.; Radi, R., Molecular basis of intramolecular electron transfer in proteins during radical-mediated oxidations: computer simulation studies in model tyrosine-cysteine peptides in solution. *Arch Biochem Biophys* **2012**, *525* (1), 82-91.

41. DiMarco, T.; Giulivi, C., Current analytical methods for the detection of dityrosine, a biomarker of oxidative stress, in biological samples. *Mass Spectrom Rev* **2007**, *26* (1), 108-20.
42. Li, Y.; Polozova, A.; Gruia, F.; Feng, J., Characterization of the degradation products of a color-changed monoclonal antibody: tryptophan-derived chromophores. *Anal Chem* **2014**, *86* (14), 6850-7.
43. Grossweiner, L. I., Photochemistry of proteins: a review. *Curr Eye Res* **1984**, *3* (1), 137-44.
44. Haywood, J.; Mozziconacci, O.; Allegre, K. M.; Kerwin, B. A.; Schöneich, C., Light-induced conversion of Trp to Gly and Gly hydroperoxide in IgG1. *Mol Pharm* **2013**, *10* (3), 1146-50.
45. Mozziconacci, O.; Okbazghi, S.; More, A. S.; Volkin, D. B.; Tolbert, T.; Schöneich, C., Comparative Evaluation of the Chemical Stability of 4 Well-Defined Immunoglobulin G1-Fc Glycoforms. *J Pharm Sci* **2016**, *105* (2), 575-587.
46. Hensel, M.; Steurer, R.; Fichtl, J.; Elger, C.; Wedekind, F.; Petzold, A.; Schlothauer, T.; Molhoj, M.; Reusch, D.; Bulau, P., Identification of potential sites for tryptophan oxidation in recombinant antibodies using tert-butylhydroperoxide and quantitative LC-MS. *PLoS One* **2011**, *6* (3), e17708.
47. Wei, Z.; Feng, J.; Lin, H. Y.; Mullapudi, S.; Bishop, E.; Tous, G. I.; Casas-Finet, J.; Hakki, F.; Strouse, R.; Schenerman, M. A., Identification of a single tryptophan residue as critical for binding activity in a humanized monoclonal antibody against respiratory syncytial virus. *Anal Chem* **2007**, *79* (7), 2797-805.
48. Folzer, E.; Diepold, K.; Bomans, K.; Finkler, C.; Schmidt, R.; Bulau, P.; Huwyler, J.; Mahler, H. C.; Koulov, A. V., Selective Oxidation of Methionine and Tryptophan Residues in a Therapeutic IgG1 Molecule. *J Pharm Sci* **2015**, *104* (9), 2824-31.
49. Sreedhara, A.; Lau, K.; Li, C.; Hosken, B.; Macchi, F.; Zhan, D.; Shen, A.; Steinmann, D.; Schöneich, C.; Lentz, Y., Role of surface exposed tryptophan as substrate generators for the antibody catalyzed water oxidation pathway. *Mol Pharm* **2013**, *10* (1), 278-88.
50. Mallaney, M.; Wang, S. H.; Sreedhara, A., Effect of ambient light on monoclonal antibody product quality during small-scale mammalian cell culture process in clear glass bioreactors. *Biotechnol Prog* **2014**, *30* (3), 562-70.
51. Stroop, S. D.; Conca, D. M.; Lundgard, R. P.; Renz, M. E.; Peabody, L. M.; Leigh, S. D., Photosensitizers form in histidine buffer and mediate the photodegradation of a monoclonal antibody. *J Pharm Sci* **2011**, *100* (12), 5142-55.
52. Ha, E.; Wang, W.; Wang, Y. J., Peroxide formation in polysorbate 80 and protein stability. *J Pharm Sci* **2002**, *91* (10), 2252-64.
53. DeRosa, M. C.; Crutchley, R. J., Photosensitized singlet oxygen and its applications. *Coordin Chem Rev* **2002**, *233*, 351-371.
54. Wright, A.; Bubb, W. A.; Hawkins, C. L.; Davies, M. J., Singlet oxygen-mediated protein oxidation: evidence for the formation of reactive side chain peroxides on tyrosine residues. *Photochem Photobiol* **2002**, *76* (1), 35-46.

55. Valliere-Douglass, J. F.; Connell-Crowley, L.; Jensen, R.; Schnier, P. D.; Trilisky, E.; Leith, M.; Follstad, B. D.; Kerr, J.; Lewis, N.; Vunnum, S.; Treuheit, M. J.; Balland, A.; Wallace, A., Photochemical degradation of citrate buffers leads to covalent acetonation of recombinant protein therapeutics. *Protein Sci* **2010**, *19* (11), 2152-63.
56. Gomes, A.; Fernandes, E.; Lima, J. L., Fluorescence probes used for detection of reactive oxygen species. *J Biochem Biophys Methods* **2005**, *65* (2-3), 45-80.
57. Shah, D. D.; Zhang, J.; Maity, H.; Mallela, K. M. G., Effect of photo-degradation on the structure, stability, aggregation, and function of an IgG1 monoclonal antibody. *Int J Pharm* **2018**, *547* (1-2), 438-449.
58. Bommana, R.; Chai, Q.; Schöneich, C.; Weiss, W. F. t.; Majumdar, R., Understanding the Increased Aggregation Propensity of a Light-Exposed IgG1 Monoclonal Antibody Using Hydrogen Exchange Mass Spectrometry, Biophysical Characterization, and Structural Analysis. *J Pharm Sci* **2018**, *107* (6), 1498-1511.
59. Luis, L. M.; Hu, Y.; Zamiri, C.; Sreedhara, A., Determination of the Acceptable Ambient Light Exposure during Drug Product Manufacturing for Long-Term Stability of Monoclonal Antibodies. *PDA J Pharm Sci Technol* **2018**, *72* (4), 393-403.
60. Bane, J.; Mozziconacci, O.; Yi, L.; Wang, Y. J.; Sreedhara, A.; Schöneich, C., Photo-oxidation of IgG1 and Model Peptides: Detection and Analysis of Triply Oxidized His and Trp Side Chain Cleavage Products. *Pharm Res* **2017**, *34* (1), 229-242.
61. Qi, P.; Volkin, D. B.; Zhao, H.; Nedved, M. L.; Hughes, R.; Bass, R.; Yi, S. C.; Panek, M. E.; Wang, D.; Dalmonte, P.; Bond, M. D., Characterization of the photodegradation of a human IgG1 monoclonal antibody formulated as a high-concentration liquid dosage form. *J Pharm Sci* **2009**, *98* (9), 3117-30.
62. Bessa, J.; Boeckle, S.; Beck, H.; Buckel, T.; Schlicht, S.; Ebeling, M.; Kiialainen, A.; Koulov, A.; Boll, B.; Weiser, T.; Singer, T.; Rolink, A. G.; Iglesias, A., The immunogenicity of antibody aggregates in a novel transgenic mouse model. *Pharm Res* **2015**, *32* (7), 2344-59.
63. Bertolotti-Ciarlet, A.; Wang, W.; Lownes, R.; Pristatsky, P.; Fang, Y.; McKelvey, T.; Li, Y.; Li, Y.; Drummond, J.; Prueksaritanont, T.; Vlasak, J., Impact of methionine oxidation on the binding of human IgG1 to Fc Rn and Fc gamma receptors. *Mol Immunol* **2009**, *46* (8-9), 1878-82.
64. Dion, M. Z.; Leiske, D.; Sharma, V. K.; Zuch de Zafra, C. L.; Salisbury, C. M., Mitigation of Oxidation in Therapeutic Antibody Formulations: a Biochemical Efficacy and Safety Evaluation of N-Acetyl-Tryptophan and L-Methionine. *Pharm Res* **2018**, *35* (11), 222.
65. Hogan, K. L.; Leiske, D.; Salisbury, C. M., Characterization of N-Acetyl-Tryptophan Degradation in Protein Therapeutic Formulations. *J Pharm Sci* **2017**, *106* (12), 3499-3506.
66. Shah, I. S.; Lovell, S.; Mehzabeen, N.; Battaile, K. P.; Tolbert, T. J., Structural characterization of the Man5 glycoform of human IgG3 Fc. *Mol Immunol* **2017**, *92*, 28-37.
67. Zheng, K.; Bantog, C.; Bayer, R., The impact of glycosylation on monoclonal antibody conformation and stability. *MAbs* **2011**, *3* (6), 568-76.
68. Zhou, Q.; Qiu, H., The Mechanistic Impact of N-Glycosylation on Stability,

- Pharmacokinetics, and Immunogenicity of Therapeutic Proteins. *J Pharm Sci* **2019**, *108* (4), 1366-1377.
69. Cymer, F.; Beck, H.; Rohde, A.; Reusch, D., Therapeutic monoclonal antibody N-glycosylation - Structure, function and therapeutic potential. *Biologicals* **2018**, *52*, 1-11.
 70. Co, M. S.; Scheinberg, D. A.; Avdalovic, N. M.; McGraw, K.; Vasquez, M.; Caron, P. C.; Queen, C., Genetically engineered deglycosylation of the variable domain increases the affinity of an anti-CD33 monoclonal antibody. *Mol Immunol* **1993**, *30* (15), 1361-7.
 71. Leibiger, H.; Wustner, D.; Stigler, R. D.; Marx, U., Variable domain-linked oligosaccharides of a human monoclonal IgG: structure and influence on antigen binding. *Biochem J* **1999**, *338* (Pt 2), 529-38.
 72. Mimura, Y.; Katoh, T.; Saldova, R.; O'Flaherty, R.; Izumi, T.; Mimura-Kimura, Y.; Utsunomiya, T.; Mizukami, Y.; Yamamoto, K.; Matsumoto, T.; Rudd, P. M., Glycosylation engineering of therapeutic IgG antibodies: challenges for the safety, functionality and efficacy. *Protein Cell* **2018**, *9* (1), 47-62.
 73. Jefferis, R., Glycosylation of recombinant antibody therapeutics. *Biotechnol Prog* **2005**, *21* (1), 11-6.
 74. Jefferis, R., Glycosylation of natural and recombinant antibody molecules. *Adv Exp Med Biol* **2005**, *564*, 143-8.
 75. Beck, A., Biosimilar, biobetter and next generation therapeutic antibodies. *MAbs* **2011**, *3* (2), 107-10.
 76. Valliere-Douglass, J. F.; Kodama, P.; Mujacic, M.; Brady, L. J.; Wang, W.; Wallace, A.; Yan, B.; Reddy, P.; Treuheit, M. J.; Balland, A., Asparagine-linked oligosaccharides present on a non-consensus amino acid sequence in the CH1 domain of human antibodies. *J Biol Chem* **2009**, *284* (47), 32493-506.
 77. Plomp, R.; Dekkers, G.; Rombouts, Y.; Visser, R.; Koeleman, C. A.; Kammeijer, G. S.; Jansen, B. C.; Rispens, T.; Hensbergen, P. J.; Vidarsson, G.; Wuhrer, M., Hinge-Region O-Glycosylation of Human Immunoglobulin G3 (IgG3). *Mol Cell Proteomics* **2015**, *14* (5), 1373-84.
 78. Liu, H.; Ponniah, G.; Zhang, H. M.; Nowak, C.; Neill, A.; Gonzalez-Lopez, N.; Patel, R.; Cheng, G.; Kita, A. Z.; Andrien, B., In vitro and in vivo modifications of recombinant and human IgG antibodies. *MAbs* **2014**, *6* (5), 1145-54.
 79. Valliere-Douglass, J. F.; Brady, L. J.; Farnsworth, C.; Pace, D.; Balland, A.; Wallace, A.; Wang, W.; Treuheit, M. J.; Yan, B., O-fucosylation of an antibody light chain: characterization of a modification occurring on an IgG1 molecule. *Glycobiology* **2009**, *19* (2), 144-52.
 80. Martinez, T.; Pace, D.; Brady, L.; Gerhart, M.; Balland, A., Characterization of a novel modification on IgG2 light chain. Evidence for the presence of O-linked mannosylation. *J Chromatogr A* **2007**, *1156* (1-2), 183-7.
 81. Liu, L., Pharmacokinetics of monoclonal antibodies and Fc-fusion proteins. *Protein Cell* **2018**, *9* (1), 15-32.
 82. Liu, L.; Gomathinayagam, S.; Hamuro, L.; Prueksaritanont, T.; Wang, W.;

- Stadheim, T. A.; Hamilton, S. R., The impact of glycosylation on the pharmacokinetics of a TNFR2:Fc fusion protein expressed in Glycoengineered *Pichia Pastoris*. *Pharm Res* **2013**, *30* (3), 803-12.
83. Kim, J. K.; Tsen, M. F.; Ghetie, V.; Ward, E. S., Catabolism of the murine IgG1 molecule: evidence that both CH2-CH3 domain interfaces are required for persistence of IgG1 in the circulation of mice. *Scand J Immunol* **1994**, *40* (4), 457-65.
 84. Hanson, Q. M.; Barb, A. W., A perspective on the structure and receptor binding properties of immunoglobulin G Fc. *Biochemistry* **2015**, *54* (19), 2931-42.
 85. Ehret, J.; Zimmermann, M.; Eichhorn, T.; Zimmer, A., Impact of cell culture media additives on IgG glycosylation produced in Chinese hamster ovary cells. *Biotechnol Bioeng* **2019**, *116* (4), 816-830.
 86. Goh, J. B.; Ng, S. K., Impact of host cell line choice on glycan profile. *Crit Rev Biotechnol* **2018**, *38* (6), 851-867.
 87. Rose, R. J.; van Berkel, P. H.; van den Bremer, E. T.; Labrijn, A. F.; Vink, T.; Schuurman, J.; Heck, A. J.; Parren, P. W., Mutation of Y407 in the CH3 domain dramatically alters glycosylation and structure of human IgG. *MAbs* **2013**, *5* (2), 219-28.
 88. Yamane-Ohnuki, N.; Satoh, M., Production of therapeutic antibodies with controlled fucosylation. *MAbs* **2009**, *1* (3), 230-6.
 89. Herter, S.; Birk, M. C.; Klein, C.; Gerdes, C.; Umana, P.; Bacac, M., Glycoengineering of therapeutic antibodies enhances monocyte/macrophage-mediated phagocytosis and cytotoxicity. *J Immunol* **2014**, *192* (5), 2252-60.
 90. Zheng, K.; Yarmarkovich, M.; Bantog, C.; Bayer, R.; Patapoff, T. W., Influence of glycosylation pattern on the molecular properties of monoclonal antibodies. *MAbs* **2014**, *6* (3), 649-58.
 91. More, A. S.; Toth, R. T. t.; Okbazghi, S. Z.; Middaugh, C. R.; Joshi, S. B.; Tolbert, T. J.; Volkin, D. B.; Weis, D. D., Impact of Glycosylation on the Local Backbone Flexibility of Well-Defined IgG1-Fc Glycoforms Using Hydrogen Exchange-Mass Spectrometry. *J Pharm Sci* **2018**, *107* (9), 2315-2324.
 92. More, A. S.; Toprani, V. M.; Okbazghi, S. Z.; Kim, J. H.; Joshi, S. B.; Middaugh, C. R.; Tolbert, T. J.; Volkin, D. B., Correlating the Impact of Well-Defined Oligosaccharide Structures on Physical Stability Profiles of IgG1-Fc Glycoforms. *J Pharm Sci* **2016**, *105* (2), 588-601.
 93. Mimura, Y.; Church, S.; Ghirlando, R.; Ashton, P. R.; Dong, S.; Goodall, M.; Lund, J.; Jefferis, R., The influence of glycosylation on the thermal stability and effector function expression of human IgG1-Fc: properties of a series of truncated glycoforms. *Mol Immunol* **2000**, *37* (12-13), 697-706.
 94. Qian, J.; Liu, T.; Yang, L.; Daus, A.; Crowley, R.; Zhou, Q., Structural characterization of N-linked oligosaccharides on monoclonal antibody cetuximab by the combination of orthogonal matrix-assisted laser desorption/ionization hybrid quadrupole-quadrupole time-of-flight tandem mass spectrometry and sequential enzymatic digestion. *Anal Biochem* **2007**, *364* (1), 8-18.

95. Giddens, J. P.; Lomino, J. V.; DiLillo, D. J.; Ravetch, J. V.; Wang, L. X., Site-selective chemoenzymatic glycoengineering of Fab and Fc glycans of a therapeutic antibody. *Proc Natl Acad Sci U S A* **2018**, *115* (47), 12023-12027.

N-glycans				
Consensus sequence		N-X-S/T; X can be any amino acids except Pro		
Core structures		GlcNAc2Man3		
Fc glycans	Glycan	ADCC	clearance	Other effect
Asn ²⁹⁷	mannose	enhance FcγRIIIa binding	increase	Reduce thermal stability ⁹⁰
	fucose	reduce FcγRIIIa binding	^a NA	No effect on thermal stability ⁹⁰
	galactose	NA	increase	NA
	bisecting GlcNAc	enhance FcγRIIIa binding	increase for Fc-fusion ^{81, 82}	NA
	^b Sialic acid NANA	NA	reduce for Fc-fusion ^{81, 82}	anti-inflammatory activity
	^c Sialic acid NGNA	reduce FcγRIIIa binding	NA	immunogenic in human
	Galα1-3Galβ1-4GlcNAc-R	NA	NA	immunogenic in human
	aglycosylated	remove FcγRIIIa binding	NA	increased protein backbone flexibility ⁹¹ , decreased solubility ⁹² , reduce thermal stability ⁹³ , faster deamidation ⁴⁵ at Asn ³¹⁵
Fab glycans		Glycoform		Antigen-binding
variable domain in ~15%-20% of serum IgG		increased bisecting GlcNAc, galactose, sialic acid; decreased core fucose		potentially increase, decrease, or no effect
Asn ⁸⁸ of cetuximab		increased bisecting GlcNAc, galactose, NGNA ⁹⁴		No effect ⁹⁵

Table 1. Summary of N-glycan sites and impact in IgGs and Fc-fusion proteins. Adapted from Liu et al¹⁵. ^aNot applicable. ^bN-acetylneuraminic acid. ^cN-glycolylneuraminic acid.

Chapter 2. Photo-induced tyrosine side chain fragmentation in IgG4-Fc: mechanisms and solvent isotope effects

2.1. INTRODUCTION

Light exposure represents an important stress condition for proteins *in vivo*, i.e. in the eye¹, and *in vitro*, i.e. for protein pharmaceuticals²⁻³. Within proteins, photo-sensitive amino acids (Trp, Tyr, Phe, Cys) can be converted into various photodegradation products via several distinct mechanisms, including photoionization and the generation of reactive oxygen species.⁴ The formation of photodegradation products can change the physical-chemical properties of proteins⁵⁻⁶. In pharmaceutical protein formulations, the chemical modification of proteins can lead to potency loss⁷⁻⁸ and, possibly, cause safety issues⁹. Therefore, the International Conference on Harmonization guidelines (Q5C)¹⁰ requires photostability tests for biomolecules, which are forced degradation studies, although some modifications have been recommended regarding the photo-irradiation conditions¹¹.

The potential for immunogenicity is a major concern for the development of protein pharmaceuticals¹²⁻¹³. Numerous studies have reported on the importance of aggregate and particle formation for immunogenicity¹⁴. However, more recent studies have recognized an additional, critical role of chemical, and especially oxidative^{9, 15} and light-induced^{9, 16}, protein modifications for immunogenicity. Importantly, when Boll et al.¹⁷ analyzed immunogenic samples of an oxidized monoclonal antibody (mAb) for common oxidation products of Met and Trp, they concluded that these did not contribute significantly to immunogenicity. Therefore, there is a need to identify chemical modifications other than conventional oxidation products, which may lead to potentially

immunogenic neo-epitopes. In this regard, we recently reported on the light-induced side chain fragmentation of Trp in a mAb¹⁸, several Fc-fragments of mAbs (mAb-Fc)¹⁹, and Trp-containing peptides²⁰. Earlier mass spectrometry experiments with Trp and Trp-containing peptides had documented such fragmentation reactions under specific conditions in the gas phase²¹, detecting 3-methyleneindolenine (3-MEI) as an important product²². In our solution studies with peptides and a protein, we detected that the electrophilic 3-MEI added to nucleophilic amino acid side chains, i.e. of Lys^{19,23}. Hence, the side chain cleavage of Trp did not only modify the Trp residue but also an adjacent Lys residue. These Trp side fragmentation are responsible for a variety of novel Trp-derived products, which should be monitored in addition to other common photoproducts from Trp such as kynurenine²⁴⁻²⁵, N-formylkynurenine²⁵, and hydroxytryptophan²⁵. Gas phase experiments also demonstrated the side chain cleavage of radical ions from Tyr-containing peptides, leading to the elimination of para-quinone methide (p-QM; 4-methylenecyclohexa-2,5-dien-1-one)²⁶⁻²⁷. This finding motivated us to evaluate whether such reaction could occur during the light-exposure of a protein in solution. We report here, that Tyr side chain cleavage proceeds selectively for three Tyr residues out of a total of eight Tyr residues in the Fc- domain of immunoglobulin G4 (IgG4-Fc) exposed to UV light. These studies with UV light enable us to formulate a reaction mechanism, which will be useful for future studies on protein degradation under ambient light, the predominant light experienced by protein pharmaceuticals during manufacturing, storage and transportation.

Immunoglobulin G (IgG) is a dimer composed of two heavy chains and two light chains, connected

by inter-chain disulfide bonds in the hinge region²⁸. The light chain is composed of one variable domain (V_L) and one constant domain (C_L), while the heavy chain is composed of one variable domain (V_H) and three constant domains (C_{H1} , C_{H2} , and C_{H3})²⁹. The IgG structure can also be divided into two fragments: the antigen-binding fragment (Fab, including V_L , C_L , V_H , and C_{H1} domains) and the crystallizable fragment (Fc, including C_{H2} and C_{H3} domains). For our experiments, we used the Fc domain of an IgG subtype, IgG4. IgG4 has unique properties compared to other subtypes, which can undergo half-molecule exchange³⁰ due to its capability of forming intra-chain disulfide bonds in the hinge region as well as relatively weak interactions between the C_{H3} domains³¹. The Fc domain of an IgG can interact with cell surface Fc binding receptors, complement proteins, and, therefore, plays an important role in IgG effector function, *in vivo* half-life and the efficacy of IgGs²⁹.

IgG4-Fc is a dimer containing 444 amino acid residues including the hinge region (Chart 1), with 2 inter-chain disulfide and 4 intra-chain disulfide bonds. We produced IgG4-Fc from the yeast *Pichia pastoris*³², which, due to incomplete glycosylation site occupancy, initially yields non-glycosylated, mono-glycosylated, and di-glycosylated forms of IgG4-Fc. The di-glycosylated IgG4-Fc (shown in Chart 1) can be purified from the other glycoforms by hydrophobic interaction chromatography (HIC)³³. The glycan, located at Asn²⁹⁷ in the C_{H2} domain³⁴⁻³⁵, was of the high mannose (HM) structure, containing GlcNAc₂-Man_(8+n) ($n = 0-4$). These covalently bound glycans are critical for the physical and chemical stability, and biological functions of IgG4-Fc³⁶. However, the micro-heterogeneity of the glycan, including the presence of GlcNAc₂-Man_(8+n) ($n=0-4$) on

Asn²⁹⁷ (Fig. S1A), introduces complexity in the characterization of photo-degradation products. For that reason, also a nonglycosylated N297Q mutant of IgG4-Fc was prepared. HM IgG4-Fc and N297Q IgG4-Fc, formulated in 20 mM sodium phosphate (pH 7.1), were photoirradiated with UV light at either $\lambda = 254$ nm or $\lambda = 295\text{--}360$ nm ($\lambda_{\text{max}} = 305$ nm) in air- or Ar- saturated solutions. Mechanistic details of the photo-induced Tyr side chain fragmentation were examined by comparison of wild-type IgG4-Fc (WT) with several mutants, and by quantification of product solvent isotope effects.

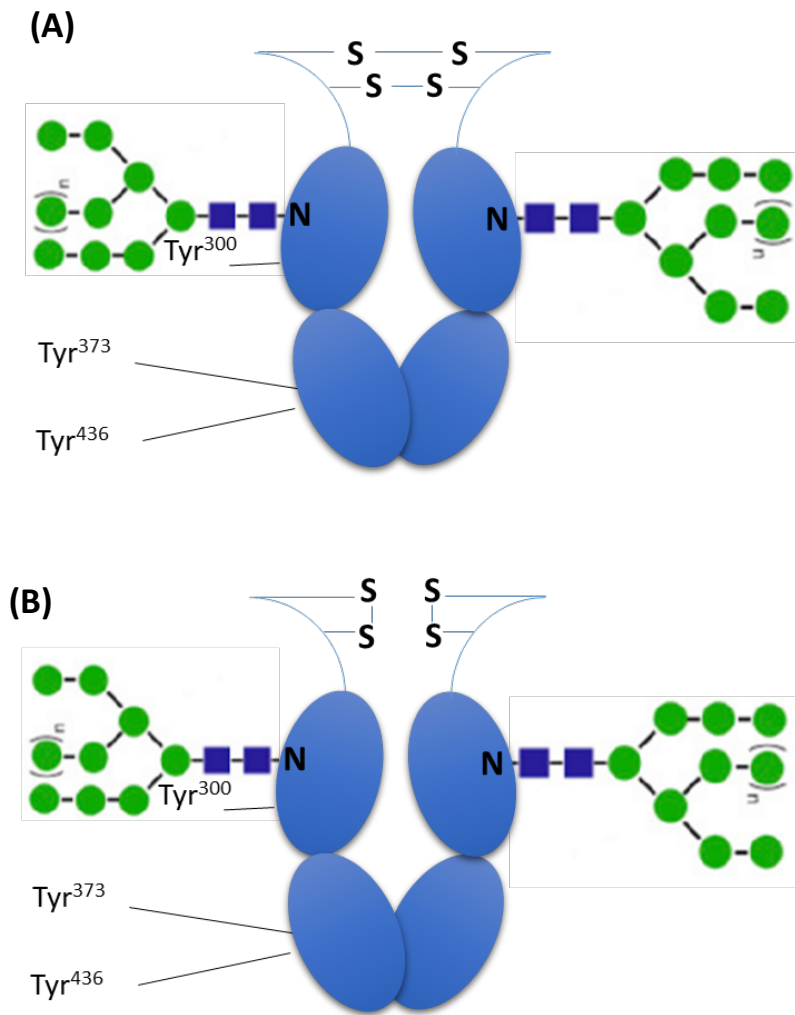


Chart 1. High mannose ($\text{GlcNAc}_2\text{Man}_{(8+n)}$ ($n=0-4$)) WT IgG4-Fc structures with intra-hinge disulfide bonds (A) or inter-hinge disulfide bonds (B), where Asn^{297} is glycosylated. The positions of Tyr^{300} ($\text{C}_\text{H}2$ domain), Tyr^{373} ($\text{C}_\text{H}3$ domain), and Tyr^{436} ($\text{C}_\text{H}3$ domain) are highlighted.

2.2. EXPERIMENTAL SECTION

2.2.1. Materials. The SacI-HF® enzyme for cDNA linearization was supplied by New England BioLabs (Ipswich, MA). Dextrose, sodium chloride, sodium phosphate (monobasic, anhydrous) and glycine were supplied by Fisher (Fair Lawn, NJ). Yeast nitrogen base (YNB) was purchased from Sunrise Biosciences (San Diego, CA). Bacto Tryptone and Yeast Extract were obtained from Becton Dickinson and Company (Franklin Lakes, NJ). Zeocin was supplied by Invitrogen (Carlsbad, CA). His-Protein G was expressed from *E. coli* Rosetta (Novagen, Burlington, MA) and purified on a Ni²⁺-nitrilotriacetic acid (NTA)-agarose column. Protein G resin was then produced by coupling recombinantly-expressed protein G with Sepharose CL-4B (Sigma-Aldrich, Saint Louis, MO) using divinyl sulfone as a coupling reagent³⁷⁻³⁸. Ethylenediaminetetraacetic acid (EDTA) was supplied by EM Science (Gibbstown, NJ, USA). Ammonium sulfate (Ultra pure grade) was supplied by AMRESCO (Solon, OH). Rabbit anti-antigen human IgG (Fc) Pierce antibody® for dot plot analysis was supplied by Thermo Scientific (Rockford, IL, USA). Antifoam 204, 2-mercaptoethanol, dithiothreitol (DTT), iodoacetamide (IAA), ammonium bicarbonate, guanidine hydrochloride, sodium phosphate (dibasic), N-acetyl-L-tyrosine and L-glutathione disulfide (GSSG) were provided by Sigma-Aldrich (Saint Louis, MO). GluC was supplied by Promega Corporation (Madison, WI). The SDS gradient gels (Mini-PROTEAN® TGX™ Gels, 4-20%) were provided by Bio-Rad (Richmond, CA, USA).

2.2.2. Production of WT IgG4-Fc. WT IgG4-Fc, including non-glycosylated, mono-glycosylated,

and di-glycosylated forms, was produced in an OCH1/PNO1 deleted and STT3D added *Pichia pastoris* yeast strain as described elsewhere³³. Briefly, IgG4-Fc cDNA cloned in a pPICZ α A *Pichia* vector (Invitrogen, Carlsbad, CA) was sequenced with 100% accuracy and linearized with the SacI-HF enzyme (Table S1). The yeast was then transformed with the linearized IgG4-Fc cDNA through electroporation³⁹. Colonies transformed with IgG4-Fc cDNA were screened by Yeast Extract Peptone Dextrose (YPD) plate containing 100 μ g/mL zeocin. The YPD plate contains 1% yeast extract (w/v), 2% peptone (w/v), 2% dextrose (w/v), and 1.5% agar (w/v). High expression colonies were screened by dot blot analysis with rabbit anti-antigen human IgG (Fc) using small scale (2.5 mL) expression systems. A selected high expression colony was used for 1L scale IgG4-Fc production.

The selected colony was inoculated with 2.5 mL of 100 μ g/mL zeocin-containing YPD medium as a starting culture and grown under shaking at 26 °C for 72 hr. The 2.5 mL culture was transferred to 50 mL of YPD media (100 μ g/mL zeocin) and grown under shaking at 26 °C for 72 hr. Then, the 50 mL cell culture was transferred to a 1 L spinner flask containing BMGY (buffered glycerol-complex media, 1% yeast extract, 2% peptone, 2% glycerol, 0.34% of yeast nitrogen base and 1% ammonium sulfate, and 4×10^{-5} % biotin)⁴⁰ buffered with 100 mM potassium phosphate at pH 6.0. The 1L cell culture was grown at room temperature under constant delivery of air for 72 hr. Then 2% of methanol (v/v) was added every 24 hr for inducing protein expression for 3 times before harvesting.

2.2.3. Purification of high mannose (HM) IgG4-Fc. Yeast cells were harvested and centrifuged at 4629 g for 20 min on an Avanti™ J-25I centrifuge (Beckman Coulter, Palo Alto, CA) using a JLA 10500 rotor (Beckman Coulter, Palo Alto, CA). The supernatant was collected and filtered with 5 layers of 90 mm Whatman filter pads to remove insoluble particles. An in-house prepared protein G affinity column (15 mL column volume) was equilibrated with 10 column volumes (CV) of 20 mM sodium phosphate, pH 6.0. The filtered supernatant was loaded onto the equilibrated column to allow IgG4-Fc to bind to the column. The column was then washed with 5 CV of 500 mM NaCl in 20 mM sodium phosphate (pH 6.0) to minimize nonspecific protein binding to the column. IgG4-Fc was then eluted with 100 mM glycine/HCl at pH 2.7, and the protein fraction was immediately neutralized with 1M Tris/HCl (pH 9.0), and subsequently dialyzed into 20 mM sodium phosphate at pH 7.0 at 4°C for 24 hrs before freezing at -80°C.

The protein G-purified IgG4-Fc was further purified by hydrophobic interaction chromatography (HIC) to separate di-glycosylated IgG4-Fc from mono-glycosylated and non-glycosylated IgG4-Fc. Samples (25 mg) were dissolved in 1 M ammonium sulfate and 20 mM sodium phosphate at pH 7.0 and filtered through a 0.2 µm filter (“Nalgene” Rapid-Flow 75 mm Filter Unit, Thermo Scientific, Rockford, IL) before loading onto the HIC column.

For HIC purification on an ÄKTAmicro chromatographic system, 125 mL of phenyl sepharose high performance resin (GE Healthcare, Uppsala, Sweden) were packed into an XK 26 column (GE Healthcare) and washed with 600 mL of filtered double-distilled water. Mobile phase A was

1 M ammonium sulfate in 20 mM sodium phosphate at pH 7.0, and mobile phase B was 20 mM sodium phosphate at pH 7.0. All buffers were filtered before loading onto the column. A volume of 675 mL mobile phase A was loaded to equilibrate the column. IgG4-Fc samples, dissolved in mobile phase A, were injected onto the column, followed by 50 mL of mobile phase A to wash the sample loop. In the following, unbound proteins were washed off with 240 mL of 100% mobile phase A. Subsequently, a linear gradient changing mobile phase B from 0% to 33% within 144 minutes was applied at 2 mL/min, followed by changing mobile phase B from 33% to 55% within 141 minutes. Then the column was washed with 55% of 750 mL containing mobile phase B. A flow rate of 2 mL/min was used for the full gradient. The eluate was monitored at 214 nm. The protein fractions were collected with a fraction collector. The collected fractions were dialyzed into 20 mM sodium phosphate, pH 7.0, for 24 hr. After characterization by LC-MS analysis and SDS-PAGE, HM IgG4-Fc fractions were combined and then dialyzed into 5 mM EDTA in 20 mM sodium phosphate, pH 7.0, to eliminate trace amounts of transition metals. After 12hr, HM IgG4-Fc (0.22 mg/mL) was dialyzed back into 20 mM sodium phosphate (pH 7.0) and stored at -80°C.

2.2.4. Cloning, expression and purification of N297Q-IgG4-Fc, H435R/Y436F-IgG4-Fc and

W381F-IgG4-Fc. A forward primer, 5'-CGGGAGGAGCAGTTCCAGAGCACGTACCGTGTG-3', and a reverse primer, 3'-GCCCTCCTCGTCAAGGTCTCGTGTCATGGCACAC-5', were designed for the mutant N297Q-IgG4-Fc. A forward primer, 5'-gcatgaggctctgcacaacagattcacacagaagagcctctccc-3', and a reverse primer, 3'-cgtactccgagacgtgtgtctaaagtgtcttctcggagaggg-5', were designed for the double mutant

H435R/Y436F-IgG4-Fc. A forward primer, 5'-gacatcgccgtggagttcgagagcaatgggcag-3', and a reverse primer, 3'-ctgtageggcacctcaagctctcgttaccgctc-5', were designed for the mutant W381F-IgG4-Fc. The primers were synthesized by Eurofins Genomics (Louisville, KY). A QuikChange Lightning Site-Directed Mutagenesis Kit (Agilent Technologies, Inc., Santa Clara, CA) was used for mutagenesis. Successfully mutated cDNA-transformed colonies were selected with 25 µg/mL zeocin-containing low salt lysogeny broth (LB) plate (1% tryptone, 0.5% NaCl, and 0.5% yeast extract) and inoculated in 6 mL LB culture overnight. The plasmids of the selected colonies were extracted with a miniprep kit (QIAGEN, Valencia, CA), and sequenced by the University of California Berkeley DNA Sequencing Facility (Berkeley, CA) with 100% accuracy. The plasmids were then linearized with the SacI-HF enzyme and transformed to an OCH1/STT3D/PNO1/Bmt1/Bmt2 KO yeast strain following the same procedures as for WT IgG4-Fc. All mutant IgG4-Fc were purified by protein G chromatography as described for WT IgG4-Fc. Since the two mutants, H435R/Y436F-IgG4-Fc and W381F-IgG4-Fc, contained >90% of HM structure [GlcNAc₂Man_(8+n) (n=0-4)] after affinity column purification (Figures S6 and S7), the two mutants were not further purified by HIC.

2.2.5. Characterization of WT, W381F, and H435R/Y436F IgG4-Fc by intact protein LC-MS analysis. Intact protein mass spectra were obtained under reducing conditions. An aliquot of 100 µg of IgG4-Fc was reduced with 10 mM DTT for 10 min at room temperature, and injected onto a C4 column (50 mm, 4.6 mm i.d.; 300-Å pore size, 5 µm particle size, Vydac 214 MS, Grace, Deerfield, IL), connected to an Agilent 1200 series LC (Agilent Technologies, Santa Clara, CA)

coupled to an Agilent 6520 Quadrupole Time-of-Flight mass spectrometer (Agilent Technologies, Santa Clara, CA). The mass spectrometer was operated with an electrospray ionization source in the positive ion mode with the mass range acquired from m/z 300 to m/z 3000 at a scan rate of 1 spectrum/second. Mobile phase A was 99.9% H₂O, 0.08 % formic acid, and 0.02 % trifluoroacetic acid, mobile phase B was 99.9% acetonitrile, 0.08% formic acid, and 0.02% trifluoroacetic acid. A linear gradient changing mobile phase B from 5 to 90% within 7 minutes was applied and the intact protein eluted at 5.5 minutes at a flow rate of 0.5 mL/min. The Agilent MassHunter Acquisition software was used for data collection, and the Agilent Mass Hunter Qualitative Analysis software (version B.03.01) was applied to data analysis. The obtained m/z values were de-convoluted through a maximum entropy deconvolution function through the Agilent Mass Hunter Qualitative Analysis software.

2.2.6. Sodium dodecyl sulfate - polyacrylamide gel electrophoresis (SDS-PAGE). For SDS-PAGE under non-reducing conditions, 20 μ L of 0.22 mg/mL HM IgG4-Fc were combined with 20 μ L of 2X loading dye (2x Laemmli sample buffer, BIO-RAD, Richmond, CA) and loaded onto the SDS gradient gel (Mini-PROTEAN® TGX™ Gels, 4-20%, BIO-RAD, Richmond, CA). For SDS-PAGE under reducing conditions, 1 μ L of 2-mercaptoethanol was added to 20 μ L solution, and the mixture was boiled in a water bath for 5 min prior to loading the mixture onto the gradient gel. For calibration, 4 μ L of a Precision Plus Protein Dual Color standard marker (BIO-RAD, Richmond, CA) was used in lane 1 of the SDS-PAGE. The electrophoresis was run at 200 volt until the front dye arrived at the bottom of the gel. When the run finished, the gel was stained with 0.05%

Coomassie Brilliant Blue (BIO-RAD, Hercules, CA) for 30 min and destained with 30% methanol, 10% acetic acid and 60% water (v:v:v). The Canon solution menu EX software and canoscan (Canon, Costa Mesa, CA) were used to record the gel images.

2.2.7. Peptide mapping with GluC. Control and photo-irradiated samples were processed side by side for enzymatic digestion by GluC. Aliquots of 500 μ L were denatured by addition of 500 μ L of 6M guanidine hydrochloride in 50 mM ammonium bicarbonate, pH 8, and subsequently reduced by addition of 10 μ L of 500 mM DTT in 50 mM ammonium bicarbonate (pH 8.0) for 1hr at 37 °C. The reduced samples were then alkylated with 50 μ L of 500 mM IAA in 200 mM ammonium bicarbonate for 1 hr at 37 °C. The samples were then transferred to Amicon Ultra Centrifugal Filter Units with 3kDa cutoff, and centrifuged at 16,900 g for 15 min at 4°C until the whole solution was concentrated to about 200 μ L. Volumes of 250 μ L of 5mM ammonium bicarbonate (pH 8.0) were added twice to the filter and centrifuged to wash out residual denaturing and alkylating agents. The filters were reverse-flipped, and the proteins on the top were collected at 300 g for 4 min at 4°C. The collected proteins were digested with GluC in 5 mM ammonium bicarbonate, pH 8, with a protein: enzyme ratio of 10:1 (w/w) for 5 hr at 37°C. The GluC was divided into two aliquots containing 11 μ g each. The first aliquot was added and the mixture was incubated at 37°C. After 2 hours, the second aliquot was added. The digested peptides were collected by centrifugation with Microcon Centrifugal Filters with 10kDa cutoff at 16,900 g for 10 min to eliminate undigested protein and the enzyme GluC, and the flow-through was collected and stored at -80 °C until further analysis.

2.2.8. HPLC-MS/MS analysis. HPLC-MS/MS analysis was performed on two different systems, a nanoAcquity ultra performance liquid chromatography system (Waters Corporation, Milford, MA), coupled to a Waters Xevo-G2 mass spectrometer (Waters Corporation, Milford, MA) and a nanoAcquity ultra performance liquid chromatography system (Waters Corporation, Milford, MA) coupled to a Synapt-G2 mass spectrometer (Waters Corporation, Milford, MA).

2.2.8.1 Analysis on the Xevo-G2 mass spectrometer. Aliquots of 4 μ L of enzymatic digests were loaded and desalted on a trap column (nanoACQUITY UPLC 2G-V/M Trap 5 μ m Symmetry C18 180 μ m x 20 mm, Waters, Milford, MA), eluted at 4 μ L/min for 3 min with 97% of mobile phase A (0.1% formic acid in water, Optima, Fisher Chemical, Fair Lawn, NJ) and 3% of mobile phase B (0.1% formic acid in acetonitrile, Optima, Fisher Chemical, Fair Lawn, NJ). The eluted peptides were moved at a velocity of 300 nL/min to an analytical column (ACQUITY UPLC Peptide CSH C18 NANOACQUITY column 10K psi, 1.7 μ m, 75 μ m x 250mm, Waters, Milford, MA), and eluted with a linear gradient changing mobile phase B from 3% to 35% within 50 min, followed by a linear gradient changing mobile phase B from 35% to 95% within 20 min. Subsequently, the column was washed with 95% mobile phase B for 10 min, before re-equilibrating to 97% of mobile phase A. Mass spectra were collected for 80 min in the positive electrospray ionization mode at a scan rate of 1 scan/second, with a mass range of m/z 200 to m/z 2000. MS/MS analysis was performed in the MS^E mode with the collision energy switching between 18 V and 45 V. Since no major peaks co-eluted with the observed photo-products under our chromatographic conditions, all the CID spectra collected from Xevo-G2 were obtained in the MS^E mode.

2.2.8.2 Analysis on the Synapt-G2 mass spectrometer. Aliquots of 5 μL of enzymatic digests from N297Q IgG4-Fc were loaded onto a CSH C18 column (1.7 μm , 300 μm x 100 mm, Waters, Milford, MA) with 99% mobile phase A (0.8% formic acid in water) and 1% mobile phase B (acetonitrile: isopropanol; 95: 5; v: v) for 1 min at 10 $\mu\text{L}/\text{min}$. The column was equilibrated with a linear gradient changing mobile phase B from 1% to 6% at 10 $\mu\text{L}/\text{min}$. Subsequently, the injected peptides were eluted with successive gradients changing mobile phase B from 6% to 21% within 35 min at 10 $\mu\text{L}/\text{min}$, from 21% to 26% within 16 min at a flow rate of 10 $\mu\text{L}/\text{min}$, and from 26% to 95% of mobile phase B for 1 min at 11 $\mu\text{L}/\text{min}$. The column was washed with 95% mobile phase B for 4 min at 11 $\mu\text{L}/\text{min}$, followed by a change of mobile phase B from 95% to 60% within 1 min at a velocity of 14 $\mu\text{L}/\text{min}$. The column was then washed with 60% mobile phase B for 2 min at 10 $\mu\text{L}/\text{min}$, before it was re-equilibrated to 99% of mobile phase A. Mass spectra were collected in the positive electrospray ionization mode at a scan rate of 1 scan/2 seconds, with a mass range of m/z 50 to m/z 2000. MS/MS analysis was performed in the data dependent acquisition (DDA) mode with the collision energy ramped from 18 V to 28 V for low masses of 250 Da to 880 Da, and ramp from 30 V to 55 V for high masses of 880 Da to 2000 Da.

The data collected on the Xevo-G2 and Synapt-G2 instruments were analyzed with Protein Prospector (<http://prospector.ucsf.edu/>) and the MassLynx software (Waters Inc., Milford, CA). All assignments were conducted manually.

2.2.9. Photoirradiation of WT, N297Q, W381F and H435R/Y436F IgG4-Fc. Photoirradiation was performed in a UV irradiator (Rayonet®, The Southern New England Ultraviolet Company, Branford, CT) equipped with 4 UV lamps emitting at $\lambda = 254$ nm (Rayonet®, catalog # RPR-2537Å) or with $\lambda_{\text{max}} = 305$ nm (Rayonet®, catalog# RPR-3000 Å; these lamps emit 95% of light between $\lambda = 265$ -340 nm). We used the iodide-iodate actinometer⁴¹⁻⁴² to quantify the photon flux at 254 nm for 4 RPR 2537A lamps to 1.5×10^{-8} einstein/s. Due to the broad spectrum of the RPR-3000A lamps, an actinometry was not performed for photo-irradiation at $\lambda_{\text{max}} = 305$ nm. For light exposure at 254 nm, 500 μ L air-saturated solutions of 0.22 mg/mL HM IgG4-Fc in 20 mM sodium phosphate, pH 7.1, were placed in ca. 13x100 mm quartz vials (Product #8683; Ace Glass Inc.; Vineland, NJ), sealed with rubber stoppers, and irradiated for 0, 15 or 30 min. For light-exposure with $\lambda_{\text{max}} = 305$ nm, 500 μ L of air-saturated solution of 0.22 mg/mL HM IgG4-Fc in 20 mM sodium phosphate, pH 7.1, were placed in 13x100 mm borosilicate vials (Fisher Scientific) sealed with rubber stoppers and irradiated for 0, 30 or 60 min. The cutoff for UV light of borosilicate glass is at $\lambda = 295$ nm. Control, non-irradiated samples were kept in a dark place. For comparison, photo-irradiation was also performed in Ar-saturated solutions. Here, 500 μ L solutions in either quartz or borosilicate vials, sealed with rubber stoppers, were carefully purged with Ar for 1 hour prior to photo-irradiation.

2.3. RESULTS

2.3.1. WT IgG4-Fc production and initial characterization. The average yield of HM IgG4-Fc

from spinner flasks was 10 mg/L. To express sufficient protein for HIC purification, WT IgG4-Fc was expressed in 10 one liter spinner flasks. Due to incomplete glycosylation at Asn²⁹⁷ by *Pichia pastoris*, protein G-purified WT IgG4-Fc contained non-glycosylated, mono-glycosylated and di-glycosylated IgG4-Fc. Different batches of affinity column-purified IgG4-Fc were analyzed by MS and SDS-PAGE, and batches of similar quality were combined and subjected to HIC purification. Di-glycosylated HM IgG4-Fc, mainly containing GlcNAc₂Man_(8+n) (n= 0-4), eluted in the early fractions of HIC, and was collected. The quality of HM IgG4-Fc used for photostability studies was initially characterized by LC-MS analysis after reduction (Supporting Information, Fig. S1A) and by SDS-PAGE under reducing and non-reducing conditions (Fig. S1B). The purity of HM IgG4-Fc was calculated by addition of the peak areas for all detected HM forms [GlcNAc₂Man_(8+n) (n= 0-4)], divided by the sum of the peak area recorded for both non-glycosylated protein and IgG4-Fc [GlcNAc₂Man_(8+n) (n= 0-4)]. The theoretical and observed masses for each glycoform are listed in Fig.S1A. The WT HM IgG4-Fc utilized for our photostability studies was of 99.1% purity, and showed a single band during SDS-PAGE under reducing conditions (Fig. S1B, lane 1), migrating with an apparent molecular weight between 25 kDa and 37 kDa. However, when analyzed by SDS-PAGE under non-reducing conditions, two bands were obtained (Fig. S1B, lane 2), migrating with apparent molecular weights between 25 kDa and 37 kDa and between 50 kDa and 75 kDa, respectively. These indicate the presence under denaturing conditions of both monomers (with intra-disulfide bond formation in the hinge region; see Chart 1) and dimers (with inter-disulfide bonds in the hinge region). The content of dimers of IgG4-Fc is about 76%, while the content of monomers is about 24%, based on a densitometry

analysis with ImageJ (National Institutes of Health, Washington D.C., USA).

2.3.2. Photoirradiation of WT HM IgG4-Fc and N297Q IgG4-Fc. WT HM IgG4-Fc (0.22 mg/mL) and the nonglycosylated N297Q IgG4-Fc (0.22 mg/mL) in 20 mM sodium phosphate, pH 7.1, were photoirradiated at 254 nm in quartz tubes or at $\lambda_{\text{max}} = 305$ nm in Pyrex tubes under air or Ar atmosphere. Ar saturation was achieved by placing protein samples in quartz or Pyrex vials, sealed with rubber stoppers, and saturated through headspace equilibration with Ar for 90 min. We confirmed that the absence or presence of 5 mM EDTA had no effect on product formation, so that all subsequent experiments were carried out in the absence of EDTA. IgG4-Fc (control and photoirradiated) were then reduced with DTT, alkylated with IAA, and digested with GluC side by side, prior to analysis by HPLC-MS/MS.

Three Tyr-containing peptides from GluC-treated IgG4-Fc revealed Tyr side chain fragmentation under light exposure: Tyr³⁷³ in the sequence MTKNQVSLTC(+57)LVKGFY³⁷³PSDIAVE/WE, referred to as peptide 1 (where the subsequence E/WE indicates that we detected peptides without and with one missed cleavage between E and W; the mass adduct of + 57 Da indicates that Cys is carbamidomethylated), Tyr⁴³⁶ in the sequence ALHNHY⁴³⁶TQKSLSLSLGK, referred to as peptide 2, and Tyr³⁰⁰ in the sequence QFN²⁹⁷STY³⁰⁰RVVSVLTVLHQDWLNGKE (where Asn²⁹⁷ is glycosylated), referred to as peptide 3. To elucidate the influence of glycosylation on photoproduct formation, the N297Q mutant was photoirradiated; in N297Q IgG4-Fc the Tyr³⁰⁰-containing sequence QFQ²⁹⁷STY³⁰⁰RVVSVLTVLHQDWLNGKE is referred to as peptide 3'. All

photoproducts derived from Tyr side chain fragmentation were identified by HPLC-MS/MS analysis on the Xevo-G2 in the MS^E mode or on the Synapt-G2 in the DDA mode, and are summarized in Table 1. The characterization of the products is described in more detail in the following sections.

2.3.2.1. MS/MS identification of photoproducts from Tyr³⁷³ side chain cleavage.

Fragmentation of the Tyr³⁷³ side chain from peptide 1 yields three peptide backbone cleavage products, MTKNQVSLTC(+57)LVKGF-NH₂, M(+16)TKNQVSLTC(+57)LVKGF-NH₂, and MTKNQVSLTC(+57)LVKGF³⁷³PSDIAVE, referred to as products **1**, **2**, and **3**, respectively, in Table 1.

i) Product 1 (m/z 575.61): The MS/MS analysis of product **1** shows nearly a complete series of b and y ions, which are presented in Fig. 1A (Xevo-G2) and Fig.S2A (Synapt-G2). Specifically, the b14 fragment and the series of y ions from y2 to y9, and y13, indicate the presence of a C-terminal amide group (-CONH₂).

ii) Product 2 (m/z 580.96): Product **2** is a secondary oxidation product resulting from product **1**, where Met³⁵⁸ is oxidized to methionine sulfoxide. The MS/MS spectrum of product **2** is shown in Fig. 1B (Xevo-G2) and Fig. S2B (Synapt-G2). The presence of b3 confirms a mass addition of +16 to the sequence MTK. The loss of 64 amu from the b4 and a10 ions (resulting in b4-64 and a10-NH₃-64) reflects the loss⁴³ of CH₃SOH from the side chain of methionine sulfoxide, indicating that the +16 mass addition is located on the Met residue of the sequence MTK. Specifically, the y14-NH₃ fragment ion in Fig. S2B is consistent with methionine sulfoxide on the N-terminal Met.

Overall, the MS/MS spectra of product **2** are very similar to those of product **1**, confirming the peptide backbone cleavage between Phe³⁷² and Tyr³⁷³ during light exposure.

Figure 1. Collision-induced dissociation (CID) spectra of products **1** and **2** derived from Tyr³⁷³ side chain fragmentation collected from Xevo-G2 in the MS^E mode. Product information is listed in Table 1.

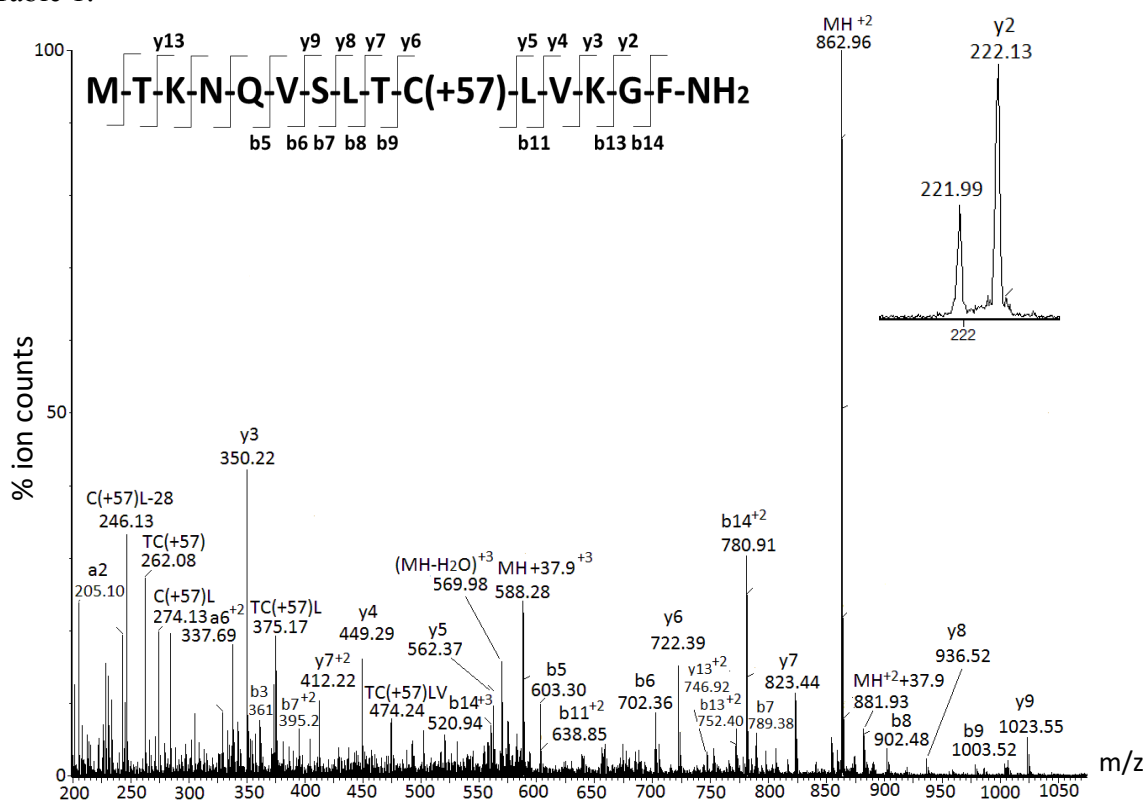


Fig. 1A. MS/MS spectrum of product **1** resulting from peptide backbone cleavage induced by Tyr³⁷³ side chain fragmentation, analyzed on the Xevo-G2 mass spectrometer in the MS^E mode.

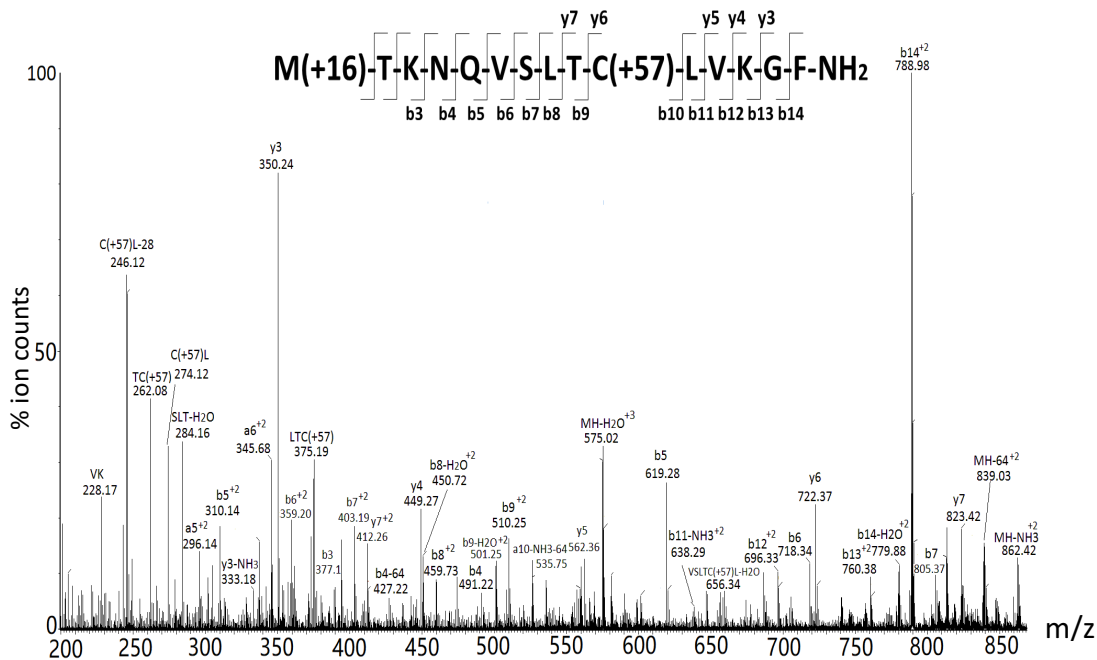


Fig. 1B. MS/MS spectrum of product **2** with an oxidized methionine, a secondary oxidation product of product **1**, analyzed with Xevo-G2 in the MS^E mode.

iii) Product **3** (m/z 832.08): The MS/MS spectrum of product **3** is presented in Fig. S2C (Synapt-G2 DDA), indicating the photo-induced side chain conversion of Tyr³⁷³ into Gly³⁷³, specifically through the characteristic b15 and b16 ions.

2.3.2.2. MS/MS identification of photoproducts from Tyr⁴³⁶ side chain cleavage. Side chain fragmentation of Tyr⁴³⁶ from the sequence ALHNHY⁴³⁶TQKSLSLSLGK (peptide **2**) yielded four products, referred to as products **4**, **5**, **6**, and **7**, respectively, which are listed in Table 1.

i) Product **4** (m/z 448.50): The MS/MS spectra of product **4**, where Tyr⁴³⁶ is converted into Gly⁴³⁶ are shown in Fig. 2A and Fig. S3A. The ions with m/z 597.67 (z=3) and m/z 448.5 (z=4) are

consistent with a mass loss of 106 amu from the original Tyr-containing sequence ALHNHY⁴³⁶TQKSLSLSLGK. The fragment ions b5, b8 and y9 reveal that the loss of 106 amu does not originate from the peptide sequences ALHNH and KLSLSLSLGK, indicating that the mass loss of 106 is derived from the peptide sequence YTQ. The only amino acid in this sequence, which can lose 106 amu, is Tyr, and, therefore, we propose the conversion of Tyr into Gly, analogous to the conversion of Tyr³⁷³ to Gly³⁷³ characterized for product **3** (see above).

ii) Products **5** and **6** (m/z 609.30 and m/z 618.30): The MS/MS spectra of product **5** (O=CH-CO-TQKSLSLSLGK) and of its hydrated form, product **6** ((OH)₂CH-CO-TQKSLSLSLGK) are presented in Fig. S3B (Synapt-G2) and Fig. 2B (Xevo-G2). The nature of the y9 fragment indicates that there is no modification on the sequence KLSLSLSLGK. Therefore, the modification is located on the N-terminal sequence TQ. Based on the observation of both a free aldehyde (product **5**) and a hydrated form (product **6**), we propose the formation of a glyoxal amide derivative on the N-terminal sequence TQ. As expected, both products **5** and **6** show many similar fragment ions (y3, y7, y8, y9). MS/MS spectra of peptide aldehyde hydrates have been reported⁴⁴⁻⁴⁶.

iii) Product **7** (m/z 387.89): The MS/MS spectra of product **7** are displayed in Fig. 2C (Xevo-G2) and Fig. S3C (Synapt-G2), and show a nearly complete series of fragment ions from y2 to y10. This fragmentation pattern indicates that product **7** has the sequence TQKSLSLSLGK.

Figure 2. CID spectra of products **4**, **6**, and **7** derived from Tyr⁴³⁶ side chain fragmentation collected from the Xevo-G2 mass spectrometer in the MS^E mode. Product information is listed in Table 1.

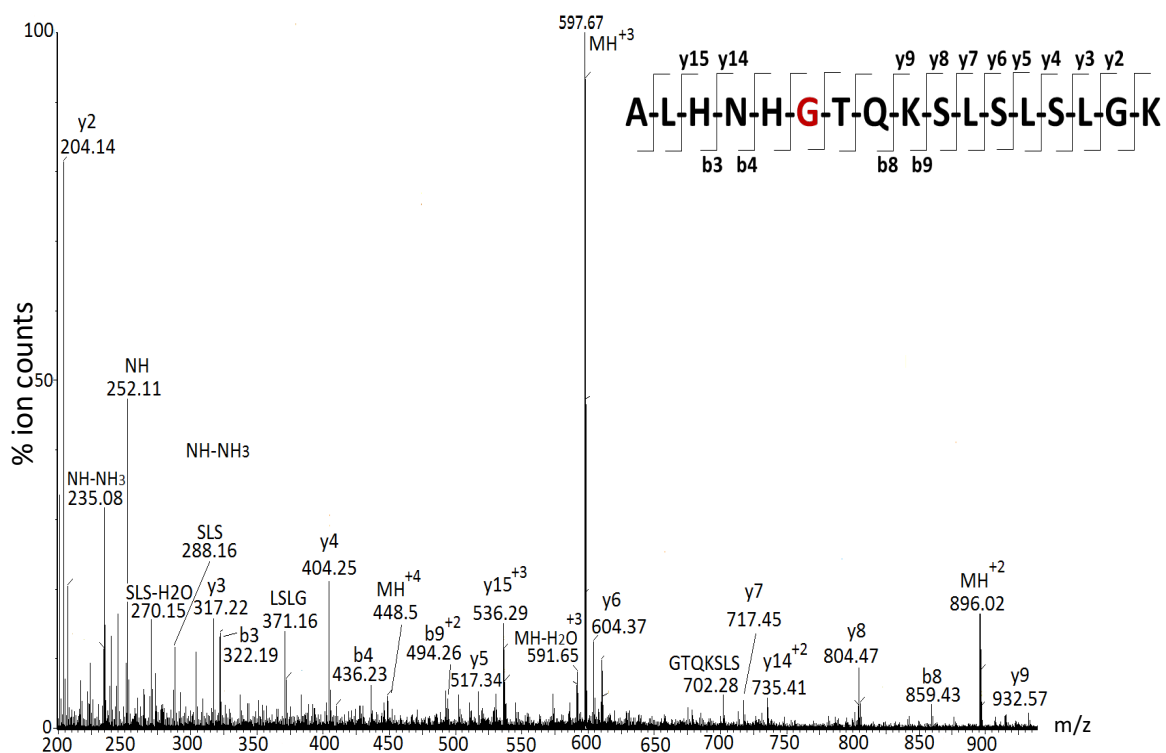


Fig. 2A. MS/MS of product **4** derived from Tyr⁴³⁶ side chain fragmentation and conversion into Gly⁴³⁶, analyzed on the Xevo-G2 mass spectrometer in the MS^E mode.

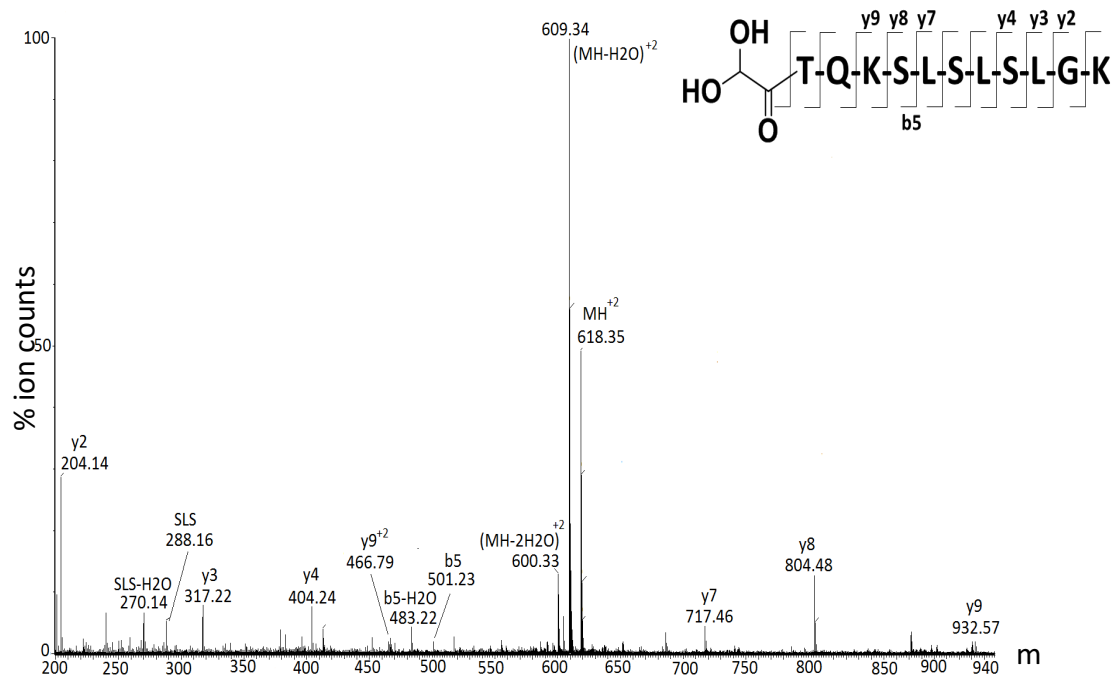


Fig. 2B. MS/MS spectrum of product **6** resulting from peptide backbone cleavage forming a glyoxal amide derivative, induced by Tyr⁴³⁶ side chain fragmentation, analyzed on the Xevo-G2 mass spectrometer in the MS^E mode.

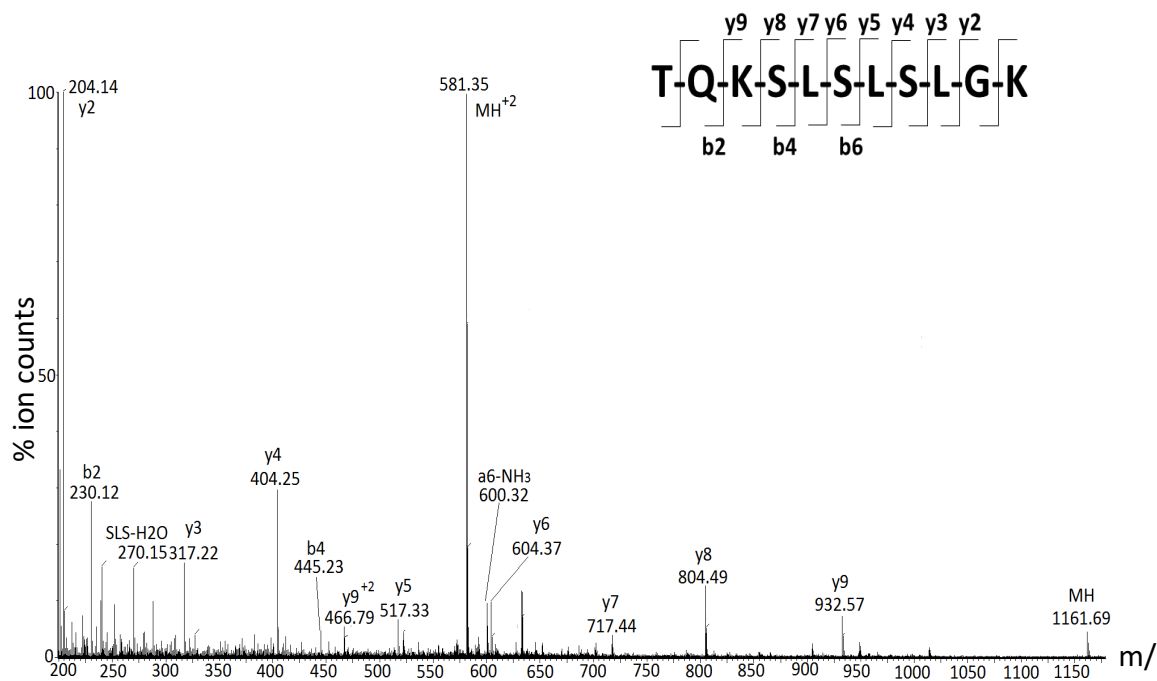


Fig. 2C. MS/MS spectrum of product 7 derived from peptide backbone cleavage induced by side chain fragmentation of Tyr⁴³⁶, analyzed on the Xevo-G2 mass spectrometer in the MS^E mode.

2.3.2.3. MS/MS identification of photoproducts from Tyr300 side chain cleavage. Side chain fragmentation of Tyr³⁰⁰ from QFN²⁹⁷STY³⁰⁰RVVSVLTVLHQDWLNGKE (peptide 3 in WT IgG4-Fc) and QFQ²⁹⁷STY³⁰⁰RVVSVLT VLHQDWLNGKE (peptide 3' in N297Q IgG4-Fc) yielded two products, products **8** and **9**, which are listed in Table 1.

i) Product 8 (m/z 686.11): The MS/MS spectrum of product **8** is shown in Fig. S4A. This product is generated by photo-induced conversion of Tyr³⁰⁰ into Gly³⁰⁰ in peptide 3', showing a loss of 106 amu from the native peptide, similar to the data presented for product **4**. The nature of the y16 and b3 ions indicate no modification on the sequences QFQ and VSVLTVLHQDWLNGKE, and the nature of the y19 and b8 fragment ions locate the mass loss of 106 amu to the original sequence YRV. Hence, we propose the conversion of the sequence YRV to GRV. Product **8** was detected only after photo-irradiation of N297Q IgG4-Fc.

ii) Product 9 (m/z 723.05): The MS/MS spectrum of product **9** is presented in Fig. S4B. Specifically, the nature of the y17 fragment locates a glyoxal amide modification on the N-terminal amino acid Arg. The mass spectrum presented in Fig. S4B shows data derived from the hydrated form of the glyoxal amide-containing product.

2.3.2.4. Other photoproducts. A number of additional chemical modifications, including methionine sulfoxide at Met²⁵², Met³⁵⁸ and Met⁴²⁶; asparagine deamidation at Asn³¹⁵; tryptophan oxidation, e.g. N-formylkynurenine formation at Trp³¹³, tryptophan side chain cleavage product, VVSVLTVLHQD-NH₂, at Trp³¹³; and vinyl thiols generated from Cys²⁶¹, Cys³²¹, Cys³⁶⁷, and Cys⁴²⁵, were observed during photo-irradiation. These products are summarized in Table S2. The

yields of oxidation products generated from Met and Trp were significantly lower in Ar-saturated compared to air-saturated solutions. The formation of oxidation products under Ar is likely due to the presence of residual oxygen in Ar-saturated solutions. We also detected the formation of di-tyrosine cross-links by fluorescence spectroscopy, monitoring the characteristic fluorescence emission around 420-425 nm⁴⁷. However, to date we could not identify these cross-links by mass spectroscopy in our proteolytic digests.

2.3.3. Quantification of the photodegradation products. Our photo-irradiation experiments were conducted mainly in air-saturated conditions. In the presence of oxygen, peptide back bone cleavage is the main degradation pathway induced by Tyr side chain fragmentation, represented by products **1, 2, 5, 6, 7** and **9**. In contrast, the product yields for photo-induced Tyr conversion into Gly (products **3, 4, 8**) were relatively low in air-saturated solutions. Hence, we did not include products **3, 4,** and **8** in the quantification of reaction products under air atmosphere. In addition, we excluded product **9** from the quantification as its native peptide (peptide 3) is glycosylated at Asn²⁹⁷ in HM WT IgG4-Fc, which leads to uncertainties in obtaining the peak area of the native peptide 3.

The yields of the respective photoproducts were calculated by means of MassLynx. Briefly, extracted ion chromatograms (XIC) of the photo-products were generated from base peak intensity chromatograms based on their respective m/z values (± 0.05 Da) to include all the peaks of interest. The XIC were further integrated with a peak-to-peak noise amplitude of 500 to calculate

the areas of the extracted peaks, which were used as numerators referred to as “area of photoproduct” in equation 1. The peak areas for the respective native peptides were obtained in the same way as those of the photo-products; these are referred to as the “area of the native peptide” in equation 1. All quantitative data are displayed in Table 2.

$$\text{yield (\%)} \text{ relative to conversion of native peptide} = \frac{\text{area of photoproduct} \times 100}{\text{area of photoproduct} + \text{area of native peptide}} \text{ Equation 1}$$

2.3.4. Conformational effects on photo-product formation. The role of protein conformation on photo-product formation was examined by photo-irradiation of WT HM IgG4-Fc at $\lambda_{\text{max}} = 305\text{nm}$ in the presence of 0, 10, 25 and 40% (v/v) 1-propanol. The effect of 1-propanol on the secondary structure of WT HM IgG4-Fc was determined by circular dichroism (CD) spectroscopy, as displayed in Fig. S5. For 0% and 10% (v/v) 1-propanol, the CD spectra demonstrate similar patterns, where the range of 220 - 230 nm shows the lowest ellipticity. However, the presence of 25% and 40% 1-propanol, respectively, leads to significantly decreased ellipticity in the range of 200 – 240 nm, indicating that the secondary structure of the IgG4-Fc is altered from a beta sheet to a random coil structure⁴⁸ in the presence of increasing amount of 1-propanol. Three photoproducts resulting from Tyr side chain fragmentation, products **1**, **2**, and **7**, show overall decreasing yields with increasing 1-propanol content (Fig. 3). In contrast, products **5** and **6** respond differently, showing an initial increase of yields with a change of 1-propanol between 0 and 10% (v/v), followed by a decrease of yields upon raising the 1-propanol content to 40% (v/v). Common to all products is the decrease of yields upon increasing the 1-propanol content from 10 to 40%

(v/v), suggesting that the co-solvent disrupts a conformation and/or pathway critical for Tyr side chain cleavage. Note, that in order to remove 1-propanol quantitatively for digestion and MS studies, the photo-irradiated samples were subjected to Amicon filtration twice, resulting in some loss of products, reflected in the generally lower percentages of yields compared to those listed in Table 2. Qualitatively similar results were obtained when acetonitrile was added between 10 and 40% (v/v) to aqueous solutions of WT HM IgG4-Fc.

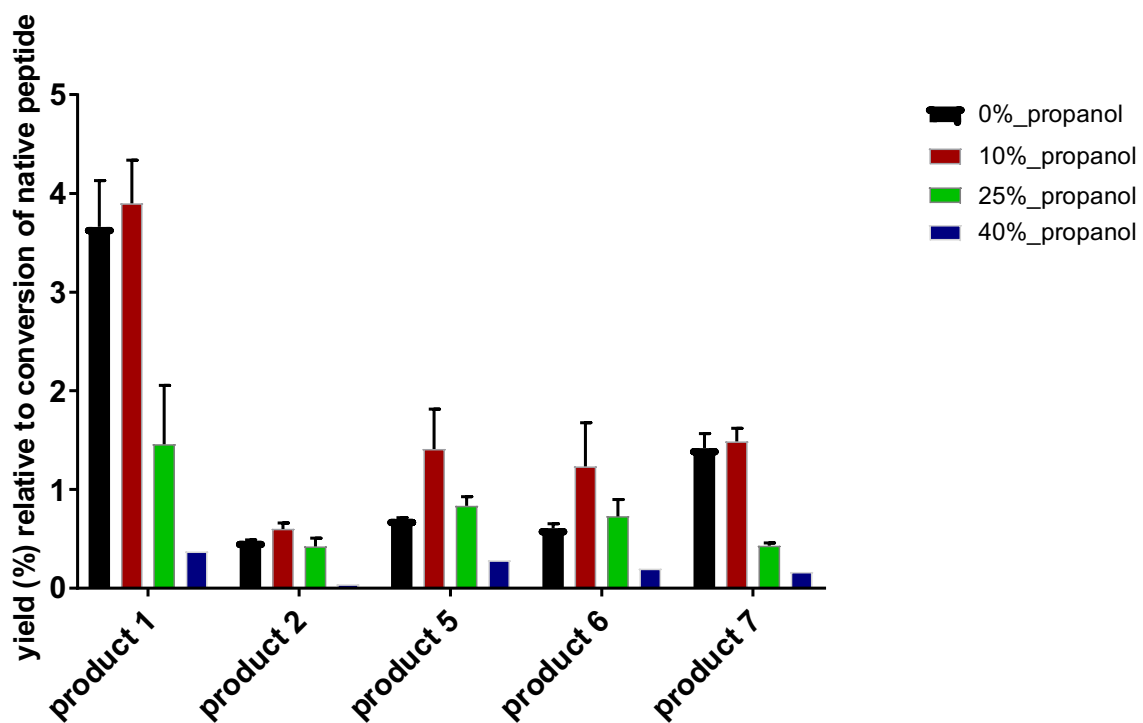


Figure 3. Conformational role in Tyr side chain fragmentation photoirradiated at wavelength > 295 nm for 60 min in the presence of 0%, 10%, 25% and 40% of 1-propanol. For 0%, 10% and 25% 1-propanol, n = 2. For 40% 1-propanol, n = 1.

2.3.5. Solvent isotope effects (SIE). HM IgG4-Fc (0.22 mg/mL) in 20 mM sodium phosphate in either H₂O or D₂O solutions (pH, pD = 7.1) was photoirradiated at 254 nm for 20 min in quartz tubes under air. After photo-irradiation, samples were buffer-exchanged to 20 mM sodium phosphate in H₂O, followed by denaturation, reduction and alkylation as described in section 2.7. The photolytic conversion (%) of native peptides in H₂O and D₂O is plotted in Fig. 4, where either no (product **1**) or inverse product solvent isotope effects (products **2**, **5**, **6** and **7**) are observed. The numerical values for product yields and the inverse product isotope effects are displayed in Table 2. Interestingly, product **1** (MTKNQVSLC(+57)LVKGF-NH₂) reveals no SIE while the Met-oxidized product, product **2** (M(+16)TKNQVSLC(+57)LVKGF-NH₂), shows an inverse SIE of 1.46. This inverse SIE may reflect Met sulfoxide formation through a singlet oxygen pathway, where singlet oxygen has a longer life time in D₂O than in H₂O⁴⁹. Products **5**, **6** and **7** from Tyr⁴³⁶ from peptide 2 show significant inverse SIE between 1.89 and 2.02, indicating a potential role for proton transfer in the mechanism leading to the cleavage of Tyr⁴³⁶. The mechanism will be discussed in detail in the Discussion section

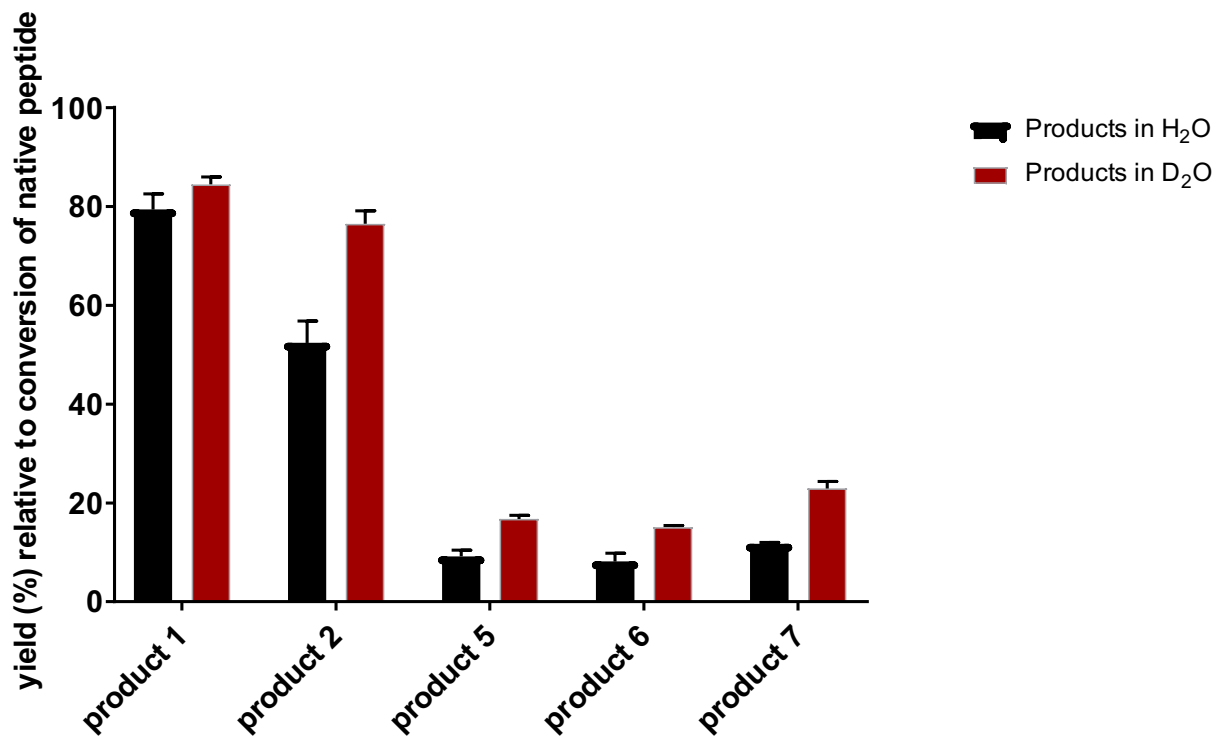


Figure 4. Product solvent isotope effects on HM WT IgG4-Fc Tyr side chain fragmentation during photoirradiation at 254 nm for 20 min. The sequences of the products are listed in Table 1. The error bars plotted indicate standard errors from three independent experiments (n=3).

2.3.6. Comparison of WT HM and W381F HM IgG4-Fc. WT and W381F IgG4-Fc at 0.71 mg/mL in 20 mM sodium phosphate (pH 7.1) were placed in quartz vials sealed with rubber stoppers and saturated through headspace equilibration with air or Ar for 90 min. Photo-irradiation of WT and W381F IgG4-Fc was conducted side by side at $\lambda = 254$ nm for 15 min. Products **1**, **2**, **5**, **6** and **7** were quantified under air, and the results are shown in Fig. 5A. Furthermore, the conversion (%) of Tyr³⁷³ and Tyr⁴³⁶ into Gly³⁷³ and Gly⁴³⁶, products **3** and **4**, was quantified in Ar-saturated solution and the data are shown in Fig. 5B. The yields of photo-products under air for W381F IgG4-Fc are at least three-fold lower compared to the yields for WT IgG4-Fc (Fig. 5A). In addition, the photo-products observed under Ar are lower by a factor of 2.0 -4.0 in W381F compared to WT IgG4-Fc (Fig.5B). These data suggest that Trp³⁸¹ plays a critical role in the mechanisms leading to Tyr side chain fragmentation.

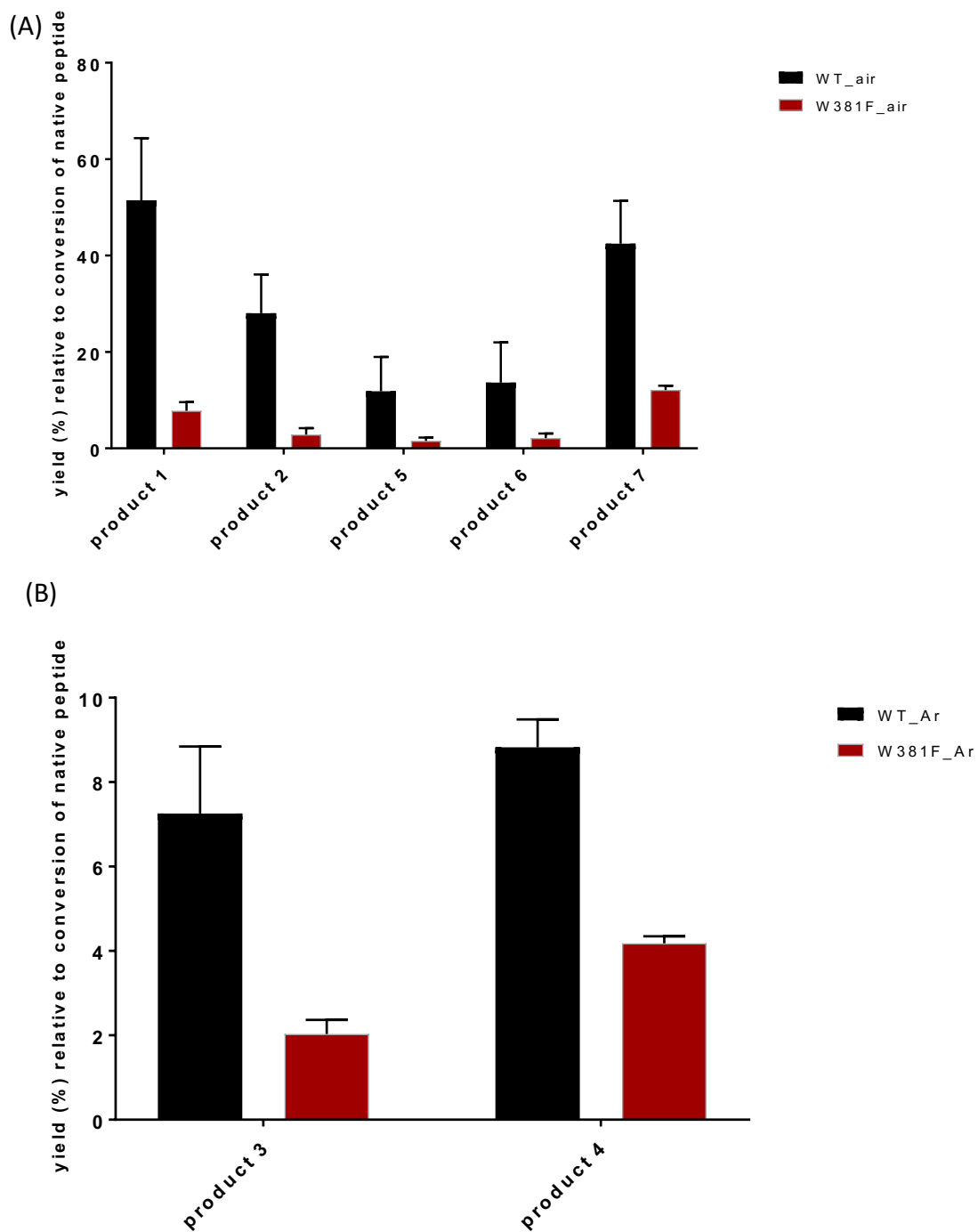


Figure 5. Quantification of light-induced Tyr side chain fragmentation product yields in WT and W381F IgG4-Fc for photoirradiation at 254 nm for 15 min. (A) Air-saturation. (B) Ar-saturation. Data show mean values and the range (n=2).

2.3.7. Comparison of WT HM and H435R/Y436F HM IgG4-Fc. The double mutant H435R/Y436F was characterized by intact protein LC-MS under reducing conditions (Fig. S7). The double mutant H435R/Y436F IgG4-Fc was initially designed to change the chromatographic behavior during purification. However, for our mechanistic investigation only the replacement of Tyr⁴³⁶ by Phe⁴³⁶ is important while we do not expect any effect of the replacement of His⁴³⁵ by Arg⁴³⁵, under our photoirradiation conditions ($\lambda_{\max} = 305$ nm). WT and H435R/Y436F IgG4-Fc (0.22 mg/mL) in 20 mM sodium phosphate (pH 7.1) in Pyrex tubes were photoirradiated at $\lambda_{\max} = 305$ nm for 1 hr. Fig. 6 summarizes the yields of photo-products from WT and H435R/Y436F IgG4-Fc. The Tyr³⁷³ cleavage products, products **1** and **2**, from peptide 1, MTKNQVSLTC(+57)LVKGFY³⁷³PSDIAVE, where Tyr is not mutated, show similar yields for WT and in the double mutant H435R/Y436F IgG4-Fc (Fig. 6). However, Tyr⁴³⁶ cleavage products, products **5**, **6** and **7**, from peptide 2, ALHNH⁴³⁵Y⁴³⁶TQKSLSLSLGK, were only observed for WT IgG4-Fc. In contrast, these products were not observed for the double mutant, which contains a modified peptide sequence, ALHNR⁴³⁵F⁴³⁶TQKSLSLSLGK of H435R/Y436F IgG4-Fc (Fig. 6). These data confirm that these products originate from the cleavage of Tyr⁴³⁶.

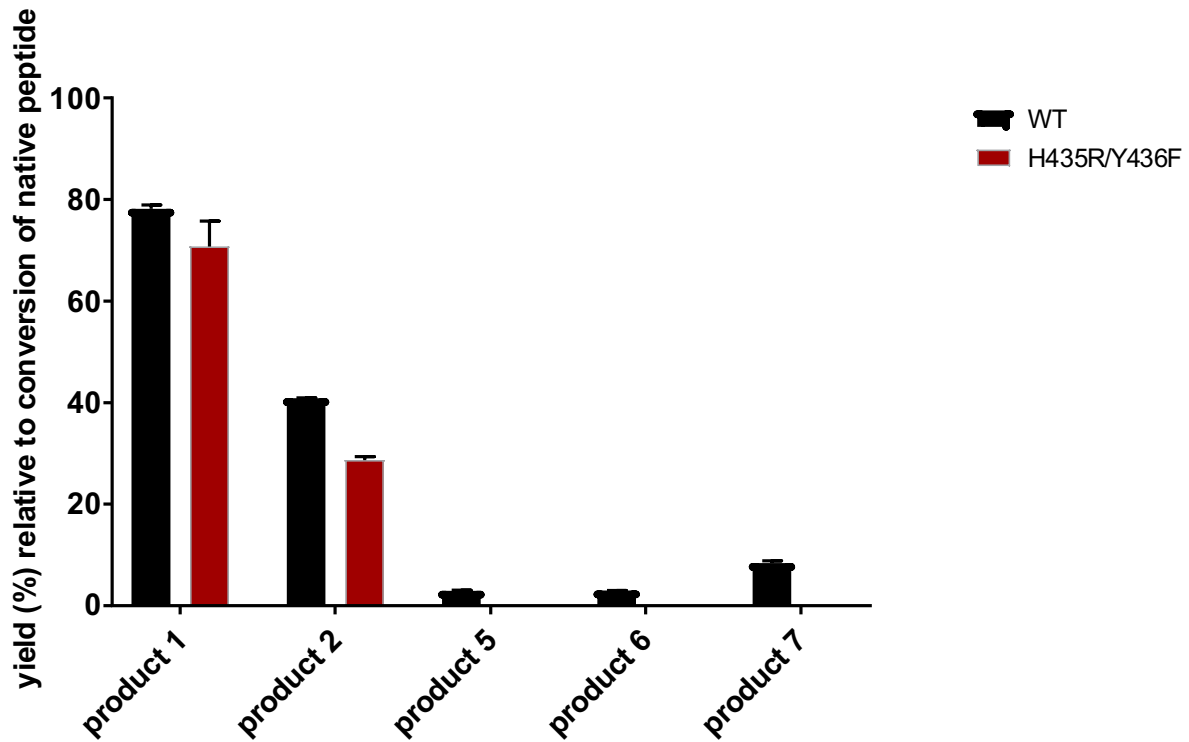


Figure 6. Quantification of light-induced Tyr side chain fragmentation product yields from non-mutated MTKNQVSLTC(+57)LVKGFY³⁷³PSDIAVE in WT and H435R/Y436F mutant, as well as product yields from ALHNR⁴³⁵⁻⁴³⁶F⁴³⁶TQKSLSLSLGK in the mutant. Photoirradiation was conducted at $\lambda_{\text{max}} = 305$ nm. Data show mean values and the range (n=2).

2.3.8. Photo-irradiation of N-acetyl-tyrosine (N-Ac-Tyr) in the presence of oxidized glutathione (GSSG). The identification of Tyr side chain fragmentation products in photo-irradiated IgG4-Fc solutions suggests the elimination of quinone-methide from Tyr residues. For mechanistic confirmation, we photo-irradiated N-Ac-Tyr in the presence of GSSG. In this experiment, GSSG serves to accept an electron generated by photo-ionization of N-Ac-Tyr, ultimately yielding GS⁻/GSH. Any one-electron oxidized N-Ac-Tyr can undergo side chain cleavage, eliminating a protonated quinone-methide, which can be trapped by GS⁻/GSH, generated from GSSG, yielding an addition product. The efficient addition of quinone methides to thiols had been demonstrated before⁵⁰⁻⁵².

1 mM N-Ac-Tyr and 200 μ M GSSG were dissolved in 20 mM sodium phosphate buffer, pH 6.8. The mixtures were placed in quartz vials sealed with rubber stoppers, saturated with Ar for 1hr, and subsequently irradiated for 30 min at $\lambda = 254$ nm. Control, non-irradiated samples were saturated with Ar for 1hr and then placed in the dark. Experiments were conducted in triplicates. The resultant photoproducts were analyzed by HPLC-MS/MS on a Xevo-G2 mass spectrometer. The product expected from the addition of GS⁻/GSH to quinone methide has a theoretical m/z of 414.13 amu, which was identified in the photo-irradiated solutions by data dependent acquisition (DDA). MS/MS data, together with the proposed fragment structures are displayed in Fig. 7. The fragment ions mainly result from the fragmentation of peptide bonds and the newly formed thioether bond of the glutathionyl moiety. However, specifically, the ion with m/z 285.14 represents a fragment from the addition product. The adduct of GS⁻/GSH to quinone methide (m/z

414.19) was only observed when both GSSG and N-Ac-Tyr were photo-irradiated together, and not in controls lacking either GSSG or N-Ac-Tyr. When we performed photo-irradiations in the presence of air rather than Ar, the yield of trapped quinone methide dropped ca. 3-fold.

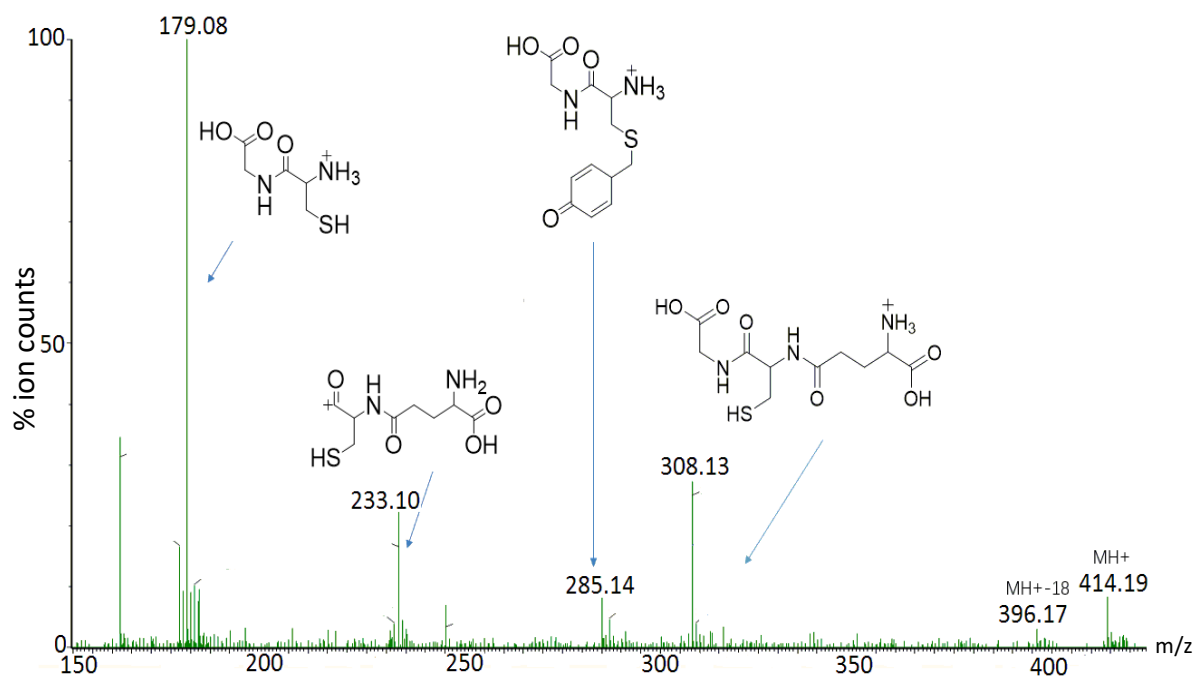


Figure 7. MS/MS of the precursor ion with m/z 414, which corresponds to the adduct of GS⁻/GSH to quinone methide. Here, the adduct is shown where GSH added to the 4-methylene moiety of 4-methylenecyclohexa-2,5-dien-1-one.

2.4. DISCUSSION

Under light exposure, Tyr³⁰⁰ in the C_{H2} domain and Tyr³⁷³ and Tyr⁴³⁶ in the C_{H3} of IgG4-Fc were observed to undergo ^αC-^βC cleavage of the Tyr side chain. The corresponding photo-degradation products, including several peptide backbone cleavage products, and Gly, were identified by peptide mapping and HPLC-MS/MS analysis. Based on these degradation products, a mechanism for Tyr side chain fragmentation is proposed and displayed in Scheme 1.

2.4.1. Tyr side chain fragmentation mechanism. We propose that the photolytic side chain cleavage of Tyr involves an intermediate Tyr radical cation (TyrOH⁺) (Scheme 1, reaction 1). In reaction 1, the Tyr radical cation is generated directly via photo-ionization of Tyr. However, an alternative pathway involves electron-transfer from Tyr to another photochemically generated radical cation, i.e., from Trp (see below). Formation of the Tyr radical cation is followed by the elimination of a protonated quinone methide and the formation of a carbon-centered glycy radical (Scheme 1, reaction 2). Under Ar, the electron generated via reaction 1 can reduce an adjacent disulfide bond (RSSR), leading to a thiol (RSH) and a thiyl radical (RS[•])⁵³. The glycy radical generated in reaction 2 can, therefore, abstract a hydrogen atom from RSH, producing Gly (Scheme 1, reaction 3). The conversion of Tyr into Gly was detected for Tyr³⁷³ (product **3**), Tyr⁴³⁶ (product **4**), and Tyr³⁰⁰ (product **8**) (Table 1). In the presence of O₂, the glycy radical converts into a peroxy radical (Scheme 1, reaction 4). The latter can eliminate superoxide to generate a carbocation (Scheme 1, reaction 5)⁵⁴, which, in water, cleaves the HN-^αC bond into glyoxal amide and a C-terminal amide (Scheme 1, reaction 6). Evidence for this mechanism is provided by the

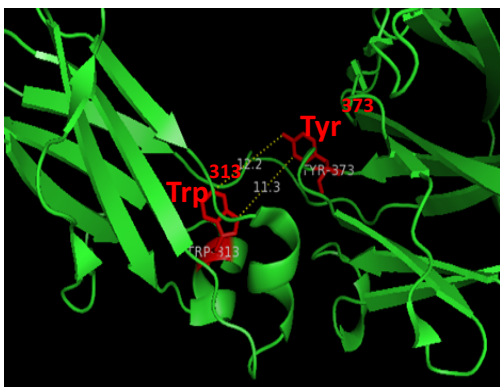
generation of products **1**, **2**, **5**, **6** and **9** under our experimental condition. Alternatively, two peroxy radicals can recombine and generate alkoxy radicals (Scheme 1, reaction 7)⁵⁵. These alkoxy radicals further react via reactions 8 and 9 (Scheme 1) to yield an isocyanate derivative, which can react with water (Scheme 1, reaction 10). Evidence for this mechanism is provided by the formation of product **7** (Table 1).

2.4.2. Effect of IgG4-Fc conformation on Tyr side chain cleavage. The role of IgG4-Fc conformation on photo-induced Tyr side chain fragmentation was examined through the addition of various amounts of 1-propanol, which has been shown to alter protein structure⁵⁶⁻⁵⁷. We used CD spectroscopy (Fig. S2) to demonstrate that 1-propanol induced changes in the IgG4-Fc secondary structure when present in the solution at $\geq 25\%$ (v/v). The structural change caused by $\geq 25\%$ (v/v) 1-propanol is sufficient to lower the yields of Tyr side chain fragmentation. Mechanistically, the reduced efficiency of Tyr side chain cleavage can be rationalized in multiple ways: first, a solvent-induced conformational change can affect the formation of TyrOH⁺, for example by electron transfer to a photo-ionized Trp residue, Trp⁺ (Reactions 12-14). Second, a solvent-induced conformational change may affect the life-time of TyrOH⁺, which, through deprotonation, can convert into the neutral tyrosyl radical (TyrO[•]) (Scheme 1, reaction 11), which should be resistant to side chain fragmentation.

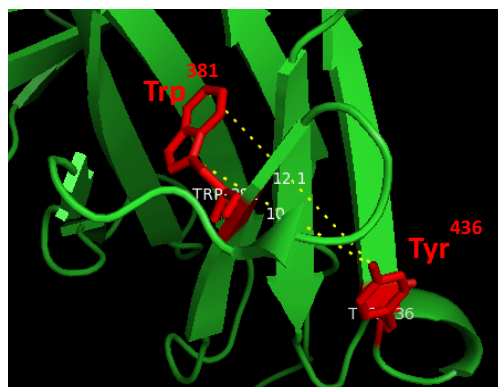
In order to evaluate a role of electron transfer from Tyr to Trp⁺ for the initiation of Tyr side chain cleavage, we inspected the crystal structure of IgG4-Fc (PDB 4C54)^{31, 58}. The structure revealed

three Trp residues located adjacent to Tyr³⁷³, Tyr⁴³⁶ and Tyr³⁰⁰, respectively, displayed in Fig. 8: Trp³¹³ is located 11.3 Å from Tyr³⁷³, Trp³⁸¹ is located 12.1 Å from Tyr⁴³⁶, and Trp³¹³ is located 18.1 Å from Tyr³⁰⁰. These spatial distances are reported to be sufficiently close for electron transfer between Tyr and Trp residues⁵⁹. We then representatively mutated Trp³⁸¹ into Phe³⁸¹, which resulted in a significant reduction of Tyr side chain cleavage (Figure 5A and 5B). The remaining, low yields of Tyr cleavage products are likely the result of electron transfer from Tyr to alternative photo-ionized Trp residues, or of direct photo-ionization of Tyr^{45,46,47}.

(A)



(B)



(C)

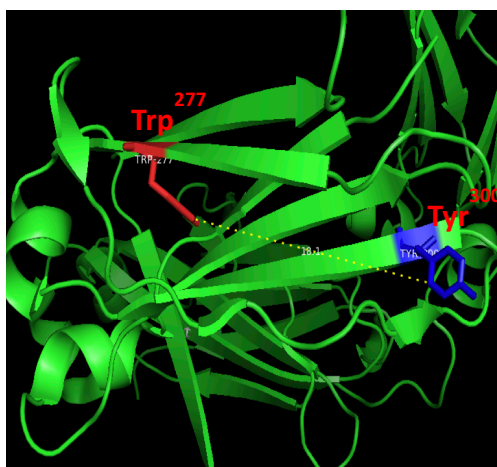


Figure 8. Tyr³⁷³ (A), Tyr⁴³⁶ (B), and Tyr³⁰⁰ (C) in the crystal structure of IgG4-Fc (PDB 4C54) displayed with PyMOL are adjacent to Trp³¹³, Trp³⁸¹, and Trp²⁷⁷, respectively.

In order to evaluate, whether the yield and/or the lifetime of $\text{TyrOH}^{\cdot+}$ influences the yields of Tyr side chain cleavage products, we measured the product solvent isotope effects. Interestingly, products **5-7** showed significant inverse product solvent isotope effects between 1.89 and 2.02. These products originate from side chain cleavage of Tyr^{436} . However, no significant product solvent isotope effect was measured for product **1**, resulting from side chain cleavage of Tyr^{373} (the inverse product solvent isotope effect for product **2**, revealing oxidation of Met to Met sulfoxide, is likely the result of singlet oxygen reaction with Met). The increased yields of products **5-7** in D_2O can be rationalized with a slower rate constant of deprotonation of $\text{TyrOD}^{\cdot+}$ via reaction 11, allowing for a more efficient side chain cleavage (reaction 2). In general, slower rates of D^+ transfer vs H^+ transfer have been observed for proton-coupled electron transfer reactions of tyrosyl radicals⁶⁰⁻⁶². While these reactions concern proton/deuterium transfer to a tyrosyl radical prior to reduction, a similarly slower deuterium vs proton transfer to base can be expected for the deprotonation of $\text{TyrOD}^{\cdot+}$ vs deprotonation of $\text{TyrOH}^{\cdot+}$. However, we also need to discuss some additional aspects of potential relevance to the observed product solvent isotope effect. First, it was reported that the reverse electron transfer from Trp to tyrosyl radical is slower in D_2O ⁶². Considering that tyrosyl radical and tyrosyl radical cation exist in equilibrium 11, the efficiency of such reverse electron transfer may affect the yields of side chain cleavage products. However, such reverse electron transfer from Trp to tyrosyl radical occurs predominantly in the acidic and alkaline pH region⁶²⁻⁶³ and not at the pH/pD = 7.1 of our experiments. Second, deprotonation of $\text{Trp}^{\cdot+}$ to the neutral Trp radical may affect the yield of $\text{TyrOH}^{\cdot+}$, which can be directly generated by electron transfer reaction 14 (Scheme 2). It can be expected that deprotonation of $\text{Trp}^{\cdot+}$ occurs slower in

D₂O as compared to H₂O, potentially resulting in higher yields of TyrOH⁺ in D₂O as compared to H₂O.

The general possibility for Tyr side chain cleavage following the one-electron oxidation of Tyr was confirmed in a model experiment where N-acetyl-tyrosine (NATS) was photo-irradiated in the presence of GSSG. Here, photo-induced electron transfer from NATS to GSSG leads to the generation of TyrOH⁺ and GS⁻/GSH. The quinone methide generated through side chain cleavage of TyrOH⁺ has electrophilic properties, amenable to the addition of GS⁻/GSH. The reaction product of this addition was detected by HPLC-MS/MS analysis.

2.5. CONCLUSION

The present paper discovers three Tyr residues undergo side chain cleavage under UV light stress, and result in peptide back bone cleavages and conversion into Gly. Based on our knowledge, the photo-induced Tyr side chain cleavage reaction is first reported in a protein solution. These reactions may be relevant to light-induced inactivation, aggregation, fragmentation or immunogenicity of protein therapeutics.

2.6. Acknowledgements

We gratefully acknowledge support of H.K. by a Graduate Fellowship from the Genentech Foundation, and experimental assistance by Drs. S. Okbazghi and I.S. Shah.

2.7. REFERENCES

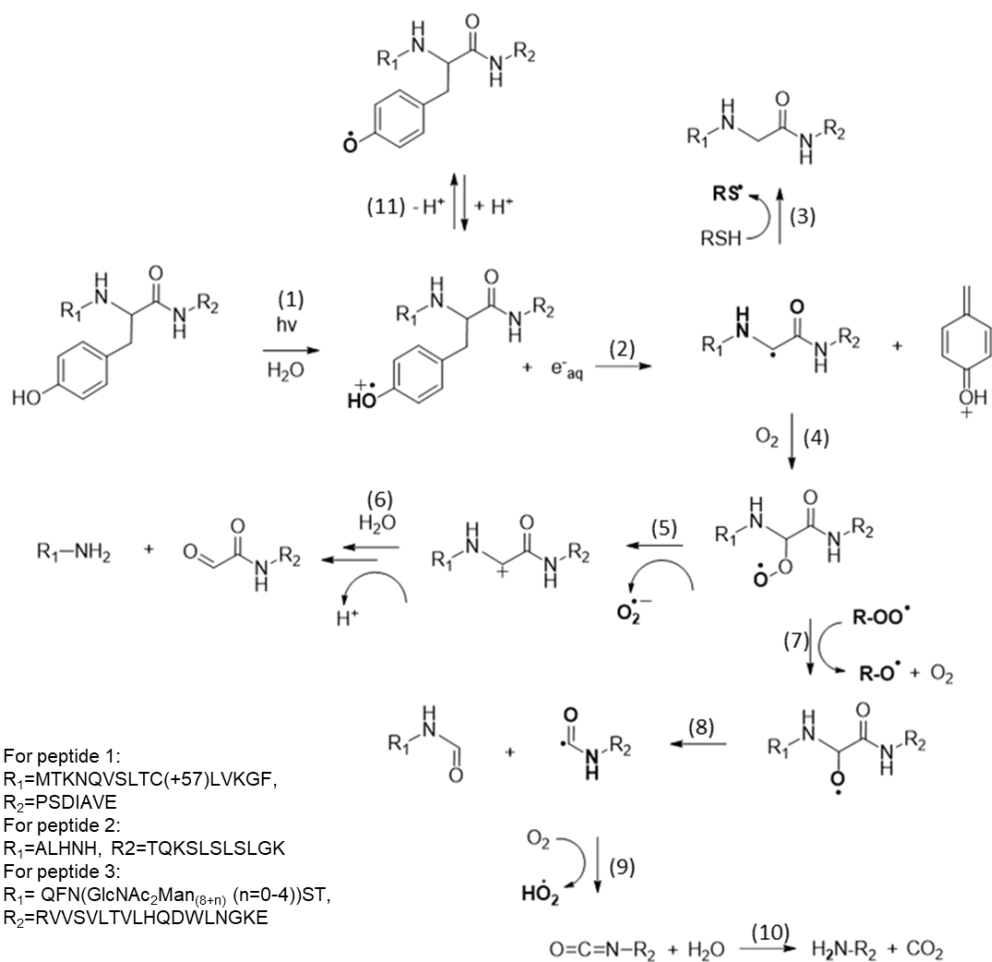
1. Noell, W. K., Possible mechanisms of photoreceptor damage by light in mammalian eyes. *Vision Res* **1980**, *20* (12), 1163-71.
2. Schoneich, C., Novel chemical degradation pathways of proteins mediated by tryptophan oxidation: tryptophan side chain fragmentation. *J Pharm Pharmacol* **2017**.
3. Schoneich, C., Sulfur Radical-Induced Redox Modifications in Proteins: Analysis and Mechanistic Aspects. *Antioxid Redox Signal* **2017**, *26* (8), 388-405.
4. Kerwin, B. A.; Remmele, R. L., Jr., Protect from light: photodegradation and protein biologics. *J Pharm Sci* **2007**, *96* (6), 1468-79.
5. Hermeling, S.; Schellekens, H.; Maas, C.; Gebbink, M. F.; Crommelin, D. J.; Jiskoot, W., Antibody response to aggregated human interferon alpha2b in wild-type and transgenic immune tolerant mice depends on type and level of aggregation. *J Pharm Sci* **2006**, *95* (5), 1084-96.
6. Cockrell, G. M.; Wolfe, M. S.; Wolfe, J. L.; Schoneich, C., Photoinduced aggregation of a model antibody-drug conjugate. *Mol Pharm* **2015**, *12* (6), 1784-97.
7. Wang, W.; Vlasak, J.; Li, Y.; Pristatsky, P.; Fang, Y.; Pittman, T.; Roman, J.; Wang, Y.; Prueksaritanont, T.; Ionescu, R., Impact of methionine oxidation in human IgG1 Fc on serum half-life of monoclonal antibodies. *Mol Immunol* **2011**, *48* (6-7), 860-6.
8. Pan, H.; Chen, K.; Chu, L.; Kinderman, F.; Apostol, I.; Huang, G., Methionine oxidation in human IgG2 Fc decreases binding affinities to protein A and FcRn. *Protein Sci* **2009**, *18* (2), 424-33.
9. Bessa, J.; Boeckle, S.; Beck, H.; Buckel, T.; Schlicht, S.; Ebeling, M.; Kiialainen, A.; Koulov, A.; Boll, B.; Weiser, T.; Singer, T.; Rolink, A. G.; Iglesias, A., The immunogenicity of antibody aggregates in a novel transgenic mouse model. *Pharm Res* **2015**, *32* (7), 2344-59.
10. Quality of biotechnological products: stability testing of biotechnological/biological products. Annex to the ICH Harmonised Tripartite Guideline for the Stability Testing of New Drug Substances and Products. *Dev Biol Stand* **1998**, *93*, 211-9.
11. Baertschi, S. W.; Alsante, K. M.; Tonnesen, H. H., A critical assessment of the ICH guideline on photostability testing of new drug substances and products (Q1B): Recommendation for revision. *J Pharm Sci* **2010**, *99* (7), 2934-40.
12. Baker, M. P.; Reynolds, H. M.; Lumicisi, B.; Bryson, C. J., Immunogenicity of protein therapeutics: The key causes, consequences and challenges. *Self Nonself* **2010**, *1* (4), 314-322.
13. De Groot, A. S.; Scott, D. W., Immunogenicity of protein therapeutics. *Trends Immunol* **2007**, *28* (11), 482-90.
14. Ratanji, K. D.; Derrick, J. P.; Dearman, R. J.; Kimber, I., Immunogenicity of therapeutic proteins: influence of aggregation. *J Immunotoxicol* **2014**, *11* (2), 99-109.
15. Luo, Q.; Joubert, M. K.; Stevenson, R.; Ketchem, R. R.; Narhi, L. O.; Wypych, J., Chemical modifications in therapeutic protein aggregates generated under different stress conditions. *J*

- Biol Chem* **2011**, *286* (28), 25134-44.
16. Fradkin, A. H.; Mozziconacci, O.; Schoneich, C.; Carpenter, J. F.; Randolph, T. W., UV photodegradation of murine growth hormone: chemical analysis and immunogenicity consequences. *Eur J Pharm Biopharm* **2014**, *87* (2), 395-402.
 17. Boll, B.; Bessa, J.; Folzer, E.; Rios Quiroz, A.; Schmidt, R.; Bulau, P.; Finkler, C.; Mahler, H. C.; Huwyler, J.; Iglesias, A.; Koulov, A. V., Extensive Chemical Modifications in the Primary Protein Structure of IgG1 Subvisible Particles Are Necessary for Breaking Immune Tolerance. *Mol Pharm* **2017**, *14* (4), 1292-1299.
 18. Haywood, J.; Mozziconacci, O.; Allegre, K. M.; Kerwin, B. A.; Schoneich, C., Light-induced conversion of Trp to Gly and Gly hydroperoxide in IgG1. *Mol Pharm* **2013**, *10* (3), 1146-50.
 19. Mozziconacci, O.; Okbazghi, S.; More, A. S.; Volkin, D. B.; Tolbert, T.; Schoneich, C., Comparative Evaluation of the Chemical Stability of 4 Well-Defined Immunoglobulin G1-Fc Glycoforms. *J Pharm Sci* **2016**, *105* (2), 575-87.
 20. Bane, J.; Mozziconacci, O.; Yi, L.; Wang, Y. J.; Sreedhara, A.; Schoneich, C., Photo-oxidation of IgG1 and Model Peptides: Detection and Analysis of Triply Oxidized His and Trp Side Chain Cleavage Products. *Pharm Res* **2017**, *34* (1), 229-242.
 21. Kang, H.; Dedonder-Lardeux, C.; Jouvét, C.; Martrenchard, S.; Gregoire, G.; Desfrancois, C.; Schermann, J. P.; Barat, M.; Fayeton, J. A., Photo-induced dissociation of protonated tryptophan TrpH(+): A direct dissociation channel in the excited states controls the hydrogen atom loss. *Phys Chem Chem Phys* **2004**, *6* (10), 2628-2632.
 22. Bagheri-Majdi, E.; Ke, Y. Y.; Orlova, G.; Chu, I. K.; Hopkinson, A. C.; Siu, K. W. M., Copper-mediated peptide radical ions in the gas phase. *J Phys Chem B* **2004**, *108* (30), 11170-11181.
 23. Mozziconacci, O.; Schoneich, C., Effect of conformation on the photodegradation of Trp- and cystine-containing cyclic peptides: octreotide and somatostatin. *Mol Pharm* **2014**, *11* (10), 3537-46.
 24. Weckler, A. T.; Yin, J.; Tao, P. L.; Kabakoff, B.; Sreedhara, A.; Deperalta, G., Photodisruption of the Structurally Conserved Cys-Cys-Trp Triads Leads to Reduction-Resistant Scrambled Intrachain Disulfides in an IgG1 Monoclonal Antibody. *Mol Pharmaceut* **2018**, *15* (4), 1598-1606.
 25. Ronsein, G. E.; Oliveira, M. C. B.; Miyamoto, S.; Medeiros, M. H. G.; Di Mascio, P., Tryptophan oxidation by singlet molecular oxygen [O-2 ((1)Delta(g))]: Mechanistic studies using O-18-labeled hydroperoxides, mass spectrometry, and light emission measurements. *Chemical Research in Toxicology* **2008**, *21* (6), 1271-1283.
 26. Madler, S.; Lau, J. K.; Williams, D.; Wang, Y.; Saminathan, I. S.; Zhao, J.; Siu, K. W.; Hopkinson, A. C., Fragmentation of peptide radical cations containing a tyrosine or tryptophan residue: structural features that favor formation of [x(n-1) + H] (+) and [z(n-1) + H] (+) ions. *J Phys Chem B* **2014**, *118* (23), 6123-33.
 27. Joly, L.; Antoine, R.; Broyer, M.; Dugourd, P.; Lemoine, J., Specific UV photodissociation of tyrosyl-containing peptides in multistage mass spectrometry. *J Mass Spectrom* **2007**, *42* (6), 818-24.

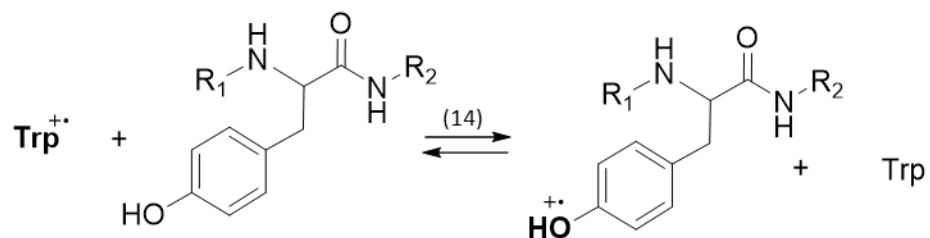
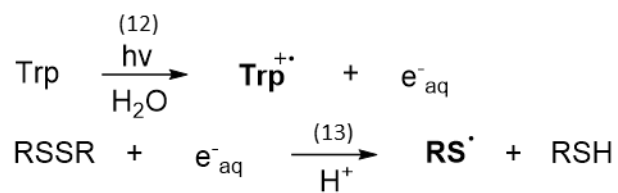
28. Fekete, S.; Guillarme, D.; Sandra, P.; Sandra, K., Chromatographic, Electrophoretic, and Mass Spectrometric Methods for the Analytical Characterization of Protein Biopharmaceuticals. *Anal Chem* **2016**, *88* (1), 480-507.
29. Vidarsson, G.; Dekkers, G.; Rispens, T., IgG subclasses and allotypes: from structure to effector functions. *Front Immunol* **2014**, *5*, 520.
30. Rispens, T.; Ooijevaar-de Heer, P.; Bende, O.; Aalberse, R. C., Mechanism of immunoglobulin G4 Fab-arm exchange. *J Am Chem Soc* **2011**, *133* (26), 10302-11.
31. Davies, A. M.; Rispens, T.; Ooijevaar-de Heer, P.; Gould, H. J.; Jefferis, R.; Aalberse, R. C.; Sutton, B. J., Structural determinants of unique properties of human IgG4-Fc. *J Mol Biol* **2014**, *426* (3), 630-44.
32. Xiao, J.; Tolbert, T. J., Site-specific chemical modification of a glycoprotein fragment expressed in yeast. *Methods Mol Biol* **2011**, *751*, 329-42.
33. Okbazghi, S. Z.; More, A. S.; White, D. R.; Duan, S.; Shah, I. S.; Joshi, S. B.; Middaugh, C. R.; Volkin, D. B.; Tolbert, T. J., Production, Characterization, and Biological Evaluation of Well-Defined IgG1 Fc Glycoforms as a Model System for Biosimilarity Analysis. *J Pharm Sci* **2016**, *105* (2), 559-74.
34. Edelman, G. M.; Cunningham, B. A.; Gall, W. E.; Gottlieb, P. D.; Rutishauser, U.; Waxdal, M. J., The covalent structure of an entire gammaG immunoglobulin molecule. *Proc Natl Acad Sci U S A* **1969**, *63* (1), 78-85.
35. Sandrine Béranger, C. M.-J., Fatena Bellahcene and Marie-Paule Lefranc Correspondence between the IMGT unique numbering for C-DOMAIN, the IMGT exon numbering, the Eu and Kabat numberings: Human IGHG. http://www.imgt.org/IMGTScientificChart/Numbering/Hu_IGHGnber.html.
36. Zheng, K.; Bantog, C.; Bayer, R., The impact of glycosylation on monoclonal antibody conformation and stability. *MAbs* **2011**, *3* (6), 568-76.
37. Xiao, J.; Tolbert, T. J., Synthesis of polymerizable protein monomers for protein-acrylamide hydrogel formation. *Biomacromolecules* **2009**, *10* (7), 1939-46.
38. Coulet, P. R.; Julliard, J. H.; Gautheron, D. C., A mild methods of general use for covalent coupling of enzymes to chemically activated collagen films. *Biotechnol Bioeng* **1974**, *16* (8), 1055-68.
39. Wu, S.; Letchworth, G. J., High efficiency transformation by electroporation of *Pichia pastoris* pretreated with lithium acetate and dithiothreitol. *Biotechniques* **2004**, *36* (1), 152-4.
40. Choi, B. K.; Bobrowicz, P.; Davidson, R. C.; Hamilton, S. R.; Kung, D. H.; Li, H.; Miele, R. G.; Nett, J. H.; Wildt, S.; Gerngross, T. U., Use of combinatorial genetic libraries to humanize N-linked glycosylation in the yeast *Pichia pastoris*. *Proc Natl Acad Sci U S A* **2003**, *100* (9), 5022-7.
41. Rahn, R. O., Potassium iodide as a chemical actinometer for 254 nm radiation: Use of iodate as an electron scavenger. *Photochem Photobiol* **1997**, *66* (4), 450-455.
42. Rahn, R. O.; Stefan, M. I.; Bolton, J. R.; Goren, E.; Shaw, P. S.; Lykke, K. R., Quantum yield of the iodide-iodate chemical actinometer: Dependence on wavelength and concentration.

- Photochem Photobiol* **2003**, *78* (2), 146-152.
43. Paizs, B.; Suhai, S., Fragmentation pathways of protonated peptides. *Mass Spectrom Rev* **2005**, *24* (4), 508-48.
 44. Bure, C.; Gobert, W.; Lelievre, D.; Delmas, A., In-source fragmentation of peptide aldehydes and acetals: influence of peptide length and charge state. *J Mass Spectrom* **2001**, *36* (10), 1149-55.
 45. Bure, C.; Le Falher, G.; Lange, C.; Delmas, A., Fragmentation study of peptide acetals and aldehydes using in-source collision-induced dissociation. *J Mass Spectrom* **2004**, *39* (7), 817-23.
 46. Bure, C.; Marceau, P.; Meudal, H.; Delmas, A. F., Synthesis and analytical investigation of C-terminally modified peptide aldehydes and ketone: application to oxime ligation. *J Pept Sci* **2012**, *18* (3), 147-54.
 47. Heinecke, J. W.; Li, W.; Daehnke, H. L.; Goldstein, J. A., Dityrosine, a Specific Marker of Oxidation, Is Synthesized by the Myeloperoxidase-Hydrogen Peroxide System of Human Neutrophils and Macrophages. *Journal of Biological Chemistry* **1993**, *268* (6), 4069-4077.
 48. Whitmore, L.; Wallace, B. A., Protein secondary structure analyses from circular dichroism spectroscopy: methods and reference databases. *Biopolymers* **2008**, *89* (5), 392-400.
 49. Baier, J.; Maier, M.; Engl, R.; Landthaler, M.; Baumler, W., Time-resolved investigations of singlet oxygen luminescence in water, in phosphatidylcholine, and in aqueous suspensions of phosphatidylcholine or HT29 cells. *J Phys Chem B* **2005**, *109* (7), 3041-6.
 50. Jiang, J. S.; Zeng, D. X.; Li, S. W., Photogenerated Quinone Methides as Protein Affinity Labeling Reagents. *Chembiochem* **2009**, *10* (4), 635-638.
 51. Lo, L. C.; Chiang, Y. L.; Kuo, C. H.; Liao, H. K.; Chen, Y. J.; Lin, J. J., Study of the preferred modification sites of the quinone methide intermediate resulting from the latent trapping device of the activity probes for hydrolases. *Biochem Biophys Res Commun* **2005**, *326* (1), 30-5.
 52. Arumugam, S.; Guo, J.; Mbua, N. E.; Friscourt, F.; Lin, N. N.; Nekongo, E.; Boons, G. J.; Popik, V. V., Selective and reversible photochemical derivatization of cysteine residues in peptides and proteins. *Chem Sci* **2014**, *5* (4), 1591-1598.
 53. Correia, M.; Neves-Petersen, M. T.; Parracino, A.; di Gennaro, A. K.; Petersen, S. B., Photophysics, photochemistry and energetics of UV light induced disulphide bridge disruption in apo-alpha-lactalbumin. *J Fluoresc* **2012**, *22* (1), 323-37.
 54. Crean, C.; Geacintov, N. E.; Shafirovich, V., Pathways of arachidonic acid peroxy radical reactions and product formation with guanine radicals. *Chem Res Toxicol* **2008**, *21* (2), 358-73.
 55. Hawkins, C. L.; Davies, M. J., Generation and propagation of radical reactions on proteins. *Biochim Biophys Acta* **2001**, *1504* (2-3), 196-219.
 56. Zhao, F.; Ghezzi-Schoneich, E.; Aced, G. I.; Hong, J.; Milby, T.; Schoneich, C., Metal-catalyzed oxidation of histidine in human growth hormone. Mechanism, isotope effects, and inhibition by a mild denaturing alcohol. *J Biol Chem* **1997**, *272* (14), 9019-29.
 57. Wicar, S.; Mulkerrin, M. G.; Bathory, G.; Khundkar, L. H.; Karger, B. L., Conformational

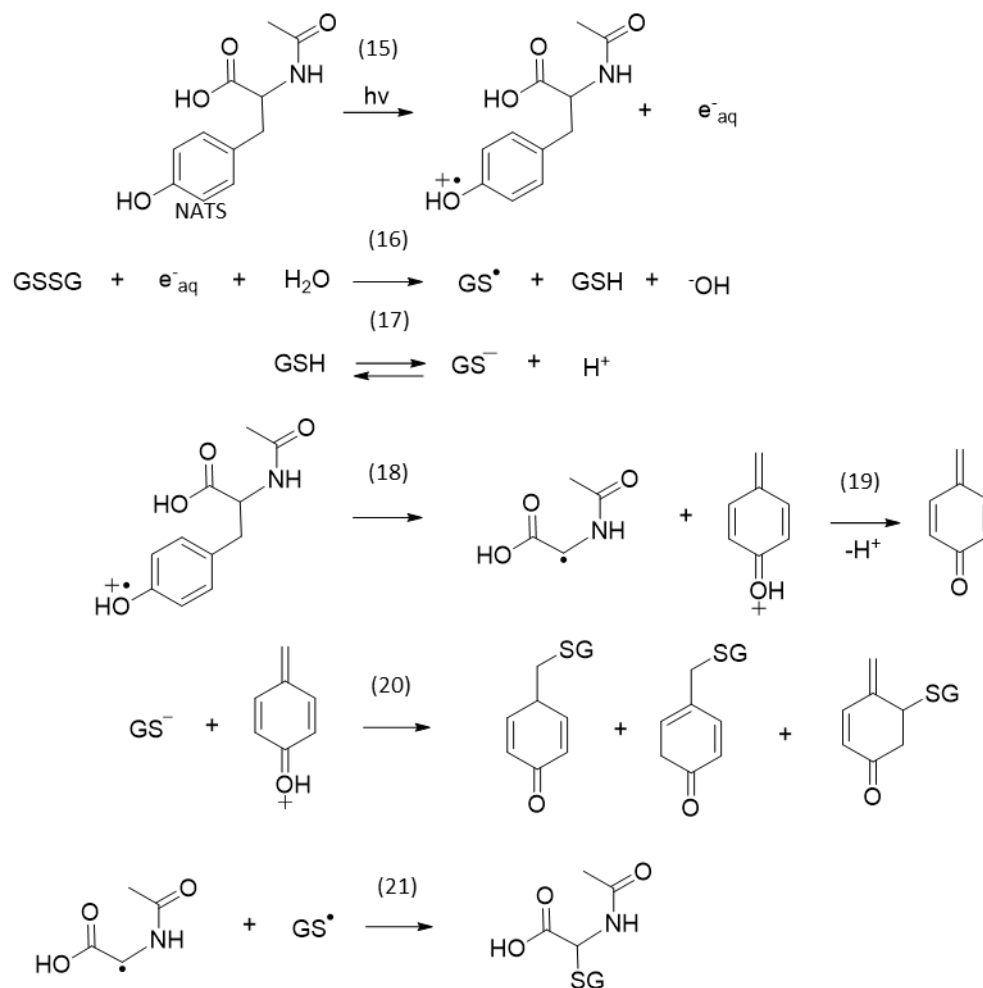
- changes in the reversed phase liquid chromatography of recombinant human growth hormone as a function of organic solvent: the molten globule state. *Anal Chem* **1994**, *66* (22), 3908-15.
58. Davies, A. M.; Rispens, T.; Ooijevaar-de Heer, P.; Aalberse, R. C.; Sutton, B. J., Room temperature structure of human IgG4-Fc from crystals analysed in situ. *Mol Immunol* **2017**, *81*, 85-91.
 59. Chang, M. C.; Yee, C. S.; Stubbe, J.; Nocera, D. G., Turning on ribonucleotide reductase by light-initiated amino acid radical generation. *Proc Natl Acad Sci USA* **2004**, *101* (18), 6882-7.
 60. Jenson, D. L.; Barry, B. A., Proton-coupled electron transfer in photosystem II: proton inventory of a redox active tyrosine. *J Am Chem Soc* **2009**, *131* (30), 10567-73.
 61. Offenbacher, A. R.; Burns, L. A.; Sherrill, C. D.; Barry, B. A., Redox-linked conformational control of proton-coupled electron transfer: Y122 in the ribonucleotide reductase beta2 subunit. *J Phys Chem B* **2013**, *117* (28), 8457-68.
 62. Reece, S. Y.; Stubbe, J.; Nocera, D. G., pH Dependence of charge transfer between tryptophan and tyrosine in dipeptides. *Biochim Biophys Acta* **2005**, *1706* (3), 232-8.
 63. Butler, J.; Land, E. J.; Prutz, W. A.; Swallow, A. J., Reversibility of Charge-Transfer between Tryptophan and Tyrosine. *J Chem Soc Chem Comm* **1986**, (4), 348-349.



Scheme 1. Proposed photolytic processes of Tyr side chain fragmentation in IgG4-Fc under air-saturation when Tyr is photo-ionized.



Scheme 2. Proposed mechanisms of electron transfer reactions between Tyr and photo-ionized Trp.



Scheme 3. Proposed mechanism of photo-irradiation of N-acetyl-tyrosine (NATS) in the presence of GSSG at 254 nm under Ar-saturation, where GSSG is oxidized glutathione and GSH is reduced glutathione.

Table 1. Photoproducts derived from Tyr side chain fragmentation in HM WT and N297Q IgG4-Fc at $\lambda = 254$ nm and $\lambda_{\max} = 305$ nm. The label “√” indicates the corresponding photoproduct is observed, whereas “x” indicates that the photoproduct is not observed under the condition. Products 1- 7, and 9 were observed in photoirradiated HM WT IgG4-Fc. All the products were observed in N297Q IgG4-Fc under irradiation.




Product	Photoproducts	Position	$\lambda = 254$ nm		$\lambda_{\max} = 305$ nm		mass/ charge	Charge
			Ar	air	Ar	air		
1	MTKNQVSLTC(+57)LVKGF -NH ₂	Tyr ³⁷³	√	√	√	√	575.61	3
2	M(+16)TKNQVSLTC(+57)L VKGF-NH ₂	Tyr ³⁷³	√	√	√	√	580.96	3
3	MTKNQVSLTC(+57)LVKGF GPSDIAVE	Tyr ³⁷³	√	√	X	X	832.08	3
4	ALHNHGTQKSLSLSLGK	Tyr ⁴³⁶	√	X	√	X	448.50	4
5	 TQKSLSLSLGK	Tyr ⁴³⁶	√	√	√	√	609.30	2
6	 [TQKSLSLSLGK]+ 18	Tyr ⁴³⁶	√	√	√	√	618.30	2
7	TQKSLSLSLGK	Tyr ⁴³⁶	√	√	√	√	387.89	3
8	QFQSTGRVVSVLTVLHQD WLNKKE	Tyr ³⁰⁰	√	√	√	X	686.11	4
9	 [RLVVSVLTVLHQ DWLNKKE]+18	Tyr ³⁰⁰	√	√	√	√	723.05	3

Table 2. Deprotonation mechanistic studies on HM WT IgG4-Fc Tyr side chain fragmentation during photoirradiation at 254 nm for 20 min. The sequences of the products are listed in Table 1

Products	Reaction position	%conversion of native peptide in H ₂ O (\pm SE)	%conversion of native peptide in D ₂ O (\pm SE)	%conversion of native peptide [D ₂ O/H ₂ O]
1	Tyr 373	76.2 \pm 3.4	78.5 \pm 1.9	1.03
2	Tyr 373	47.8 \pm 4.6	68.8 \pm 2.8	1.44
5	Tyr 436	8.6 \pm 0.98	16.3 \pm 0.79	1.89
6	Tyr 436	7.6 \pm 1.3	14.6 \pm 0.39	1.92
7	Tyr 436	11.0 \pm 0.26	22.3 \pm 1.3	2.02

Table 3: Photoproduct formation under Ar- and air-saturated conditions at $\lambda=254$ nm or $\lambda_{\max}=305$ nm for WT and several mutants. Product details are displayed in Table 1. Photo-products of WT IgG4-Fc are summarized in Table 1.

Tyr residue	N297Q (254nm)		W381F (254nm)		H435R/Y436F (305nm)
	Ar	air	Ar	air	air
Tyr ³⁷³	1,2,3	1,2,3	1,2,3	1,2	1,2
Tyr ⁴³⁶	4,5,6,7	5,6,7	4,5,6,7	5,6,7	Very little or NA
Tyr ³⁰⁰	8,9	9	9	9	9

Supplementary Figures

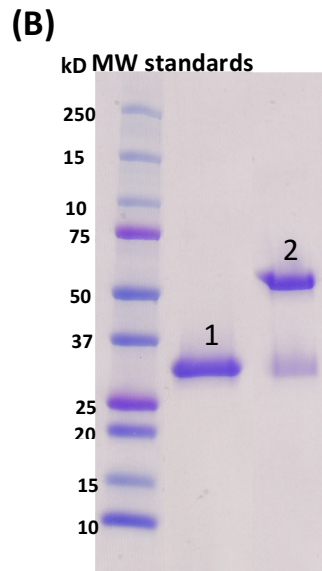
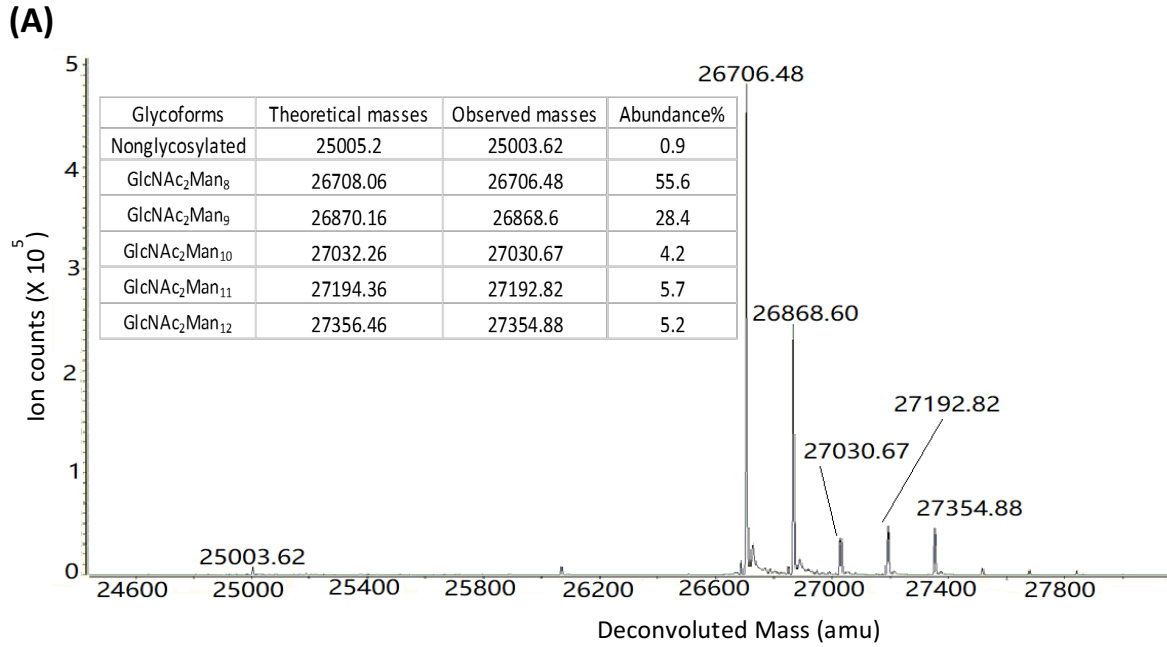


Figure S1. Characterization of WT HM IgG4-Fc. (A) Intact IgG4-Fc MS analysis under reducing conditions; (B) Intact IgG4-Fc characterization on SDS-PAGE under reducing (lane 1) and non-reducing conditions (lane 2).

Figure S2. Collision-induced dissociation(CID) mass spectra of products **1**, **2**, and **3** resulting from Tyr³⁷³ side chain fragmentation under photoirradiation. Product information is listed in Table 1.

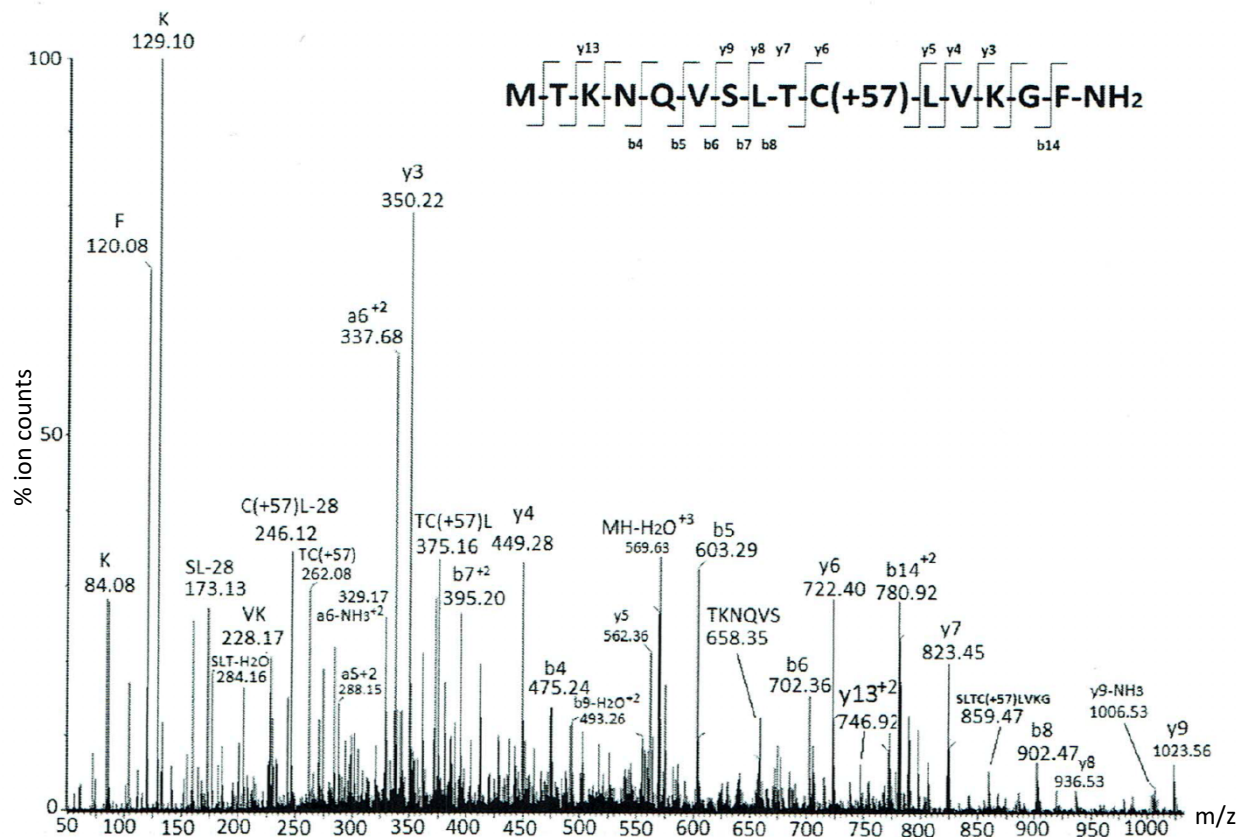


Fig. S2A. MS/MS spectrum of product 1 resulting from peptide backbone cleavage induced by Tyr373 side chain fragmentation, analyzed with Synapt-G2 in the data dependent acquisition (DDA) mode.

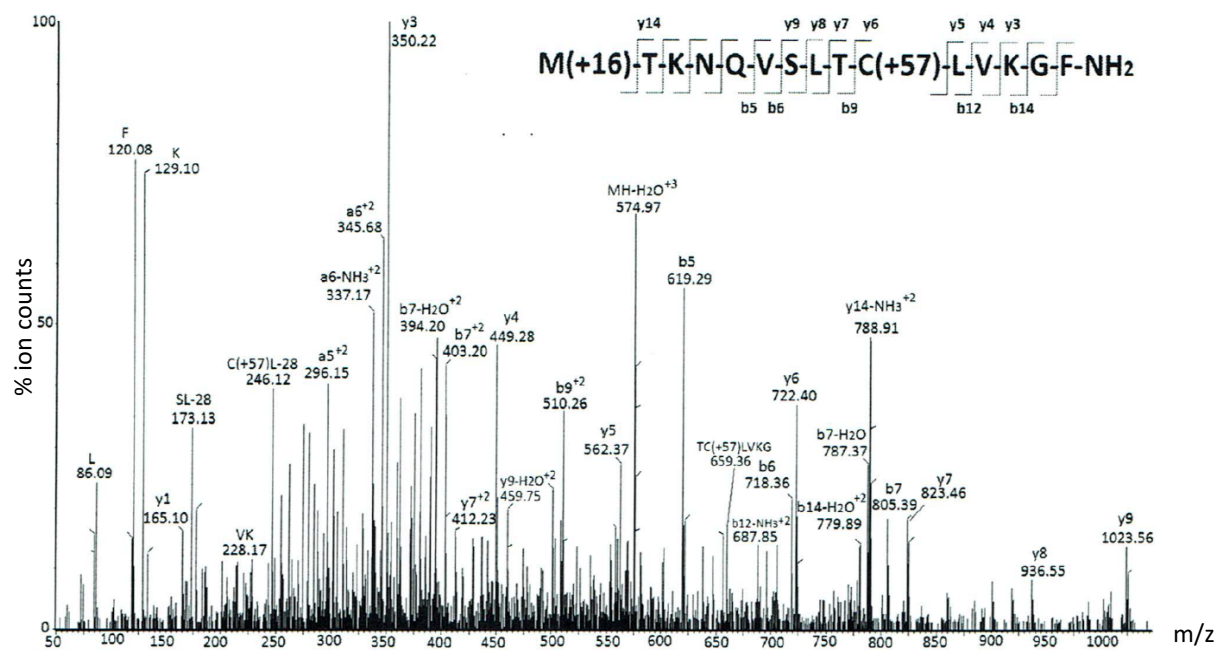


Fig. S2B. MS/MS spectrum of product 2 with an oxidized methionine, a secondary oxidation product of product 1, analyzed with Synapt-G2 in the DDA mode.

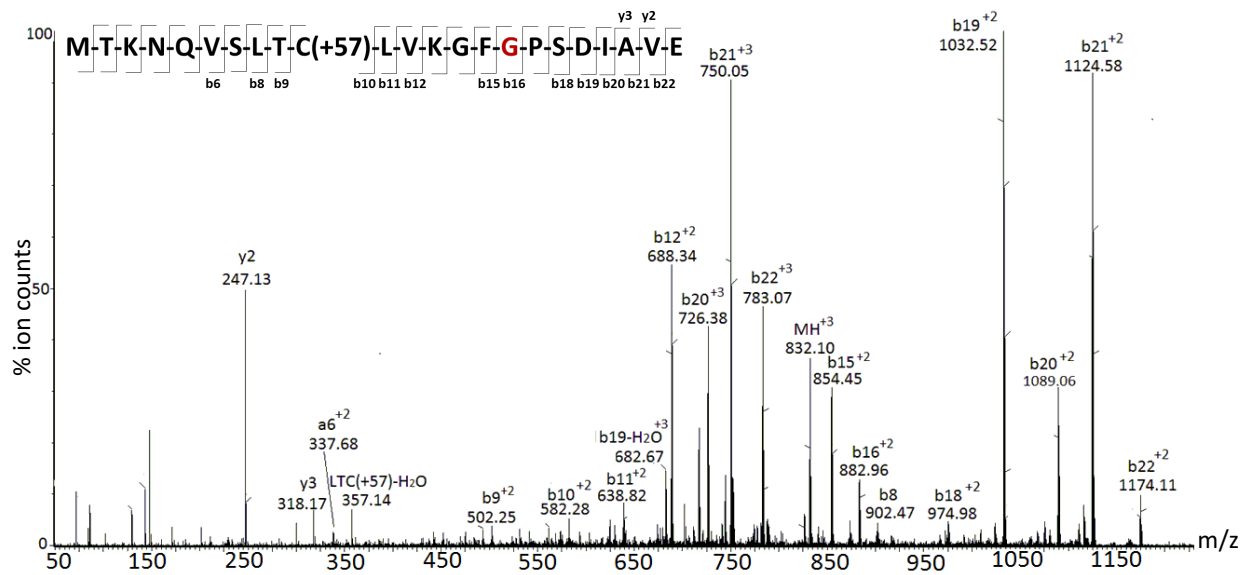


Fig. S2C. MS/MS spectrum of product 3 resulting from Tyr³⁷³ conversion into Gly³⁷³, analyzed with Synapt-G2 in the DDA mode.

Figure S3. CID mass spectra of products **4**, **5**, and **7** resulting from Tyr⁴³⁶ side chain fragmentation under photoirradiation. Product information is listed in Table 1.

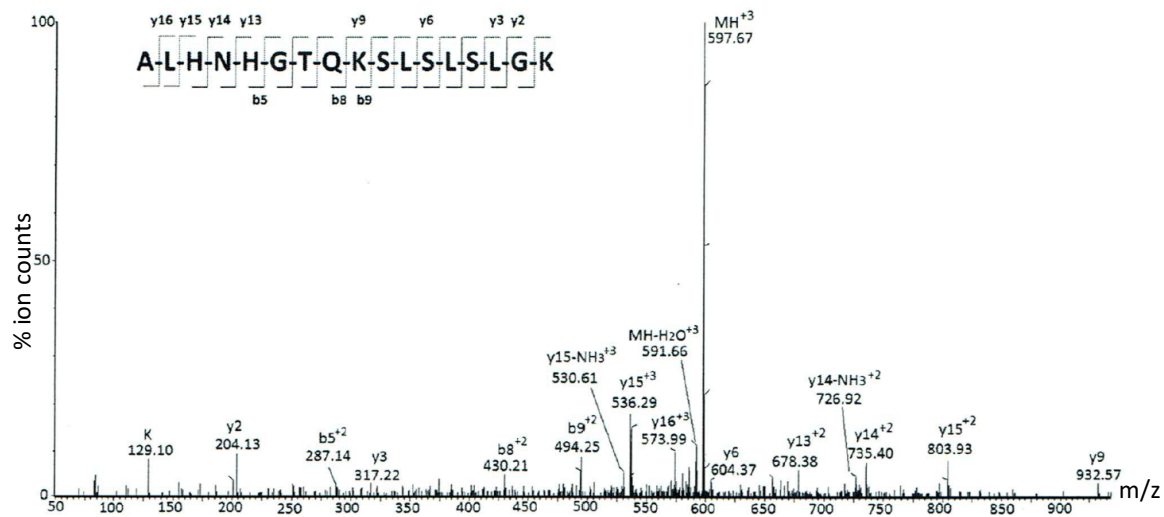


Fig. S3A. MS/MS spectrum of product **4** derived from Tyr⁴³⁶ conversion into Gly⁴³⁶, analyzed with Synapt-G2 in the DDA mode.

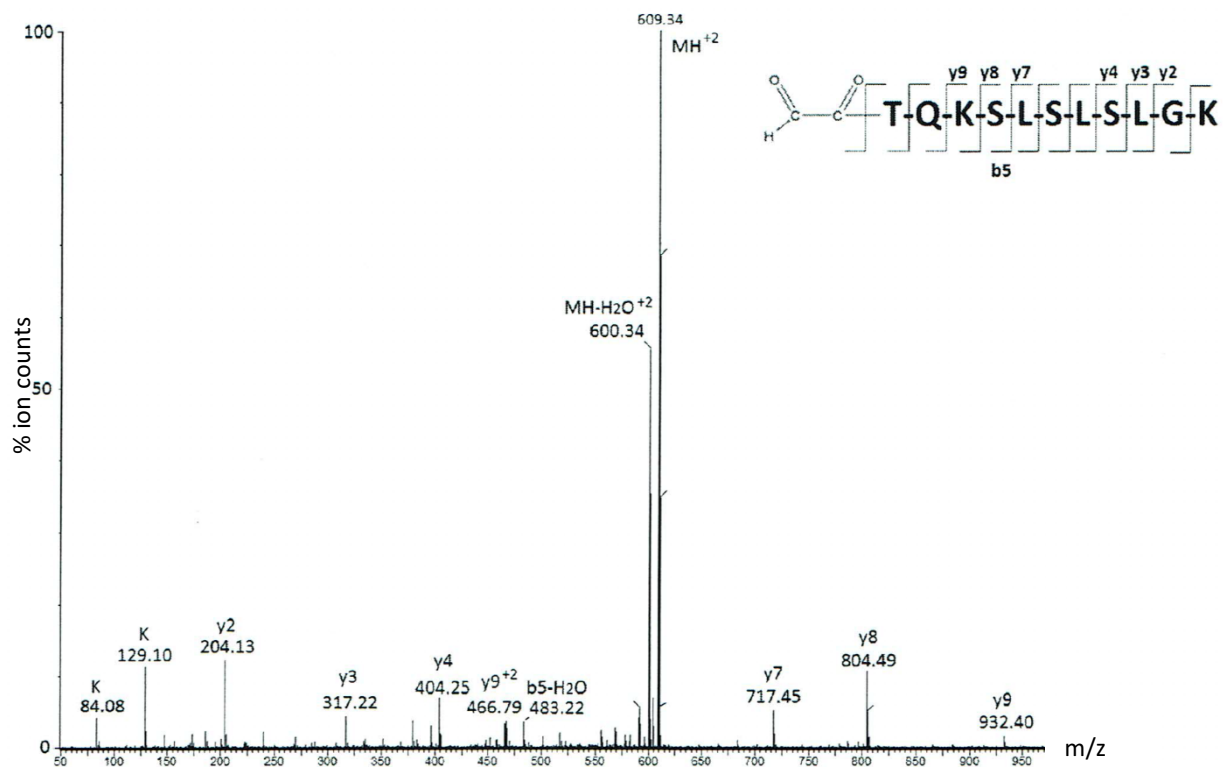


Fig. S3B. MS/MS spectrum of product **5** resulting from peptide backbone cleavage forming a glyoxal derivative, induced by Tyr⁴³⁶ side chain fragmentation, analyzed with Synapt-G2 in the DDA mode.

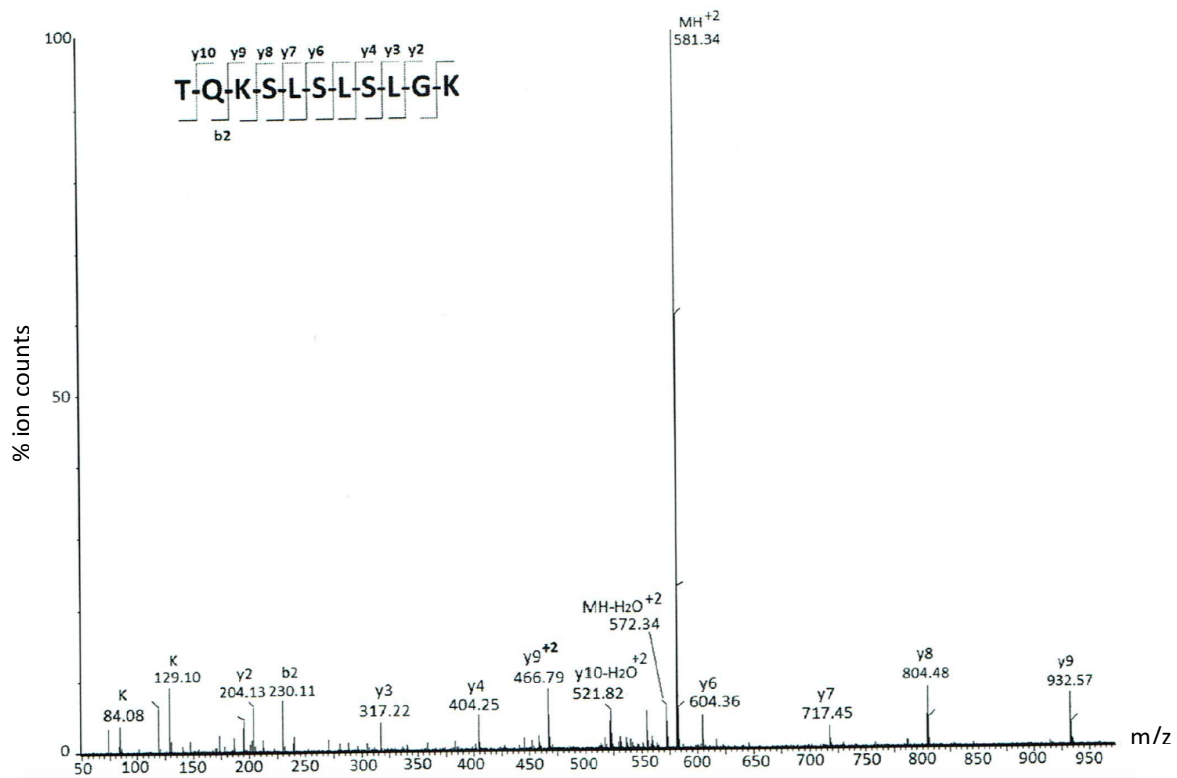


Fig. S3C. MS/MS spectrum of product 7 derived from peptide backbone cleavage induced by side chain fragmentation of Tyr⁴³⁶, analyzed with Synapt-G2 in the DDA mode.

Figure S4. CID mass spectra of products **8** and **9** resulting from Tyr³⁰⁰ side chain fragmentation under photoirradiation. Product information is listed in Table 1.

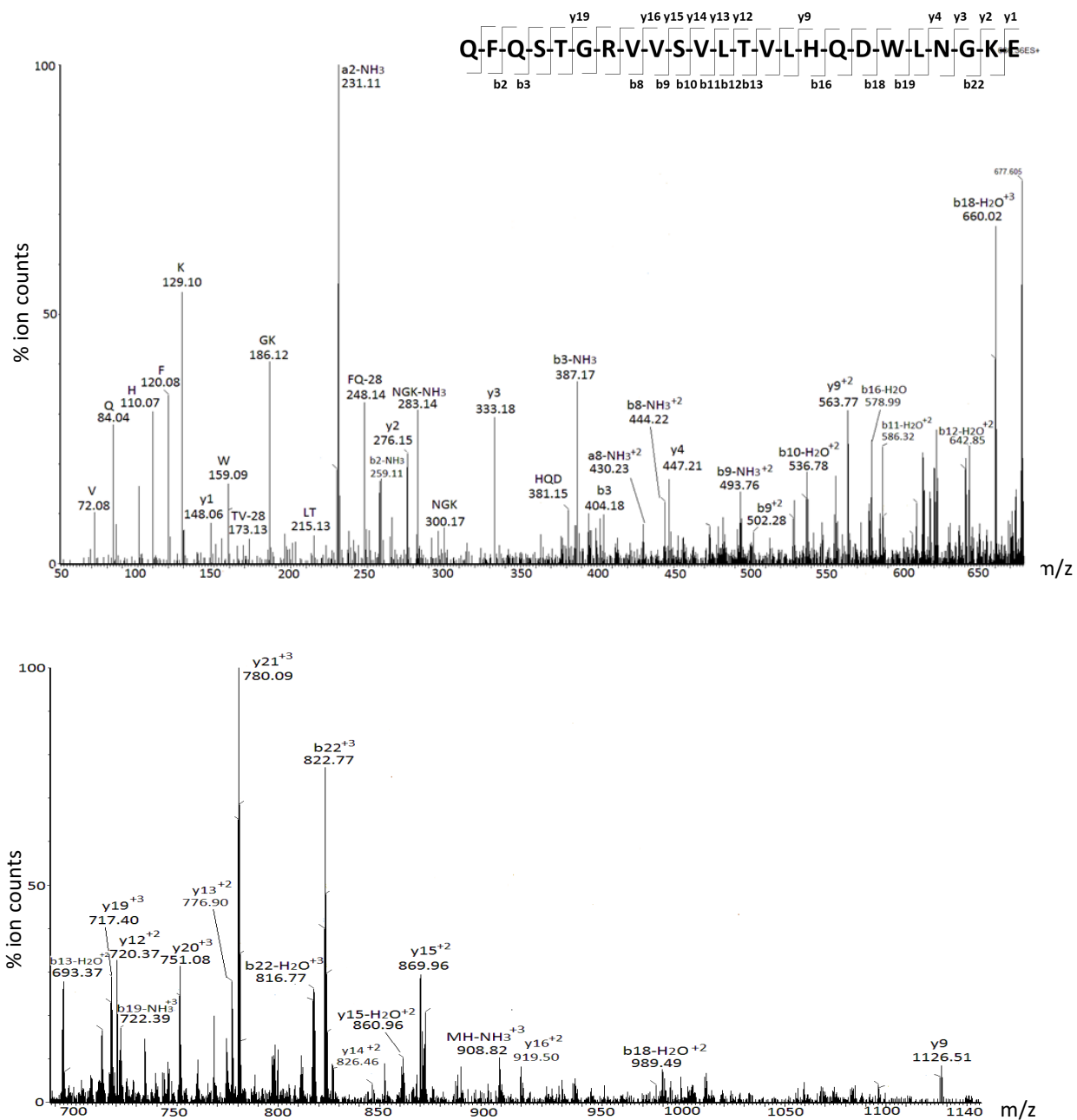


Fig. S4A. MS/MS spectrum of product **8** derived from Tyr³⁰⁰ conversion into Gly³⁰⁰, analyzed with Synapt-G2 in the DDA mode.

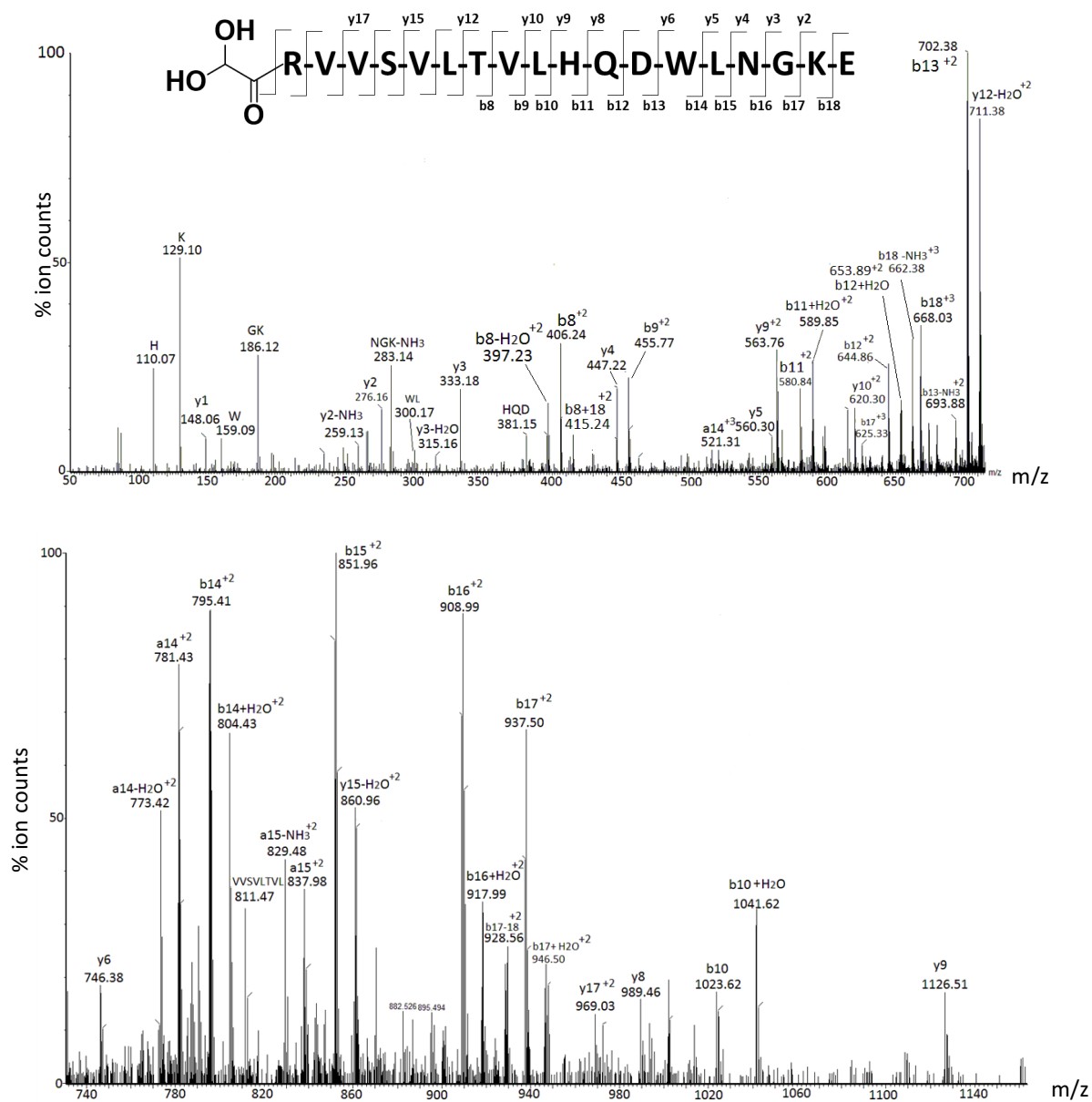


Fig. S4B. MS/MS spectrum of product 9 resulting from peptide backbone cleavage forming a glyoxal derivative, induced by Tyr³⁰⁰ side chain fragmentation, analyzed with Synapt-G2 in the DDA mode.

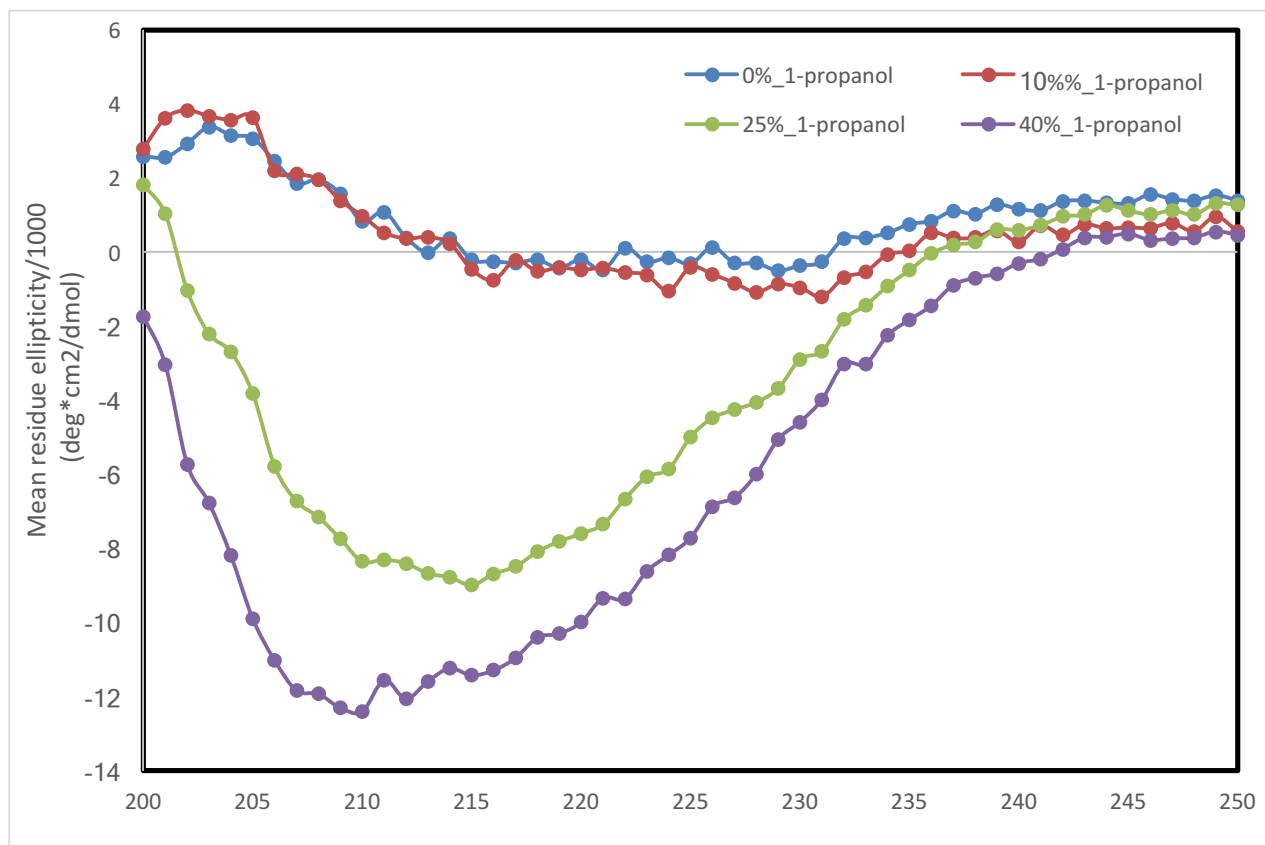


Figure S5. CD analysis of WT HM IgG4-Fc secondary structure in the presence of 1-propanol.

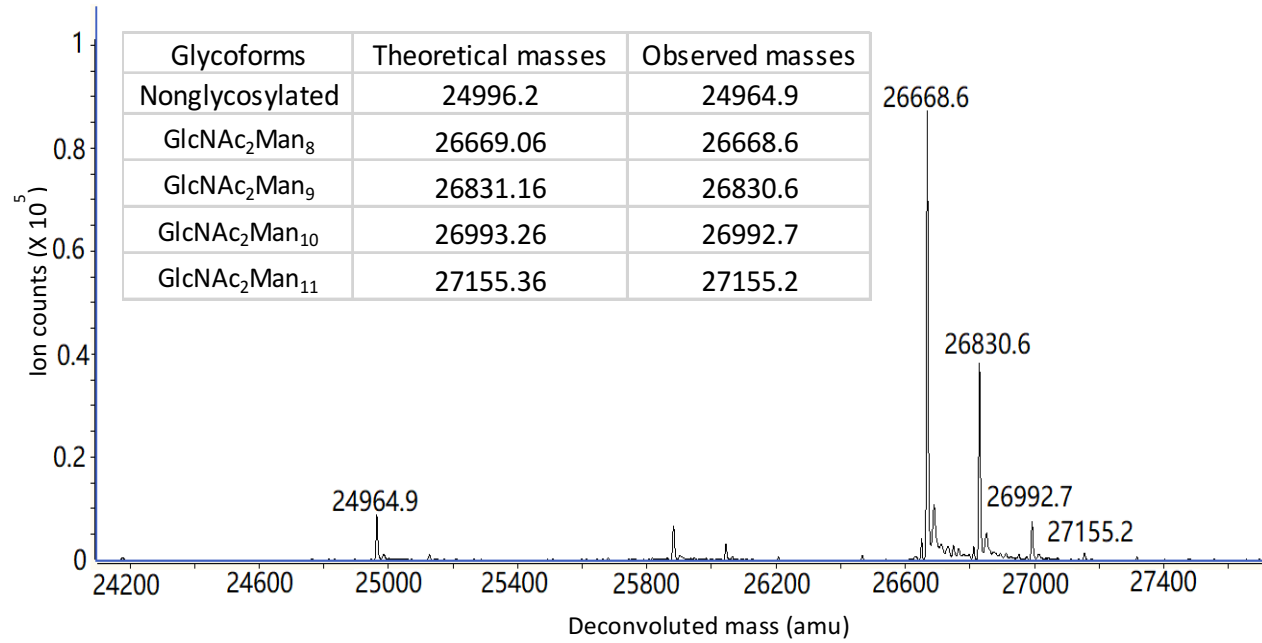


Figure S6. Intact protein MS characterization of the W381F HM IgG4-Fc mutant. The protein was reduced with dithiothreitol (DTT).

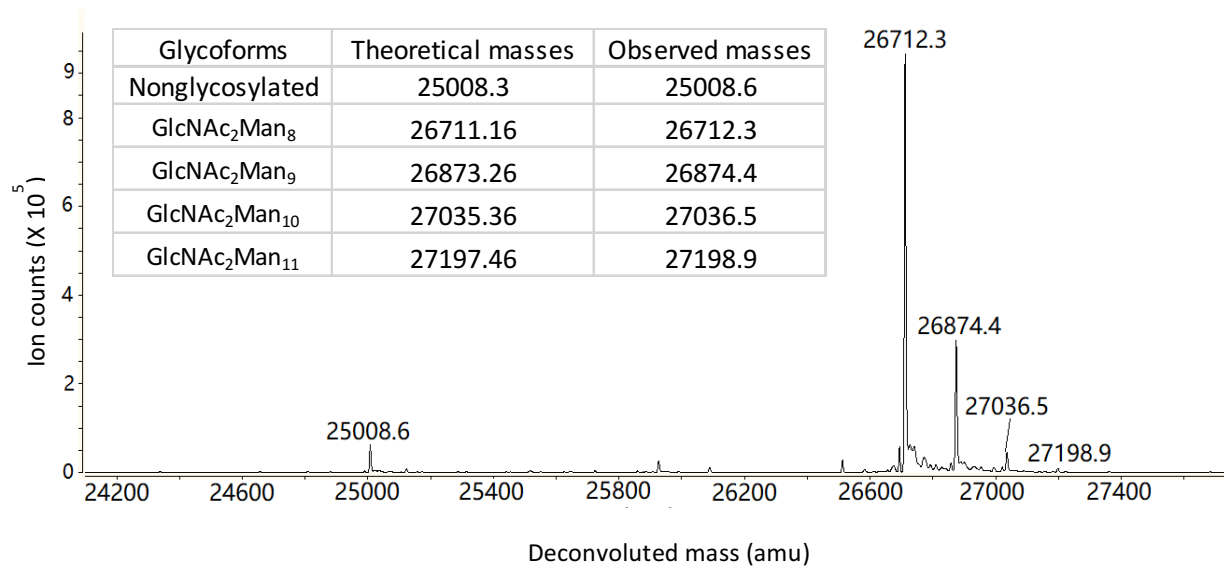


Figure S7. Intact protein MS characterization of the H435R/Y436F HM IgG4-Fc mutant. The protein was reduced with DTT.

Table S1. IgG4-Fc full amino acid sequence from Cys²²⁶ to Lys⁴⁴⁷ with Eu numbering.

<u>Eu numbering</u>	<u>IgG4 Fc</u>
225	-
226	C
227	P
228	S
229	C
230	P
231	A
232	P
233	E
234	F
235	L
236	G
237	G
238	P
239	S
240	V
241	F
242	L
243	F
244	P
245	P
246	K
247	P
248	K
249	D
250	T
251	L
252	M
253	I
254	S
255	R
256	T
257	P
258	E
259	V
260	T
261	C
262	V

263	V
264	V
265	D
266	V
267	S
268	Q
269	E
270	D
271	P
272	E
273	V
274	Q
275	F
276	N
277	W
278	Y
279	V
280	D
281	G
282	V
283	E
284	V
285	H
286	N
287	A
288	K
289	T
290	K
291	P
292	R
293	E
294	E
295	Q
296	F
297	N
298	S
299	T
300	Y
301	R
302	V
303	V

304	S
305	V
306	L
307	T
308	V
309	L
310	H
311	Q
312	D
313	W
314	L
315	N
316	G
317	K
318	E
319	Y
320	K
321	C
322	K
323	V
324	S
325	N
326	K
327	G
328	L
329	P
330	S
331	S
332	I
333	E
334	K
335	T
336	I
337	S
338	K
339	A
340	K
341	G
342	Q
343	P
344	R

345	E
346	P
347	Q
348	V
349	Y
350	T
351	L
352	P
353	P
354	S
355	Q
356	E
357	E
358	M
359	T
360	K
361	N
362	Q
363	V
364	S
365	L
366	T
367	C
368	L
369	V
370	K
371	G
372	F
373	Y
374	P
375	S
376	D
377	I
378	A
379	V
380	E
381	W
382	E
383	S
384	N
385	G

386	Q
387	P
388	E
389	N
390	N
391	Y
392	K
393	T
394	T
395	P
396	P
397	V
398	L
399	D
400	S
401	D
402	G
403	S
404	F
405	F
406	L
407	Y
408	S
409	R
410	L
411	T
412	V
413	D
414	K
415	S
416	R
417	W
418	Q
419	E
420	G
421	N
422	V
423	F
424	S
425	C
426	S

427	V
428	M
429	H
430	E
431	A
432	L
433	H
434	N
435	H
436	Y
437	T
438	Q
439	K
440	S
441	L
442	S
443	L
444	S
445	L
446	G
447	K
448	*

Table S2. A summary of chemical modifications of the amino acid of WT IgG4-Fc during photoirradiation.

	Photo-induced modifications	
Amino acid	254 nm (air or argon)	$\lambda_{\text{max}} = 305 \text{ nm}$ (air or argon)
Cys²⁶¹	Vinyl thiol	Vinyl thiol
Met²⁵²	Methionine sulfoxide	Methionine sulfoxide
Asn³¹⁵	Asn deamidation	Asn deamidation
Cys³²¹	Vinyl thiol	Vinyl thiol
Met⁴²⁸	Methionine sulfoxide	Methionine sulfoxide
Trp³¹³	N-formylkynurenine	N-formylkynurenine
Cys³⁶⁷	Vinyl thiol	Vinyl thiol
Cys⁴²⁵	Vinyl thiol	Vinyl thiol

Chapter 3. Photo-induced Trp and Tyr side chain cleavage in IgG4-Fc: impact on physicochemical stability and receptor binding, and effect of N- and O-glycosylation on product formation

3.1. Introduction.

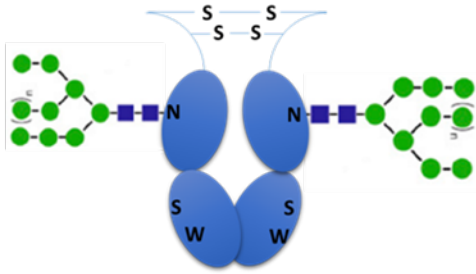
The exposure of proteins to UV and visible light¹⁻² leads to chemical modifications, which may impact function, and/or cause aggregation and potentially immunogenicity³⁻⁵. An important study by Boll et al.⁵ suggests that chemical modifications of proteins contribute to the immunogenicity of protein aggregates. However, this study also concludes that it is not routinely observed chemical modifications, such as Met sulfoxide or common Trp oxidation products, which are responsible for this contribution to immunogenicity⁵. Therefore, there is a need to identify other, potentially new, chemical modifications, which may predispose proteins to aggregation and/or immunogenicity.

In prior work we reported that protein Trp residues are prone to side chain fragmentation induced by UV light⁶⁻⁹, including the exposure to ICH light stress in an Atlas SUNTEST CPS+ system operated in the ID65 configuration¹⁰. This reaction converts Trp into a series of products including Gly. In a monoclonal antibody (mAb) of the IgG1 subclass this side chain fragmentation targets specific Trp residues such as Trp¹⁹¹ in the light chain (LC) and Trp³⁰⁹ and Trp³⁷³ in the heavy chain (HC)^{6, 10}. Trp residues are frequently part of residue clusters important for protein folding and stability¹¹⁻¹⁴. Hence, the conversion of Trp to Gly can induce a cavity in the three-dimensional structure of a protein, which may result in (local) unfolding and destabilization¹⁵. The extent of such destabilization will depend on the exact location of the targeted Trp residue and its chemical environment¹⁵. More recently, we reported for IgG4-Fc that also protein Tyr residues undergo side

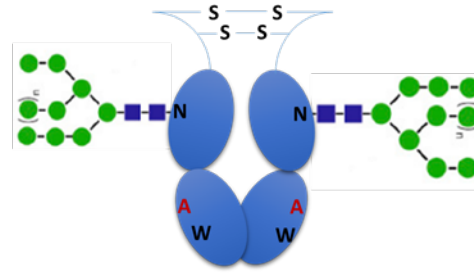
chain fragmentation during UV light exposure, likely induced by electron transfer to a photochemically generated Trp radical cation¹⁶. This reaction converts Tyr into a number of products, including Gly, suggesting that also such reaction may lead to the unfolding of protein domains containing these Tyr residues.

The purpose of the present work was to examine the consequences of photo-induced conversion of Trp and Tyr to Gly on the physicochemical properties and receptor binding of the constant region of an antibody, IgG4-Fc. For these experiments we generated Tyr-to-Gly mutants for all three Tyr residues on IgG4-Fc, which are target for photochemical conversion to Gly, and the Trp-to-Gly mutant at position Trp³⁸¹. Unfortunately, the expression yields of the Trp³⁸¹Gly mutant were low, so that we also prepared the Trp³⁸¹Ala mutant as a surrogate for the Trp³⁸¹Gly mutant, which provided larger yields of protein required for some of our biophysical studies. To our surprise, we noted that both Trp³⁸¹Gly and Trp³⁸¹Ala mutations introduced an atypical glycosylation, where > 60% of the glycoprotein was O-glycosylated at Ser³⁷⁵, confirmed by MS analysis under reducing conditions. This necessitated the characterization of any differences induced by O-glycosylation, and provided an opportunity for addressing the effects of N- vs. O-glycosylation on the physicochemical properties of IgG4-Fc and on its photo-induced degradation. For these studies additional mutants, IgG4-Fc S375A and W381A/S375A (Chart 1 and 2) were generated.

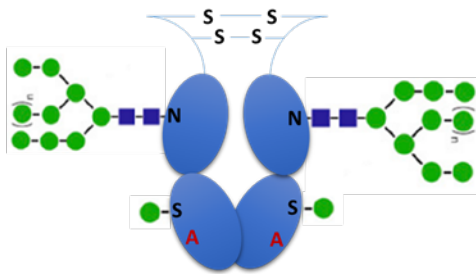
A. Wild-Type



B. S375A



C. W381A



D. S375A/W381A

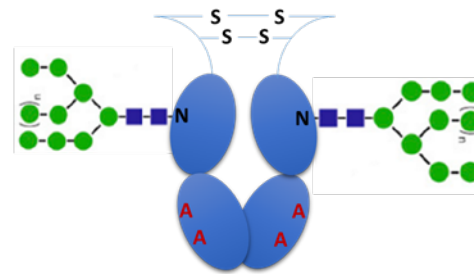
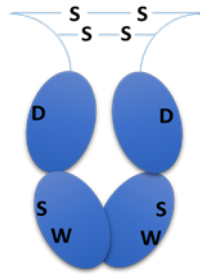
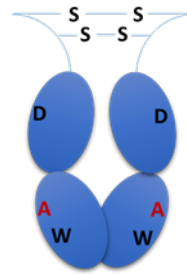


Chart 1: Wild-type (A), S375A (B), W381A (C), and S375A/W381A (D) IgG4-Fc structures with inter-hinge disulfide bonds (intra-hinge disulfide not shown), where Asn²⁹⁷ is glycosylated with high mannose (GlcNAc₂Man_(8+n) (n=0-4)) in all four IgG4-Fc, while Ser³⁷⁵ in W381A is O-glycosylated with mannose to an extent of ca. 61%.

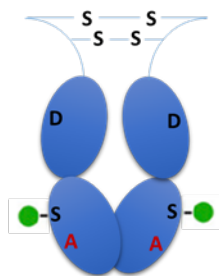
A. WT_degly



B. S375A_degly



C. W381A_degly



D. S375A/W381A_degly

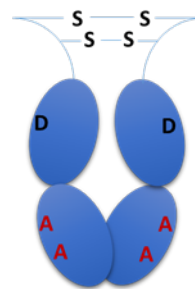


Chart 2: N-de-glycosylated structures WT_degly (A), S375A_degly (B), W381A_degly (C), and S375A/W381A_degly (D) IgG4-Fc shown with inter-hinge disulfide bonds (intra-hinge disulfide bonds not shown), where Ser³⁷⁵ in W381A is glycosylated with mannose with ~61% occupancy to an extent of ca. 61%.

Glycosylation represents a heterogeneous post-translational protein modification (PTM), which is a critical determinant of intrinsic protein properties.^{8, 17-18} In antibodies, glycosylation affects the physicochemical stability and therapeutic efficacy¹⁹⁻²⁰. Of the approximately 400 FDA- approved therapeutic proteins²¹, the majority are glycoproteins, where monoclonal antibodies (mAbs) represent a dominant fraction²². The glycans of glycoproteins are complex and (bio)synthetically difficult to control. They can vary for different expression systems, processing conditions (e.g., temperature, pH), and the native properties of proteins²³. Studies on the effect of glycosylation on the stability and function of protein pharmaceuticals are important for glycoengineering and development of therapeutic proteins^{18, 24}.

The two main types of glycosylation are N- and O-linked glycosylation²⁵. N-glycosylation involves the attachment of a carbohydrate group to the side chain N atom of Asn within a consensus sequence Asn-X-Thr/Ser, where X can be any amino acid except Pro²⁶. N-glycosylation has been extensively studied, especially in mAbs²⁷. Specifically immunoglobulin G (IgG), has become an important therapeutic for the treatment of cancer, immune, and infectious diseases due to its specificity, efficacy, long serum half-life and largely reduced side effects. IgGs consist of two heavy chains, including variable (V_H) and constant heavy chain domains (C_{H1} , C_{H2} , and C_{H3}), and two light chains containing the V_L and C_L domains. The heavy and light chains, are connected by inter-chain disulfide bonds, where the V_H , V_L , C_{H1} , and C_L domains compose the antigen-binding region (Fab), while C_{H2} and C_{H3} are parts of the constant region (which is part of the crystallizable fragment, Fc). All IgG subclasses are glycosylated at Asn²⁹⁷ in the C_{H2} domain. Crystal structures

of the IgG-Fc domain have shown that the attached N-glycans at Asn²⁹⁷ can influence the conformation of the C_H2 domain²⁸⁻²⁹, and therefore affect the interactions between Fc domain and Fc receptors. N-linked glycosylation contains a uniform core structure, GlcNAc₂Man₃, which can be further modulated by Golgi enzymes³⁰. This modulation of the glycan core structure affects the biological activity³¹⁻³³ and physico-chemical properties^{8, 29, 34-35} of IgG1. In contrast to IgG1, the effect of glycan modulation on the physico-chemical properties of IgG4 has not been extensively studied, even though also this subtype has been developed into biotherapeutics.³⁶⁻³⁷

O-glycosylation involves the covalent attachment of a carbohydrate to the hydroxyl group of Ser, Thr, or Tyr³⁸. Mammalian O-glycosylation can involve Fuc, GalNAc, GlcNAc, Man, and Glc³⁸. The lack of a consensus sequence for O-glycosylation³⁹⁻⁴⁰ leads to difficulties in the prediction and characterization of O-glycosylation. IgGs have been reported to be O-glycosylated both *in vivo* and *in vitro*⁴¹. For example, ca. 8% of IgG3, extracted from human serum revealed O-glycosylation in the hinge region⁴². Recombinant human mAb therapeutics expressed in Chinese hamster ovary (CHO) can be O-glycosylated, e.g., via O-fucosylation^{41, 43} and O-glucosylation (~10%)²⁹ in IgG1, as well as O-mannosylation at Ser in the variable regions of IgG2⁴⁴. These unexpected observations suggest that the introduction of structural heterogeneity by enzymatic O-glycosylation during the process of antibody engineering and manufacturing may be inevitable. Therefore, molecular features which predispose mAbs to O-glycosylation, and its potential consequences, need to be addressed and thoroughly characterized.

In the present work, we examined the impact of N- and O-linked glycans on the physico-chemical properties of IgG4-Fc variants. The IgG4-Fc variants containing Asn²⁹⁷ N-glycans, are referred to as WT, S375A, W381A, and S375A/W381A IgG4-Fc (Chart 1) (For WT, S375A, and S375A/W381A, the attached N-glycans are N-GlcNAc₂Man_(8+n), n= 0-4; for W381A, the attached glycans are a mixture of N- and O-glycans, predominantly N-GlcNAc₂Man_(8+n) or N-GlcNAc₂Man_(8+n)/O-Man₁, n = 0-4). These glycoforms are named as high mannose (HM). The PNGase F-treated IgG4-Fc variants are referred to as WT_degly, S375A_degly, W381A_degly, and S375A/W381A_degly (Chart 2).

3.2. Materials.

Yeast extract and peptone were purchased from Becton Dickinson and Company (Franklin Lakes, NJ). Dextrose, sodium phosphate, sodium chloride, methanol, and glycerol were purchased from Fisher (Fair Lawn, NJ). Zeocin was obtained from Invitrogen (Carlsbad, CA). Yeast nitrogen base (YNB) was obtained from Sunrise Biosciences (San Diego, CA). Rmp protein A sepharoseTM fast flow was purchased from GE Healthcare Bio-Sciences (Uppsala, Sweden). Potassium phosphate, biotin, citric acid, dithiothreitol (DTT), iodoacetamide (IAA), iodoacetic acid (IAC), ammonium bicarbonate, and guanidine hydrochloride were purchased from Sigma-Aldrich (Saint Louis, MO). The SacI-HF was bought from New England BioLabs (Ipswich, MA). GluC and Trypsin/LysC were purchased from Promega Corporation (Madison, WI). Tris (2-carboxyethyl) phosphine (TCEP) was obtained from Thermo Fisher Scientific (Waltham, MA). D₂O, D 99.9%, was

purchased from Cambridge Isotope Laboratories (Tewksbury, MA).

3.2.1. Cloning of WT, W381A, S375A, S375A/W381A, Y300G, Y373G, Y436G, and W381G.

A forward primer, 5'-CGACATCGCCGTGGAGGCTGAGAGCAATGGGCAGC-3', and a reverse primer, 5'-GCTGCCCATGCTCTCAGCCTCCACGGCGATGTCG-3', were designed for W381A. WT IgG4-Fc cDNA cloned in a pPICZ α A vector (Invitrogen, Carlsbad, CA) was used as W381A parent plasmid. A forward primer, 5'-AAGGCTTCTACCCCGCCGACATCGC CGTGG-3', and a reverse primer, 5'-CCACGGCGATGTCGGCGGGGTAGAAG CCTT-3', were designed for S375A and S375A/W381A. A forward primer, 5'-GCAGTTCAACAGCAGC GGCCGTGTGGTCAGCCTC-3', and a reverse primer, 5'-GACGCTGACCACACGGCCCGT GCTGTTGAACTGC-3', were designed for Y300G. A forward primer, 5'-CTGGTCAAAGGC TTCGGCCCCAGCGACATCGC-3', and a reverse primer, 5'-GCGATGTCGCTGGGGCCGA AGCCTTTGACCAG-3' were designed for Y373G. A forward primer, 5'- GGCTCTGCACAACCACGGCACACAGAAGAGCCTC-3', and a reverse primer, 5'- GAGGCTCTTCTGTGTGCCGTGGTTGTGCAGAGCC-3' were designed for Y436G. A forward primer, 5'-GACATCGCCGTGGAGGGTGAGAGCAATGGGCAG-3', and a reverse primer, 5'- CTGCCCATGCTCTCACCTCCACGGCGATGTC-3' were designed for W381G. WT cDNA-containing plasmid was used for S375A, Y300G, Y373G, and Y436G, W381A, and W381G cDNA-containing plasmid was used as W381A/S375A parent plasmid. The primers were bought from Eurofins Genomics (Louisville, KY). The mutagenesis was achieved with a QuikChange Lightning Site-Directed Mutagenesis Kit (Agilent Technologies, Inc., Santa Clara, CA).

Mutated cDNA-plasmids were transferred to XL10-Gold ultracomplement cells, provided by Agilent Technologies, by means of heat shock. The cells were grown in low salt lysogeny broth (LB) medium (1% tryptone, 0.5% NaCl, and 0.5% yeast extract) at 37°C for 1hr, and then plated onto a 25 µg/mL zeocin-containing LB for colony selection. The plate was incubated at 37°C overnight, and colonies grown with zeocin resistance were selected. The plasmids of selected colonies were inoculated in 6 mL of zeocin-containing LB medium (25 µg/mL), amplified by shaking at 250 rpm at 37°C overnight, purified with a miniprep Kit (QIAGEN, Valencia, CA), and sequenced by the University of California Berkeley DNA Sequence Facility (Berkeley, CA). Those cDNA-plasmids showing 100% sequence accuracy were linearized with SacI-HF, and electroporation transferred to a pno11/och1 KO and STT3D added *Pichia pastoris* yeast strain³³. Those yeast colonies grown with zeocin resistance (100 µg/mL) were selected for IgG4-Fc production.

3.2.2. Expression of IgG4-Fc. For IgG-Fc expression we followed a procedure which was described previously³³. Briefly, a starting medium of 2.5 mL YPD containing 1% yeast extract (w/v), 2% peptone (w/v), 2% dextrose (w/v), and 2.5 mg zeocin was inoculated with the selected yeast colonies and shaken in an incubator (New Brunswick Innova 4200 Incubator-Shaker, Edison, NJ, USA) at 250 rpm at 26°C. After 72 hr, the 2.5 mL yeast cells were transferred to 50 mL YPD medium placed in a 250 mL Erlenmeyer flask, and the yeast culture was grown under shaking at 26°C. After 72 hr, the 50 mL yeast cells were transferred to a 1 L spinner flask containing buffered glycerol-complex media, referred to as BMGY⁴⁵ (1% yeast extract, 2% peptone, 2% glycerol,

0.34% of yeast nitrogen base and 1% ammonium sulfate, 4×10^{-5} % biotin, and 100 mM potassium phosphate, pH 6.0), followed by addition of two drops of sterilized antifoam. The 1L yeast cell culture was grown at room temperature (RT) for 72 hr on a stir plate under a constant flow of air, which was filtered by a 0.2 μm Millipore Express® PES membrane. The protein production was induced by addition of a final content of 1% methanol (v:v) to the 1 L spinner flask every 24 hr for 3 times. After 72 hr of induction, the yeast cells were harvested, and IgG4-Fc was purified.

3.2.3. Purification of IgG4-Fc using affinity chromatography. The yeast cells were transferred to centrifuge bottles and centrifuged in an Avanti™ J-25I centrifuge (Beckman Coulter, Palo Alto, CA) with a JLA-10500 rotor (Beckman Coulter, Palo Alto, CA) at 6,693 g for 20 min at 4°C. After the centrifugation, the supernatant was collected and filtered by six layers of 90 mm Whatman filter pads. IgG4-Fc was purified from the supernatant with a pre-packed column containing rmp Protein A Sepharose™ Fast Flow resin. The mobile phase was controlled by a Masterflex L/S economy pump system (Cole Parmer Instrument, Chicago, IL), and the eluting fractions were monitored by an ISCO model UA-5 absorbance detector at 214 nm. The column (10 mL) was initially equilibrated with 10 column volumes (CV) of 20 mM sodium phosphate (pH 7.0). Afterwards, the filtered supernatant was applied to the column at a flow rate of 1.5 mL/min, followed by wash with high salt concentration (500 mM NaCl in 20 mM sodium phosphate, pH 7.0) until the intensity of the UV absorption at 214 nm dropped to baseline level. Then equilibration buffer (10 CV) was applied to wash off residual salt. Bound IgG4-Fc was eluted with 50 mM citric acid (pH 3.0) and immediately dialyzed in 2 L of 20 mM sodium phosphate (pH 7.0). The dialysis

buffer was exchanged twice. IgG4-Fc of good quality (evaluated by HPLC-MS and SDS-PAGE gel analysis) was aliquoted and stored at -80°C for further analysis.

3.2.4. PNGase F digestion of WT, S375A, W381A, S375A/W381A IgG4-Fc. The N-linked glycans of 500 µL aliquots of proteins (0.2 mg/mL, pH 7.0) were deglycosylated by mixing with 0.5 µL N-glycosidase F (PNGase F) in a protein to enzyme ratio of 500:1 (w/w) and incubating at RT for 24 hrs. The extent of the enzymatic reaction was monitored by mass spectrometry, as described in section 2.5. PNGase F was expressed in *E.coli*, purified with a Nickel column⁴⁶, and stored in 50% glycerol at -20°C for further use. Deglycosylated proteins are from here on indicated by the label “-degly”.

3.2.5. Characterization of WT, S375A, W381A, S375A/W381A, Y300G, Y373G, and Y436G IgG4-Fc by LC-MS analysis of intact proteins. The masses of intact WT and the six IgG4-Fc mutants were initially analyzed by LC-MS. Briefly, 20 µg of each protein was dissolved at 0.2 mg/mL in 20 mM sodium phosphate, pH 7.0, and reduced with 10 mM DTT for 10 min at RT. The reduced proteins were injected onto a C4 column (50 mm, 4.6 mm i.d.; 300-Å pore size, 5 µm particle size, Vydac 214 MS, Grace, Deerfield, IL), operated by an Agilent 1200 series LC system (Agilent Technologies, Santa Clara, CA). A linear gradient was operated at a flow rate of 0.5 mL/min, changing mobile phase B (99.9% acetonitrile, 0.08% formic acid, and 0.02% trifluoroacetic acid) from 5 to 90% within 7 min. Mobile phase A contained 99.9% H₂O, 0.08 % formic acid, and 0.02 % trifluoroacetic acid. The reduced protein eluted at approximately 5.5 min

and was analyzed with an online-coupled Agilent 6530 Quadrupole Time-of-Flight mass spectrometer (Agilent Technologies, Santa Clara, CA). The mass spectrometer was operated with an electrospray ionization source (ESI) in the positive mode, scanning from mass/charge (m/z) values of m/z 300 to m/z 3000 at a scan rate of 1 scan/second. The collected chromatographic data were extracted and de-convoluted with the Agilent MassHunter Qualitative Analysis software.

3.2.6. Characterization of IgG4-Fc with sodium dodecyl sulfate-polyacrylamide gel electrophoresis (SDS-PAGE). The characterization of IgG4-Fc with SDS-PAGE (Mini-PROTEAN TGX™ Gels, 4-20%, BIO-RAD, Richmond, CA) was performed under non-reducing and reducing conditions. Initially, about 3.3 μg of each protein (0.2 mg/mL) in 15 μL of 20 mM sodium phosphate was mixed with 15 μL of 2x concentration of Laemmli sample buffer, containing 20-35% of glycerol and 1-2.5% of SDS (BIO-RAD, Richmond, CA). For non-reducing conditions, the mixtures were immediately loaded onto the SDS-PAGE. For reducing conditions, 1.5 μL of 2-mercaptoethanol (14.3 M) were added, followed by boiling in a water bath for 2 min, and subsequently loaded onto the SDS-PAGE. 3 μL of a Precision Plus Dual Color standard marker (BIO-RAD, Richmond, CA) were loaded in the first lane. The gel was run at 200 volts for about 40 min until the front dye ran to the bottom of the gel. The gel was stained with 0.25% Coomassie Brilliant blue (50% methanol, 0.25% Coomassie blue, 10% acetic acid and 40% water) for 10 min, followed by staining with 0.05% Coomassie blue for 10 min, and de-staining with 30% methanol, 10% acetic acid and 60% water until the bands were clear.

3.2.7. Peptide mapping with GluC and Trypsin/LysC. Control and light-exposed protein samples were subjected to peptide mapping side by side. Aliquots of 500 μL reaction mixtures containing 0.2 mg/mL protein (in 20 mM sodium phosphate) were denatured by the addition of 500 μL of 6 M GdnHCl (in 50 mM NH_4HCO_3 , pH 8.0) and reduced with 10 μL of 500 mM DTT (in 50 mM NH_4HCO_3) for 1 hr in a water bath maintained at 37°C. Free thiols resulting from the reduction step were alkylated by reaction with 40 μL of 500 mM IAA (in 50 mM NH_4HCO_3 for GluC digestion) or IAC (in 50 mM NH_4HCO_3 for Trypsin/LysC digestion) for 1 hr in a water bath maintained at 37 °C. After 1 hr, the denaturing, reducing, and alkylating agents were removed by exchange with 5 mM NH_4HCO_3 , pH 8.0, using a 3kDa filter unit (Amicon Ultra Centrifugal Filter, County Cork, Ireland), and the protein solution was concentrated to about 200 μL through centrifugation at 16,900 g for 10 min. The concentrated protein solution was finally collected by reverse-flip of the filter, and centrifuged at 300 g for 4 min. For GluC treatment, aliquots of 40 μL (~20 μg protein) were digested. GluC solutions were prepared by dissolving 10 μg GluC in 50 μL of 5 mM NH_4HCO_3 . Two aliquots of GluC (5 μL each) with 2 μg in total were added. The first aliquot was added, and incubated at 37 °C for 3 hrs, followed by the second aliquot and incubation at 37 °C for another 3 hr. The protein to GluC ratio was about 10:1 (w:w). For Trypsin/LysC digestion, aliquots of 100 μL (~62.5 μg protein) were used. Trypsin/LysC solutions were prepared by dissolving 20 μg Trypsin/LysC in 220 μL of 5 mM NH_4HCO_3 . Two aliquots of Trypsin/LysC (10 μL each) with 1.8 μg in total were added. The protein to Trypsin/LysC ratio was about 35:1 (w:w).

3.2.8. HPLC-MS/MS. Proteolytic IgG4-Fc peptides were analyzed with a nanoAcquity ultra performance liquid chromatography system (Waters Corporation, Milford, MA), coupled to a Xevo-G2 mass spectrometer (Waters Corporation, Milford, MA). A volume of 2 μ L was injected onto a C18 guard column (nanoACQUITY UPLC 2G-V/M Trap 5 μ m Symmetry C18 180 μ m x 20mm, Waters, Milford, MA), and washed with 97% mobile phase A (0.1% formic acid in H₂O, Optima, Fisher Chemical, Fair Lawn, NJ) and 3% mobile phase B (0.1% formic acid in CH₃CN, Optima, Fisher Chemical, Fair Lawn, NJ) for 3 min at a flow rate of 4 μ L/min. After the washing step, the following gradient program was applied to move and separate the peptides onto an analytical column (ACQUITY UPLC Peptide CSH C18 NANOACQUITY column 10K psi, 1.7 μ m, 75 μ m x 250 mm, Waters, Milford, MA) at a flow rate of 300 nL/min: between 0 to 50 min, mobile phase B was linearly increased from 3% to 35%; after 50 min, mobile phase B was linearly increased from 35% to 95% within 20 min; after 70 min, the column was washed with 95% mobile phase B for 10 min prior to equilibration with 97% of mobile phase A. The peptides were ionized in an electrospray ionization (ESI) source, and analyzed in the positive mode within a m/z range of 200-2000 at a scan rate of 1 scan/second. The peptide fragment ions were analyzed in the MS^E mode, with the collision energy ramping from 18 V to 45 V, or in the data-dependent acquisition (DDA) mode with the collision energy ramping from 15 V to 40 V for low masses and ramping from 30 V to 55 V for high masses.

3.2.9. Differential scanning calorimetry (DSC). DSC was performed using a MicroCal VP-capillary calorimeter (Malvern, UK). Protein samples (0.22 mg/mL) were kept in a 96-well plate,

which was sealed using a plastic cover and stored at 5°C during the DSC run. Samples were scanned from 10 to 90°C at a scan rate of 1°C/min using a filtering period of 16 sec. Raw DSC thermograms were processed using the Origin software (Origin Lab, Northampton, MA). Buffer subtraction, baseline correction, and concentration normalization were first performed. The processed thermograms were then fit to a non-two-state equilibrium model to derive T_m values for WT, S375A, WT_degly, S375A_degly, Y300G, Y373G, and Y436G IgG4-Fc.

3.2.10. Intrinsic fluorescence. The intrinsic fluorescence spectra of the protein variants were collected using a fluorescence plate reader (Fluorescence Innovations, Inc., Minneapolis, MN), as previously described⁴⁷. This instrument is equipped with a dye laser (280-300 nm), a temperature-controlled sample plate, and a charge-coupled device detector. Samples (0.22 mg/mL) were loaded into a 384 well plate, and silicon oil was added to avoid sample evaporation during thermal ramping. The sample plate was centrifuged at 2,000 rpm for 1 min to remove air bubbles. Proteins were excited at 295 nm (>95% of the absorbance by Trp) and their emission spectra were collected from 300 to 400 nm. The temperature was ramped from 10 to 90 °C with an increment of 2.5 °C per step and an equilibration time of 2 min. The moments of spectra at each temperature were calculated employing the ThermoSpec software (Fluorescence Innovations, Inc., Minneapolis, MN) according to the following equation:

$$\text{Moment} = \frac{\int I(x)x dx}{\int I(x) dx}$$

where x and $I(x)$ are the wavelength and fluorescence intensity, respectively. The moments were then plotted as a function of temperature to generate melting curves. The melting temperature (T_m)

was calculated using a first derivative method using the Origin software (OriginLab Corporation, Northampton, MA).

3.2.11. FTIR analysis. A Tensor-27 FTIR spectrometer (Baker, Billerica, MA) equipped with a Bio-ATR cell was used to acquire the FTIR spectra. The detector was cooled with liquid nitrogen prior to use. The interferometer was continuously purged with N₂ gas to void the cell of CO₂. Samples were equilibrated for ten minutes at 20 °C prior to acquisition. Spectra were recorded from 4000 to 800 cm⁻¹ with a resolution of 4 cm⁻¹. Scans were performed in triplicate; for each replicate a total of 256 scans were averaged. Buffer subtraction, atmospheric compensation and baseline subtraction were executed using the OPUS V6.5 software (Baker, Billerica, MA). Spectra were fit as the sum of pseudo-Voigt bands (linear combinations of Gaussian and Lorentzian). Secondary structures were assigned according to Kong et al⁴⁸. Second derivative spectra were calculated using a 13 point, 2nd order Savitzky-Golay algorithm.

3.2.12. Hydrogen Exchange (HX) -Mass spectrometry analysis of WT and W381A IgG4-Fc.

The procedures used for HX mass spectrometry analysis are described in detail elsewhere⁴⁹. Briefly, HX was achieved with an H/DX PAL robot (LEAP Technologies, Carrboro, NC), and the mass differences were measured through an online Agilent 1260 Infinity LC system (Agilent Technologies, Santa Clara, CA) coupled to a quadrupole-time-of-flight mass spectrometer (Agilent 6530, Santa Clara, CA). Aliquots of 10 μL of 3.7 μM WT and W381A (in 20 mM sodium phosphate, pH 7.1) were deuterium-labeled by injection of 36 μL deuterated labeling buffer (20

mM sodium phosphate in D₂O, pH 7.1) at six time points (20 s, 100 s, 500 s, 2500 s, 12500 s, and 62500 s). Each labeling time point was conducted in triplicates. The HX reaction was conducted at the pre-set time points at room temperature, followed by combination of 43 μ L labeling mixture with 35 μ L of quench buffer, containing 200 mM sodium phosphate, 0.5 M TCEP, pH 2.5, at 1 °C. Subsequently, a volume of 75 μ L was injected and analyzed by HPLC-MS.

An injected sample was desalted on a C8 trap column through a linear gradient ranging from 0% to 50% of mobile phase B (0.1% formic acid in acetonitrile) within 1 min, followed by another 1 min elution with 50% mobile phase B. Subsequently, the mobile phase was re-equilibrated to 100% of mobile phase A (0.1% formic acid in water) within 1 min. The collected mass spectra were deconvoluted and analyzed by a built-in software, BioConfirm B.08 (Agilent 6530, Santa Clara, CA). Specifically the signals for the N-GlcNAc₂Man₉ glycoform of WT and the N-GlcNAc₂Man₉ or N-GlcNAc₂Man₈/O-Man₁ glycoforms of W381A were monitored for HX, due to their high respective intensity and abundance.

3.2.13. Deuteration controls. The maximum deuterium incorporation into both WT and W381A IgG4-Fc was evaluated separately with thoroughly denatured proteins. 10 μ L of 3.7 μ M WT and W381A stock solution, respectively, were denatured with 4 M GdnDCI for 2 hr at room temperature, followed by labeling with deuterated labeling buffer containing 20 mM Na₂HPO₄/NaH₂PO₄, 4 M GdnDCI, 20 mM TCEP, pH 7.1, and incubation for 4 hr at room temperature. Fully deuterated samples were then quenched and analyzed by HPLC-MS as

described below. GdnDCI was prepared in-house by dissolving 1.5 g of GdnHCl in 15 mL of D₂O, followed by lyophilization with a Labconco freezezone 2.5 lyophilizer (Labconco Corporation, Kansas City, MO) until the powder was dried completely. The dissolution and lyophilization steps were repeated three times.

3.2.14. Photoirradiation of glycosylated and deglycosylated WT, S375A, W381A and S375A/W381A IgG4-Fc. Photo-irradiation of the 8 IgG4-Fc proteins (4 glycosylated and 4 deglycosylated variants) was conducted in a UV irradiator (Rayonet®, The Southern New England Ultraviolet Company, Branford, CT) equipped with 4 lamps emitting between 265 nm and 340 nm, with $\lambda_{\text{max}} = 305$ nm. The ferrioxalate actinometer⁵⁰⁻⁵¹ was utilized to quantify the photon flux for four RPR-300A lamps to 1.87E^{-8} Einstein/s. A volume of 500 μL of each protein (0.22 mg/mL, pH 7.0) in 20 mM sodium phosphate was placed in Pyrex tubes, sealed with rubber stoppers, and photo-irradiated for 45 min at RT. Pyrex tubes have a wavelength-cutoff of around 295 nm. These photo-irradiation conditions correspond to light intensities of <25 Whr/m², i.e., less than 12.5% of the minimal intensity (200 Whr/m²) recommended for UV photostability testing by the ICH Q1B guideline⁵². Two independent experiments were performed. Control, non-irradiated samples were wrapped in aluminum foil and placed in the dark at RT.

3.2.15. Binding assays of WT, Y300G, Y373G, Y436G and W381A IgG4-Fc. The affinity of WT, Y300G, Y373G, Y436G and W381A to Fc γ receptor IIIA (Fc γ R IIIA) was evaluated by immobilizing biotinylated Fc γ R IIIA (the Val¹⁵⁸ polymorph; prepared as previously described³³) on

a streptavidin (SA) tip (ForteBio, Menlo Park, CA). The binding assays were described in detail elsewhere³³. Briefly, the SA tips were prepared by hydration in PBS buffer (150 mM NaCl, 50 mM sodium phosphate, pH 7.4) for 10 min, followed by hydration in PBS kinetic buffer (PBS buffer containing 1mg/mL bovine serum albumin (VWR Chemicals, Solon, OH)) for 30 min. The hydrated tip was then assembled to a ForteBio BLItz system (Menlo Park, CA), and the tip was held in a black microcentrifuge tube (Argos Technologies, Vernon Hills, IL) containing 250 μ L PBS kinetic buffer. The BLItz system, protein and buffer solutions were kept in a 25 °C incubator during the binding assays.

For receptor loading, an initial baseline (30 s) was established with PBS kinetic buffer. In the association step (3 min), 0.02 μ M Fc γ R IIIA in PBS kinetic buffer was loaded to a response level of Δ nm ca. 0.4, then the tube was switched to the PBS kinetic buffer. The response level was measured by a wavelength shift of reflected white light, referred to as light interference, recorded as binding responses (Δ nm). Last, the dissociation step (3 min) was performed with PBS kinetic buffer. For baseline collection, the baseline (30s), association (3 min) and dissociation (3 min) steps performed with PBS kinetic buffer. For sample loading, an initial baseline (30 s) was established with PBS kinetic buffer. In the association step (3min), protein solution in PBS kinetic buffer was loaded to the biosensor tip. The dissociation step (3 min) was performed with PBS kinetic buffer. Based on the binding affinity of different proteins, a series of five protein concentrations was used for each variant. For WT, a concentration series of 0.2 μ M, 0.4 μ M, 0.8 μ M, 1.6 μ M, and 3.2 μ M was prepared in PBS kinetic buffer. For Y300G, a concentration series

of 1.8 μM , 3.6 μM , 7.2 μM , 14.4 μM , and 28.8 μM was prepared in PBS kinetic buffer. For Y373G, a concentration series of 0.5 μM , 1.0 μM , 2.0 μM , 4.0 μM , and 8.0 μM was prepared in PBS kinetic buffer. For Y436G, a concentration series of 1.1 μM , 2.2 μM , 4.5 μM , 8.9 μM , and 26.7 μM was prepared in PBS kinetic buffer. For W381A, a concentration series of 0.78 μM , 1.56 μM , 3.125 μM , 6.25 μM , and 12.5 μM was prepared in PBS kinetic buffer. The protein solutions were loaded from low concentration to high concentration. The tip was regenerated with 1 mM NaOH for 30 s, followed by washing with PBS kinetic buffer for 2 min. For each sample, experiments were performed in triplicates. The tip was replaced between each replicate.

For data analysis, each run was exported as a CSV file with binding response (Δnm) and time (s), and baseline subtracted. The sensorgram data were fitted with a two-exponential association model using the program XL fit analysis (IDBS, Boston, MA) in the excel (Microsoft Corporation, Redmond, WA) software. The data were fit to the equation:

$$y = A(1 - \exp(-Bx)) + C(1 - \exp(-Dx))$$

where x corresponds to time, and B and D correspond to k_{obs} of the slow and fast phase, respectively. For the iteration, B and D were constrained to be ≥ 0 .

3.3. Results.

All samples of IgG4-Fc utilized for the experiments were 0.22 mg/mL in 20 mM sodium phosphate (pH 7.0), unless specifically stated otherwise.

3.3.1 Characterization of Y300G, Y373G, and Y436G IgG4-Fc. Y300G, Y373G, and Y436G IgG4-Fc were expressed in the *Pichia pastoris* yeast strain, purified with protein A chromatography, and initially characterized by MS analysis after reduction with DTT. PNGase F-treated Y300G, Y373G and Y436G presented one major peak (Supporting Information, Fig. S1A), suggesting that N-glycosylation at Asn²⁹⁷ represents the major glycosylation site. The MS spectra of glycosylated IgG4-Fc are presented in Fig. S1B, and the corresponding percentages of N-linked glycoforms are summarized in Table S1. Y300G reveals a higher amount of bulky HM glycoforms, e.g., a total of 37.6% comprising GlcNAc₂Man₁₁ to GlcNAc₂Man₁₆ as compared to WT, Y373G, and Y436G (which contain $\leq 21.61\%$ GlcNAc₂Man₁₁ to GlcNAc₂Man₁₆).

The overall conformational stability of WT, Y300G, Y373G, and Y436G was examined by DSC, scanning from 10 to 90°C, and the obtained thermograms were de-convoluted into two T_m values, denoted as T_{m1} and T_{m2} (Fig. 1A, Table 1). The mutation Y373G caused an approximate 10°C decrease in both T_{m1} and T_{m2} values compared to WT. The mutant Y436G presented a similar T_{m1} value, but a decrease of 5.6°C for T_{m2} compared to WT. Instead, the mutant Y300G revealed no significant differences of T_{m1} and T_{m2} compared to WT. In addition, the characterization of tertiary structure was achieved by intrinsic fluorescence spectroscopy increasing the temperature from 10 to 90°C, where the fluorescence moments (defined in Section 2.10) were plotted as a function of temperature (Fig. 1B). The corresponding T_m values are listed in Table 1. Overall, WT and Y300G present a similar T_m , while the Y436G mutant displays a 1°C decrease in T_m ; instead, the mutant Y373G showed an approximate 8°C decrease in T_m compared to WT.

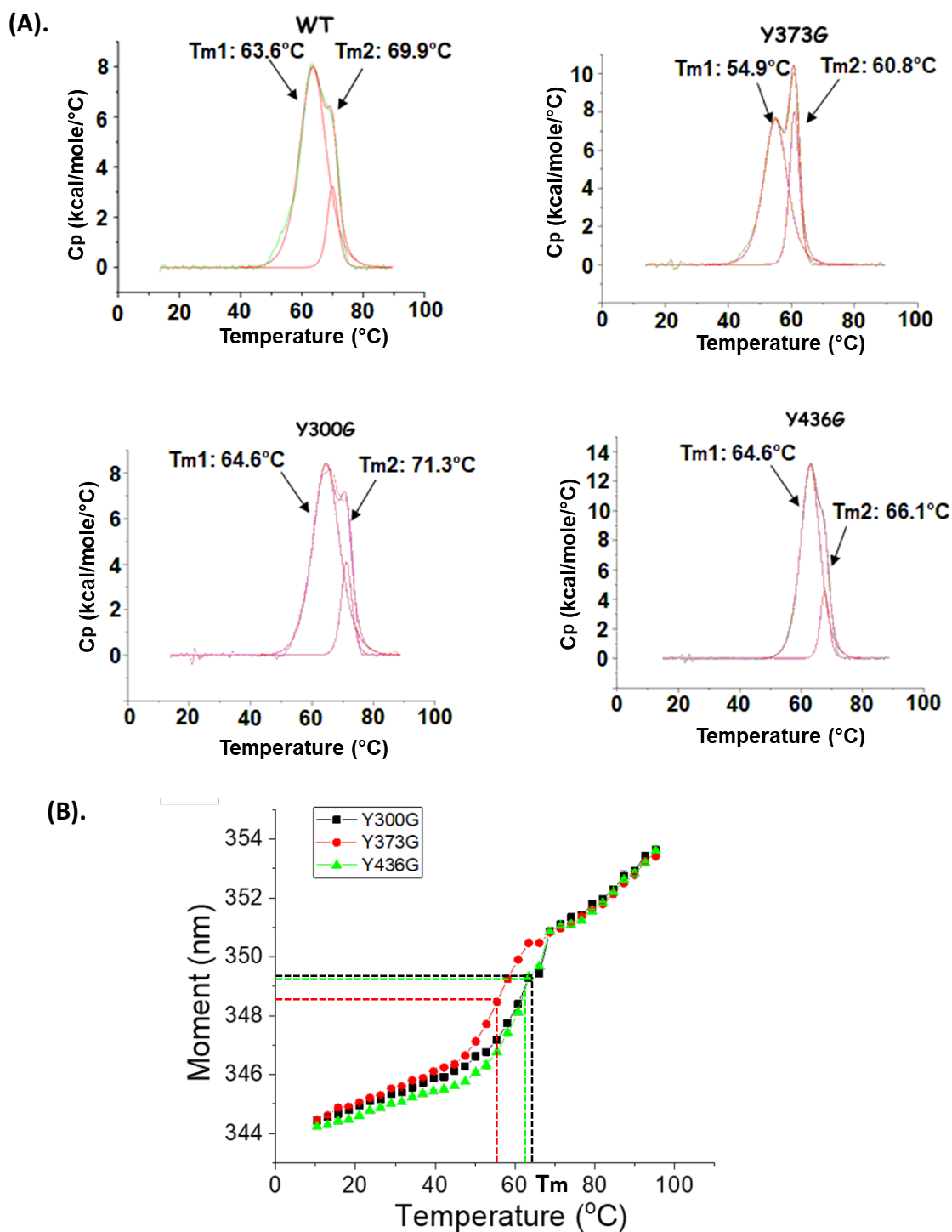


Fig. 1. (A) Representative DSC thermograms and (B) representative intrinsic fluorescence thermograms of Y300G, Y373G and Y436G. The corresponding T_m values are displayed in Table

1.

3.3.2 Initial characterization of WT, S375A, W381A, S375A/W381A, WT_degly, S375A_degly, W381A_degly, and S375A/W381A_degly IgG4-Fc by MS and SDS-PAGE. WT, S375A, W381A, S375A/W381A, WT_degly, S375A_degly, W381A_degly, and S375A/W381A_degly, were initially characterized by MS analysis after chemical reduction with DTT. The respective theoretical and observed masses are summarized in Table S2. The mass differences of 1701- 2512 Da between WT_degly and the series of glycosylated WT forms (Fig. S2 and S3) correspond to the presence of various mannosylated forms of the HM glycoform, $\text{GlcNAc}_2\text{Man}_{(8+n)}$ ($n=0-4$). WT, S375A, W381A and S375A/W381A all yield HM glycoforms (Fig. S2). WT_degly, S375A_degly and S375A/W381A_degly IgG4-Fc present one major peak (Fig. S3), indicating that they were mainly N-glycosylated at Asn^{297} prior to PNGase F treatment. W381A_degly, on the other hand, presents two major peaks, where one of them corresponds to a non-glycosylated form, and the other one corresponds to an O-glycosylated form, indicated by a mass addition of 162 ion (Table S2). The percentages of O-glycosylated WT, S375A, W381A, S375A/W381A proteins were calculated after PNGase F treatment based on the signal intensities for the O-glycosylated forms, divided by the sum of the signal intensities for de-glycosylated and O-glycosylated forms (+162) (Fig. S3). We calculate about 8.1% O-glycosylation in WT, 1.4% O-glycosylation in the S375A mutant, 61.4% O-glycosylation in W381A and 4.9% O-glycosylation in S375A/W381A. The double mutant S375A/W381A displays a significantly reduced intensity of the signal for the O-glycosylated form, suggesting that Ser^{375} is O-glycosylated in W381A. O-linked glycosylation was further confirmed by peptide mapping and HPLC-MS/MS analysis, as described in Section 3.3. On the other hand, the S375A mutant still reveals 1.4% O-glycosylation,

a relatively lower quantity as compared to WT. This indicates the potential presence of other O-glycation sites besides Ser³⁷⁵. We also calculated the relative fraction of non-glycosylated proteins (prior to PNGase F treatment), which were generally <5%, using the de-convoluted MS intensities of non-glycosylated forms, divided by the sum of the intensities of non-glycosylated forms and those of all glycosylated IgG4-Fc forms (GlcNAc₂Man_(8+n) (n=0-4)).

We used SDS-PAGE under reducing and non-reducing conditions to further monitor the purity of the glycoforms (Fig. S4). Lanes 2, 3, 4, and 5 were run under reducing conditions, and displayed single bands, respectively, indicating that proteins were obtained with good purity. Lanes 7, 8, 9 and 10 were run under non-reducing conditions, and showed two major bands, indicating the existence of intra- and inter-disulfide bonds in the hinge regions of the IgG4-Fc glycoforms⁵³. The formation of intra-disulfide bonds of IgG4-Fc subtype is mainly due to the presence of a Ser instead of a Pro residue in the core-hinge region, which leads to increased flexibility⁵⁴. Densitometry analysis with Image J (National Institutes of Health, Washington D.C., USA) quantifies about 63% inter-chain disulfide and 37% intra-chain disulfide in WT, 67% inter-chain and 33% inter-chain disulfide in W381A, 67% inter-chain disulfide and 33% intra-chain disulfide in S375A, and 77% inter-chain disulfide and 24% intra-chain disulfide in S375A/W381A.

3.3.3. HPLC-MS/MS analysis of O-mannosylation at Ser375 in W381A IgG4-Fc. The localization of the additional O-mannosylation site in W381A was determined by peptide mapping. W381A IgG4-Fc was reduced with DTT, alkylated with IAA, and digested with GluC. The GluC

digested peptides were analyzed with HPLC-MS/MS and covered 100% of the W381A IgG4-Fc primary sequence. The O-mannosylated proteolytic peptide MTKNQVSLTC(+57)LVKGFYPS(+162)³⁷⁵DIAVE (m/z 921.47, z=3) and the corresponding non-O-mannosylated peptide MTKNQVSLTC(+57)LVKGFYPS³⁷⁵DIAVE (m/z 867.45, z=3) are referred to as peak 1 and peak 2, respectively, in Fig. S5, where +57 represents a Cys residue alkylated with IAA. Peak 1 elutes about 0.5 min before peak 2, indicating the increased hydrophilicity of peak 1 due to the additional O-mannosylation. The collision-induced dissociation (CID) MS/MS spectrum of MTKNQVSLTC(+57)LVKGFYPS (+162)³⁷⁵DIAVE, collected in the data-dependent acquisition (DDA) mode, is presented in Fig. 2. The m/z values of the b15 and b16 ions indicate that the carbohydrate is not located on the subsequence MTKNQVSLTC(+57)LVKGFY. Additionally, the y3, b19, b19-162, b20, b20-162, b21, b21-162, b22 and b22-162 fragment ions indicate that the carbohydrate is located on the sequence PSD. Since O-glycosylation is mainly targeting Ser or Thr residues, our results are consistent with the carbohydrate located on Ser³⁷⁵.

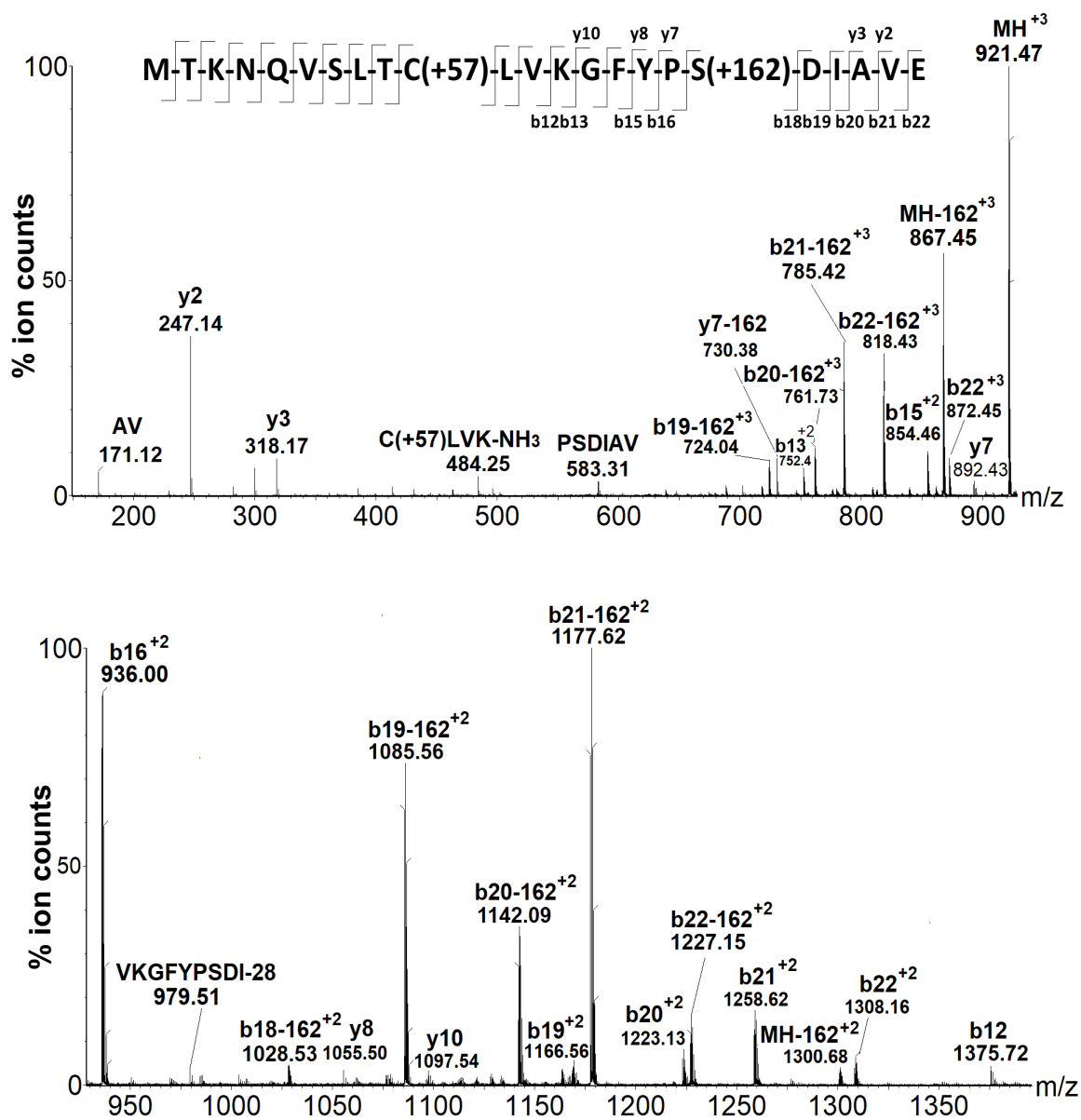


Fig. 2. MS/MS spectra of the O-glycosylated peptide MTKNQVSLTC(+57)LVKGFYPS³⁷⁵(+162) DIAVE (m/z 921.47) of W381A IgG4-Fc, where +162 indicates that Ser³⁷⁵ is mannosylated, and +57 indicates that the Cys residue is alkylated due to reaction with IAA.

3.3.4. Thermal stability of WT, S375A, W381A, S375A/W381A, WT_degly, S375A_degly, W381A_degly, and S375A/W381A_degly IgG4-Fc. The overall conformational stability of the various IgG4-Fc variants was examined by DSC. The thermograms of WT, S375A, W381A, S375A/W381A, WT_degly, S375A_degly, W381A_degly, and S375A/W381A_degly IgG4-Fc are shown in Fig. 3A and 3B, respectively. The thermograms of WT and S375A were deconvoluted into three transitions, represented by melting temperatures (T_m) referred to as T_{m1} , T_{m2} , and T_{m3} . All T_m values are summarized in Table 2. The T_{m1} of WT_degly is 5.8 °C lower compared to WT, T_{m2} is 3°C lower, and T_{m3} is 2°C lower. The T_{m1} of S375A_degly is 1 °C higher compared to S375A, T_{m2} is 2.4°C higher, and T_{m3} is 0.1°C higher. Importantly, the thermograms of W381A and W381A/S375A present no transitions in the temperature range 30 – 80°C, regardless of the presence or absence of N-linked glycans, indicating that the mutation of Trp³⁸¹ to Ala³⁸¹ results in a loss of conformation. A similar loss of conformation was detected by DSC analysis of W381G IgG4-Fc (Fig. S6A). In addition, we tried rescuing the conformational structures of W381A and W381G IgG4-Fc by the addition of indole. Such a chemical rescue approach has been recently described where a Trp to Gly mutation of a single-chain variable fragment was structurally and functionally rescued by the addition of 1000-fold concentration of indole^{15, 55}. However, the W381A and W381G IgG4-Fc (3.5 μM) were not rescued by the addition of up to 4 mM indole (>1000-fold excess of indole), indicated by the absence of any obvious thermal transition (Fig. S6B).

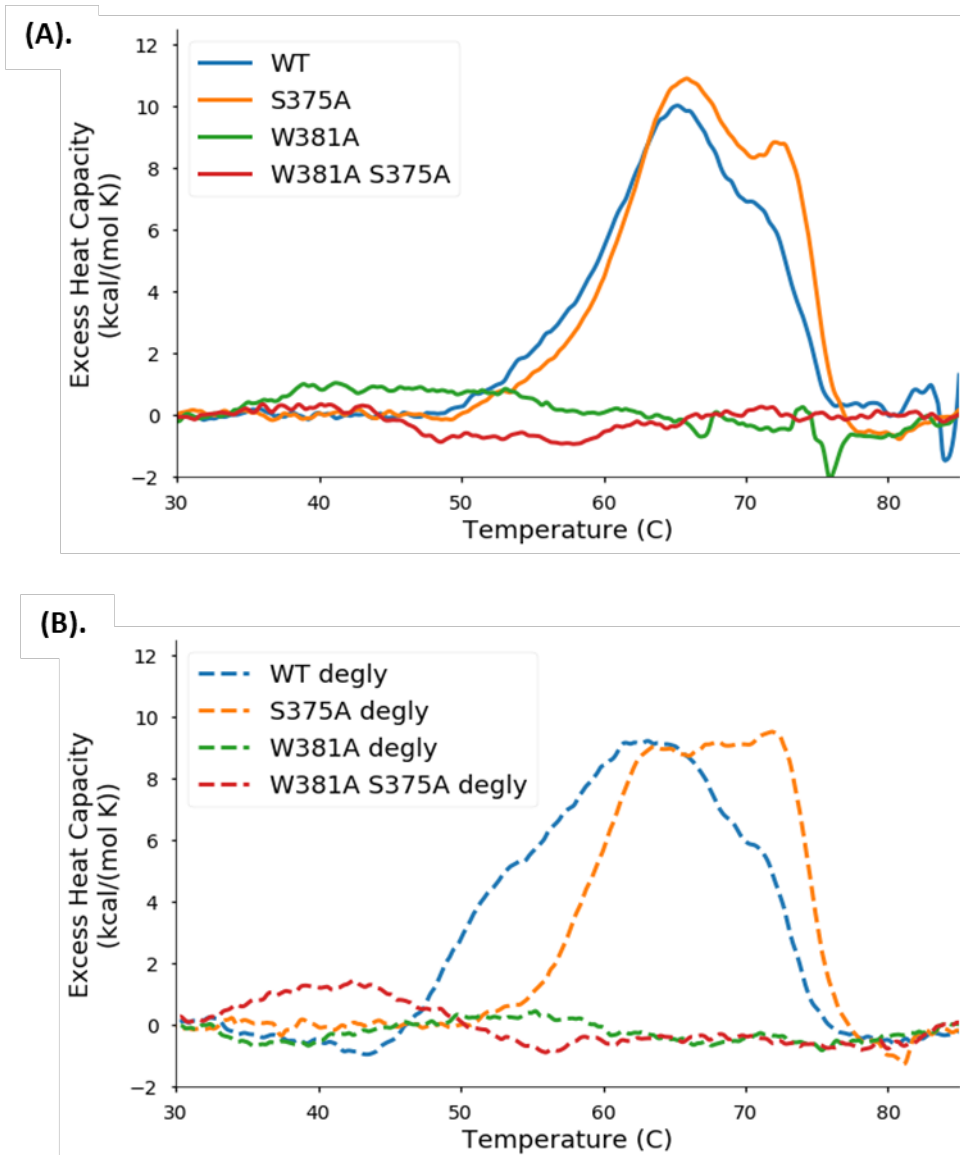


Fig. 3. Representative DSC thermograms of WT, S375A, W381A, and S375A/W381A (A) and WT_degly, S375A_degly, W381A_degly, and S375A/W381A_degly (B). All the derived T_m values of WT and S375A are summarized in Table 2.

3.3.5. Tertiary structure of WT, S375A, W381A, S375A/W381A, WT_degly, S375A_degly, W381A_degly, and S375A/W381A_degly IgG4-Fc. The tertiary structures of the IgG4-Fc variants were evaluated by intrinsic fluorescence spectroscopy with a temperature ramp from 10 to 90°C. The fluorescence moments were plotted on the y axis as a function of temperature, as shown in Fig. 4. Between 10 and 90°C, the S375A mutant displays a slight blue shift compared to WT IgG4-Fc (Fig. 4A), regardless of the presence of N-linked glycans (Fig. 4B), indicating that S375A has a relatively more compact tertiary structure compared to WT, consistent with our DSC analysis (Table 2). At 10°C, the fluorescence moments of W381A and S375A/W381A show a 2 nm-red shift compared to WT. The T_m values obtained by intrinsic fluorescence are displayed in Table 2, with 63.6 °C for glycosylated WT and S375A, and 62.6°C and 62.8°C for PNGase F-treated WT and S375A, respectively. W381A and W381A/S375A demonstrate no transition upon increasing the temperature from 10 to 90°C, indicating that the mutation of Trp³⁸¹ to Ala³⁸¹ causes a perturbation of tertiary structure in both W381A and S375A/W381A. We did not observe any differences between O-glycosylated W381A and the non-glycosylated double mutant S375A/W381A with regard to their tertiary structures monitored by intrinsic fluorescence spectroscopy.

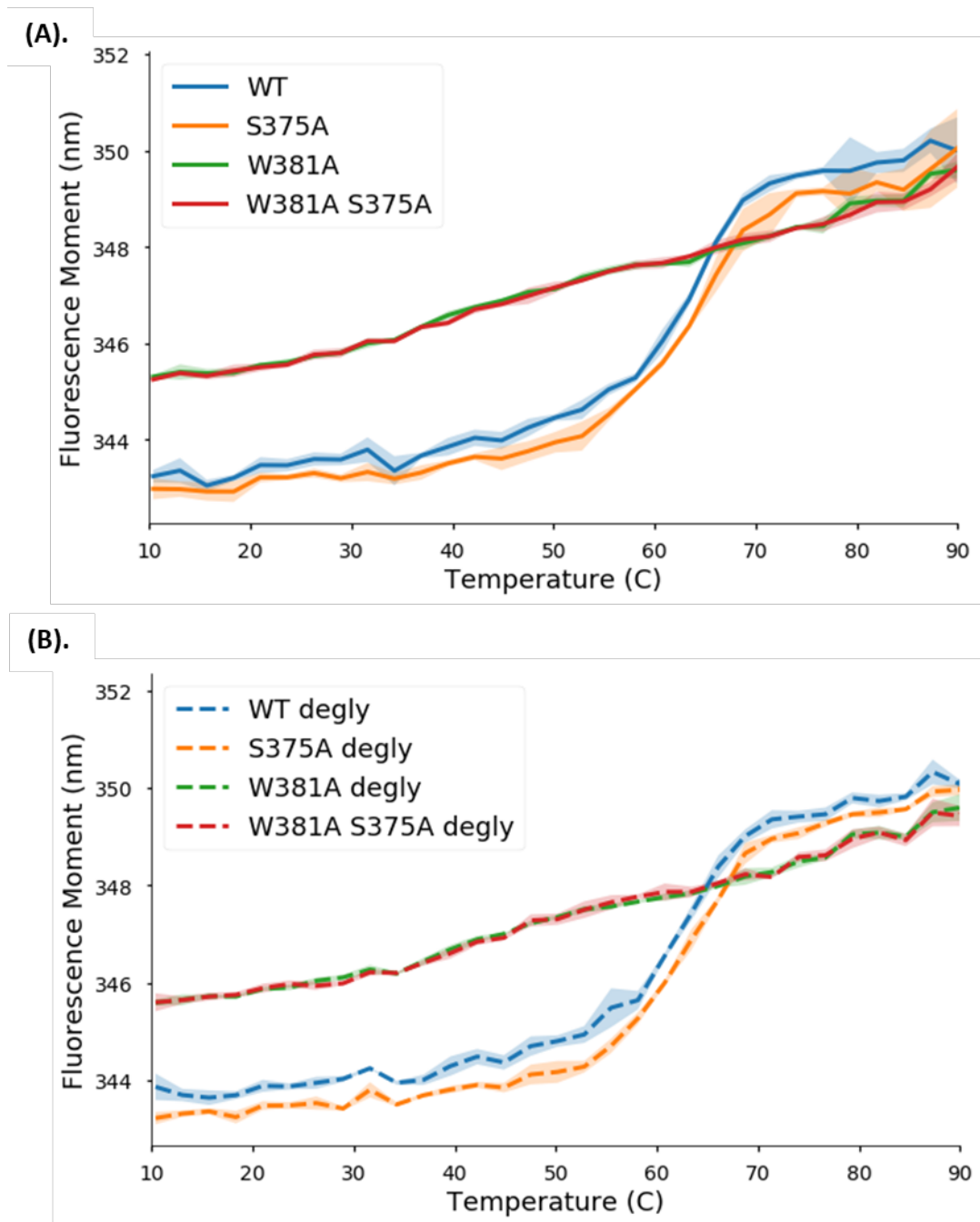


Fig. 4. Tertiary structure characterization through intrinsic fluorescence spectroscopy of (A) glycosylated WT, S375A, W381A and S375A/W381A and (B) PNGase F-treated WT_degly, S375A_degly, W381A_degly and S375A/W381A_degly. The shaded areas represent standard deviations from four independent measurements.

3.3.6. Secondary structure of WT, S375A, W381A, S375A/W381A, WT_degly, S375A_degly, W381A_degly, and S375A/W381A_degly IgG4-Fc. Fig. 5 shows the second-derivative amide I spectra of WT, S375A, W381A, and S375A/W381A IgG4-Fc and their respective N-deglycosylated forms. These spectra are stacked to facilitate comparison. All proteins reveal an overall β -sheet structure ($\sim 1630\text{ cm}^{-1}$). Here, W381A and S375A/W381A shift the β -sheet bands by 1 - 2 cm^{-1} to lower wavenumbers compared to WT and S375A. There are no substantial differences induced by PNGase F treatment for WT, W381A, and S375A, but the N-deglycosylation of the double mutant S375A/W381A IgG4-Fc induces a significant absorbance increase at wavenumbers around 1650 cm^{-1} and 1680 cm^{-1} , characteristic of random coil and β -turn structures based on the second-derivative analysis⁴⁸. Spectra were also deconvoluted and fit to individual secondary structures, displayed in Fig. S7, with little differences.

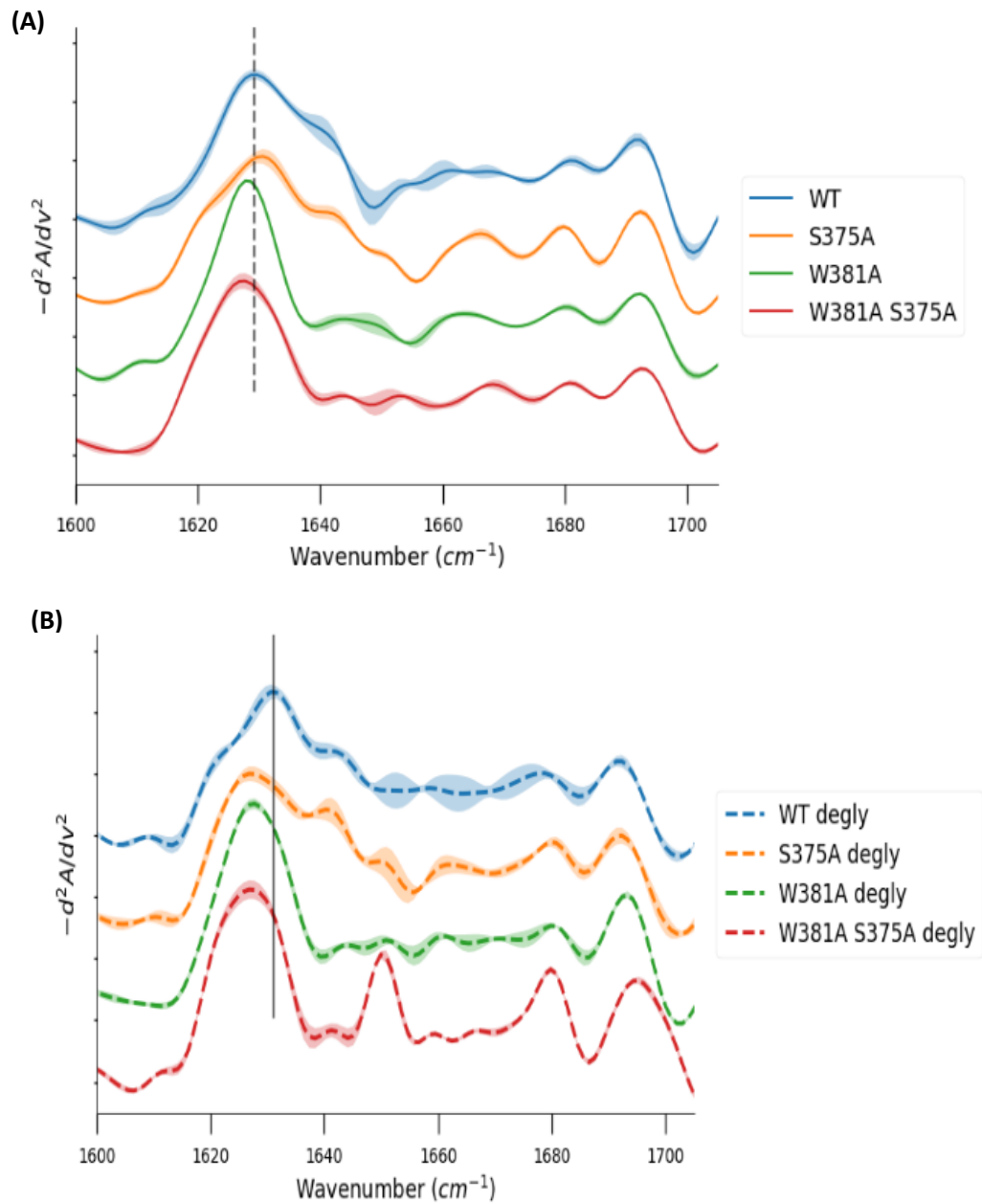


Fig. 5. Secondary-derivative amide I spectra from FTIR analysis of (A) glycosylated and (B) PNGase F-treated WT, S375A, W381A, and S375A/W381A IgG4-Fc.

3.3.7. Backbone flexibility of WT and W381A IgG4-Fc examined by HX-MS. Maximally deuterated reference proteins were generated by deuterium-labeling of denatured WT and W381A IgG4-Fc, respectively, referred to as deuteration controls. The deuteration controls of WT and W381A revealed similar deuterium incorporation of approximate 100-110 Da (data not shown). These values were utilized for the calculation of % deuteration for native WT and W381A IgG4-Fc, plotted on the y-axis as a function of HX time in Fig. 6. Two species, IgG4-Fc-GlcNAc₂Man₈ and IgG4-Fc-GlcNAc₂Man₉, were tracked for HX measurements, because of their high abundance (Fig. S2). The two GlcNAc₂Man₈ and GlcNAc₂Man₉ glycoforms demonstrate the same trend. W381A displays a constantly higher incorporation of deuterium compared to WT at the six times sampled, where for the last two HX times (12500 s and 62500 s), W381A is close to full deuteration with a % deuteration of 96.86% - 100%. This indicates that W381A presents higher backbone flexibility compared to WT. Moreover, W381A does not reach a full deuteration between 10 s and 10000s sampling time, suggesting that also this mutant is characterized by some structure, consistent with our FTIR analysis.

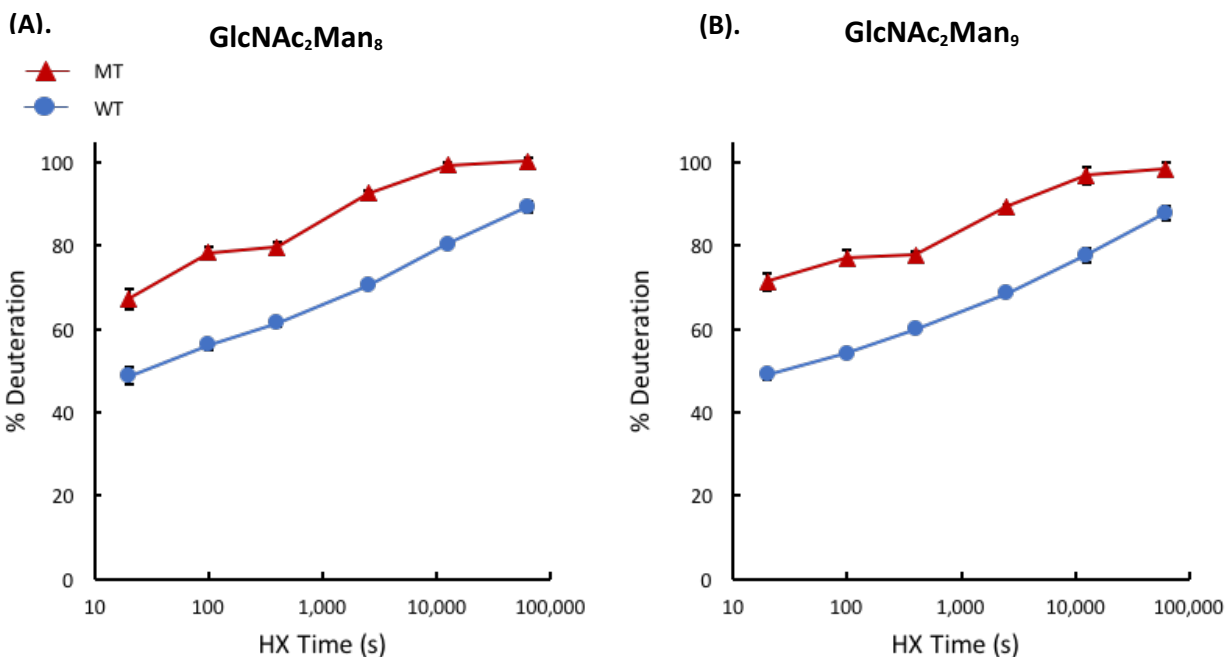


Fig. 6. HX exchange of W381A (red) and WT (blue) IgG4-Fc, showing %deuteration vs labeling time, where %deuteration is normalized on deuteration controls. (A) represents the GlcNAc₂Man₈ glycoform, whereas (B) represents the GlcNAc₂Man₉ glycoform. The error bars represent the standard deviation from three independent HX experiments.

3.3.8. Photo-degradation of WT, S375A, W381A, S375A/W381A, WT_degly, S375A_degly, W381A_degly, and S375A/W381A_degly IgG4-Fc. The photostability of the IgG4-Fc variants was evaluated by comparison of the yields of photo-products after photoirradiation at $\lambda_{\max} = 305$ nm for 45 min under air. All yields are reported as the conversion of native peptides (in %), quantified as the ratio of the peak areas of the products to the sum of peak areas for products and native peptides. The peak areas of the native and modified peptides were extracted by Masslynx (Waters Corporation, Milford, MA). As a complementary method, the total ion count (TIC) was

also utilized for relative quantification, which demonstrated a similar trend (data not shown). A total of 16 photo-products resulting from the photo-degradation of several Tyr, Met, Cys, and Trp residues were identified and quantified, as shown in Fig. 7-11 (where the products from Tyr, Met and Cys degradation were characterized after GluC digestion, and the products from Trp degradation were characterized after Trypsin/LysC digestion). All detected photo-degradation products are listed in Table 3.

During the exposure of WT IgG4-Fc to UV light, three Tyr residues, including Tyr³⁰⁰, Tyr³⁷³, and Tyr⁴³⁶, undergo side chain fragmentation to yield Gly and several peptide backbone cleavage products¹⁶. For WT and mutant IgG4-Fc, the side chain fragmentation products of Tyr³⁷³ and Tyr⁴³⁶ are summarized in Table 3 (products **1-5**) and their relative yields in Fig. 7. These compilations do not contain data on photo-products from Tyr³⁰⁰, which are typically observed best in the absence of oxygen¹⁶. As photo-irradiation was in the present work performed under air, the photo-products from Tyr³⁰⁰ were not included. The transformation of Met²⁵², Met³⁵⁸, and Met⁴²⁶ to Met sulfoxide (MetSO) is summarized in Fig. 8, and the transformation of Cys³²¹, Cys³⁶⁷ and Cys⁴²⁵ to vinyl cysteine (vinyl Cys) is presented in Fig. 9. The photo-degradation products from Trp³¹³ and Trp⁴¹⁷ are summarized in Fig. 10 and 11.

3.3.8.1. Photo-induced Tyr side chain fragmentation. The photo-induced Tyr side chain fragmentation of WT IgG4-Fc was previously documented by us¹⁶. Here, the peptide backbone cleavage products (products **1-5**; Table 3) dominate for photo-irradiation under air atmosphere, where products **1-2** resulted from the cleavage of Tyr³⁷³, and products **3, 4** and **5** result from the

cleavage of Tyr⁴³⁶. The yields of products **1-5** from S375A are similar to those of WT, but W381A and S375A/W381A show between 2.6- and 13.5-fold reduction of the yields of photoproducts **1-5** (Fig. 7A and 7B). Hence, the W381A mutation has a similar effect as our previously reported W381F mutation¹⁶. The thermal stability of W381F IgG4-Fc was evaluated by DSC and displayed in Fig. S8.

The yields of products **1** and **2** originating from Tyr³⁷³ are higher in WT_degly and S375A_degly as compared to the glycosylated WT and S375A. For example, product **1** accounts for a relative yield of 22.1% in WT, 22.8% in S375A, 30.7% in WT_degly, and 33.0% in S375A_degly, while product **2** accounts for 3.8% in WT, 4.1% in S375A, 5.5% in WT_degly, and 5.0% in S375A_degly, respectively. This indicates that the presence of N-glycans has an effect on the formation of photoproducts from Tyr³⁷³, but less from Tyr⁴³⁶ (products **3-5**), other than the fact that a two-fold reduction of product **5** was observed in S375A compared to S375A_degly. We attempted to monitor the formation of di-tyrosine by MS analysis, but could not detect it. Hence, the yields were probably below the detection limit. As an alternative, fluorescence emission between 370 and 500 nm (excitation at 320 nm) was utilized, where an emission maximum at 410-425 nm corresponds to the formation of di-tyrosine⁵⁶. As displayed in Fig. S9, we note that the fluorescence maximum shifts to ca. 430 nm for WT, Y300G, Y373G, Y436G, and to ca 439 nm for W381A, suggesting the contribution of N-formylkynurenine to the fluorescence emission, which perturbs the analysis of di-tyrosine.

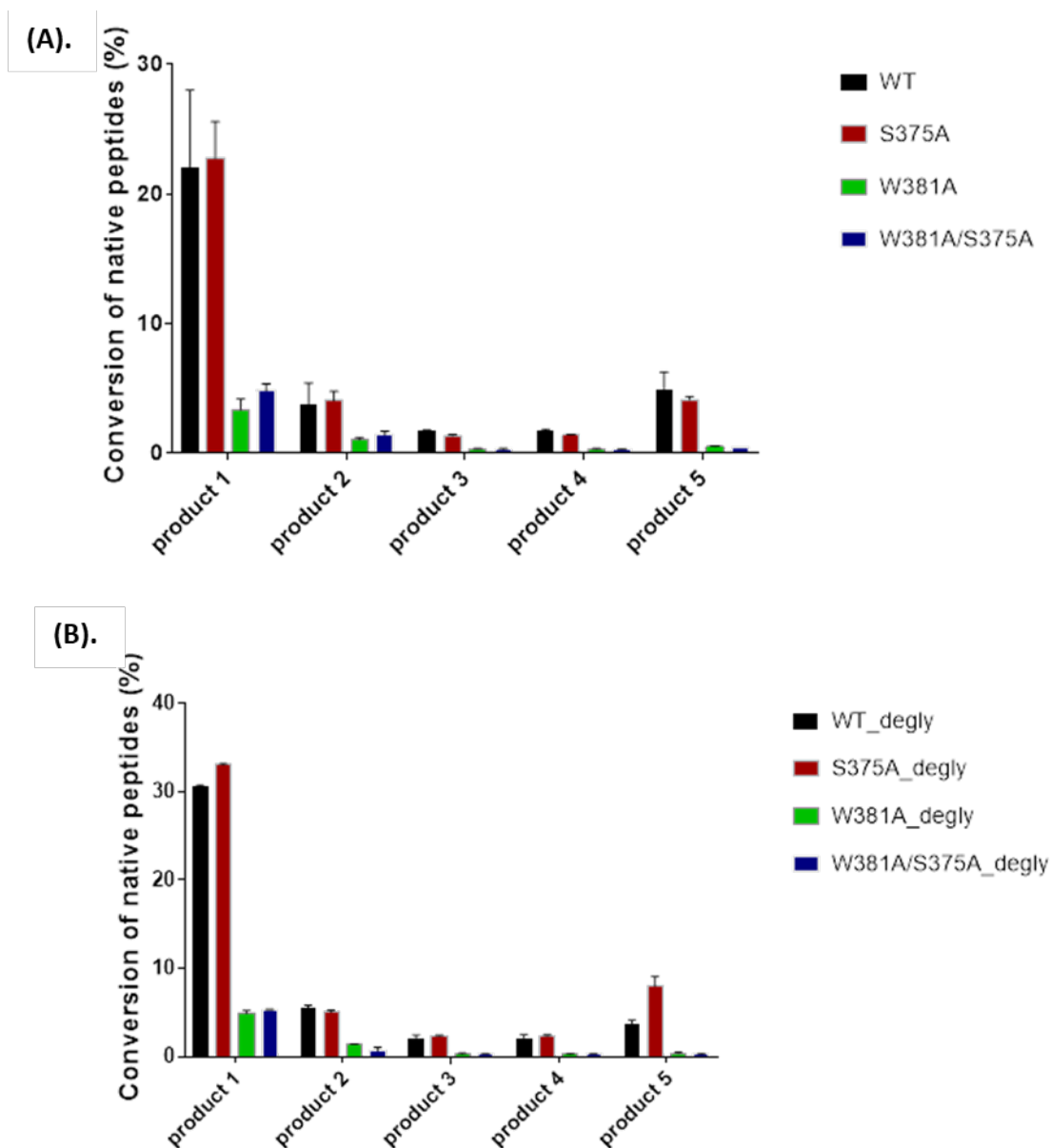


Fig. 7. Relative yields of products **1-5** originating from photo-induced side chain fragmentation of Tyr³⁷³ (products **1-2**) and Tyr⁴³⁶ (products **3-5**). Photo-irradiation was performed at $\lambda_{\max} = 305$ nm for 45 min under air. (A) Product formation from WT, S375A, W381A, and W381A/S375A IgG4-Fc. (B) Product formation from WT_degly, S375A_degly, W381A_degly, and W381A/S375A_degly. Products **1-5** are displayed in Table 3.

3.3.8.2. Formation of MetSO. Three Met residues in IgG4-Fc are transformed into MetSO after photo-irradiation under air. These include Met²⁵² in the C_H2 domain, and Met³⁵⁸ and Met⁴²⁶ in the C_H3 domain. Representative yields of MetSO, referred to as products **6**, **7**, **8**, are displayed in Fig. 8. For WT, S375A, W381A and S375A/W381A, the relative yields of MetSO rank as follows: MetSO²⁵² > MetSO⁴²⁶ > MetSO³⁵⁸. This may be due to the differences of their solvent accessibility, based on previously reported structures of WT IgG1 and IgG2⁵⁷⁻⁵⁸. The most significant differences between WT and the mutants are observed for product **7** (both glycosylated and N-deglycosylated forms), and for product **8** (Fig. 8B)

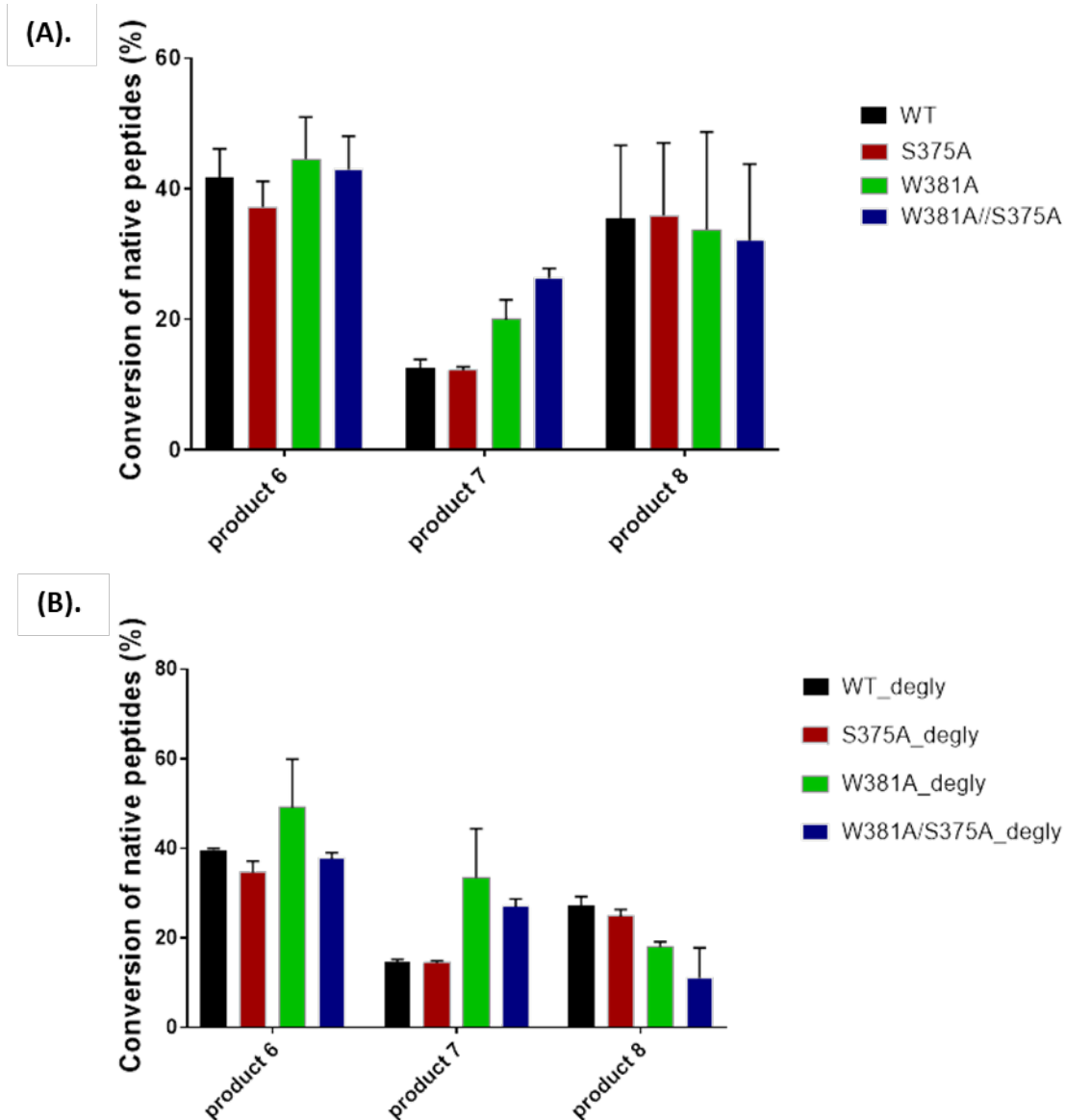


Fig. 8. Relative yields of MetSO originating from Met²⁵², Met³⁵⁸, and Met⁴²⁶, referred to as products 6, 7, and 8. Detailed peptide sequences are presented in Table 3. (A) Product yields from WT, S375A, W381A, and W381A/S375A. (B) Product yields from WT_degly, S375A_degly, W381A_degly, and W381A/S375A_degly.

3.3.8.3. Formation of vinyl Cys. The yields of photo-chemically generated vinyl Cys from Cys³²¹, Cys³⁶⁷ and Cys⁴²⁵ are displayed in Fig. 9. These products are referred to as products **9**, **10**, and **11**, respectively. Vinyl Cys forms about 1.4 -1.9 fold more in WT compared to S375A, and about 1.3-2.9 fold more in WT_degly compared to in S375A_degly. O-mannosylation does not have much of an effect on vinyl Cys formation derived from a comparison between the product yields from W381A and S375A/W381A.

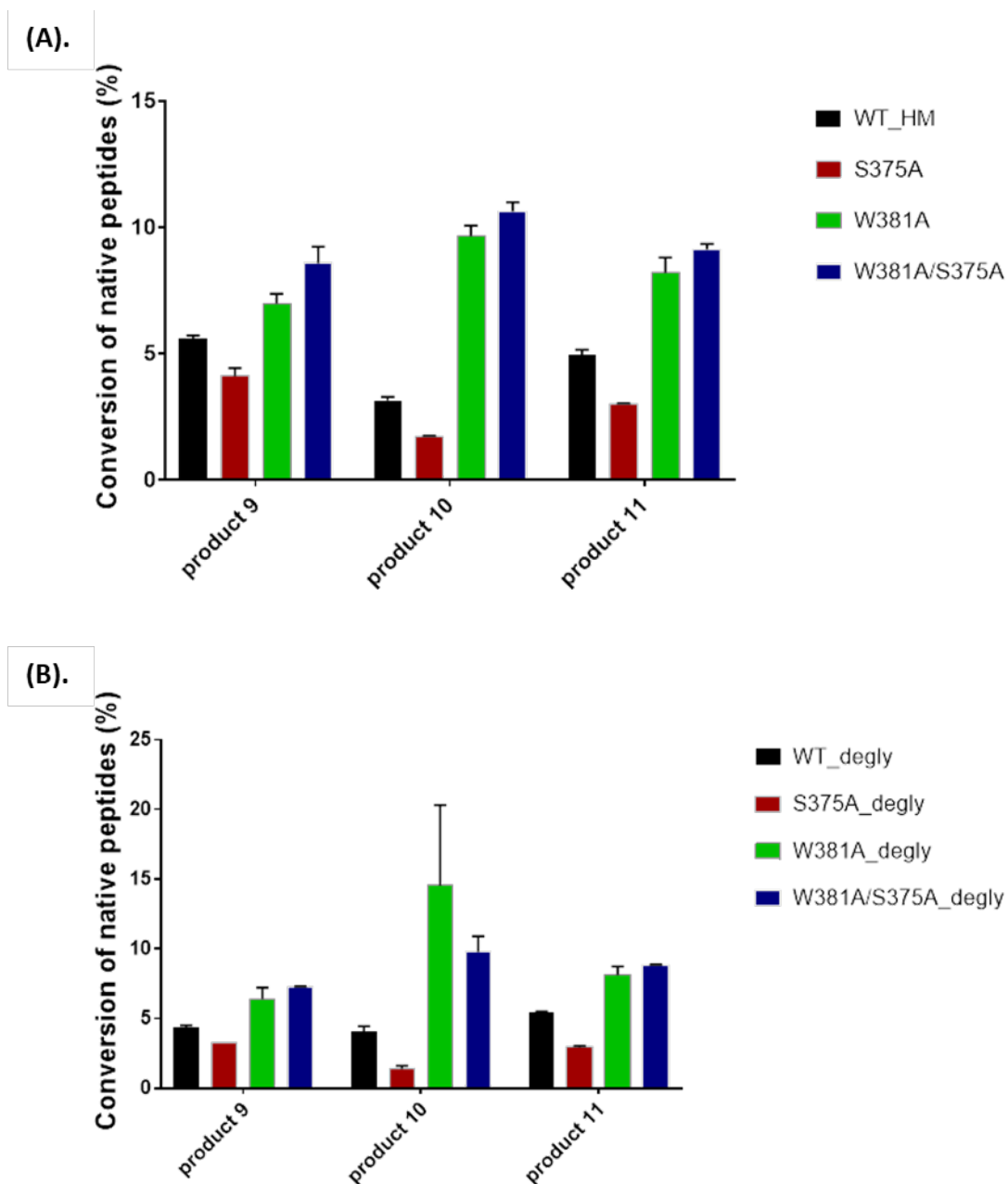


Fig. 9. Relative yields of vinyl Cys originating from Cys³²¹, Cys³⁶⁷, and Cys⁴²⁵, referred to as products **9**, **10**, and **11**. Detailed peptide sequences are presented in Table 3. (A) Product yields from WT, S375A, W381A, and W381A/S375A. (B) Product yields from WT_degly, S375A_degly, W381A_degly, and W381A/S375A_degly.

3.3.8.4. Photo-degradation of Trp. The yields of hydroxytryptophan (Trp-OH) (product **12** from Trp³¹³ and product **14** from Trp⁴¹⁷) and N-formylkynurenine (NFK) (product **13** from Trp³¹³) from the IgG4 variants are displayed in Fig. 10. The yields of kynurenine (Kyn) (product **15** from Trp³¹³) and Trp side chain fragmentation (product **16** from Trp³¹³) are displayed in Fig. 11. Overall, the mutation of Trp³⁸¹ to Ala³⁸¹ results in ca. 1.5 – 3 fold increase in the yields of Trp³¹³ and Trp⁴¹⁷ oxidation. The product yields for W381A and S375A/W381A are similar, suggesting that the presence of an O-glycan at Ser³⁷⁵ does not have much of an effect on Trp³¹³ and Trp⁴¹⁷ degradation. Interestingly, products **12**, **13**, **15**, and **16** resulting from Trp³¹³ degradation consistently demonstrate slightly higher yields for N-glycosylated IgG4-Fc (p values <0.05, one-tailed paired t-test with Excel), while product **14** from Trp⁴¹⁷ reveals slightly higher yields in N-deglycosylated IgG4-Fc (p values <0.05, one-tailed paired t-test with Excel).

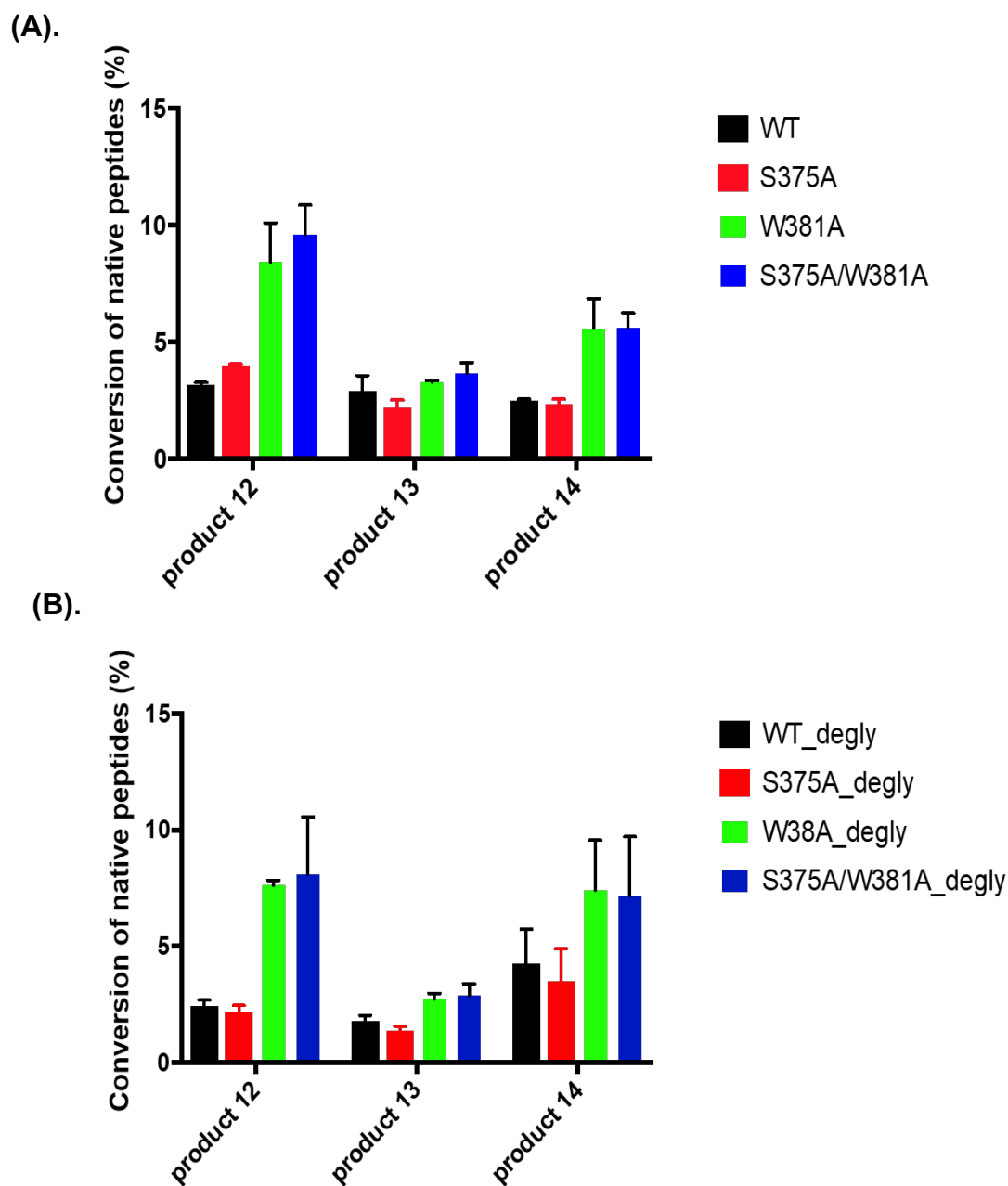


Fig. 10. Relative yields of Trp oxidation products originating from Trp³¹³ (product 12 and 13) and Trp⁴¹⁷ (product 14). Detailed peptide sequences are presented in Table 3. (A) Product yields from WT, S375A, W381A, and W381A/S375A. (B) Product yields from WT_degly, S375A_degly, W381A_degly, and W381A/S375A_degly.

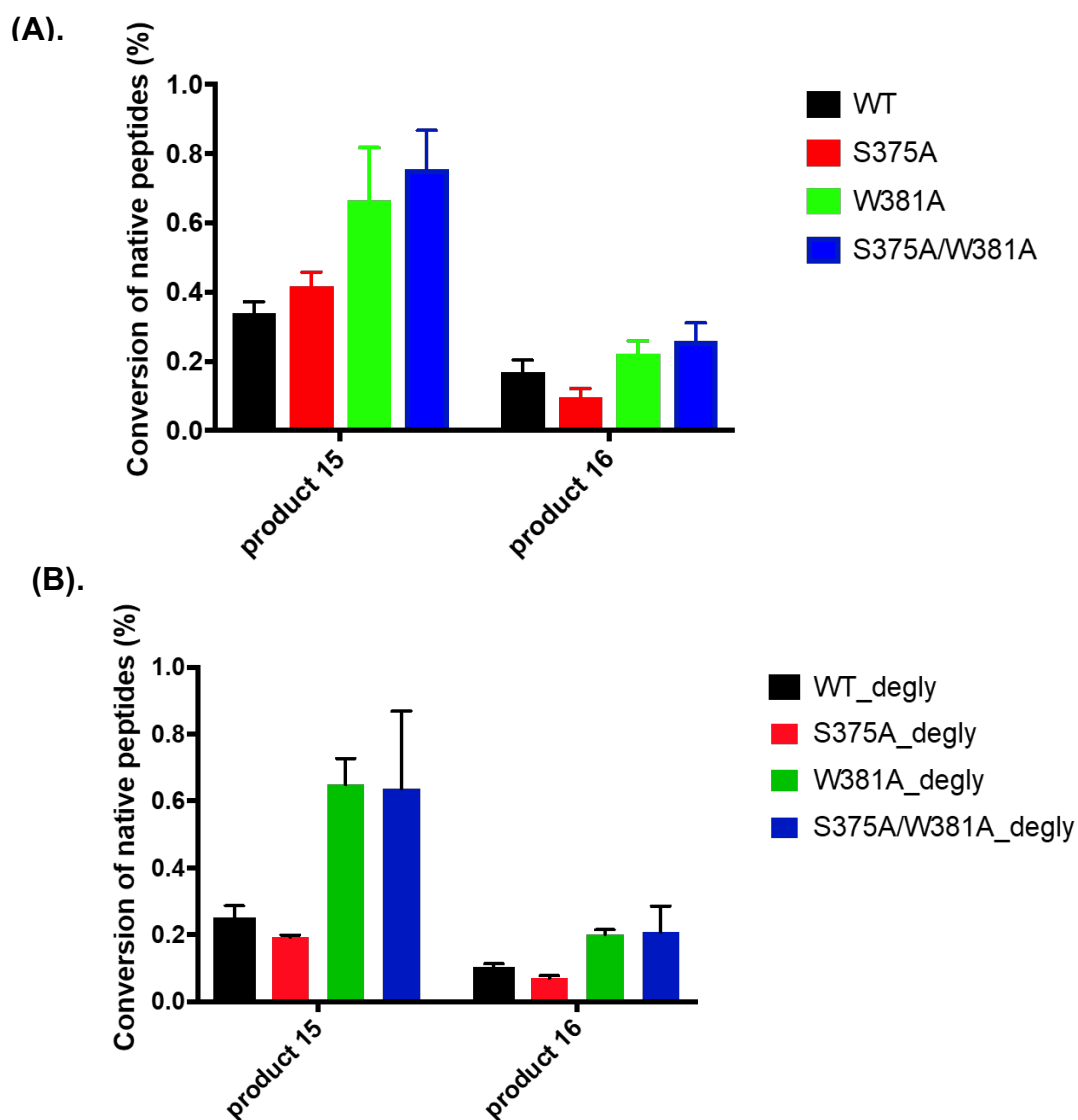
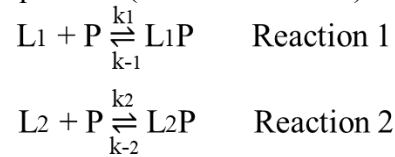


Fig. 11. Relative yields of Trp degradation originating from Trp³¹³, referred to as products **15** and **16**. Detailed peptide sequences are presented in Table 3. (A) Product yields from WT, S375A, W381A, and W381A/S375A. (B) Product yields from N-deglycosylated WT, S375A, W381A, and W381A/S375A.

3.3.9. Binding of WT, Y300G, Y373G, Y436G, and W381A IgG4-Fc to FcγRIIIA. The affinity of the IgG4-Fc variants to FcγRIII A was obtained with a BLItz system by immobilizing FcγRIIIA on SA tips. The binding responses (Δnm) as a function of time (s) were then fit to a two-exponential association model with XLFit. Two representative examples of the fits for WT and Y300G, are shown in Fig. 12A and 12B, respectively, and the fits for Y373G, Y436G and W381A are presented in Fig. S10. A dilution series of five concentrations was applied to each sample protein sample.

The experimental sensorgram of association reveals a deviation from mono-exponential kinetics (Fig. 12)⁵⁹⁻⁶⁰, requiring two parallel equilibria (Reaction 1 and 2) for kinetic analysis.



Here, L_1 and L_2 represent two forms of FcγRIIIA, based on the potential for heterogeneity of FcγR⁶¹. The variable P represents the concentration of the IgG4-Fc variants, k_1 and k_2 represent the k_{on} values, and k_{-1} and k_{-2} represent the k_{off} values for Reactions 1 and 2. Reaction 1 stands for the fast phase, and reaction 2 stands for the slow phase. Based on the relative concentrations where $[\text{Fc}\gamma\text{RIIIA}] \ll [\text{IgG4-Fc}]$, the association reactions are of pseudo first order. We obtained

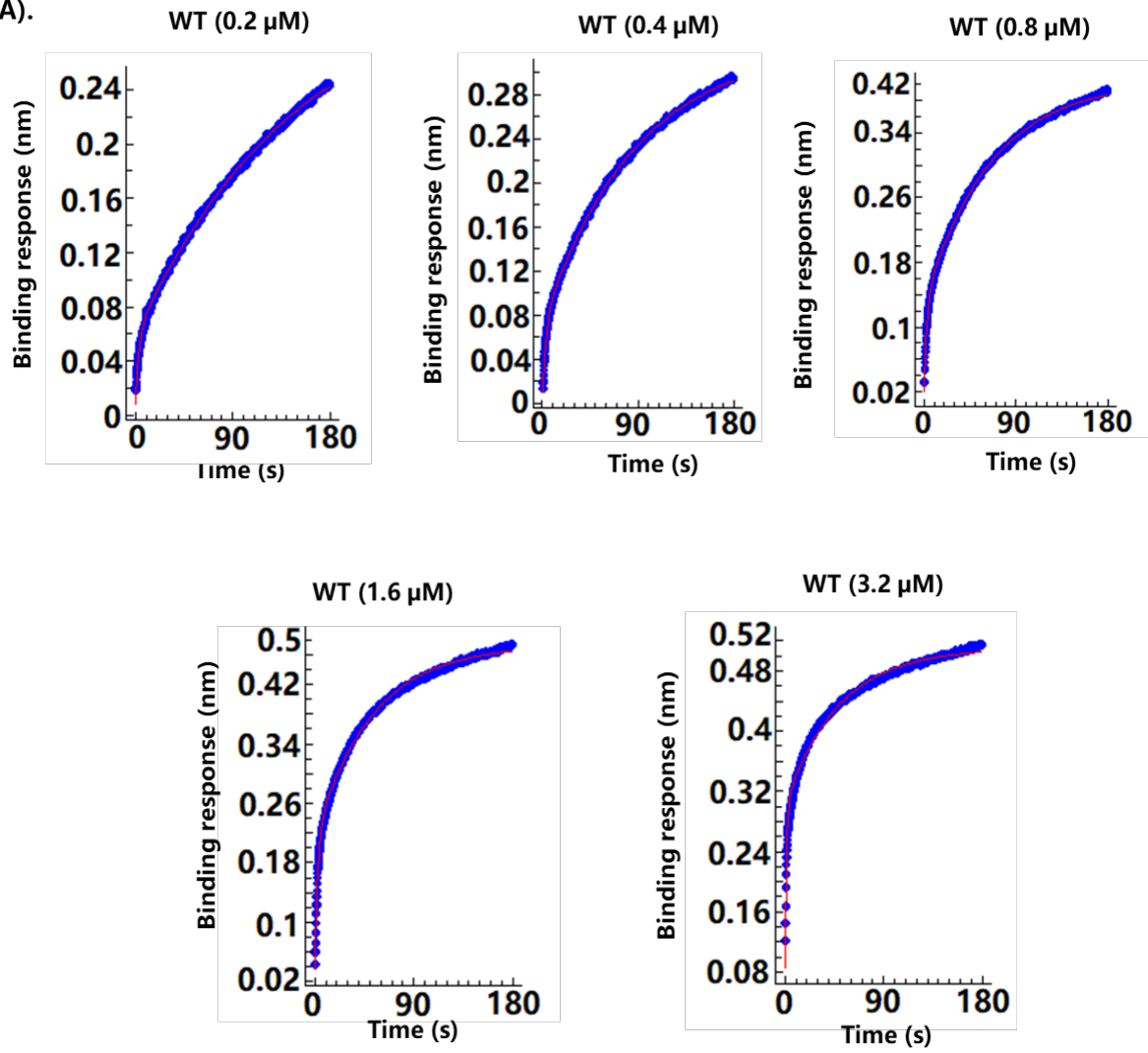
$$[\text{L}_1\text{P}] + [\text{L}_2\text{P}] = [\text{L}_1\text{P}]_{\infty}(1 - \exp(-(k_1[\text{P}_0] + k_{-1})t)) + [\text{L}_2\text{P}]_{\infty}(1 - \exp(-(k_2[\text{P}_0] + k_{-2})t)),$$

where $[\text{L}_1\text{P}]$ and $[\text{L}_2\text{P}]$ represent the concentrations of the complexes L_1P and L_2P at time t as dependent variables, respectively; $[\text{P}_0]$ represents the initial and approximately constant concentration of P. $[\text{L}_1\text{P}]_{\infty}$ and $[\text{L}_2\text{P}]_{\infty}$ represent the concentrations of L_1P and L_2P at infinite reaction time. A two-exponential association fit was applied using XL fit analysis: $y = A(1 - \exp(-$

Bx)) + C(1-exp(-Dx)), where $A = [L_1P]_{\infty}$; $B = k_1[P_0] + k_{-1}$; $C = [L_2P]_{\infty}$; $D = k_2[P_0] + k_{-2}$. Therefore, the fitting parameters, B and D correspond to k_{obs} of the fast (Fig. 13) and the slow phases (Fig. S11), which can be plotted as a function of the concentration of $[P_0]$. From the slope, we derive k_{on} ($M^{-1}s^{-1}$) (k_1 or k_2), and from the intercept, we derive k_{off} (s^{-1}) (k_{-1} or k_{-2}) (Fig. 14). The plots of k_{obs} vs. $[P_0]$ of the fast phase display a linear relation for the five IgG4-Fc variants (Fig. 13). However, the plots of k_{obs} vs. $[P_0]$ of the slow phase show linearity only for WT, Y373G, and Y300G (Fig. S11). The k_{on} and k_{off} values derived from the fast phase are consistent with the specific binding affinity between Fc and Fc γ RIII^{33, 62}. Therefore, in the following we compare the binding affinity of the IgG4-Fc variants based on the rate constants obtained from the fast phase.

By comparison, we observed the following trend of the k_{on} values: WT > Y373G > Y436G > Y300G > W381A, where k_{on} of WT is about 11.5-fold higher than k_{on} for W381A. On the other hand, the trend of k_{off} values is as follows: Y373G < W381A < WT < Y300G < Y436G, where Y373G, W381A and WT present similar k_{off} values within a 1.5-fold difference, while Y300G and Y436G display (2.0- 3.5)-fold increased k_{off} values with respect to Y373G, W381A, and WT. The equilibrium dissociation constants (K_D) were obtained by calculating the ratio of k_{off} over k_{on} , and the trend was as follows: WT < Y373G < Y436G < Y300G < W381A, where WT and Y373G present similar K_D values (1.6 -1.9 μ M), while Y436G, Y300G, and W381A display ca. 9-10 fold increased K_D values as compared to WT and Y373G, indicating that WT and Y373G have about a 10-fold higher affinity to Fc γ RIII A than Y300G, Y436G and W381A.

(A).



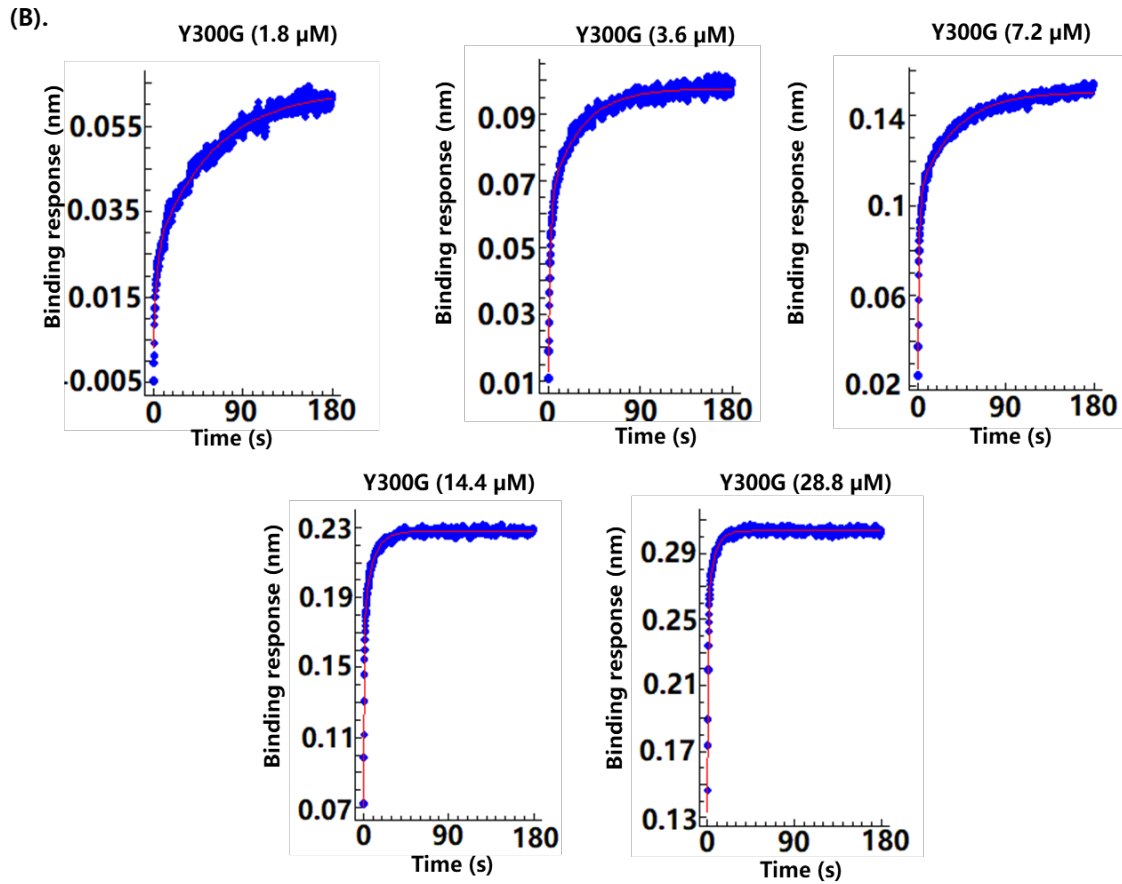


Fig. 12. BLI association sensorgrams for (A) WT and Fc γ RIII A, and (B) Y300G and Fc γ RIII A in PBS kinetic buffer (pH 7.4), where the red line corresponds to a two-phase exponential association fit, and the blue dots correspond to experimental data points.

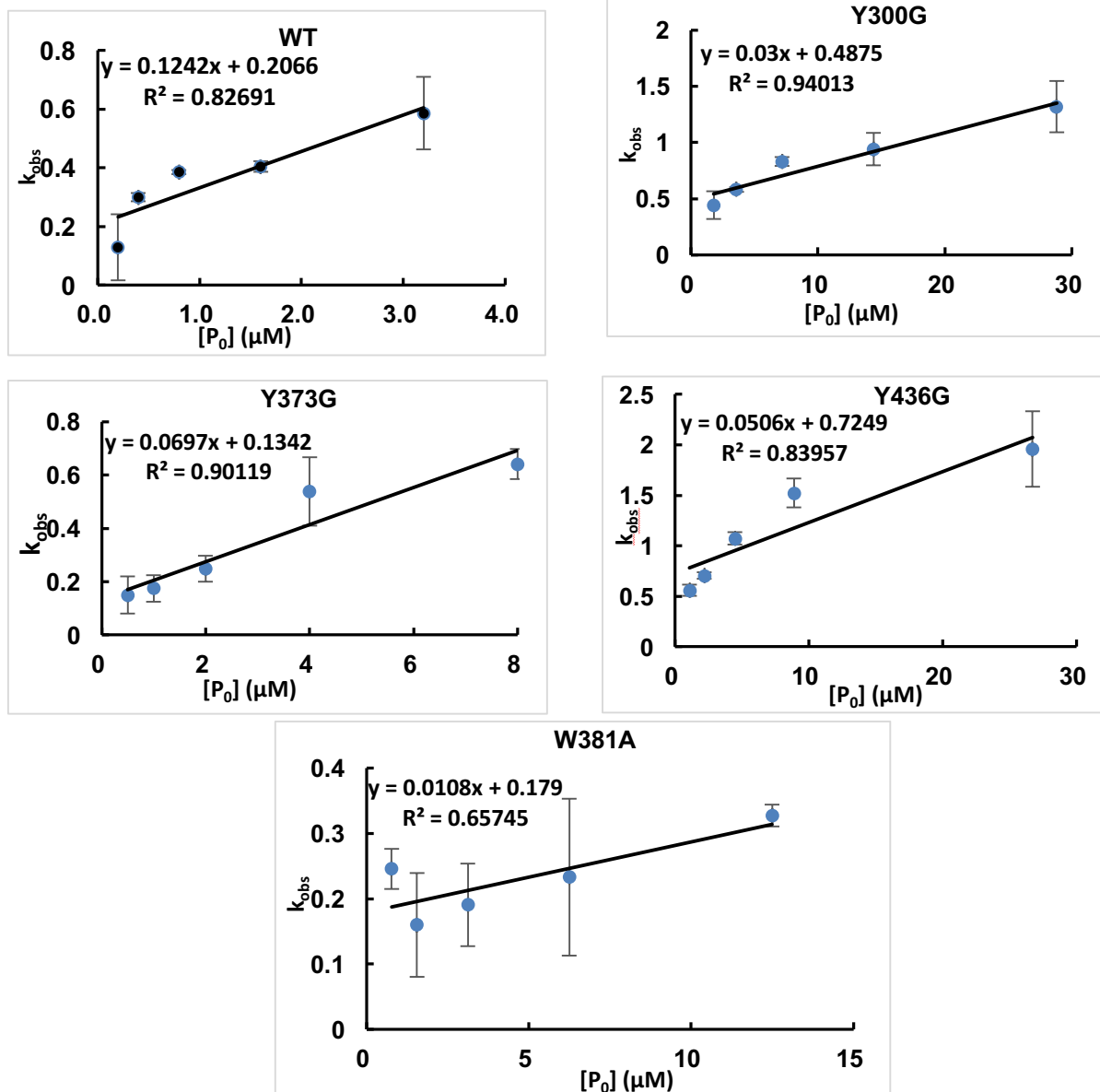


Fig. 13. Plot of k_{obs} of the fast phase as a function of concentrations of the IgG4-Fc variants. The error bars represent the standard error from three independent measurements.

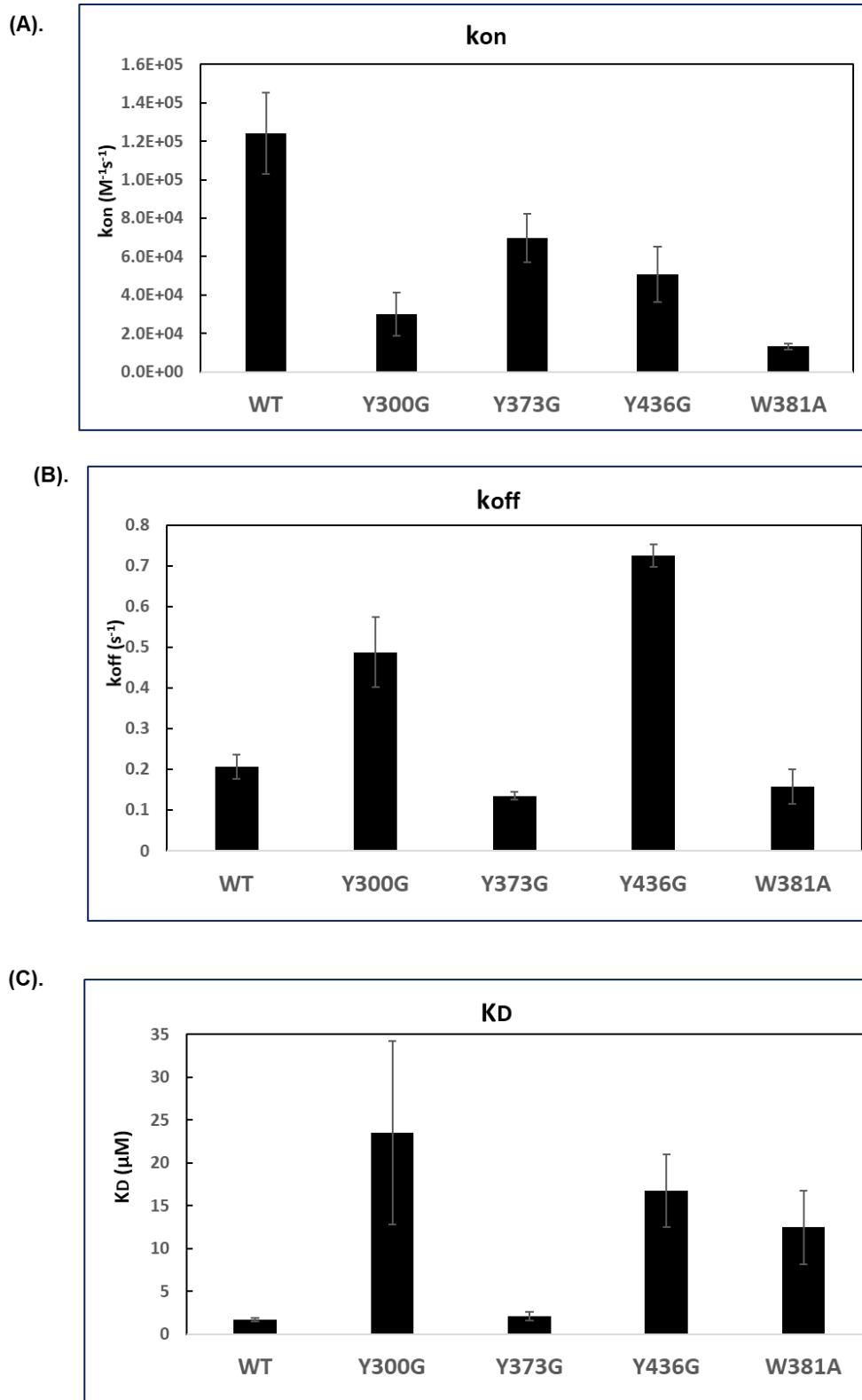


Fig. 14. k_{on} (A), k_{off} (B) and K_D (C) values of the fast phase for WT, Y300G, Y373G, Y436G, and W381A IgG4-Fc.

3.4. Discussion.

Physico-chemical stability and biological function are central for safety, potency, and comparability assessment of protein therapeutics. These properties depend on the intrinsic (primary sequence, structure, glycosylation) and extrinsic factors (pH, temperature, exposure to light, formulation additives). Here, we examined the consequences of photo-induced conversion of Trp and Tyr of IgG4-Fc to Gly^{6, 19} on the structure, backbone flexibility, and receptor binding. During preparation of the various Tyr to Gly and Trp to Gly/Ala mutants, we realized that these mutations led to a change of glycosylation, especially the formation of atypical O-glycosylation. Therefore, we designed additional mutants to evaluate the effect of N- vs O-glycosylation, and N-deglycosylation on protein structure, receptor binding, and photochemical product formation. Our results show that: (1) The conversion of Tyr³⁷³ to Gly³⁷³ significantly decreased the thermal stability of both the C_H2 and C_H3 domains of IgG4-Fc; (2) the single conversion of Trp³⁸¹ to Ala³⁸¹ or Gly³⁸¹ in the C_H3 domain of IgG4-Fc- caused overall conformational and tertiary structure perturbation; (3) the conversion of Tyr³⁰⁰ to Gly³⁰⁰ and Trp³⁸¹ to Ala³⁸¹ results in a ca. 10-fold reduction of binding affinity to the FcγRIII A; (4) an O-linked glycosylation site at Ser³⁷⁵ was enriched to more than 60% in W381A and W381G IgG4-Fc; (5) both, the mutation of a single Trp and the introduction of N-glycans have an effect on the yields of photo-induced product formation. Therefore, it is critical to characterize and control Trp and Tyr degradation during processing and storage of protein therapeutics.

3.4.1. The impact of photo-induced conversion of Tyr to Gly on the conformational stability of IgG4-Fc.

Three Tyr residues in IgG4-Fc, Tyr³⁰⁰, Tyr³⁷³, and Tyr⁴³⁶, were representatively mutated to Gly, to investigate the impact of photo-induced transformation of Tyr to Gly on the physical stability of IgG4-Fc. We observed reduced conformational stability for Y373G and Y436G, but not for Y300G, evaluated by DSC and intrinsic fluorescence spectroscopy (Fig. 1 and Table 1). However, based on our MS analysis, the mutant Y300G contains a larger fraction of bulky glycoforms (i.e., Man₁₂-Man₁₆; Table S1). The presence of bulkier glycoforms may compensate for any loss of stability possibly resulting from Tyr³⁰⁰Gly mutation⁶³. The reduced thermal stability of Y373G and Y436G indicates that the photo-induced conversion of Tyr³⁷³ and Tyr⁴³⁶ into Gly can lead to destabilization of conformational structures of IgG4-Fc.

3.4.2. Thermal stability of WT, S375A, W381A, and S375A/W381A IgG4-Fc.

Upon photoirradiation, Trp³⁸¹ (Eu numbering⁶⁴⁻⁶⁵) in IgG4-Fc¹⁶ and IgG1⁶ can be photoionized, resulting in the loss of the indole side chain, and convert to Gly and several peptide backbone cleavage products. Therefore, we evaluated the effect of such degradation on physical properties utilizing IgG4-Fc as model protein. An atypical O-glycosylation at Ser³⁷⁵ was detected in the Trp³⁸¹ mutants, W381A and W381G IgG4-Fc, and to evaluate the impact of O-glycans, S375A and the S375A/W381A mutants were prepared. During the production of W381A and W381G, the expression yields of W381A were significantly higher than of the W381G mutant. Hence, W381A was selected for some of the biophysical experiments requiring larger amounts of protein.

The thermal unfolding of IgG4-Fc was monitored by DSC, and the thermograms were fit to two or three transitions depending on the IgG4-Fc variants^{17,66}. WT IgG4-Fc presents a similar thermal stability of the C_{H2} domain as IgG4-Fc¹⁷, but an approximate 10°C reduction of T_{m2}¹⁷, corresponding to the unfolding of the C_{H3} domain¹⁷ (Table 2). The reduced thermal stability of the C_{H3} domain in IgG4-Fc can be explained by the weak C_{H3}-C_{H3} interactions^{53,67-68}, which are about three orders of magnitude weaker⁶⁹ as compared to IgG1-Fc.

The DSC and intrinsic fluorescence thermograms (10-90°C) of W381A and S375A/W381A are similar and reveal no thermal transitions, indicating that the overall conformation and tertiary structures are disrupted by the mutation of Trp³⁸¹ to Ala³⁸¹. Trp³⁸¹ sits in the hydrophobic core of C_{H3} domain, and the loss of the hydrophobic side chain leads to reduced protein conformational stability. A similar observation was reported for a four-helix-bundle protein, Rop, where the unpacking of its hydrophobic core caused not only the loss of protein activity but decreased protein stability⁷⁰. Additionally, the C_{H3}-C_{H3} interaction is critical for the assembly of the Fc domain⁶⁹, and, therefore, disruption of the inter-chain C_{H3} interactions can perturb the folding of the overall IgG4-Fc. The reduced thermal stability of proteins can potentially lead to increased aggregation propensity⁷¹, shorter shelf-life⁷²⁻⁷³, and safety issues⁷².

3.4.2.1. Backbone flexibility of WT and W381A IgG4-Fc.

Changes in protein conformation can potentially accompany in changes in the backbone flexibility

of proteins. Therefore, the backbone flexibilities of WT and W381A were evaluated by HX MS analysis. Deuteration controls were prepared with denatured WT and W381A, and display a maximum of 100 -110 Da mass increase due to deuterium incorporation. This value can be utilized to calculate the fraction of deuteration of native WT and W381A. W381A reaches full deuteration (~96 -100%) within 12500 s exposure to D₂O, whereas, WT achieves only 87.83 -89.46% deuteration even at 62500 s. Therefore, W381A possesses much higher backbone flexibility than WT IgG4-Fc. On the other hand, W381A does not reach full deuteration at the initial time point, indicating that it is not completely unstructured. These data are consistent with our FTIR analysis (Fig. 5), revealing that W381A and WT IgG4-Fc display similar amounts of secondary structure, where β -sheet shows the highest abundance (Fig S7).

3.4.2.2. The effects of N-glycans on thermal stability.

N-glycans at Asn²⁹⁷ in IgGs are critical for their thermal stability, particularly for the C_H2 domain of Fc¹⁷. Hence, the effects of N-glycans on the thermal stability of WT, S375A, W381A, and S375A/W381A IgG4-Fc were examined. PNGase F was utilized to release N-glycans from these IgG4-Fc variants, to obtain WT_degly, S375A_degly, W381A_degly, and S375A/W381A_degly IgG4-Fc. The DSC thermograms of WT_degly and S375A_degly IgG4-Fc present three transitions. For comparison, we fitted also the DSC thermograms of WT and S375A to three transitions, and derived T_{m1}, T_{m2} and T_{m3} (Table 2). As expected¹⁸, the removal of N-glycans reduced thermal stability of WT IgG4-Fc. However, the removal of N-glycans did not modify the thermal stability of S375A IgG4-Fc, indicating a possible interaction of the O-glycan at Ser³⁷⁵ with the N-glycan at

Asn²⁹⁷. W381A, S375A/W381A, and W381A_degly, S375A/W381A_degly (Chart 1 and 2) reveal no thermal transitions independent of the presence of N-glycans or O-glycans (Fig. 3 and 4), indicating that the Trp³⁸¹Ala mutation results in the loss of conformation. It must be pointed out that PNGase F dependent deglycosylation of Asn²⁹⁷ yields Asp²⁹⁷, introducing a negative charge⁷⁴ at residue 297, which may affect protein structure.

3.4.3. The impact of photo-induced conversion of Trp and Tyr on binding kinetics and equilibria with FcγRIIIA.

We evaluated the impact of light-induced conversion of Tyr to Gly on the affinity of IgG4-Fc to FcγRIIIA. We also evaluated the W381A mutant instead of W381G as the expression yields of W381A were sufficiently high to generate sufficient material for the binding experiments. As both W381A and W381G showed no significant thermal transition during DSC experiment, we concluded that the W381A mutant was a viable substitute for W381G in the receptor binding experiments. FcγRIIIA binds with the lower hinge and hinge-proximal C_H2 domain of IgG-Fc in a 1:1 stoichiometry⁷⁵. Interestingly, our BLI sensorgrams could not be fitted with monoexponential kinetics (Fig. 10 and Fig. S10). On close inspection of the literature⁷⁶, we found references^{77,78} which did not show simple mono-exponential binding kinetics of IgG to FcγR. This can be rationalized in various ways. First, our FcγRIIIA may be heterogeneous, e.g. distinct receptor populations at the biosensor surface resulting from immobilization⁷⁸. In addition, the two N-linked glycosylation sites at Asn¹⁶² and Asn⁴⁵ of FcγRIIIA may present distinct glycoforms^{79-80,81-82}. The literature shows that the binding between Fc and FcγRIIIa involves carbohydrate-carbohydrate

interactions, which require unique glycoforms of both proteins to achieve high affinity⁷³. Second, IgG4-Fc is expressed with various glycans at Asn²⁹⁷ (see Table S1)⁸³. The glycosylation at Asn²⁹⁷ in the C_{H2} domain has shown not only to affect the affinity of mAbs to FcγRIIIA but also the binding kinetics⁸⁴. Third, the presence of low levels of impurities of IgG4-Fc, e.g., ca. 2% of aggregates of mAbs, can affect binding kinetics with FcγRIIIA⁷⁸. Fourth, the sensorgrams may contain elements of non-specific reversible association in IgG4-Fc as a function of increased protein concentration. To minimize potential nonspecific binding, a 1 mg/mL BSA additive was supplemented to the running buffers and sample solutions. All the above conditions can lead to heterogeneous binding, resulting in two or more phases of association events. Thus, to achieve a better fit and more accurate results, a two-phase exponential association model was utilized to derive the k_{on} and k_{off} values for a slow and a fast phase. Here, we reported values for the fast phase based on previous knowledge⁶² of the specific binding between Fc and FcγRIIIA. Overall, Y300G and W381A display up to 10-fold reduced affinity to FcγRIIIA as compared to WT. The reduced binding affinity can be due to different reasons. Tyr³⁰⁰ residue is located in the upper C_{H2} domain adjacent to the N-glycosylated site at Asn²⁹⁷, potentially participating in interaction with FcγRIIIA⁸⁵⁻⁸⁶. The mutation Trp³⁸¹Ala causes a loss of conformation of IgG4-Fc, which may perturb the potential structural interface, or orientations of the Fc domains, critical for affinity to FcγRIIIA⁸⁷. Y436G presents relative high k_{on} and k_{off} values, which, overall, result in an 8-fold increase in K_D compared to WT, and thus weaker binding affinity. In addition, Tyr⁴³⁶ is part of a common ‘consensus’ sequence of the C_{H2}-C_{H3} interface to interact with FcRn⁸⁸, which is crucial to protect mAbs from lysosomal degradation and to maintain long serum half-life.

3.4.4. O-glycosylation at Ser³⁷⁵ in W381A and W381G IgG4-Fc.

We initially prepared the mutants W381A and W381G IgG4-Fc to evaluate the effect of Trp side chain cleavage on biophysical stability. The biophysical analysis of W381A and W381G IgG4-Fc reveals a perturbation of overall thermal stability (Fig. 3 and Fig. S6). Moreover, the expression yields of W381G were very low, suggesting that W381G is potentially even less stable than W381A⁸⁹. The lower stability would be consistent with the ca. 15% higher level of O-glycosylation at Ser³⁷⁵ in W381G as compared to W381A (Fig. S12). Since W381A was expressed with higher yields, it was selected for further production and characterization.

IgG4-Fc variants were produced in the *pno1/och1* KO and STT3D added *Pichia pastoris* yeast strain. Several IgG-Fc subtypes, e.g., IgG1-Fc⁴⁹ and IgG3-Fc⁹⁰, were previously expressed from the same system, showing <10% O-glycosylation. We obtained similar results with IgG4-Fc, displaying approximate 8.1% O-glycosylation in WT IgG4-Fc. However, the mutation of Trp³⁸¹ to Ala³⁸¹ in the C_H3 domain of IgG4-Fc leads to a surprising increase of up to 61% O-glycosylation at Ser³⁷⁵, which was confirmed by mass spectrometry analysis: (1) the identification of two major peaks in the mass spectra of W381A_degly (Fig. S3) is consistent with the presence of N-deglycosylated and O-glycosylated forms, respectively. Here, the O-glycosylated form is indicated by a mass addition of 162⁹¹⁻⁹²; (2) peptide mapping of W381A identifies Ser³⁷⁵ as the major O-glycosylated site (Fig.2); (3) the O-glycosylated form is removed in S375A/W381A_degly IgG4-Fc (Fig. S3).

O-linked glycosylation at Ser³⁷⁵ does not appear to cause the structural alterations, but occurs more easily when the structure of IgG4-Fc is perturbed, e.g., in W381A and W381G. This is particularly consistent with the observation of Neubert et al., who mapped the O-mannose glycoproteome in *Saccharomyces cerevisiae*³⁹, where O-linked mannosylation was more favored in unstructured regions and β -strands. Alternatively, protein O-mannosyltransferases can participate in protein folding quality control as a part of unfolded protein O-mannosylation (UPOM), which may explain that W381A and W381G are better substrates for O-mannosylation than the more stable WT, and reveal a higher level of O-mannose⁹³.

3.4.5. Photostability of WT, S375A, W381A, and S375A/W381A IgG4-Fc. During photo-irradiation, the formation of different photo-products can result from distinct reaction pathways. For example, the side chain fragmentation of Tyr is induced by electron transfer from Tyr to a radical cation, Trp⁺, generated by photo-ionization of Trp.¹⁶ The yield of the respective photo-products can therefore, be affected by the mutation of Trp and conformational alterations changing the distance between Tyr and Trp⁺. As such, photo-products from the side chain fragmentation of Tyr reveal a 2.6-13.5 fold reduction of yields in W381A and S375A/W381A (Fig. 7) compared to WT and S375A. The higher susceptibility of photo-degradation at Trp³¹³ and Trp⁴¹⁷ to photo-degradation in W381A, S375A/W381A, W381A_degly, and S375A/W381A_degly is likely due to the fact that Trp³⁸¹ is deleted in these mutant leading to preferred light absorption of other Trp residues, e.g., Trp³¹³ and Trp⁴¹⁷. In parallel, the increased susceptibility of Trp³¹³ and Trp⁴¹⁷ to

photo-degradation leads to an increase in photo-induced electron transfer to disulfide bonds containing Cys³²¹, Cys³⁶⁷, and Cys⁴²⁵, resulting higher vinyl Cys formation from Cys³²¹, Cys³⁶⁷, and Cys⁴²⁵.

With regard to the effect of glycans on photostability, O-glycosylation does not significantly affect the yield of photoproducts, evident from a comparison of W381A and S375A/W381A. This is likely due to the fact that the mutation of Trp to Ala has a more significant impact on photo-degradation, leading to unfolding, to which O-glycosylation, does not add much. Alternatively, the size of O-mannose is small, which does not significantly modify the structure. The presence of N-glycans, on the other hand, does play a role in the yield of photo-products. Similar observations were documented regarding IgG1-Fc⁸.

3.5. Conclusions

The present paper elucidates the impact of photo-induced Tyr and Trp side chain fragmentation on the physico-chemical stability and receptor binding of IgG4-Fc, and the effect of N- vs O-glycans on product formation. Surprisingly, the side chain cleavage of Trp³⁸¹, represented by W381G and W381A, causes a conformational perturbation of both the C_H2 and C_H3 domains of IgG4-Fc. Moreover, W381A and W381G reveal significantly enriched atypical O-glycosylation at Ser³⁷⁵. The fragmentation of Tyr side chain results in reduced thermal stability, and decreased receptor binding affinity to FcγRIIIA. These findings help elucidate photo-induced inactivation,

fragmentation and physical instability in protein therapeutics.

3.6. Acknowledgements

We gratefully acknowledge support of H.K. by a Graduate Fellowship from the Genentech Foundation.

3.7. Associated content

Fig. S1. Mass spectrometry analysis of (A) Y300G_degly, Y373G_degly, Y436G_degly and (B) Y300G, Y373G, Y436G after reduction with DTT.

Fig. S2. MS analysis of WT, S375A, W381A, and S375A/W381A IgG4-Fc after chemical reduction of disulfides.

Fig. S3. MS analysis of WT_degly, S375A_degly, W381A_degly, and S375A/W381A_degly IgG4-Fc after chemical reduction of disulfides.

Fig. S4. SDS-PAGE analysis of WT, S375A, W381A, and S375A/W381A, glycosylated proteins were run under reducing conditions; deglycosylated proteins were run under nonreducing conditions.

Fig. S5. Chromatogram of proteolytic digest of W381A IgG4-Fc analyzed with HPLC-MS/MS. Peak 1 contains the O-linked glycosylated peptide, MTKNQVSLTC(+57)LVKGFYPS³⁷⁵(+162) DIAVE (m/z 921.47). Peak 2 contains the nonglycosylated peptide, MTKNQVSLTC(+57)LV KGFYPS³⁷⁵DIAVE (m/z 867.45).

Fig. S6. Thermal stability of (A) WT, W381G, and W381A, and (B) chemical rescue with indole.

Fig. S7. Relative percentage of individual secondary structures of WT, S375A, W381A, and S375A/W381A, glycosylated and deglycosylated, analyzed by FTIR.

Fig. S8. Representative DSC thermograms of W381F. The corresponding T_m values are displayed.

Fig. S9. Dityrosine detection of WT, Y300G, Y373G, Y436G and W381A by exciting photo-irradiated IgG4-Fc at 320 nm and fluorescence emission scan from 371 – 500 nm. Photo-irradiation was performed at $\lambda_{max}=305$ nm for 45 min.

Fig. S10. BLI association of (A) Y373G and Fc γ RIII A, (B) Y436G and Fc γ RIII A, (C) W381A and Fc γ RIII A in PBS kinetic buffer (pH 7.4), where the red line corresponds to two-phase exponential association fit, and the blue dots correspond to experimental data points.

Fig. S11. Plot of k_{obs} of the slow phase as a function of concentrations of the IgG4-Fc variants, WT, Y373G, and Y300G. The error bars represent the standard error from three independent measurements. Y373G and W381A were not shown due to the absence of linear relationship between k_{obs} of their slow phase and protein concentrations.

Fig. S12. The presence of O-linked glycosylation (%) in W381G, W381A, and WT IgG4-Fc characterized by HPLC-MS analysis.

Table S1. Relative abundance (in %) of different glycoforms of Y300G, Y373G, and Y436G IgG4-Fc.

Table S2. Theoretical and observed masses of glycosylated WT, S375A, W381A, and S375A/W381A, and the N-deglycosylated variants WT_degly, S375A_degly, W381A_degly, and S375A/W381A_degly under reducing conditions.

3.8. References.

1. Mallaney, M.; Wang, S. H.; Sreedhara, A., Effect of ambient light on monoclonal antibody product quality during small-scale mammalian cell culture process in clear glass bioreactors. *Biotechnol Prog* **2014**, *30* (3), 562-70.
2. Sreedhara, A.; Yin, J.; Joyce, M.; Lau, K.; Weckslar, A. T.; Deperalta, G.; Yi, L.; John Wang, Y.; Kabakoff, B.; Kishore, R. S., Effect of ambient light on IgG1 monoclonal antibodies during drug product processing and development. *Eur J Pharm Biopharm* **2016**, *100*, 38-46.
3. Fradkin, A. H.; Mozziconacci, O.; Schöneich, C.; Carpenter, J. F.; Randolph, T. W., UV photodegradation of murine growth hormone: chemical analysis and immunogenicity consequences. *Eur J Pharm Biopharm* **2014**, *87* (2), 395-402.
4. Bessa, J.; Boeckle, S.; Beck, H.; Buckel, T.; Schlicht, S.; Ebeling, M.; Kiialainen, A.; Koulov, A.; Boll, B.; Weiser, T.; Singer, T.; Rolink, A. G.; Iglesias, A., The immunogenicity of antibody aggregates in a novel transgenic mouse model. *Pharm Res* **2015**, *32* (7), 2344-59.
5. Boll, B.; Bessa, J.; Folzer, E.; Rios Quiroz, A.; Schmidt, R.; Bulau, P.; Finkler, C.; Mahler, H. C.; Huwyler, J.; Iglesias, A.; Koulov, A. V., Extensive Chemical Modifications in the Primary Protein Structure of IgG1 Subvisible Particles Are Necessary for Breaking Immune Tolerance. *Mol Pharm* **2017**, *14* (4), 1292-1299.
6. Haywood, J.; Mozziconacci, O.; Allegre, K. M.; Kerwin, B. A.; Schöneich, C., Light-induced conversion of Trp to Gly and Gly hydroperoxide in IgG1. *Mol Pharm* **2013**, *10* (3), 1146-50.
7. Mozziconacci, O.; Schöneich, C., Effect of conformation on the photodegradation of Trp- and cystine-containing cyclic peptides: octreotide and somatostatin. *Mol Pharm* **2014**, *11* (10), 3537-46.
8. Mozziconacci, O.; Okbazghi, S.; More, A. S.; Volkin, D. B.; Tolbert, T.; Schöneich, C., Comparative Evaluation of the Chemical Stability of 4 Well-Defined Immunoglobulin G1-Fc Glycoforms. *J Pharm Sci* **2016**, *105* (2), 575-587.
9. Steinmann, D.; Mozziconacci, O.; Bommana, R.; Stobaugh, J. F.; Wang, Y. J.; Schöneich, C., Photodegradation Pathways of Protein Disulfides: Human Growth Hormone. *Pharm Res* **2017**, *34* (12), 2756-2778.
10. Bane, J.; Mozziconacci, O.; Yi, L.; Wang, Y. J.; Sreedhara, A.; Schöneich, C., Photo-oxidation of IgG1 and Model Peptides: Detection and Analysis of Triply Oxidized His and Trp Side Chain Cleavage Products. *Pharm Res* **2017**, *34* (1), 229-242.
11. Heringa, J.; Argos, P., Side-chain clusters in protein structures and their role in protein folding. *J Mol Biol* **1991**, *220* (1), 151-71.
12. Jonasson, P.; Aronsson, G.; Carlsson, U.; Jonsson, B. H., Tertiary structure formation at specific tryptophan side chains in the refolding of human carbonic anhydrase II. *Biochemistry* **1997**, *36* (17), 5142-8.
13. Chang, Y.; Zajicek, J.; Castellino, F. J., Role of tryptophan-63 of the kringle 2 domain of tissue-type plasminogen activator in its thermal stability, folding, and ligand binding properties. *Biochemistry* **1997**, *36* (25), 7652-63.

14. Samanta, U.; Pal, D.; Chakrabarti, P., Environment of tryptophan side chains in proteins. *Proteins* **2000**, *38* (3), 288-300.
15. Kaiser, C. E.; Rincon Pabon, J. P.; Khowsathit, J.; Castaldi, M. P.; Kazmirski, S. L.; Weis, D. D.; Zhang, A. X.; Karanicolas, J., Modulating Antibody Structure and Function through Directed Mutations and Chemical Rescue. *ACS Synth Biol* **2018**, *7* (4), 1152-1162.
16. Kang, H.; Tolbert, T. J.; Schöneich, C., Photo-induced tyrosine side chain fragmentation in IgG4-Fc: mechanisms and solvent isotope effects. *Mol Pharm* **2018**.
17. More, A. S.; Toprani, V. M.; Okbazghi, S. Z.; Kim, J. H.; Joshi, S. B.; Middaugh, C. R.; Tolbert, T. J.; Volkin, D. B., Correlating the Impact of Well-Defined Oligosaccharide Structures on Physical Stability Profiles of IgG1-Fc Glycoforms. *J Pharm Sci* **2016**, *105* (2), 588-601.
18. Zheng, K.; Bantog, C.; Bayer, R., The impact of glycosylation on monoclonal antibody conformation and stability. *MAbs* **2011**, *3* (6), 568-76.
19. Golay, J.; Da Roit, F.; Bologna, L.; Ferrara, C.; Leusen, J. H.; Rambaldi, A.; Klein, C.; Introna, M., Glycoengineered CD20 antibody obinutuzumab activates neutrophils and mediates phagocytosis through CD16B more efficiently than rituximab. *Blood* **2013**, *122* (20), 3482-91.
20. Robak, T., GA-101, a third-generation, humanized and glyco-engineered anti-CD20 mAb for the treatment of B-cell lymphoid malignancies. *Curr Opin Investig Drugs* **2009**, *10* (6), 588-96.
21. Lagasse, H. A.; Alexaki, A.; Simhadri, V. L.; Katagiri, N. H.; Jankowski, W.; Sauna, Z. E.; Kimchi-Sarfaty, C., Recent advances in (therapeutic protein) drug development. *F1000Res* **2017**, *6*, 113.
22. Usmani, S. S.; Bedi, G.; Samuel, J. S.; Singh, S.; Kalra, S.; Kumar, P.; Ahuja, A. A.; Sharma, M.; Gautam, A.; Raghava, G. P. S., THPdb: Database of FDA-approved peptide and protein therapeutics. *PLoS One* **2017**, *12* (7), e0181748.
23. Werner, R. G.; Kopp, K.; Schlueter, M., Glycosylation of therapeutic proteins in different production systems. *Acta Paediatr* **2007**, *96* (455), 17-22.
24. Zheng, K.; Yarmarkovich, M.; Bantog, C.; Bayer, R.; Patapoff, T. W., Influence of glycosylation pattern on the molecular properties of monoclonal antibodies. *MAbs* **2014**, *6* (3), 649-58.
25. Spiro, R. G., Protein glycosylation: nature, distribution, enzymatic formation, and disease implications of glycopeptide bonds. *Glycobiology* **2002**, *12* (4), 43R-56R.
26. Apweiler, R.; Hermjakob, H.; Sharon, N., On the frequency of protein glycosylation, as deduced from analysis of the SWISS-PROT database. *Biochim Biophys Acta* **1999**, *1473* (1), 4-8.
27. Cymer, F.; Beck, H.; Rohde, A.; Reusch, D., Therapeutic monoclonal antibody N-glycosylation - Structure, function and therapeutic potential. *Biologicals* **2018**, *52*, 1-11.
28. Higel, F.; Seidl, A.; Sorgel, F.; Friess, W., N-glycosylation heterogeneity and the influence on structure, function and pharmacokinetics of monoclonal antibodies and Fc fusion proteins. *Eur J Pharm Biopharm* **2016**, *100*, 94-100.

29. Yamaguchi, Y.; Nishimura, M.; Nagano, M.; Yagi, H.; Sasakawa, H.; Uchida, K.; Shitara, K.; Kato, K., Glycoform-dependent conformational alteration of the Fc region of human immunoglobulin G1 as revealed by NMR spectroscopy. *Biochim Biophys Acta* **2006**, *1760* (4), 693-700.
30. Bieberich, E., Synthesis, Processing, and Function of N-glycans in N-glycoproteins. *Adv Neurobiol* **2014**, *9*, 47-70.
31. Kaneko, Y.; Nimmerjahn, F.; Ravetch, J. V., Anti-inflammatory activity of immunoglobulin G resulting from Fc sialylation. *Science* **2006**, *313* (5787), 670-3.
32. Thomann, M.; Reckermann, K.; Reusch, D.; Prasser, J.; Tejada, M. L., Fc-galactosylation modulates antibody-dependent cellular cytotoxicity of therapeutic antibodies. *Mol Immunol* **2016**, *73*, 69-75.
33. Okbazghi, S. Z.; More, A. S.; White, D. R.; Duan, S.; Shah, I. S.; Joshi, S. B.; Middaugh, C. R.; Volkin, D. B.; Tolbert, T. J., Production, Characterization, and Biological Evaluation of Well-Defined IgG1 Fc Glycoforms as a Model System for Biosimilarity Analysis. *J Pharm Sci* **2016**, *105* (2), 559-74.
34. Liu, H.; Bulseco, G. G.; Sun, J., Effect of posttranslational modifications on the thermal stability of a recombinant monoclonal antibody. *Immunol Lett* **2006**, *106* (2), 144-53.
35. Kayser, V.; Chennamsetty, N.; Voynov, V.; Forrer, K.; Helk, B.; Trout, B. L., Glycosylation influences on the aggregation propensity of therapeutic monoclonal antibodies. *Biotechnol J* **2011**, *6* (1), 38-44.
36. Zhang, T.; Song, X.; Xu, L.; Ma, J.; Zhang, Y.; Gong, W.; Zhang, Y.; Zhou, X.; Wang, Z.; Wang, Y.; Shi, Y.; Bai, H.; Liu, N.; Yang, X.; Cui, X.; Cao, Y.; Liu, Q.; Song, J.; Li, Y.; Tang, Z.; Guo, M.; Wang, L.; Li, K., The binding of an anti-PD-1 antibody to Fcγ3b has a profound impact on its biological functions. *Cancer Immunol Immunother* **2018**, *67* (7), 1079-1090.
37. Scapin, G.; Yang, X.; Prosser, W. W.; McCoy, M.; Reichert, P.; Johnston, J. M.; Kashi, R. S.; Strickland, C., Structure of full-length human anti-PD1 therapeutic IgG4 antibody pembrolizumab. *Nat Struct Mol Biol* **2015**, *22* (12), 953-8.
38. Darula, Z.; Medzihradzky, K. F., Analysis of Mammalian O-Glycopeptides-We Have Made a Good Start, but There is a Long Way to Go. *Mol Cell Proteomics* **2018**, *17* (1), 2-17.
39. Neubert, P.; Halim, A.; Zausser, M.; Essig, A.; Joshi, H. J.; Zatorska, E.; Larsen, I. S.; Loibl, M.; Castells-Ballester, J.; Aebi, M.; Clausen, H.; Strahl, S., Mapping the O-Mannose Glycoproteome in *Saccharomyces cerevisiae*. *Mol Cell Proteomics* **2016**, *15* (4), 1323-37.
40. Nishikawa, I.; Nakajima, Y.; Ito, M.; Fukuchi, S.; Homma, K.; Nishikawa, K., Computational prediction of O-linked glycosylation sites that preferentially map on intrinsically disordered regions of extracellular proteins. *Int J Mol Sci* **2010**, *11* (12), 4991-5008.
41. Liu, H.; Ponniah, G.; Zhang, H. M.; Nowak, C.; Neill, A.; Gonzalez-Lopez, N.; Patel, R.; Cheng, G.; Kita, A. Z.; Andrien, B., In vitro and in vivo modifications of recombinant and human IgG antibodies. *MAbs* **2014**, *6* (5), 1145-54.
42. Plomp, R.; Dekkers, G.; Rombouts, Y.; Visser, R.; Koeleman, C. A.; Kammeijer, G. S.; Jansen, B. C.; Rispen, T.; Hensbergen, P. J.; Vidarsson, G.; Wuhrer, M., Hinge-Region O-

- Glycosylation of Human Immunoglobulin G3 (IgG3). *Mol Cell Proteomics* **2015**, *14* (5), 1373-84.
43. Valliere-Douglass, J. F.; Brady, L. J.; Farnsworth, C.; Pace, D.; Balland, A.; Wallace, A.; Wang, W.; Treuheit, M. J.; Yan, B., O-fucosylation of an antibody light chain: characterization of a modification occurring on an IgG1 molecule. *Glycobiology* **2009**, *19* (2), 144-52.
 44. Martinez, T.; Pace, D.; Brady, L.; Gerhart, M.; Balland, A., Characterization of a novel modification on IgG2 light chain. Evidence for the presence of O-linked mannosylation. *J Chromatogr A* **2007**, *1156* (1-2), 183-7.
 45. Choi, B. K.; Bobrowicz, P.; Davidson, R. C.; Hamilton, S. R.; Kung, D. H.; Li, H.; Miele, R. G.; Nett, J. H.; Wildt, S.; Gerngross, T. U., Use of combinatorial genetic libraries to humanize N-linked glycosylation in the yeast *Pichia pastoris*. *Proc Natl Acad Sci U S A* **2003**, *100* (9), 5022-7.
 46. Loo, T.; Patchett, M. L.; Norris, G. E.; Lott, J. S., Using secretion to solve a solubility problem: High yield expression in *Escherichia coli* and purification of the bacterial glycoamidase PNGase F. *Protein Expres Purif* **2002**, *24* (1), 90-98.
 47. Wei, Y.; Larson, N. R.; Angalakurthi, S. K.; Russell Middaugh, C., Improved Fluorescence Methods for High-Throughput Protein Formulation Screening. *SLAS TECHNOLOGY: Translating Life Sciences Innovation* **2018**, 2472630318780620.
 48. Kong, J.; Yu, S., Fourier transform infrared spectroscopic analysis of protein secondary structures. *Acta Biochim Biophys Sin (Shanghai)* **2007**, *39* (8), 549-59.
 49. More, A. S.; Toth, R. T. t.; Okbazghi, S. Z.; Middaugh, C. R.; Joshi, S. B.; Tolbert, T. J.; Volkin, D. B.; Weis, D. D., Impact of Glycosylation on the Local Backbone Flexibility of Well-Defined IgG1-Fc Glycoforms Using Hydrogen Exchange-Mass Spectrometry. *J Pharm Sci* **2018**, *107* (9), 2315-2324.
 50. Hatchard, C. G.; Parker, C. A., A New Sensitive Chemical Actinometer .2. Potassium Ferrioxalate as a Standard Chemical Actinometer. *Proc R Soc Lon Ser-A* **1956**, *235* (1203), 518-536.
 51. Lee, J.; Seliger, H. H., Quantum Yield of Ferrioxalate Actinometer. *J Chem Phys* **1964**, *40* (2), 519-&.
 52. Quality of biotechnological products: stability testing of biotechnological/biological products. Annex to the ICH Harmonised Tripartite Guideline for the Stability Testing of New Drug Substances and Products. *Dev Biol Stand* **1998**, *93*, 211-9.
 53. Rispens, T.; Ooijevaar-de Heer, P.; Bende, O.; Aalberse, R. C., Mechanism of immunoglobulin G4 Fab-arm exchange. *J Am Chem Soc* **2011**, *133* (26), 10302-11.
 54. Silva, J. P.; Vetterlein, O.; Jose, J.; Peters, S.; Kirby, H., The S228P mutation prevents in vivo and in vitro IgG4 Fab-arm exchange as demonstrated using a combination of novel quantitative immunoassays and physiological matrix preparation. *J Biol Chem* **2015**, *290* (9), 5462-9.
 55. Deckert, K.; Budiardjo, S. J.; Brunner, L. C.; Lovell, S.; Karanicolas, J., Designing allosteric control into enzymes by chemical rescue of structure. *J Am Chem Soc* **2012**, *134* (24), 10055-

- 60.
56. Heinecke, J. W.; Li, W.; Daehnke, H. L., 3rd; Goldstein, J. A., Dityrosine, a specific marker of oxidation, is synthesized by the myeloperoxidase-hydrogen peroxide system of human neutrophils and macrophages. *J Biol Chem* **1993**, *268* (6), 4069-77.
 57. Pan, H.; Chen, K.; Chu, L.; Kinderman, F.; Apostol, I.; Huang, G., Methionine oxidation in human IgG2 Fc decreases binding affinities to protein A and FcRn. *Protein Sci* **2009**, *18* (2), 424-33.
 58. Liu, D.; Ren, D.; Huang, H.; Dankberg, J.; Rosenfeld, R.; Cocco, M. J.; Li, L.; Brems, D. N.; Remmele, R. L., Jr., Structure and stability changes of human IgG1 Fc as a consequence of methionine oxidation. *Biochemistry* **2008**, *47* (18), 5088-100.
 59. Grunwald, C.; Kuhlmann, J.; Woll, C., In deuterated water the unspecific adsorption of proteins is significantly slowed down: results of an SPR study using model organic surfaces. *Langmuir* **2005**, *21* (20), 9017-9.
 60. Robelek, R.; Wegener, J., Label-free and time-resolved measurements of cell volume changes by surface plasmon resonance (SPR) spectroscopy. *Biosens Bioelectron* **2010**, *25* (5), 1221-4.
 61. Hayes, J. M.; Frostell, A.; Karlsson, R.; Muller, S.; Martin, S. M.; Pauers, M.; Reuss, F.; Cosgrave, E. F.; Anneren, C.; Davey, G. P.; Rudd, P. M., Identification of Fc Gamma Receptor Glycoforms That Produce Differential Binding Kinetics for Rituximab. *Mol Cell Proteomics* **2017**, *16* (10), 1770-1788.
 62. Vidarsson, G.; Dekkers, G.; Rispens, T., IgG subclasses and allotypes: from structure to effector functions. *Front Immunol* **2014**, *5*, 520.
 63. Rose, R. J.; van Berkel, P. H.; van den Bremer, E. T.; Labrijn, A. F.; Vink, T.; Schuurman, J.; Heck, A. J.; Parren, P. W., Mutation of Y407 in the CH3 domain dramatically alters glycosylation and structure of human IgG. *MAbs* **2013**, *5* (2), 219-28.
 64. Edelman, G. M.; Cunningham, B. A.; Gall, W. E.; Gottlieb, P. D.; Rutishauser, U.; Waxdal, M. J., The covalent structure of an entire gammaG immunoglobulin molecule. *Proc Natl Acad Sci U S A* **1969**, *63* (1), 78-85.
 65. Sandrine Béranger, C. M.-J., Fatena Bellahcene and Marie-Paule Lefranc Correspondence between the IMGT unique numbering for C-DOMAIN, the IMGT exon numbering, the Eu and Kabat numberings: Human IGHG. http://www.imgt.org/IMGTScientificChart/Numbering/Hu_IGHGnber.html.
 66. Jung, S. K.; Lee, K. H.; Jeon, J. W.; Lee, J. W.; Kwon, B. O.; Kim, Y. J.; Bae, J. S.; Kim, D. I.; Lee, S. Y.; Chang, S. J., Physicochemical characterization of Remsima. *MAbs* **2014**, *6* (5), 1163-77.
 67. van der Neut Kolfschoten, M.; Schuurman, J.; Losen, M.; Bleeker, W. K.; Martinez-Martinez, P.; Vermeulen, E.; den Bleker, T. H.; Wiegman, L.; Vink, T.; Aarden, L. A.; De Baets, M. H.; van de Winkel, J. G.; Aalberse, R. C.; Parren, P. W., Anti-inflammatory activity of human IgG4 antibodies by dynamic Fab arm exchange. *Science* **2007**, *317* (5844), 1554-7.
 68. Ishikawa, T.; Ito, T.; Endo, R.; Nakagawa, K.; Sawa, E.; Wakamatsu, K., Influence of pH on heat-induced aggregation and degradation of therapeutic monoclonal antibodies. *Biol Pharm*

- Bull* **2010**, *33* (8), 1413-7.
69. Rispens, T.; Davies, A. M.; Ooijevaar-de Heer, P.; Absalah, S.; Bende, O.; Sutton, B. J.; Vidarsson, G.; Aalberse, R. C., Dynamics of inter-heavy chain interactions in human immunoglobulin G (IgG) subclasses studied by kinetic Fab arm exchange. *J Biol Chem* **2014**, *289* (9), 6098-109.
 70. Munson, M.; Balasubramanian, S.; Fleming, K. G.; Nagi, A. D.; OBrien, R.; Sturtevant, J. M.; Regan, L., What makes a protein a protein? Hydrophobic core designs that specify stability and structural properties. *Protein Science* **1996**, *5* (8), 1584-1593.
 71. Brader, M. L.; Estey, T.; Bai, S.; Alston, R. W.; Lucas, K. K.; Lantz, S.; Landsman, P.; Maloney, K. M., Examination of thermal unfolding and aggregation profiles of a series of developable therapeutic monoclonal antibodies. *Mol Pharm* **2015**, *12* (4), 1005-17.
 72. Telikepalli, S. N.; Kumru, O. S.; Kalonia, C.; Esfandiary, R.; Joshi, S. B.; Middaugh, C. R.; Volkin, D. B., Structural characterization of IgG1 mAb aggregates and particles generated under various stress conditions. *J Pharm Sci* **2014**, *103* (3), 796-809.
 73. Laptos, T.; Omersel, J., The importance of handling high-value biologicals: Physico-chemical instability and immunogenicity of monoclonal antibodies. *Exp Ther Med* **2018**, *15* (4), 3161-3168.
 74. Tarentino, A. L.; Gomez, C. M.; Plummer, T. H., Jr., Deglycosylation of asparagine-linked glycans by peptide:N-glycosidase F. *Biochemistry* **1985**, *24* (17), 4665-71.
 75. Subedi, G. P.; Barb, A. W., The Structural Role of Antibody N-Glycosylation in Receptor Interactions. *Structure* **2015**, *23* (9), 1573-1583.
 76. Bruhns, P.; Iannascoli, B.; England, P.; Mancardi, D. A.; Fernandez, N.; Jorieux, S.; Daeron, M., Specificity and affinity of human Fcγ receptors and their polymorphic variants for human IgG subclasses. *Blood* **2009**, *113* (16), 3716-25.
 77. Derebe, M. G.; Nanjunda, R. K.; Gilliland, G. L.; Lacy, E. R.; Chiu, M. L., Human IgG subclass cross-species reactivity to mouse and cynomolgus monkey Fcγ receptors. *Immunol Lett* **2018**, *197*, 1-8.
 78. Dorion-Thibaudeau, J.; Raymond, C.; Lattova, E.; Perreault, H.; Durocher, Y.; De Crescenzo, G., Towards the development of a surface plasmon resonance assay to evaluate the glycosylation pattern of monoclonal antibodies using the extracellular domains of CD16a and CD64. *J Immunol Methods* **2014**, *408*, 24-34.
 79. Ferrara, C.; Stuart, F.; Sondermann, P.; Brunker, P.; Umana, P., The carbohydrate at FcγRIIIa Asn-162. An element required for high affinity binding to non-fucosylated IgG glycoforms. *J Biol Chem* **2006**, *281* (8), 5032-6.
 80. Shibata-Koyama, M.; Iida, S.; Okazaki, A.; Mori, K.; Kitajima-Miyama, K.; Saitou, S.; Kakita, S.; Kanda, Y.; Shitara, K.; Kato, K.; Satoh, M., The N-linked oligosaccharide at FcγRIIIa Asn-45: an inhibitory element for high FcγRIIIa binding affinity to IgG glycoforms lacking core fucosylation. *Glycobiology* **2009**, *19* (2), 126-34.
 81. Hayes, J. M.; Frostell, A.; Cosgrave, E. F.; Struwe, W. B.; Potter, O.; Davey, G. P.; Karlsson, R.; Anneren, C.; Rudd, P. M., Fcγ receptor glycosylation modulates the binding of IgG glycoforms: a requirement for stable antibody interactions. *J Proteome Res* **2014**, *13*

- (12), 5471-85.
82. Ferrara, C.; Grau, S.; Jager, C.; Sondermann, P.; Brunker, P.; Waldhauer, I.; Hennig, M.; Ruf, A.; Rufer, A. C.; Stihle, M.; Umana, P.; Benz, J., Unique carbohydrate-carbohydrate interactions are required for high affinity binding between Fcγ₃ and antibodies lacking core fucose. *Proc Natl Acad Sci U S A* **2011**, *108* (31), 12669-74.
 83. Jefferis, R.; Lund, J.; Pound, J. D., IgG-Fc-mediated effector functions: molecular definition of interaction sites for effector ligands and the role of glycosylation. *Immunol Rev* **1998**, *163*, 59-76.
 84. Kanda, Y.; Yamada, T.; Mori, K.; Okazaki, A.; Inoue, M.; Kitajima-Miyama, K.; Kuni-Kamochi, R.; Nakano, R.; Yano, K.; Kakita, S.; Shitara, K.; Satoh, M., Comparison of biological activity among nonfucosylated therapeutic IgG1 antibodies with three different N-linked Fc oligosaccharides: the high-mannose, hybrid, and complex types. *Glycobiology* **2007**, *17* (1), 104-118.
 85. Sondermann, P.; Huber, R.; Oosthuizen, V.; Jacob, U., The 3.2-A crystal structure of the human IgG1 Fc fragment-Fc γ₃ complex. *Nature* **2000**, *406* (6793), 267-73.
 86. Davies, A. M.; Rispen, T.; Ooijsaar-de Heer, P.; Gould, H. J.; Jefferis, R.; Aalberse, R. C.; Sutton, B. J., Structural determinants of unique properties of human IgG4-Fc. *J Mol Biol* **2014**, *426* (3), 630-44.
 87. Hanson, Q. M.; Barb, A. W., A perspective on the structure and receptor binding properties of immunoglobulin G Fc. *Biochemistry* **2015**, *54* (19), 2931-42.
 88. DeLano, W. L.; Ultsch, M. H.; de Vos, A. M.; Wells, J. A., Convergent solutions to binding at a protein-protein interface. *Science* **2000**, *287* (5456), 1279-83.
 89. Mezzasalma, T. M.; Kranz, J. K.; Chan, W.; Struble, G. T.; Schalk-Hihi, C.; Deckman, I. C.; Springer, B. A.; Todd, M. J., Enhancing recombinant protein quality and yield by protein stability profiling. *J Biomol Screen* **2007**, *12* (3), 418-28.
 90. Shah, I. S.; Lovell, S.; Mehzabeen, N.; Battaile, K. P.; Tolbert, T. J., Structural characterization of the Man₅ glycoform of human IgG3 Fc. *Mol Immunol* **2017**, *92*, 28-37.
 91. Gong, B.; Burnina, I.; Lynaugh, H.; Li, H., O-linked glycosylation analysis of recombinant human granulocyte colony-stimulating factor produced in glycoengineered *Pichia pastoris* by liquid chromatography and mass spectrometry. *J Chromatogr B Analyt Technol Biomed Life Sci* **2014**, *945-946*, 135-40.
 92. Neubert, P.; Strahl, S., Protein O-mannosylation in the early secretory pathway. *Curr Opin Cell Biol* **2016**, *41*, 100-8.
 93. Goder, V.; Melero, A., Protein O-mannosyltransferases participate in ER protein quality control. *J Cell Sci* **2011**, *124* (Pt 1), 144-53.

Table 1. Melting temperature (T_m) of Y300G, Y373G, and Y436G from DSC and fluorescence.

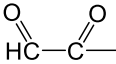
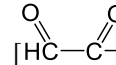
Experiments were conducted in triplicate.

	T_m1 (DSC)	T_m2 (DSC)	T_m (Fluorescence)
WT	65.12 ± 0.1	71.68 ± 0.1	63.6 ± 0.3
Y300G	64.6 ± 0.1	71.3 ± 0.1	63.5 ± 0.1
Y373G	54.9 ± 0.1	60.8 ± 0.04	55.3 ± 0.1
Y436G	64.6 ± 0.1	66.1 ± 0.1	62.1 ± 0.1

Table 2. Melting temperature (T_m) of WT, S375A, WT_degly, and S375A_degly from DSC and fluorescence. Experiments were conducted in triplicate.

	T _m 1 (DSC)	T _m 2 (DSC)	T _m 3 (DSC)	T _m (Fluorescence)
WT	60.0 ± 0.1	65.9 ± 0.1	71.8 ± 0.4	63.6 ± 0.3
S375A	62.2 ± 0.1	66.8 ± 0.2	72.7 ± 0.1	63.6 ± 0.2
WT_degly	54.2 ± 0.7	62.9 ± 0.6	69.9 ± 0.5	62.6 ± 0.4
S375A_degly	63.3 ± 0.2	69.2 ± 0.2	72.8 ± 0.1	62.8 ± 0.2

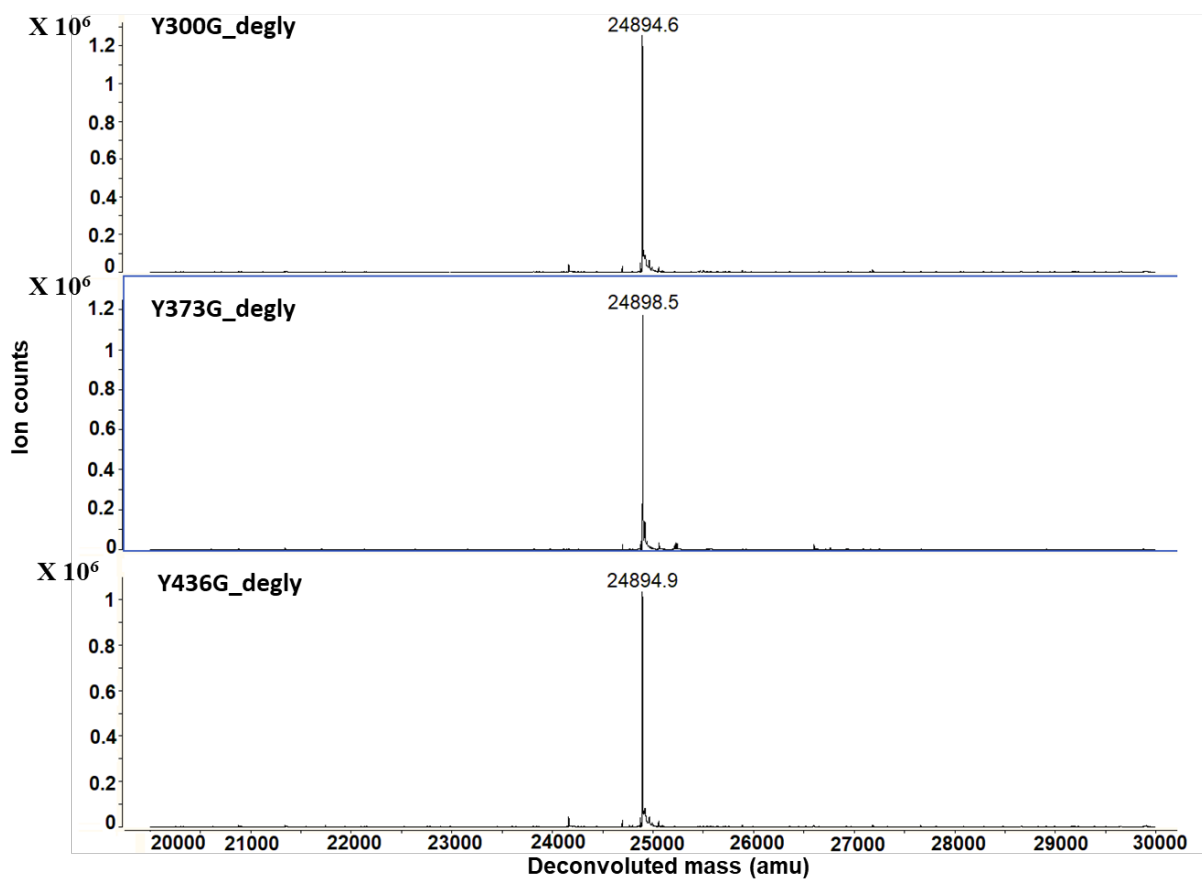
Table 3. Photo-degradation products identified by HPLC-MS/MS through peptide mapping. The corresponding modified residue is listed in the “position” column. The mass modification of +57 or +58 of Cys indicates the alkylation by IAA or IAC, respectively, M(+16) is the formation of methionine sulfoxide, C(+55) is the formation of vinyl thiol, W(+16), W(+32), and W(+4) are the formation of Trp-OH, NFK, and Kyn, respectively.

Product	Photoproducts	Position	m/z	z
1	MTKNQVSLTC(+57)LVKGF-NH ₂	Tyr ³⁷³	575.61	3
2	M(+16)TKNQVSLTC(+57)LVKGF-NH ₂	Tyr ³⁷³	580.96	3
3	 TQKSLSLSLGK	Tyr ⁴³⁶	609.30	2
4	 [TQKSLSLSLGK]+18	Tyr ⁴³⁶	618.30	2
5	TQKSLSLSLGK	Tyr ⁴³⁶	387.89	3
6	FLGGPSVFLFPPKPKDTLM(+16)ISRTPE	Met ²⁵²	698.38	4
7	M(+16)TKNQVSLTC(+57)LVKGFYPSDI AVE	Met ³⁵⁸	872.76	3
8	GNVFSC(+57)SVM(+16)HE	Met ⁴²⁶	641.75	2
9	YKC(+55)KVSNGLPSSIE	Cys ³²¹	569.96	3
10	MTKNQVSLTC(+55)LVKGFYPSDIAVE	Cys ³⁶⁷	866.76	3
11	GNVFSC(+55)SVMHE	Cys ⁴²⁵	632.75	2
12	VVSVLTVLHQDW(+16)LNGK	Trp ³¹³	608.65	3
13	VVSVLTVLHQDW(+32)LNGK	Trp ³¹³	613.99	3

14	SRW(+16)QEGNVFSC(+58)SVMHEALH NHYTQK	Trp ⁴¹⁷	613.26	5
15	VVSVLTVLHQDW(+4)LNGK	Trp ³¹³	604.65	3
16	VVSVLTVLHQDW-NH ₂	Trp ³¹³	604.84	2

Fig. S1. Mass spectrometry analysis of (A) Y300G_degly, Y373G_degly, Y436G_degly and (B) Y300G, Y373G, Y436G after reduction with DTT.

(A).



(B).

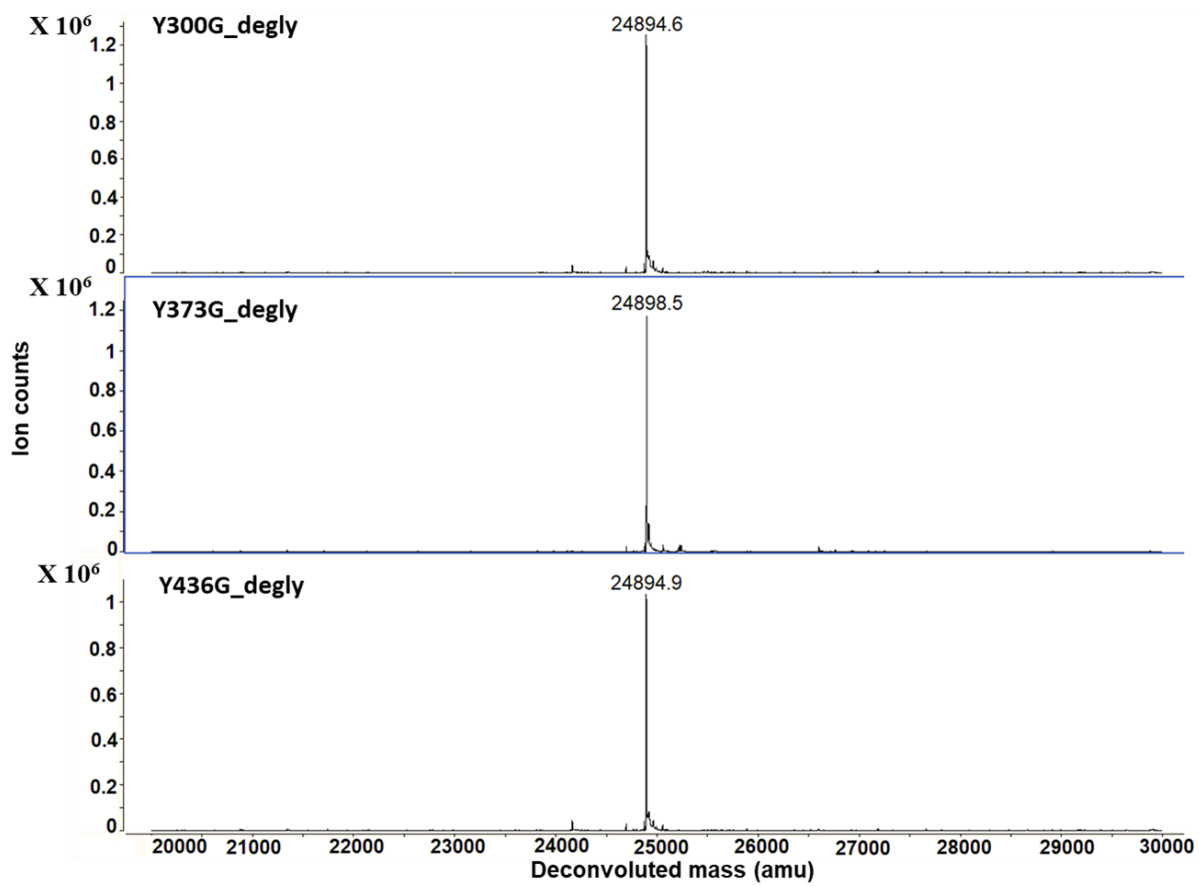


Fig. S2. MS analysis of WT, S375A, W381A, and S375A/W381A IgG4-Fc after chemical reduction of disulfides.

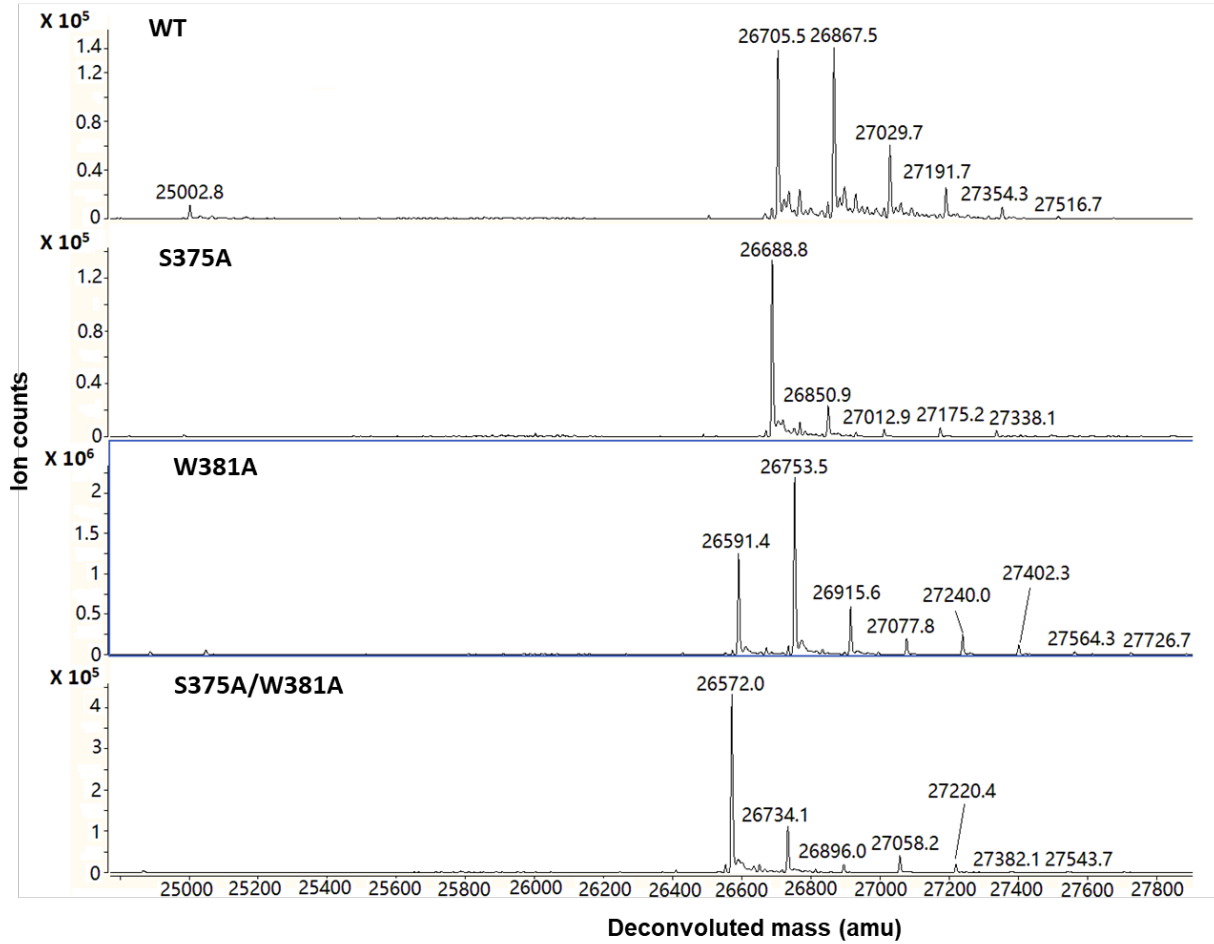


Fig. S3. MS analysis of WT_degly, S375A_degly, W381A_degly, and S375A/W381A_degly

IgG4-Fc after chemical reduction of disulfides.

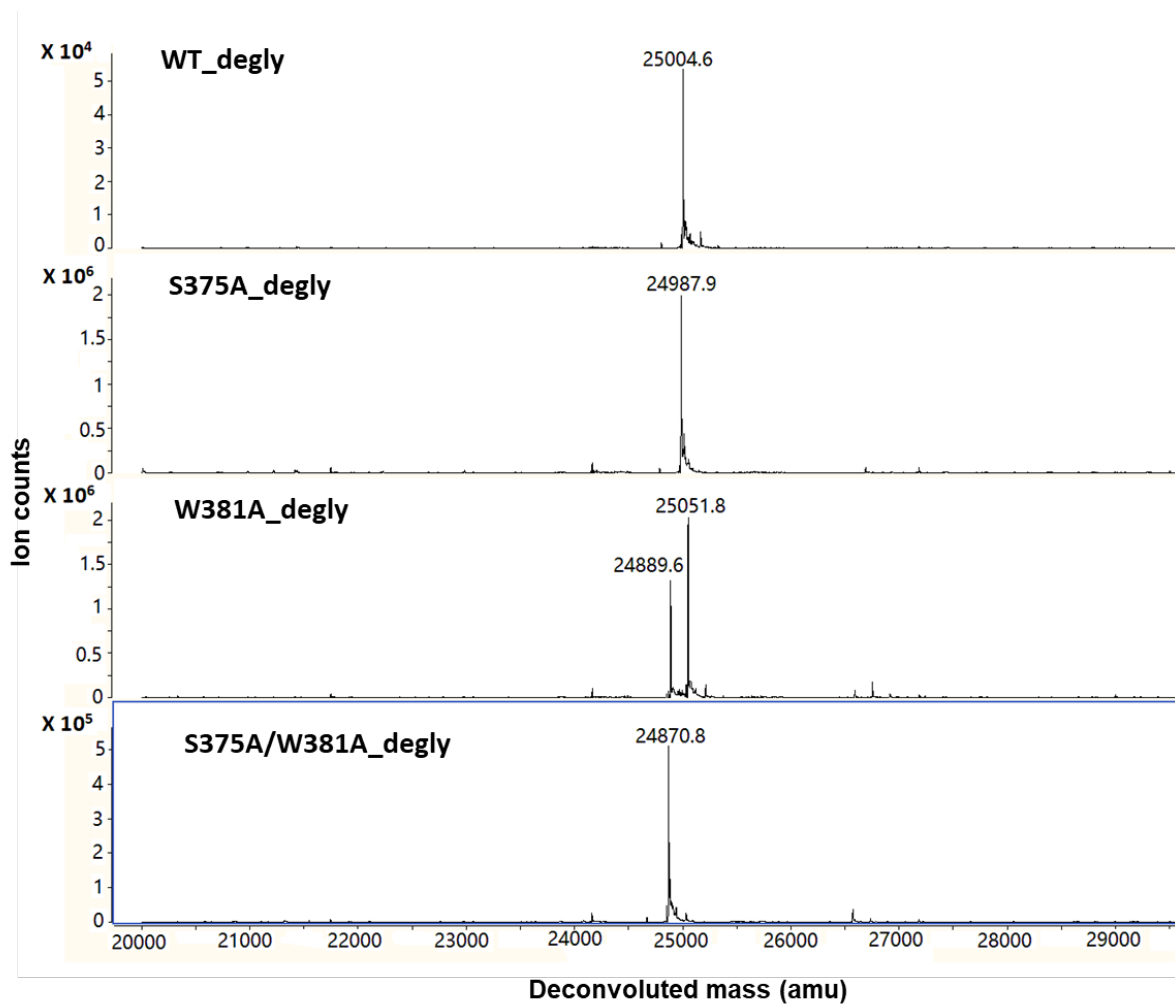


Fig. S4. SDS-PAGE analysis of WT, S375A, W381A, and S375A/W381A, glycosylated proteins were run under reducing conditions; deglycosylated proteins were run under nonreducing conditions.

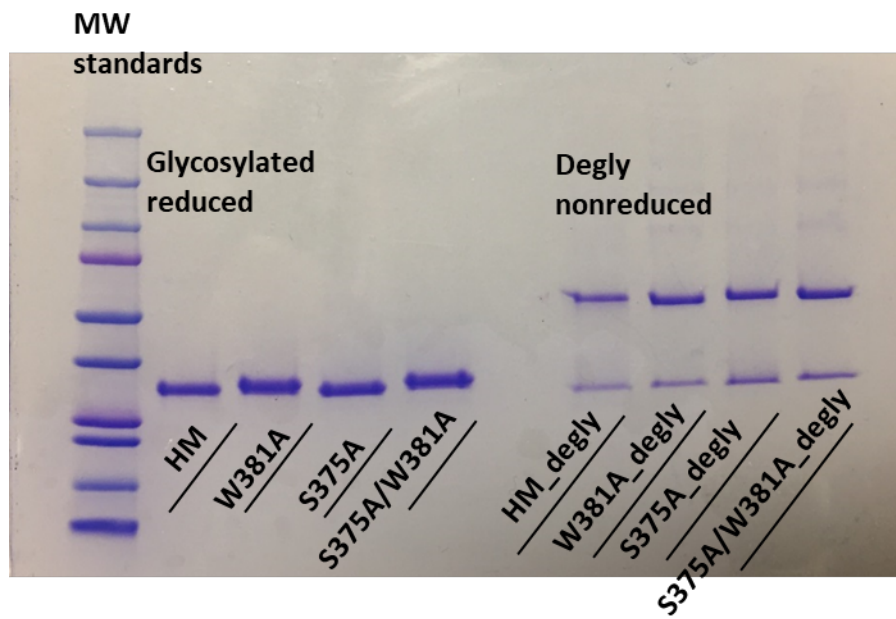


Fig. S5. Chromatogram of proteolytic digest of W381A IgG4-Fc analyzed with HPLC-MS/MS.

Peak 1 contains the O-linked glycosylated peptide, MTKNQVSLTC(+57)LVKGFYPS³⁷⁵(+162)DIAVE (m/z 921.47). Peak 2 contains the nonglycosylated peptide, MTKNQVSLTC(+57)LVKGFYPS³⁷⁵DIAVE (m/z 867.45).

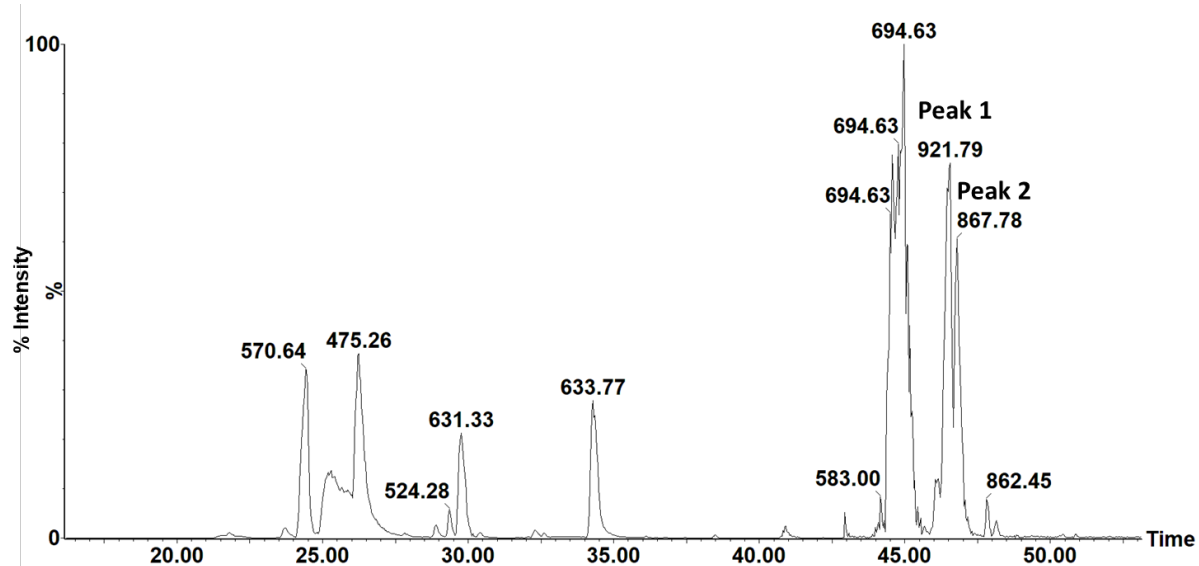


Fig. S6. Thermal stability of (A) WT, W381G, and W381A, and (B) chemical rescue with indole.

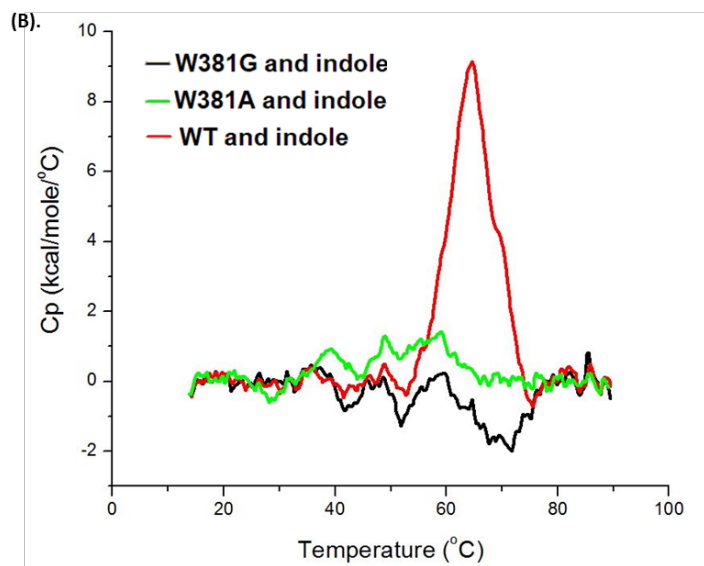
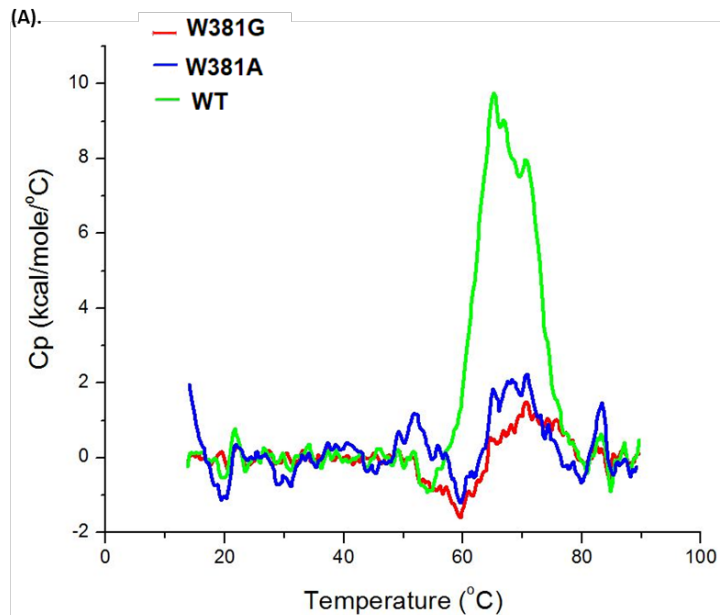


Fig. S7. Relative percentage of individual secondary structures of WT, S375A, W381A, and S375A/W381A, glycosylated and deglycosylated, analyzed by FTIR.

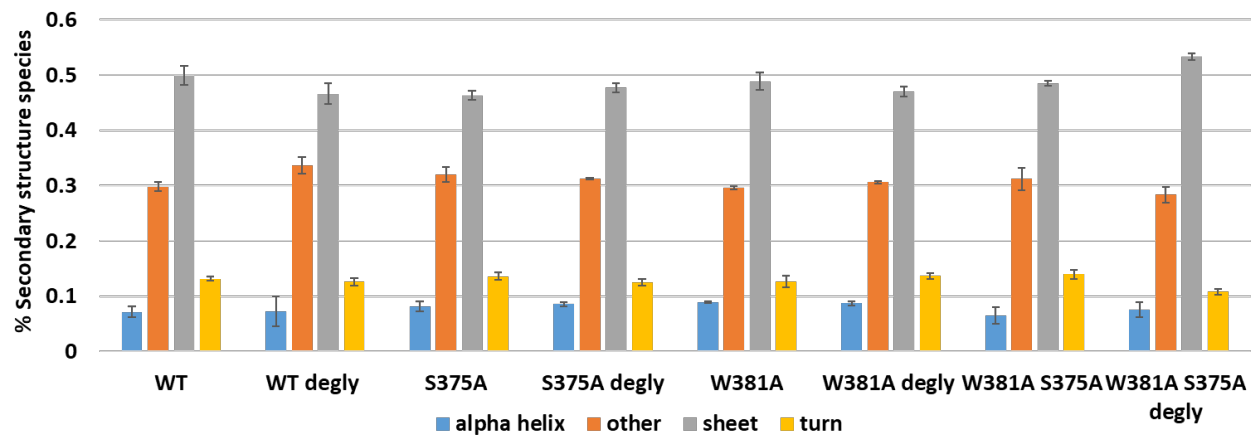


Fig. S8. Representative DSC thermograms of W381F. The corresponding T_m values are displayed.

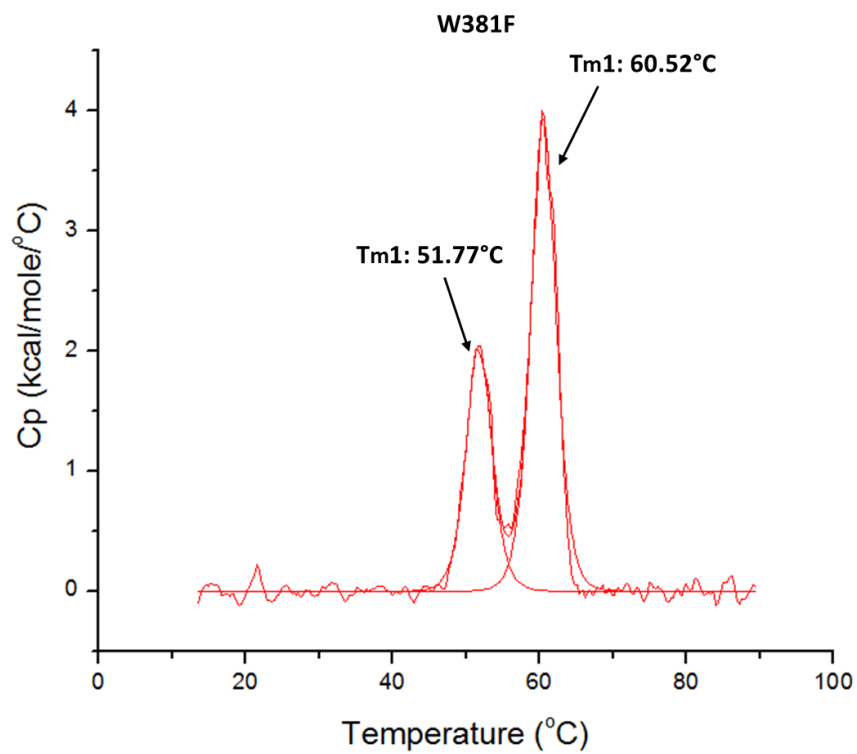


Fig. S9. Dityrosine detection of WT, Y300G, Y373G, Y436G and W381A by exciting photo-irradiated IgG4-Fc at 320 nm and fluorescence emission scan from 371 – 500 nm. Photo-irradiation was performed at $\lambda_{\text{max}}=305$ nm for 45 min.

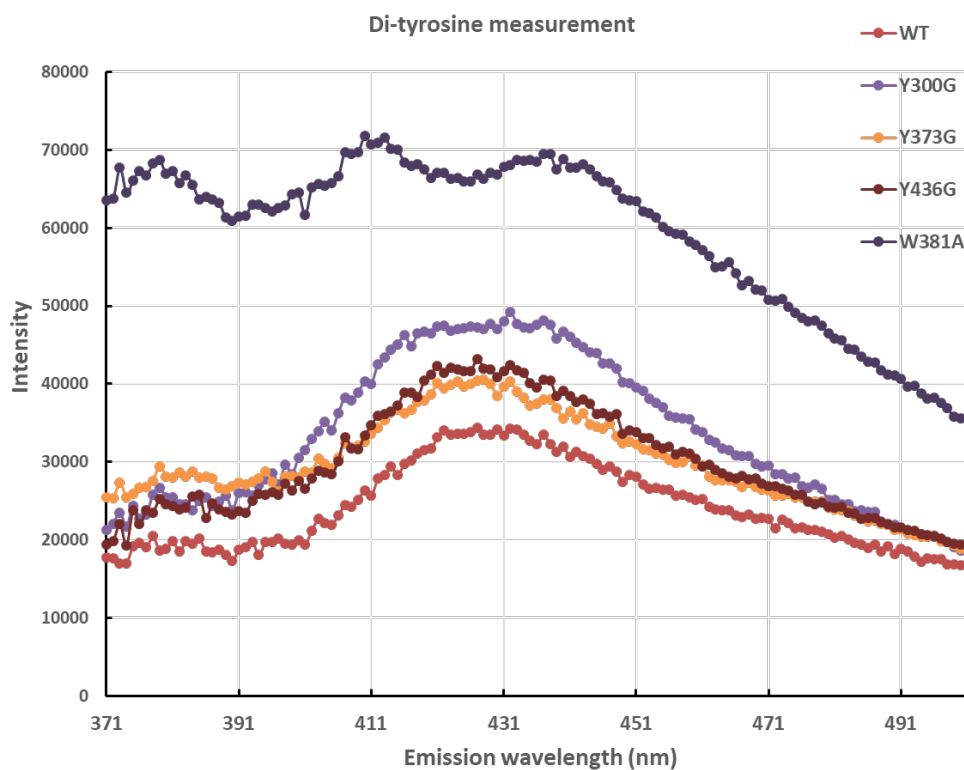
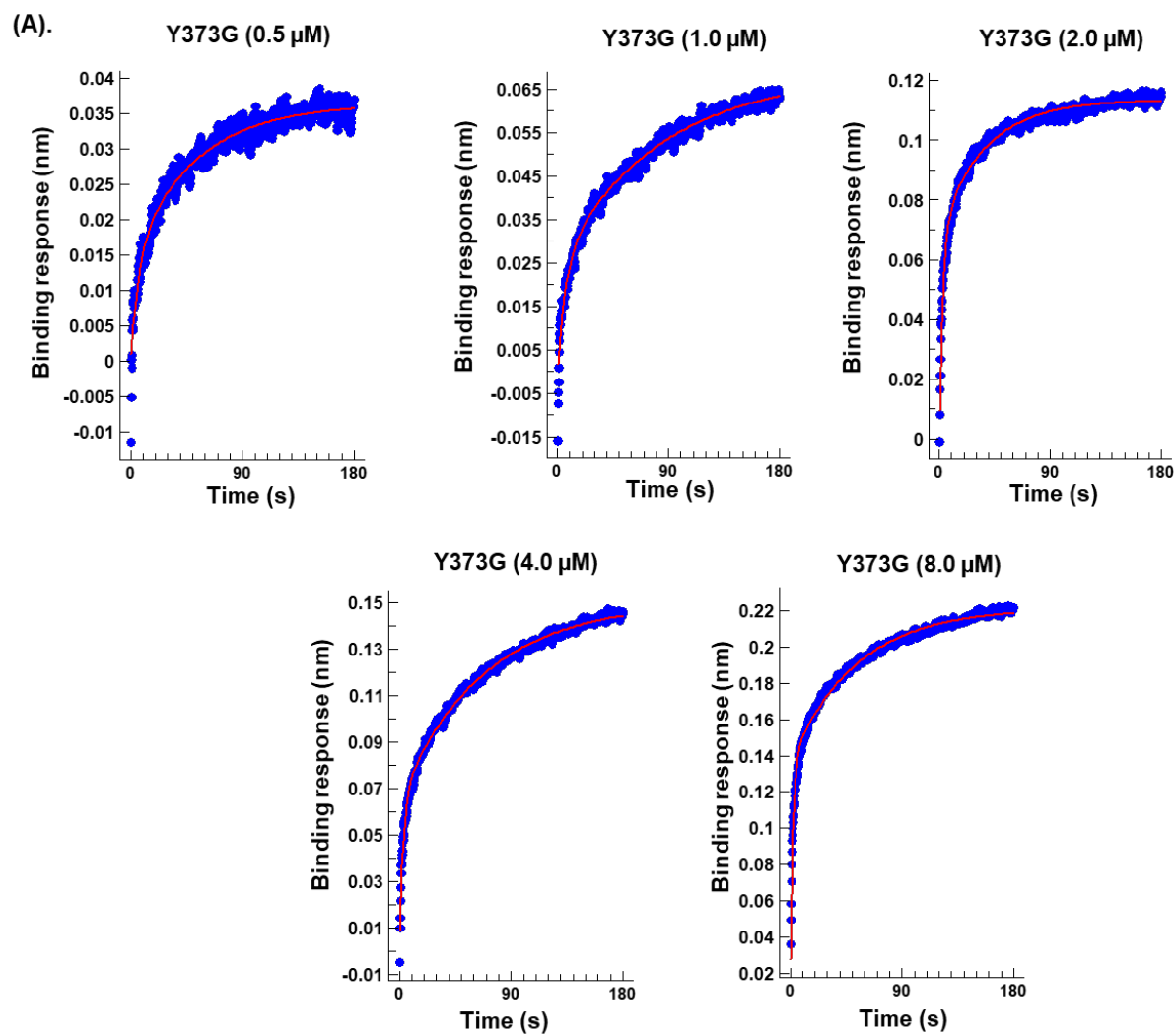
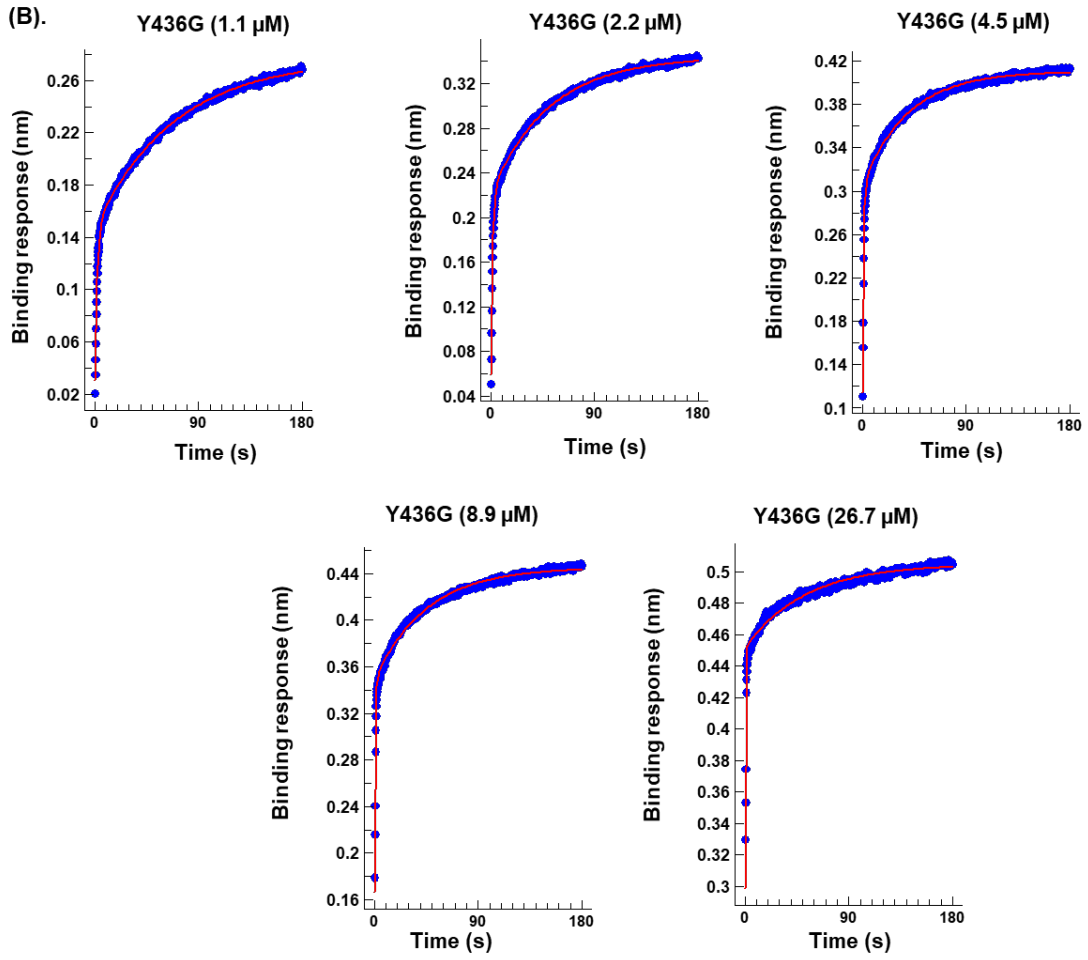


Fig. S10. BLI association of (A) Y373G and Fc γ RIII A, (B) Y436G and Fc γ RIII A, (C) W381A and Fc γ RIII A in PBS kinetic buffer (pH 7.4), where the red line corresponds to two-phase exponential association fit, and the blue dots correspond to experimental data points.





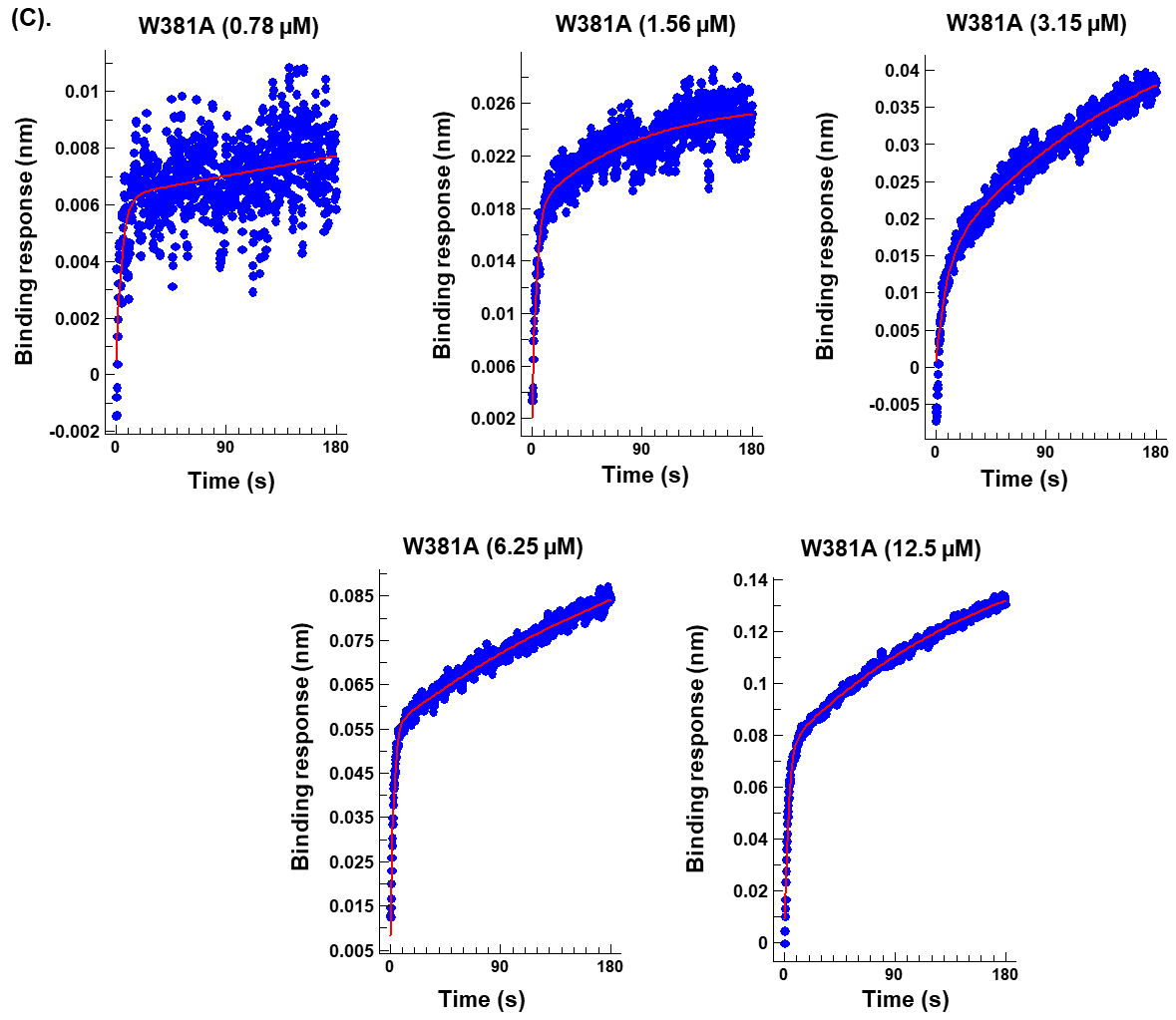


Fig. S11. Plot of k_{obs} of the slow phase as a function of concentrations of the IgG4-Fc variants, WT, Y373G, and Y300G. The error bars represent the standard error from three independent measurements. Y373G and W381A were not shown due to the absence of linear relationship between k_{obs} of their slow phase and protein concentrations.

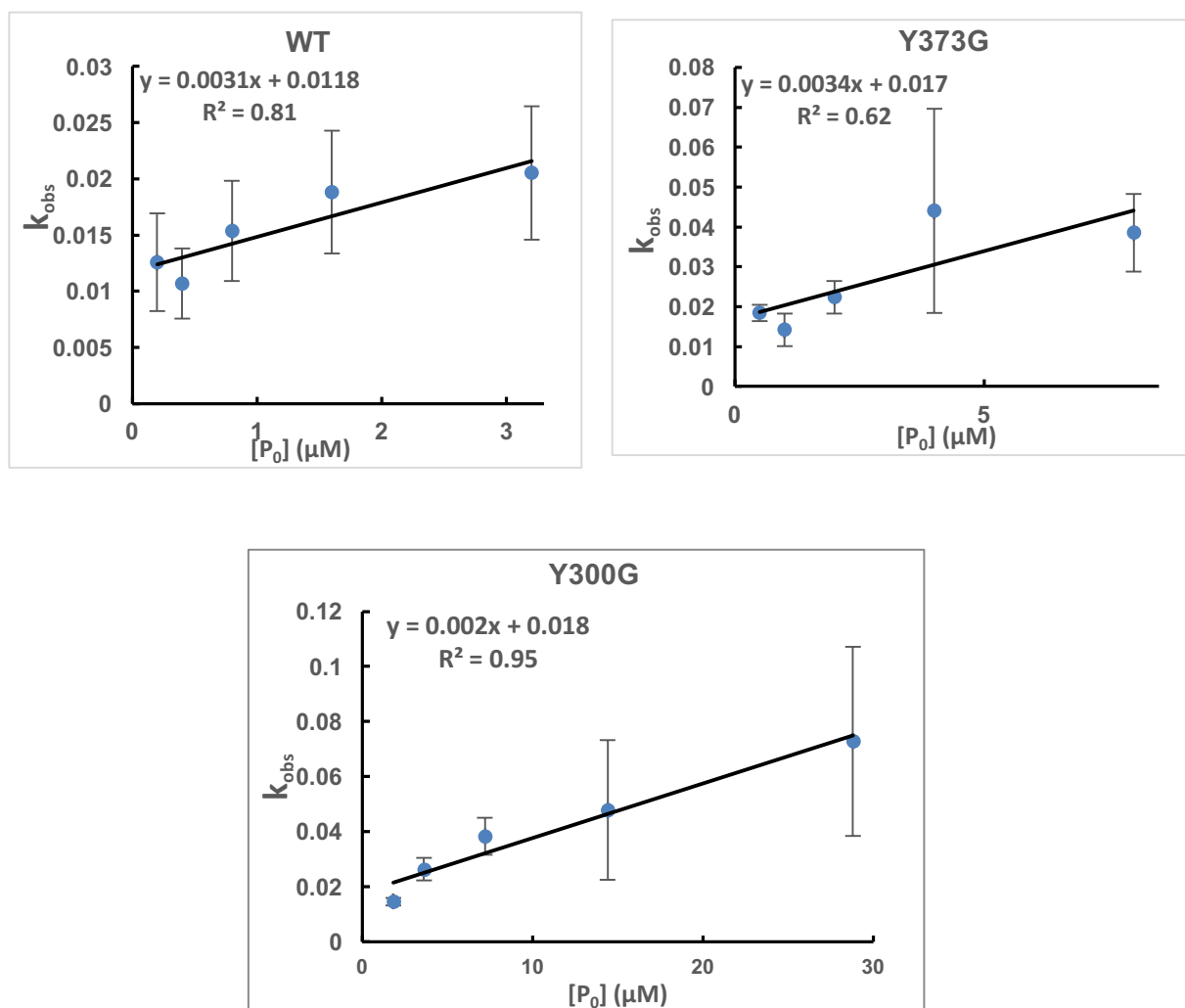


Fig. S12. The presence of O-linked glycosylation (%) in W381G, W381A, and WT IgG4-Fc characterized by HPLC-MS analysis.

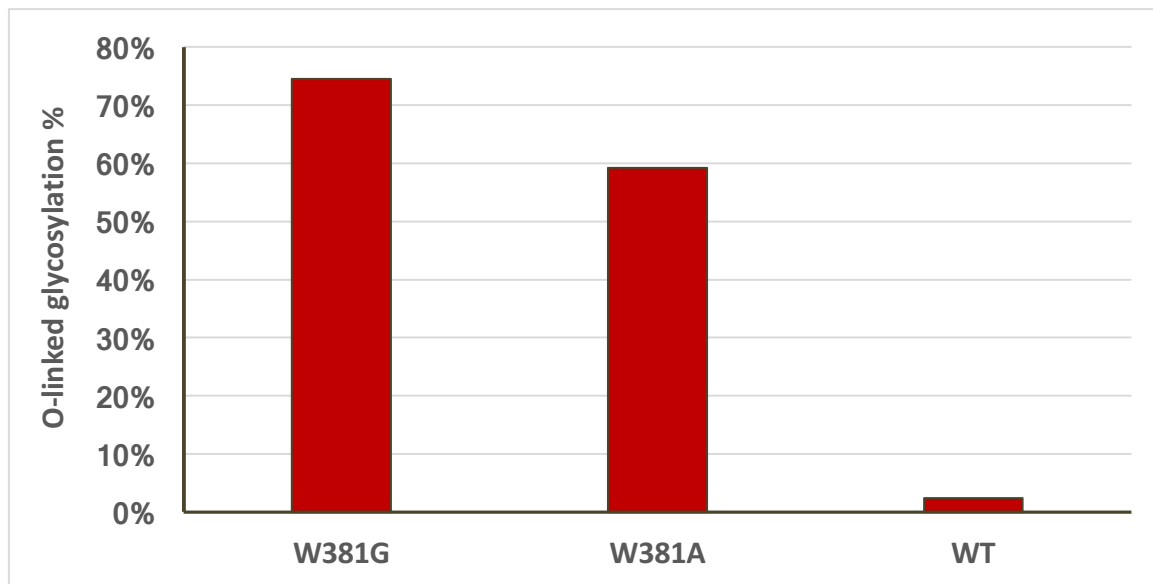


Table S1. Relative abundance (in %) of different glycoforms of Y300G, Y373G, and Y436G IgG4-

Fc.

	WT	Y300G	Y373G	Y436G
No glycan	2.89	0.69	2.69	0.77
Man8	35.61	34.87	52.06	64.48
Man9	36.58	21.43	19.40	18.70
Man10	15.49	5.24	4.24	3.74
Man11	6.49	14.22	10.06	6.46
Man12	2.46	13.12	7.17	4.04
Man13	0.48	2.74	1.20	0.70
Man14	0.00	2.92	1.58	0.58
Man15	0.00	3.93	1.37	0.49
Man16	0.00	0.84	0.23	0.05

Table S2. Theoretical and observed masses of glycosylated WT, S375A, W381A, and S375A/W381A, and the N-deglycosylated variants WT_degly, S375A_degly, W381A_degly, and S375A/W381A_degly under reducing conditions.

	Theoretical	Observed			
WT_degly	25006.24	25004.6			
S375A_degly	24990.24	24987.9			
W381A_degly	24891.11	^a 24889.6/25051.8			
W381A/S375_degly	24875.11	24870.8			
	Theoretical				
	GlcNAc ₂ Man ₈	GlcNAc ₂ Man ₉	GlcNAc ₂ Man ₁₀	GlcNAc ₂ Man ₁₁	GlcNAc ₂ Man ₁₂
WT	26707.7	26869.75	27031.81	27193.86	27355.91
S375A	26691.7	26853.75	27015.81	27177.86	27339.91
W381A	26592.56	26754.61	26912.66	27078.72	27240.77
W381A/S375A	26576.56	26738.61	26900.66	27062.72	27224.77
	Observed				
	GlcNAc ₂ Man ₈	GlcNAc ₂ Man ₉	GlcNAc ₂ Man ₁₀	GlcNAc ₂ Man ₁₁	GlcNAc ₂ Man ₁₂
WT	26705.5	26867.5	27029.7	27191.7	27354.3
S375A	26688.8	26850.9	27012.9	27175.2	27338.1
W381A	26591.4	26753.5	26915.6	27077.8	27240
W381A/S375A	26572	26734.1	26896	27058.2	27220.4

^aW381A_degly presents two masses, 24889.6 and 25051.8, corresponding to the absence and presence of O-glycan, respectively.

Chapter 4. Effects of glycan structure on the physicochemical stability, photostability, and receptor binding of IgG4-Fc

1. Introduction.

Monoclonal antibodies (mAbs), primarily IgGs, represent important therapeutics owing to their target specificity and long serum half-life(1-3). Among the four human isotypes of IgG (i.e., IgG1, 2, 3 and 4), isotypes 1, 2 and 4 have been developed into therapeutic mAbs. IgG3-based mAbs are usually not developed due to their susceptibility to proteolysis, the existence of many allotypes, and the shorter half-life *in vivo*(4). The four IgG isotypes are highly conserved with respect to their primary residual sequences, presenting more than 90% similarity(5). However, each isotype reveals a distinctive profile with regard to biological effector functions and immune complexes(5). For example, IgG4 displays no affinity to complement component 1q (C1q) and a low affinity to Fc receptors(6). Because of this IgG4 has been preferably selected as an isotype for therapeutic mAbs when a host effector function is undesirable or unnecessary. For example, IgG4-based mAbs have been selected for immune-checkpoint therapy, blocking the inhibitory interaction between programmed death protein-1 (PD-1) on immune cells and the ligand PD-L1 on tumor cells by binding to PD-1 on immune cells and allowing an effective immune response to be initiated against tumor cells(7). By the end of 2018, 10 IgG4-based mAbs were introduced into the market among approximately 80 approved mAbs in the USA and the EU(8, 9). Therefore, IgG4 is an essential IgG subclass for the development of effective immunotherapies.

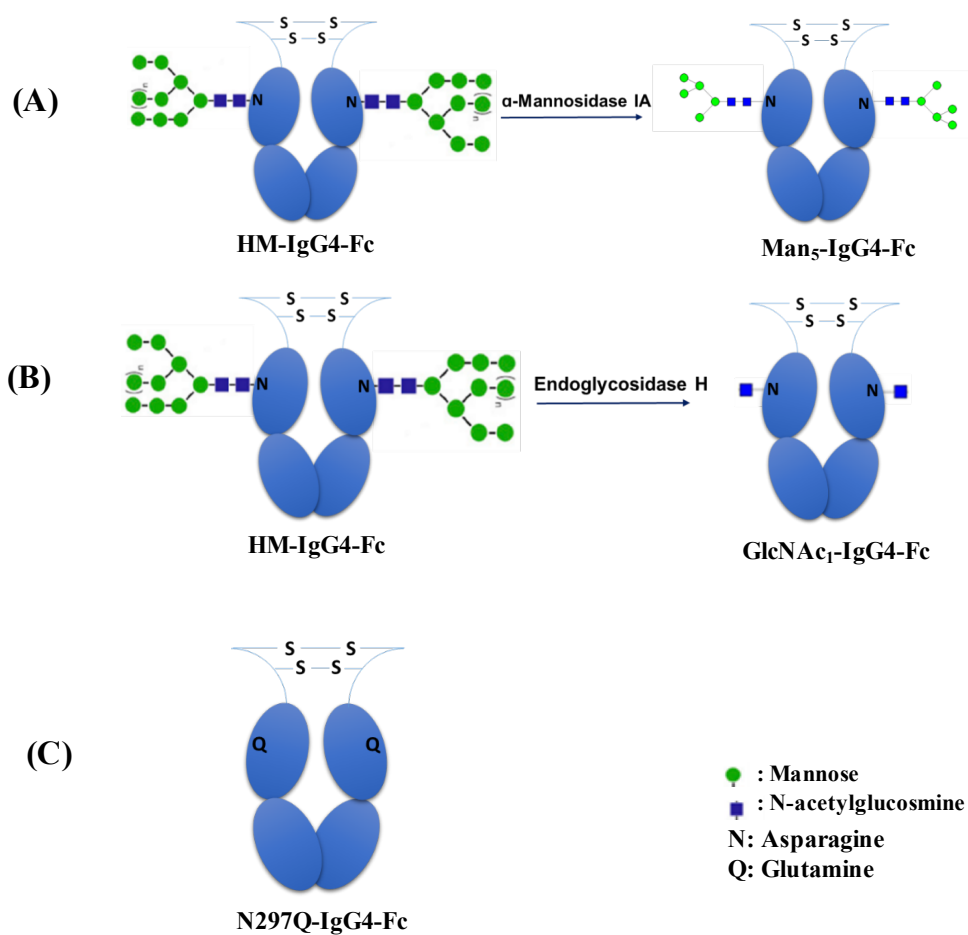
Glycosylation at Asn²⁹⁷ (Eu numbering(10)) is a heterogeneous, conserved, and critical post-translational modification (PTM) of IgGs. It contributes to their biological function and physicochemical stability(11-13). However, glycan structures are difficult to control and can be

affected by host cell genotypes, strains, culture conditions, protein sequences, the manufacturing process(14) as well as the length of storage(15). Hence, glycosylation at Asn²⁹⁷ is a critical quality attribute (CQA) that is required to be strictly defined and controlled(16), (17). Several analytical approaches have been developed to qualitatively and quantitatively monitor oligosaccharide profiles of mAbs, including fluorescence detection of 2-aminobenzamide (AB) labeled glycans and HPLC-MS analysis of released glycans, glycopeptides and glycoproteins(18). Analytical results suggest that variations of glycan structures constantly exist among biosimilars and reference products(19). Alterations in glycan structures have been shown to affect physico-chemical properties(11, 12, 20, 21) and biological effector functions(13, 17) of IgG1 or the crystallizable fragment of IgG1 (IgG1-Fc), but such knowledge is limited with regard to IgG4.

IgG4-Fc is a dimer, composed of a lower hinge region, and the C_H2 and C_H3 domains (Scheme 1). Although IgG4-Fc presents a structure similar to IgG1-Fc, it reveals several unique properties such as the capability of undergoing half-molecule exchange(22). Half-molecule exchange refers to a process where an IgG4-Fc dimer dissociates into monomers, and the dissociated monomer exchanges with an adjacent monomer to reform a new dimer(23). The capability of IgG4 to undergo half-molecule exchange has been investigated by mutagenesis(24) and by a high-resolution crystal structure of IgG4-Fc(23), where two amino acid modifications were found to be essential for such exchange. One is the replacement of Ser²²⁸ by Pro²²⁸ (Eu numbering(10)) in the core-hinge region(22), which enhances the flexibility of the hinge, allowing the formation of inter- and intra-chain disulfides. The other is the presence of a bulkier Arg⁴⁰⁹ instead of a Lys⁴⁰⁹ in the

C_{H3} domain, which disrupts the essential hydrogen bond interaction between Asn³⁹⁰ in one C_{H3} domain and Ser⁴⁰⁰ in the other C_{H3} domain, leading to the dissociation of C_{H3}-C_{H3}(24). Many IgG4 therapeutics are designed for hinge stabilization via mutating Ser²²⁸ to Pro²²⁸ to prevent half molecule exchange *in vivo*(25). In addition, the crystal structure of IgG4 presents an altered conformation (compared to IgG1) of the C_{H2} FG loop (residues 325-331), which may explain reduced affinity of IgG4-Fc to Fcγ receptor IIIA (FcγRIIIA) relative to IgG1-Fc. A variety of studies of FcγRIIIA binding to IgG1 have shown that the interaction is complex, with both antibody and receptor glycosylation altering binding(26-31). IgG1 Asn²⁹⁷ glycan structures, e.g., the attachment of core fucose, significantly reduce the binding affinity of IgG1 to FcγRIIIA, and this has been attributed to carbohydrate-carbohydrate interactions or entropic effects. FcγRIIIA glycosylation at N162, has also been demonstrated to alter IgG1 binding, with Man₅ FcγRIIIA glycoforms exhibiting higher affinity. The affinity of IgG-Fc to FcγRIIIA is important in eliciting antibody-dependent cellular cytotoxicity (ADCC) which can be important in the mechanism of action of mAb therapeutics. The purpose of this work was to evaluate the effect of glycan structure on the physico-chemical properties, photochemical stability and receptor binding of IgG4-Fc. These are critical parameters, which could affect shelf-life and *in vivo* half-life of IgG4-based protein therapeutics. We selected photostability studies as representative for chemical stability studies in view of our recent results, demonstrating that the UV exposure of wild-type IgG4-Fc leads to the side chain cleavage of specific Tyr residues(32). The mechanism of this reaction involves photo-induced electron transfer between Tyr and an intermediate Trp radical cation and is controlled by solvent-dependent changes of protein conformation(32). Therefore, we expect

differences in the yields of Tyr-derived reaction products depending on the effect of glycan structure on the dynamics of IgG4-Fc. In addition, we monitored the photo-induced formation of methionine sulfoxide (MetSO) and disulfide cleavage products.



Scheme 1. A scheme presentation of three glycosylated IgG4 including HM, Man₅, and GlcNAc₁, where HM was obtained from yeast expression, Man₅ (A) and GlcNAc₁ (B) were obtained from in vitro enzymatic remodeling of HM. N297Q IgG4-Fc (C) was obtained through site-directed mutation.

Previous studies reported the affinity between FcγRIIIA and human serum-derived IgG4 with an equilibrium dissociation constant of 4-5 μM, where IgG4 potentially contained a mixture of various glycoforms(6). However, the affinity of specific glycoforms of IgG4 to FcγRIIIA is unknown. Considering that the micro-heterogeneity of Asn²⁹⁷ glycans may impact the binding affinity of the Fc domain to FcγRIIIA, we prepared three well-defined glycosylated and one non-glycosylated IgG4-Fc. The designed IgG4-Fc variants include GlcNAc₂Mn_(8+n) (n =0-4), referred to as high mannose (HM); GlcNAc₂Man₅, referred to as Man₅; GlcNAc₁ and the N297Q mutant, as displayed in Scheme 1. Binding affinities to FcγRIIIA of the four IgG4-Fc were evaluated and correlated with physico-chemical properties.

2. Materials and methods. Yeast extract, peptone, and agar were purchased from Becton Dickinson and Company (Franklin Lakes, NJ). Yeast nitrogen base (YNB) was bought from Sunrise Biosciences (San Diego, CA). Zeocin was provided by Invitrogen (Carlsbad, CA). Rmp protein A sepharoseTM fast flow, phenyl sepharoseTM high performance and XK 26 emptyTM columns were obtained from GE Healthcare Bio-Sciences (Uppsala, Sweden). Endo H was provided by NEB Biolab (Ipswich, MA). Dextrose, sodium chloride, methanol, glycerol, ammonium hydroxide, phosphoric acid, and sodium phosphate were obtained from Fisher (Fair Lawn, NJ). Biotin, citric acid, ammonium bicarbonate, dithiothreitol (DTT), and iodoacetamide (IAA) were obtained from Sigma-Aldrich (Saint Louis, MO). 0.1% formic acid in H₂O and 0.1% formic acid in acetonitrile were provided by Optima Fisher Chemical (Fair Lawn, NJ).

2.1 Expression of wild-type IgG4-Fc. For the expression of wild-type IgG4-Fc, we followed an approach described by Okbazghi et al(33, 34). Briefly, the gene of IgG4-Fc-cDNA was transferred to pno1/och1/bmt 1/bmt 2 deleted and STT3D added *Pichia pastoris* yeast strain through electroporation(34). The successfully transformed yeast colonies were screened on a yeast extract-peptone-dextrose (YPD, 1% yeast extract, 2% peptone, 2% dextrose and 1.5% agar) plate containing 100 µg/mL zeocin. A selected single colony was then inoculated in a 2.5 mL YPD culture media containing 100 µg/mL zeocin, and shaken at 27 °C for 72 hr. The 2.5 mL YPD cell culture was transferred to a 250 mL YPD medium containing 100 µg/mL zeocin, and shaken at 27 °C for ca. 72 hr before transfer to an NBS BioFlo 415 fermenter (Eppendorf, Enfield, CT). The fermenter was prepared in the following way: initially, 7 L of a media base composed of 1% yeast extract, 2% peptone, and 2% glycerol with anti-foam were prepared and sterilized. After the media was cooled, the temperature was set to 30 °C., and 0.34% of yeast nitrogen base, 1% ammonium sulfate, and 4×10^{-5} % biotin were filter sterilized and added to the fermenter. The pH of the medium was adjusted to 6 and maintained during fermentation by addition of concentrated ammonium hydroxide. Finally, the 250 mL yeast cell culture was added to the fermenter. The yeast cells were allowed to grow until the batch glycerol was consumed, followed by an additional addition of 300 mL of glycerol. Once the added glycerol was also consumed, methanol was added by peristaltic pump to induce the production of IgG4-Fc, initially at a rate of 1% (v/v) per 24 hr and increasing to approximately 4% (v/v) once the culture was acclimated to metabolize methanol. For induction, the cells were grown at 25 °C for approximately 3 days prior to harvest. Protein A-purified IgG4-Fc yielded non-glycosylated, mono-glycosylated, and di-glycosylated IgG4-Fc with a yield of ca.

150 mg/L, which is sufficient for analytical characterization. Therefore, in total, one batch was prepared.

2.2 Purification of IgG4-Fc with protein A affinity chromatography. Yeast cells harvested from the fermentation batch were centrifuged at 6,693 g for 20 min on an Avanti J-25I centrifuge (Beckman Coulter, Palo Alto, CA) with a JLA-10500 rotor at 4°C. After centrifugation, the supernatant was combined and filtered with five layers of 90 mm Whatman type 1 filter pads, where the flow-through was collected. A volume of approximate 100 mL of Sepharose Fast Flow protein A (GE Healthcare, Uppsala, Sweden) was packed into a XK50/20 column container (GE Healthcare). The column was equilibrated with 10 column volumes of 20 mM sodium phosphate, pH 7, followed by loading the filtered yeast culture supernatant to allow IgG4-Fc to bind. Non-specific binders were washed out with high salt wash buffer, containing 500 mM NaCl in 20 mM sodium phosphate, pH 7.0. IgG4-Fc was eluted with 50 mM citric acid, pH 3.0, and immediately neutralized with Tris-HCl, pH 9.0. The eluted IgG4-Fc was dialyzed overnight in 20 mM sodium phosphate, pH 7.0, at 4°C prior to further purification.

2.3 Purification of HM IgG4-Fc with hydrophobic interaction chromatography (HIC).

Protein A-purified IgG4-Fc contained di-, mono-, and non-glycosylated IgG4-Fc, where the major glycosylation form was HM, $\text{GlcNAc}_2\text{Man}_{(8+n)}$ ($n=0-4$) (Fig. 1). To obtain a more homogeneous protein solution, a second purification step utilizing HIC chromatography was applied to remove mono- and non-glycosylated IgG4-Fc and potential aggregates. Briefly, a volume of 75 mL phenyl

spharoseTM high-performance resin was packed into an XK26 column and operated by an ÄKTA micro system controlled by the Unicorn 5.20 software (Amersham Biosciences, Piscataway, NJ). Initially, the packed column was washed with 8 column volumes (CV) of distilled water, followed by equilibrating with 9 CV of mobile phase A (1 M ammonium sulfate in 20 mM sodium phosphate, pH 7.0). An IgG4-Fc solution was prepared by mixing with 1 M ammonium sulfate in 20 mM sodium phosphate, pH 7.0, and loaded onto the HIC column through an autosampler loop controlled by a MINIPULS 2 pump (Gilson, Lewis Center, OH) loading at ca. 2 mL/min. After loading, the sample loop was washed with 50 mL mobile phase A to wash off the residual IgG4-Fc. To elute different patterns of glycosylated IgG4-Fc, a linear gradient was applied ranging from 0% to 33% of mobile phase B (20 mM sodium phosphate, pH 7.0) for 288 mL, from 33% to 55% of mobile phase B for 282 mL, followed by a constant level of mobile phase B at 55% for 750 mL. Di-glycosylated IgG4-Fc eluted in the early fractions, and was collected for future use. The eluates were monitored by UV absorption at 220 nm. All the aqueous solutions were filtered with a 0.22 µm filter prior to loading onto the column.

2.4 Expression and purification of *B.t.* α -1,2-mannosidase. *E. coli* cells containing the His-*B.t.* α -1,2-mannosidase-cDNA(35, 36) were inoculated into 6 mL LB media, containing 50 µg/mL kanamycin, and shaken at 37°C for 12 hr. The 6 mL cell culture was then transferred to 1 L LB medium, containing 50 µg/mL kanamycin in a baffled flask and shaken at 37°C. After 12 hr, the cells were induced with 0.2 mM isopropyl β -D-1-thiogalactopyranoside (IPTG), and shaken for an additional 12 hr for enzyme production. The cells were harvested by centrifugation at 6,693 g

for 30 min on an Avanti J-25I centrifuge (Beckman Coulter, Brea, CA) with a JLA-10500 rotor at 4°C. The pellets were collected and suspended in 30 mL of 50 mM sodium phosphate containing 5 mM β -mercaptoethanol, pH 7.5, and then sonicated on ice. The cell lysate was then centrifuged at 15,000 rpm for 30 min, where the supernatant was collected and filtered, followed by loading onto a Ni^{2+} -NTA-agarose column. The column (ca. 5 mL) was initially equilibrated with 50 mM sodium phosphate, pH 7.5, and 5 mM β -mercaptoethanol for 10 CV, followed by loading of the supernatant. The column was washed with 50 mM sodium phosphate, pH 7.5, and eluted with 50 mM sodium phosphate, pH 7.5, containing 250 mM imidazole. The enzyme was dialyzed overnight against 20 mM MES buffer, pH 6.6, at 4 °C, followed by the addition of a final content at 50% glycerol, to store the enzyme in 50% glycerol, 10 mM MES, pH 6.6 at -20 °C.

2.5 *In vitro* enzymatic synthesis of Man₅ IgG4-Fc. Di-glycosylated Man₅ IgG4-Fc were obtained by truncating HM IgG4-Fc through *in vitro* enzymatic remodeling with α -1,2-mannosidase, respectively(13). To obtain Man₅ IgG4-Fc, 2 mL HM IgG4-Fc at 2 mg/mL were mixed with 8 mL solution containing 5 mM CaCl_2 , 150 mM NaCl, 10 mM MES, pH 6.6, and α -mannose IA at an enzyme:protein ratio of 1:8 (w:w). The mixture was placed in a dialysis bag, and kept in a 2 L dialysis bottle containing the reaction buffer. The reaction was conducted at room temperature, covered with aluminum foil, at a constant moderate stir rate. The dialysis buffer was exchanged once every 24 hr for 4 days. The expected and observed masses for Man₅ IgG4-Fc under reducing conditions are 26221.76 Da and 26220.2 Da, respectively (Fig. 1A).

2.6 *In vitro* enzymatic synthesis of GlcNAc₁ IgG4-Fc. To obtain GlcNAc₁ IgG4-Fc, 8 mg of HM IgG4-Fc in a volume of 31 mL 20 mM sodium phosphate, pH 7.1, were digested with 5 µL Endo H, and incubated at room temperature for approximate 18 hr. The completeness of the enzymatic reaction was monitored by HPLC-MS analysis. The enzymes, Endo H and *B.t.* α-1,2-mannosidase, were removed using protein A affinity chromatography, respectively. The expected and observed masses for GlcNAc₁ IgG4-Fc under reducing conditions are 25207.88 Da and 25207.7 Da, respectively (Fig. 1A).

2.7 Mutagenesis, production and purification of N297Q IgG4-Fc. A forward primer, 5'-CGGGAGGAGCAGTTCCAGAGCACGTACCGTGTG-3', and a reversed primer, 3'-GCCCTCCT CG TCAAGGTCTCGTGCATGGCACAC-5', were designed to produce the non-glycosylated N297Q IgG4-Fc. The site-directed mutation was achieved with a QuikChange Lightning Site-Directed Mutagenesis Kit (Agilent Technologies, Inc., Santa Clara, CA). The mutated N297Q IgG4-Fc cDNA-transformed colonies were screened with low salt broth (LB) plate (1% tryptone, 0.5% NaCl, 0.5% yeast extract, and 1.5% agar) containing 25 µg/mL zeocin, inoculated in 6 mL LB media, and grown at 37 °C for 12 hr with shaking. The plasmids were then extracted with a miniprep kit (QIAGEN, Valencia, CA), sequenced by the University of California Berkeley DNA Sequencing Facility (Berkeley, CA) with 100% accuracy, and linearized with the SacI-HF (NEB Biolab, Ipswich, MA). The linearized plasmids were then transferred to an och1/pno1/bmt1/bmt2 deleted and STT3D added *Pichia pastoris* yeast strain. The successfully N297Q-IgG4-Fc cDNA-transformed yeast colony, selected by tolerance to 100 µg/mL zeocin

containing YPD plate, was inoculated in a 2 mL YPD culture with 100 µg/mL zeocin and grown at 27 °C for 72 hr with shaking, followed by transfer to a 50-mL flask containing 100 µg/mL zeocin, and grown at 27 °C for 72 hr with shaking. The 50 mL yeast cells were then scaled up to a 1 L spinner flask, containing buffered glycerol-complex media(37) (1% yeast extract, 2% peptone, 2% glycerol, 0.34% of yeast nitrogen base and 1% ammonium sulfate, 4×10^{-5} % biotin, and 100 mM potassium phosphate, pH 6.0), with a constant flow of air and stirring, followed by growth at room temperature. After 72 hr, the expression of N297Q IgG4-Fc was induced by the addition of 1% (v/v) MeOH every 24 hr for three times before harvesting the cells. N297Q IgG4-Fc was purified in the same manner as WT IgG4-Fc.

2.8 Characterization of IgG4-Fc with intact protein HPLC-MS and sodium dodecyl sulfate-polyacrylamide gel electrophoresis (SDS-PAGE). The initial characterization of the four glycoforms of IgG4-Fc was evaluated by LC-MS analysis of the intact protein under reducing conditions. A volume of 90 µL of 0.22 mg/mL IgG4-Fc protein solution, after reduction with 10 mM DTT for 5 min at room temperature, was loaded onto a C4 column (50 mm, 4.6 mm i.d.; 300-Å pore size, 5 µm particle size, Vydac 214 MS, Grace, Deerfield, IL), coupled to an Agilent 1200 series LC system (Agilent Technologies, Santa Clara, CA). The analytes were eluted by a linear gradient, changing mobile phase B (99.9% acetonitrile, 0.08% formic acid, and 0.02% trifluoroacetic acid) from 5 to 90% within 7 min. Mobile phase A was 99.9% H₂O, 0.08 % formic acid, and 0.02 % trifluoroacetic acid. The IgG4-Fc was ionized in an electrospray ionization (ESI) source, and analyzed in the positive mode by an Agilent 6520 Quadrupole Time-of- Flight mass

spectrometer (Agilent Technologies, Santa Clara, CA). A scan rate of 1 scan/second and a mass/charge (m/z) range of m/z 300 to m/z 3000 were applied. The acquired raw file was extracted and deconvoluted by the Agilent MassHunter Qualitative Analysis software to obtain the molecular weight and relative intensities of different IgG4-Fc species (Fig. 1A).

SDS-PAGE analysis was conducted under reducing and non-reducing conditions. For non-reducing conditions, 20 μ L of 0.2 mg/mL IgG4-Fc in 20 mM sodium phosphate were mixed with Laemmli sample buffer (containing 20-35% of glycerol and 1-2.5% of SDS, BIO-RAD, Richmond, CA) at a 1:1 (v:v) ratio, followed by loading onto a 4% -20% gradient PAGE gel (Mini-PROTEAN TGX™ Gels, BIO-RAD, Richmond, CA). For reducing conditions, an additional 1.5 μ L of 2-mercaptoethanol (14.3 M) were added to the protein solution, followed by boiling for 5 min to achieve full reduction. The gel was run at 200 volts until the front dye reached the bottom. A typical stain with 0.25% Coomassie Brilliant Blue and destain with 30% methanol, 10% acetic acid, 60% water was applied until the bands became clear (Fig. 1B).

2.9 Peptide mapping. Aliquots of 500 μ L at 0.22 mg/mL of photo-irradiated and controlled IgG4-Fc were denatured with 3 M GdnHCl, reduced with 5 mM DTT, and alkylated with 20 mM IAA in 50 mM NH_4HCO_3 . The reduction and alkylation was conducted at 37 °C for 1 hr, respectively, in the presence of GdnHCl. Excess amounts of reducing and alkylating agents were removed with Amicon Ultra Centrifugal Filter Units with 10 kDa cutoff by centrifugation at 16,900 g for 10 min. The protein solution was collected by reverse flip of the filter and centrifugation at 300 g for 4 min.

Peptides were obtained by digestion with GluC (Promega Corporation, Madison, WI) at a w:w ratio of 10:1 (protein:enzyme) at 37 °C for 6 hr. The obtained peptides were analyzed by HPLC-MS/MS.

2.10 HPLC-MS/MS analysis. An aliquot of 4 μ L of GluC-digested IgG4-Fc was injected onto a nanoAcquity ultra performance liquid chromatography (UPLC) system (Waters Corporation, Milford, MA) coupled to a Xevo-G2 mass spectrometer (Waters Cooperation, Milford, MA), equipped with an electrospray ionization source (ESI). The injected peptides were initially loaded onto a C18 trap column (nanoACQUITY UPLC 2G-V/M Trap 5 μ m Symmetry C18 180 μ m x 20mm, Waters, Milford, MA), and desalted for 3 min isocratically with 97% of mobile phase A (0.1% formic acid in water) and 3% of mobile phase B (0.1% formic acid in acetonitrile) at a flow rate of 4 μ L/min. The peptides were eluted to and fractionated on an analytical C18 column (ACQUITY UPLC Peptide CSH C18 NANOACQUITY column 10K psi, 1.7 μ m, 75 μ m x 250 mm, Waters, Milford, MA) with a linear gradient of mobile phase B changing from 3% to 35% within 50 minutes at a flow rate of 300 nL/min, followed by a linear gradient changing mobile phase B from 35% to 95% between 50 and 70 min. The column was subsequently washed with 95% mobile phase B for 10 min before re-equilibration with 97% of mobile phase A. The analytes were ionized by ESI, and analyzed in the positive mode with an m/z range of 200-2000 at a scan rate of 1 scan/second. The fragment ions were collected in the MS^E mode after collision-induced dissociation (CID).

2.11 Photo-degradation. Photoirradiation was conducted in a UV irradiator (Rayonet®, The Southern New England Ultraviolet Company, Branford, CT), equipped with 4 lamps (Rayonet®, catalog# RPR-3000A) emitting continuous wavelengths between 265 nm and 340 nm, with a maximum emission at $\lambda_{\text{max}} = 305$ nm. We used the ferrioxalate actinometer(38, 39) to quantify the photon flux to 1.87×10^{-8} Einstein/s. Aliquots of 500 μL of IgG4-Fc (HM, Man₅, GlcNAc₁, and N297Q at 0.22 mg/mL, pH 7.1) in 20 mM sodium phosphate were placed in Pyrex tubes, and capped with rubber stoppers. Pyrex tubes have a wavelength cutoff of 295 nm. The photoirradiation was conducted for 30 min at RT. These photo-irradiation conditions ensured that our samples were exposed to light intensities of $< 20 \text{ Whr/m}^2$, i.e., $< 10\%$ of the minimum light exposure (200 Whr/m^2) advised by the ICH Q1B guideline for UV photostability testing(40). Control samples were placed in the dark at RT. Two independent experiments were conducted.

2.12 Differential scanning calorimetry (DSC). The thermal stability of the four IgG4-Fc glycoforms was evaluated using a MicroCal VP-capillary calorimeter (Malvern, UK). A volume of 400 μL of 0.22 mg/mL IgG4-Fc was placed in a 96-well plate at 5 °C, sealed with a plastic cover. Thermograms were obtained within a temperature of 10°C-90°C at a scan rate of 1°C/min with a filtering period of 16 s. The built-in Origin software (Origin Lab, Malvern, UK) was utilized for the analysis of the raw thermograms after the processing of buffer subtraction, baseline correction and concentration normalization. T_m values were then derived from the processed thermograms by a fit to a non-two-state equilibrium model(41).

2.13 Intrinsic fluorescence. The intrinsic fluorescence of the four IgG4-Fc glycoforms was measured by excitation with a dye laser emitting from 280 nm to 300 nm, a temperature-controlled fluorescence plate reader, and a charge coupled device detector (Fluorescence Innovations, Inc., Minneapolis, MN). The fluorescence was examined within a temperature range between 10°C and 90°C at an increment rate of 2.5 °C/step. A volume of 20 µL containing 0.22 mg/mL IgG4-Fc was applied to a 384 well plate, followed by loading 2 µL silicon oil on top of the protein solution to minimize sample evaporation. The excitation was conducted at 295 nm, and the emission spectra were collected between 300 nm and 400 nm. The fluorescence center of mass, defined as moment, was calculated as follows, using the ThermoSpec software (Fluorescence Innovations, Inc.):

$$\text{Moment} = \frac{\int I(x)xdx}{\int I(x)dx}$$

where x is the wavelength, and I(x) is the intensity. The fluorescence moment was plotted as a function of temperature, and T_m values were derived from the 1st derivative of the plot.

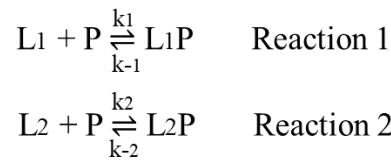
2.14 Biolayer interferometry (BLI) binding assays. Binding affinities of the four IgG4-Fc to FcγRIIIA were evaluated by BLI using a BLItz system (ForteBio, Menlo Park, CA) via immobilizing biotinylated FcγRIIIA to a streptavidin tip (SA; ForteBio, Menlo Park, CA). The biotinylated FcγRIIIA (Val¹⁵⁸) was prepared as described(13). IgG4-Fc was dialyzed into 2 L PBS buffer (39.3 mM Na₂HPO₄, 150 mM NaCl, and 10.65 mM NaH₂PO₄, pH 7.4) at 4 °C. The dialysis buffer was exchanged once after 12 hr. PBS kinetic buffer, containing 1 mg/mL BSA (VWR Chemicals, Solon, Ohio) in PBS, was prepared. After dialysis, IgG4-Fc was mixed with 10 mg/mL BSA (prepared in PBS buffer) at a ratio of 9:1 (v:v) to obtain a protein mixture in 1 mg/mL BSA

in PBS buffer, pH 7.4, to minimize non-specific binding. A series of five concentrations were applied for each IgG4-Fc glycoforms. For HM, a series of 0.2 μM , 0.4 μM , 0.8 μM , 1.6 μM , and 3.2 μM was applied. For Man₅, a series of 0.0478 μM , 0.0958 μM , 0.192 μM , 0.383 μM , and 0.766 μM was applied. For GlcNAc₁, a series of 2.7 μM , 3.28 μM , 5.4 μM , 6.57 μM and 13.14 μM was applied. For N297Q, two concentrations, 11.35 μM and 16.27 μM , were applied.

The SA tip was prepared by hydration in PBS for 10 min, followed by hydration in PBS kinetic buffer for 30 min. The SA tip was then loaded onto the BLItz system. For Fc γ RIIIA loading, a 30 s of baseline was first established with 250 μL of PBS kinetic buffer. In the 3-min receptor loading step, 0.02 μM of Fc γ RIIIA in PBS kinetic buffer was loaded until the response level reaches 0.4 Δnm . BLI measures the interaction of proteins at the surface of the SA tips (equipped with biosensors), which results in a shift of light wavelength (Δnm), referred to as light interference. After the response level reached $\Delta\text{nm}= 0.4$, the Fc γ RIIIA solution was exchanged with a PBS kinetic buffer. In the 3-min dissociation step, the tips were dipped into PBS kinetic buffer. For collection of a blank, tips were dipped into 250 μL PBS kinetic buffer in all three binding steps, including 30 s of baseline collection, 180 s of association and 180 s of dissociation. For sample analysis, in the 30-s baseline step, tips were dipped into PBS kinetic buffer, then in the 3-min association step the sample was loaded at various concentrations, and finally the tips were dipped into PBS kinetic buffer in the 3-min dissociation step. For each IgG4-Fc variant, the samples were loaded from the lowest to the highest concentrations. Between each sample run, a regeneration step was applied through washing with 1 mM NaOH for 30 s, followed by washing with PBS

kinetic buffer for 2 min. A minimum of two independent replicates were conducted. The tip was replaced between each replicate.

The association sensorgrams of IgG4-Fc and FcγRIIIA cannot be fit by mono-exponential kinetics(42-45) (Fig. S1). Instead, a model based on two separate association equilibria (Reactions 1 and 2), a fast and a slow one, led to excellent kinetic fits. Here, L₁ and L₂ represent two variants within a heterogeneous population of FcγRIIIA(46, 47), P represents IgG4-Fc, k₁ and k₂ represent the k_{on} values for Reactions 1 and 2, respectively, and k₋₁ and k₋₂ represent the k_{off} values for Reactions 1 and 2, respectively.



Kinetically, the reactions are of pseudo first order due to the excess quantity of P (IgG4-Fc). The following equations were used for the kinetic fits.

$$[L_1P] + [L_2P] = [L_1P]_{\infty}(1-\exp(-(k_1[P_0] + k_{-1})t)) + [L_2P]_{\infty}(1-\exp(-(k_2[P_0] + k_{-2})t)) \quad (1)$$

$$y = A(1-\exp(-Bx)) + C(1-\exp(-Dx)) \quad (2)$$

where in equation 1, [L₁P] and [L₂P] are the concentrations of complex L₁P and L₂P at time t as dependent variables, respectively. [P₀] is the initial and constant concentration of P, based on [P] » [L]. [L₁P]_∞ and [L₂P]_∞ are the concentrations of L₁P and L₂P at infinite reaction time. A two-exponential association fit was applied using XL fit analysis (IDBS, Boston, MA) as displayed in equation 2, where A = [L₁P]_∞; B = k₁[P₀] + k₋₁; C = [L₂P]_∞; D = k₂[P₀] + k₋₂. The values for B and D

were constrained to be ≥ 0 . The fitting parameters B and D correspond to k_{obs} of the fast and the slow phase, respectively. Linear plots of k_{obs} as a function of the concentration of $[P_0]$ were obtained, where the slopes represent k_{on} ($\text{M}^{-1}\text{s}^{-1}$) (k_1 or k_2), and the intercepts represents k_{off} (s^{-1}) (k_{-1} or k_{-2}). The k_{on} and k_{off} values derived from the fast phase are consistent with previously reported binding affinities between Fc and Fc γ RIII(5, 6, 13). Hence, in the present work, we focus mainly on the kinetic parameters derived from the fast phase. The k_{on} and k_{off} from the slow phase were derived for HM and Man₅ IgG4-Fc.

3. Results. The physicochemical stability of the four IgG4-Fc variants (0.22 mg/mL) was analyzed in 20 mM sodium phosphate, pH 7.1, while binding assays were performed in PBS, pH 7.4.

3.1 Initial characterization of HM, Man₅, GlcNAc₁, and N297Q IgG4-Fc. HM, Man₅ and GlcNAc₁-IgG4-Fc were derived from the same batch of a 10 L-fermenter production. N297Q was expressed in 1L-scale spinner flasks. To ensure that the three glycosylated IgG4-Fc variants and the non-glycosylated IgG4-Fc were of adequate quality, an initial characterization with HPLC-MS and SDS-PAGE analysis was performed (Fig. 1). In the reducing gel (Fig. 1B, right panel), single bands of HM, Man₅, GlcNAc₁, and N297Q were observed, migrating between 25 kD and 37 kD, indicating that the four IgG4-Fc variants were obtained with good purity. In the non-reducing gel (Fig. 1B, left panel), HM displays two bands, and a reduced mobility compared to Man₅, GlcNAc₁ and N297Q. The differential mobility in both the reducing and non-reducing gels results from the differences of glycan mass and branching associated with each IgG4-Fc form. The two bands, predominantly observed for HM in the non-reducing gel, are consistent with both intra- and inter-

chain disulfide bonds in the hinge region, where intra-chain disulfide bond formation leads to dissociation of an IgG4-Fc dimer. The intra- and inter-chain disulfides were quantified by densitometry analysis with Image J (National Institutes of Health, Washington D.C., US). Here, inter-chain disulfides account for 50.6% for HM, 70.5% for Man₅, 67.4% for GlcNAc₁, and 80.3% for N297Q IgG4-Fc. In turn, intra-chain disulfides are present at 49.4% for HM, 29.5% for Man₅, 32.6% for GlcNAc₁ and 19.7% for N297Q IgG4-Fc.

Intact protein HPLC-MS was applied to analyze the homogeneity of the glycoforms of HM, Man₅ and GlcNAc₁ IgG4-Fc (Fig. 1A). The signal intensities of glycosylated and nonglycosylated forms were recorded utilizing MassHunter Qualitative Analysis. The homogeneity of HM was calculated as the sum of intensity of Man₈ to Man₁₂ forms divided by the sum of intensity of nonglycosylated and Man₈ to Man₁₂ forms. The homogeneity of GlcNAc₁ was calculated as the intensity of GlcNAc₁ form divided by the sum of nonglycosylated and GlcNAc₁ forms. The homogeneity of Man₅ was calculated as the intensity of Man₅ form divided by the sum of intensity of nonglycosylated and Man₅ to Man₉ forms. HM, GlcNAc₁ and Man₅ presented a homogeneity of 97.1%, 96.4%, and 86.7%, respectively. N297Q was obtained through site-directed mutation and the homogeneity was 100%.

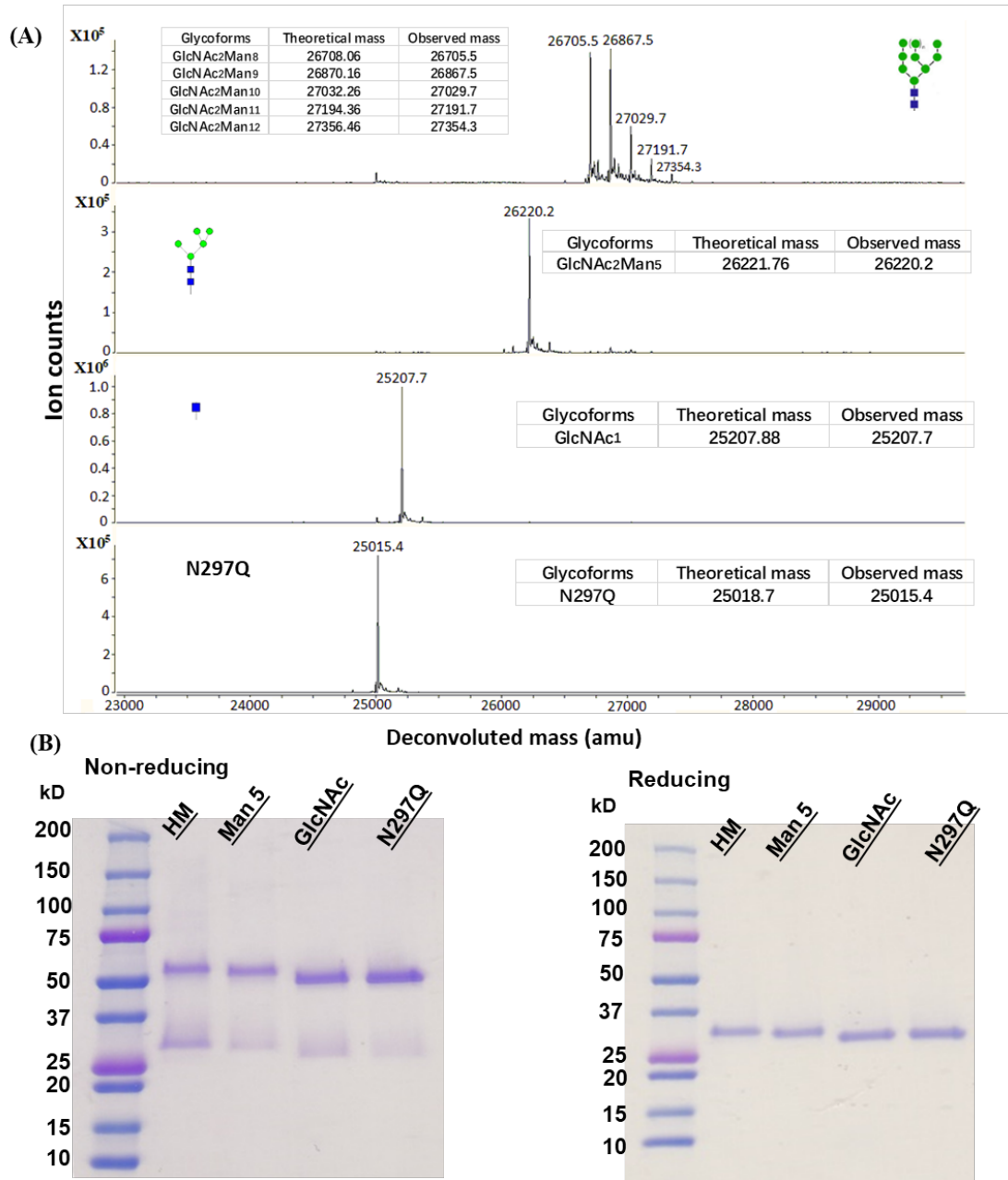


Fig. 1. Initial characterization of intact GlcNAc₂Man_(8+n) (n =0-4), GlcNAc₂Man₅, GlcNAc₁, and N297Q IgG4-Fc with (A) MS under reducing conditions after treatment with DTT and (B) SDS-PAGE under non-reducing (left) and reducing conditions (right).

3.2 DSC. The overall conformational stability of the four IgG4-Fc glycoforms was evaluated by

DSC using a temperature ramp from 10 to 90°C with 1°C increments (Fig. 2). All of the four IgG4-Fc variants display two thermal transitions, corresponding to the unfolding of the C_H2 and C_H3 domains, respectively. Melting temperatures of the transitions, represented as T_{m1} and T_{m2}, were derived and are listed in Table 1. Overall, the thermal stability of HM, Man₅, and GlcNAc₁ does not vary significantly, where T_{m1} and T_{m2} values show only small differences within 1°C. On the other hand, N297Q IgG4-Fc shows a reduction of approximate 3°C for T_{m1} as compared to the other three glycoforms. N297Q does not reveal significant changes of T_{m2} compared to the other glycoforms.

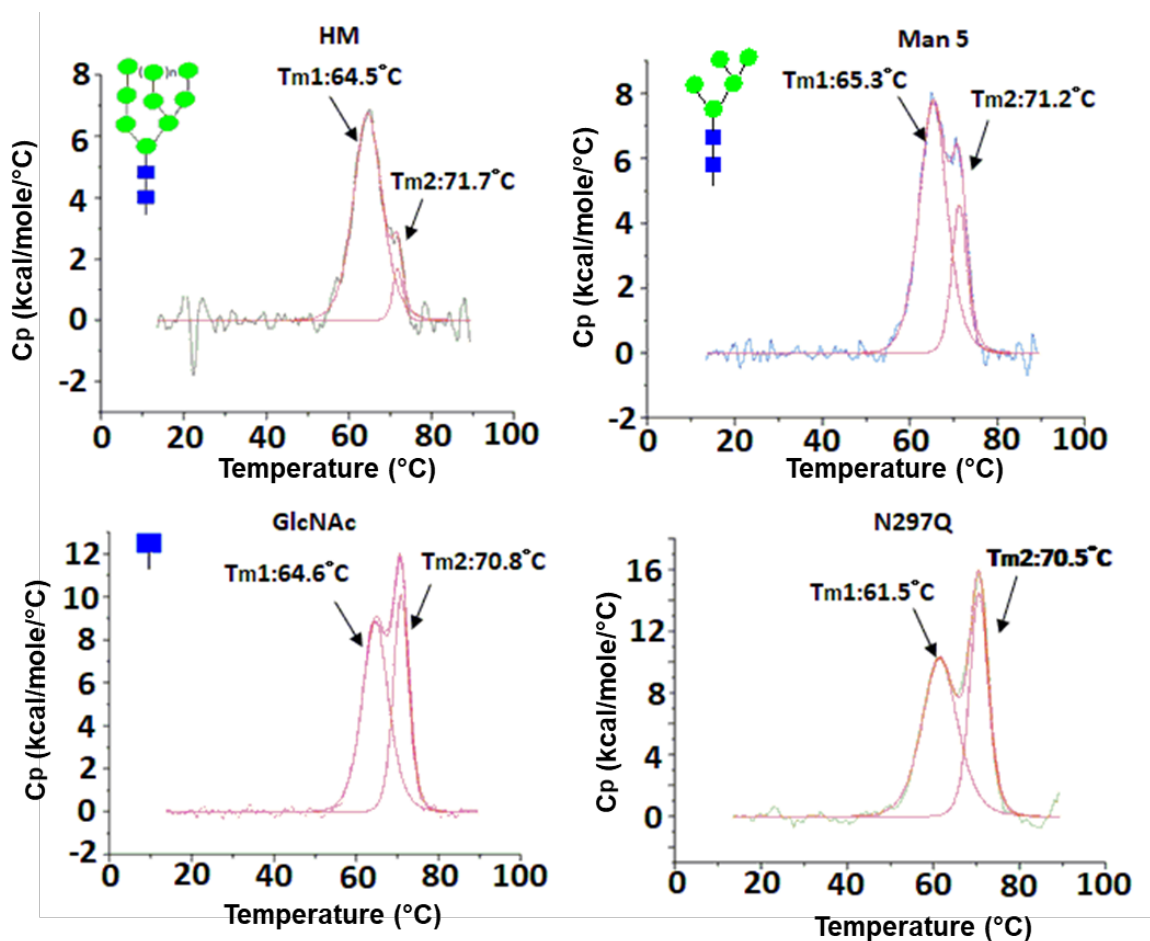
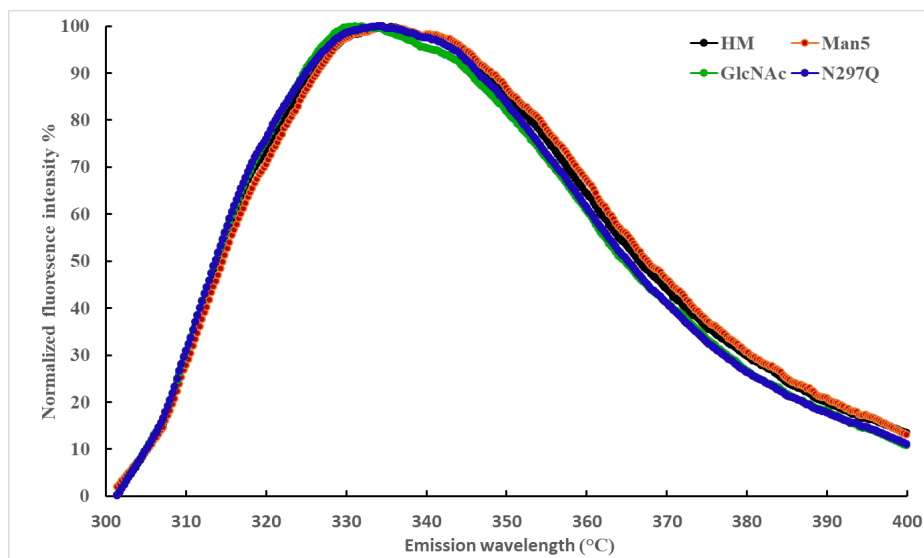


Fig. 2. Thermograms of HM, Man₅, GlcNAc₁, N297Q examined by DSC from 10°C to 90°C. Corresponding T_m values are displayed in Table 1, where T_{m1} represents the melting temperature of the C_H2 domain, and T_{m2} represents the melting temperature of the C_H3 domain.

3.3. Intrinsic fluorescence. The tertiary structures of the four IgG4-Fc variants were evaluated by intrinsic fluorescence spectroscopy through excitation at 295 nm, and emission measurements between 300 nm and 400 nm. The fluorescence emission spectra of the four IgG4-Fc recorded at 25°C (Fig. 3A) reveal a maximum fluorescence intensity at similar wavelengths, between 337 and 340 nm. This suggests, that the four IgG4-Fc variants present similar tertiary structure. A

temperature ramp from 10 to 90 °C was applied to evaluate the thermal stability of the four IgG4-Fc variants, and the fluorescence moment plotted as a function of temperature (Fig. 3B). The respective transition values T_m were derived and are listed in Table 1. These data suggest the thermal stability ranks in the following order: Man₅ ~ HM > GlcNAc₁ > N297Q IgG4-Fc.

(A).



(B).

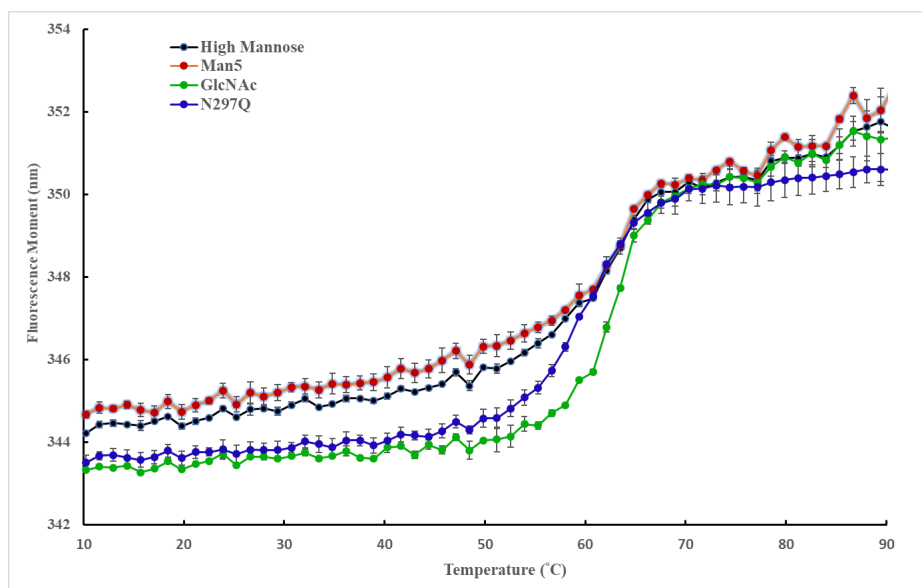


Fig. 3. Intrinsic fluorescence of HM, Man₅, GlcNAc, and N297Q of IgG4-Fc, where (A) is the normalized fluorescence intensity (%) as a function of wavelength, (B) is fluorescence moment (nm) as a function of temperature (°C). Three independent experiments were performed.

3.4 Photostability. The photostability of the four IgG4-Fc variants was evaluated by photo-

irradiation at $\lambda_{\text{max}} = 305$ nm for 30 min. The conversion of native peptides (%) into eleven photoproducts was quantified, and relative yields of the photoproducts are displayed in Fig. 4. These products include five peptide backbone cleavage products resulting from photo-induced Tyr side chain fragmentation(32), three Met sulfoxide products (MetSO), and three vinyl Cys products. Detailed information on the nature of the photoproducts is provided in Table 2.

3.4.1 Formation of Tyr side chain fragmentation products. Two Tyr residues in IgG4-Fc, Tyr³⁷³ and Tyr⁴³⁶, were monitored to quantify photo-induced tyrosine side chain fragmentation. The mechanism of such Tyr fragmentation was documented in a previous publication(32). In the presence of O₂, the major degradation products are peptide backbone cleavage products (Table 2), including product **1** from Tyr³⁷³, and products **3**, **4** and **5** from Tyr⁴³⁶. Product **2** (from Tyr³⁷³) is a secondary oxidation product, derived from Met oxidation of product **1**. Products **1-5** were formed with higher relative yields in GlcNAc₁ and N297Q IgG4-Fc, presenting more than 1.5- and 2-fold increase over the yields obtained from HM and Man₅ IgG4-Fc, respectively. It appears, that the size of the glycans inversely correlates with the relative yields of products **1-5** (Fig. 4A and 4B).

3.4.2 Formation of MetSO. IgG4-Fc contains three Met residues, Met²⁵², Met³⁵⁸, and Met⁴²⁶. Their corresponding oxidation products, referred to as products **6**, **7** and **8** (Fig. 4C), show an increase of yields in the following order: MetSO²⁵² > MetSO⁴²⁶ > MetSO³⁵⁸. This trend is similar to observed trends for peroxide-treated IgG1 and photo-oxidized IgG2(48). The glycan structure does not significantly affect the yields of MetSO (products **6-8**, Fig. 4C).

3.4.3 Formation of Vinyl Cys Three Cys residues in IgG4-Fc, Cys³²¹, Cys³⁶⁷, and Cys⁴²⁵, were monitored to quantify the yield of vinyl Cys formation. Their corresponding products are referred

to as products **9**, **10**, and **11** (Fig. 4D). Interestingly, their relative yields follow an opposite trend as compared to the yields of Tyr derived products, where HM shows the most efficient formation of vinyl Cys. The other IgG4-Fc variants, Man₅, GlcNAc₁, and N297Q, show approximate half the yields as compared to HM IgG4-Fc.

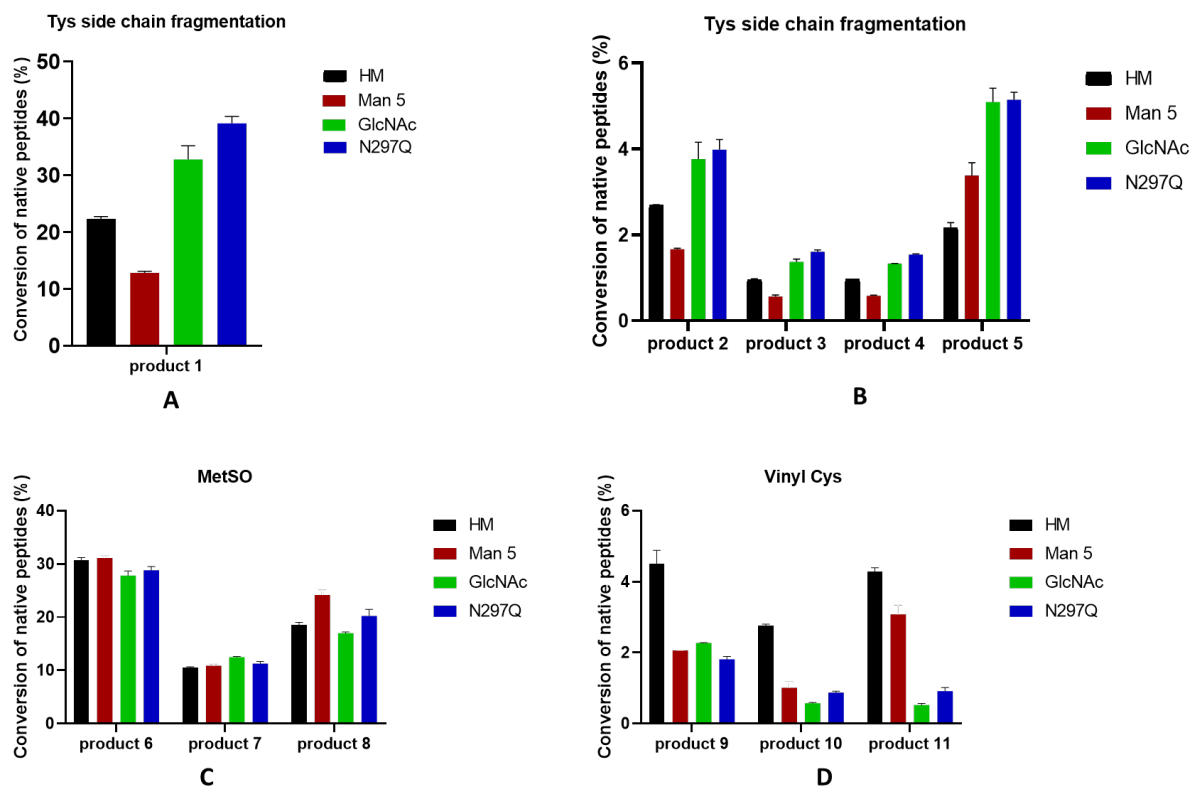


Fig. 4. Conversion of native peptides resulting from Tyr (A and B), Met (C) and Cys (D) photo-degradation. The photoirradiation was conducted at λ_{\max} = 305 nm for 30 min. Detailed peptide sequences information is presented in Table 2. Product yields from the four IgG4-Fc: HM, Man₅, GlcNAc₁ and N297Q are plotted. Two independent replicates were performed.

3.5 Binding of IgG4-Fc variants to FcγRIIIA. The effect of glycan structure at Asn²⁹⁷ in IgG4-Fc on binding to FcγRIIIA(Val¹⁵⁸) was evaluated using biolayer interferometry on a BLItz system. The equilibrium binding for HM, Man₅, GlcNAc₁, and N297Q IgG4-Fc is displayed in Fig. 5. The sensorgrams for the association between IgG4-Fc and FcγRIIIA are displayed in Fig. 6. All binding curves were well fit to bi-exponential kinetics, indicative of at least two separate association equilibria, potentially reflecting the glycan heterogeneity of FcγRIIIA (28, 29, 42, 45). For comparison, also the surface plasmon resonance data by Bruhns et al. (6) suggest more than one process in the interaction of FcγRIIIA(Val¹⁵⁸) with full length IgG4. In the two-exponential association model used for the kinetic fits ($y = A(1-\exp(-Bx)) + C(1-\exp(-Dx))$), $B = k_{obs,1} = k_1[P_0] + k_{-1}$ and $D = k_{obs,2} = k_2[P_0] + k_{-2}$, as described in Section 2.13. Here, k_1 and k_2 represent the k_{on} values for Reactions 1 and 2, respectively, and k_{-1} and k_{-2} represent the k_{off} values for Reactions 1 and 2, respectively. This two-exponential association model leads to good quality curve fits (Fig. 6, in red) for HM, Man₅, and GlcNAc₁ IgG4-Fc (Fig. 6, experimental data in blue). No measurable binding to FcγRIIIA was observed for the non-glycosylated variant N297Q IgG4-Fc (Fig. 5 and Fig. 6D). The values for k_{obs} were plotted as a function of the concentration $[P_0]$, from where k_{on} ($M^{-1}s^{-1}$) was derived from the slope, and the k_{off} (s^{-1}) was derived from the intercept. The plots for the fast phase are shown in Fig. 5, while the plots for the slow phase are shown in Fig. S2 (for the slow phase, linear plots were only obtained for HM and Man₅ IgG4-Fc). The fitting parameters for the fast phase correspond more closely to the affinity between IgG4 and FcγRIIIA (6), and, therefore, we primarily compared the IgG4-Fc variants based on the kinetic parameters for the fast phase. Equilibrium dissociation K_D constants were calculated as the ratio of k_{off} over

k_{on} . All values for k_{on} , k_{off} , and K_D for HM, Man_5 , and $GlcNAc_1$ IgG4-Fc are summarized in Table 3.

Man_5 IgG4-Fc reveals a two-fold increase of k_{on} compared to HM IgG4-Fc, resulting in a ca. two-fold reduction of K_D . The lower K_D of Man_5 indicates a ca. two-fold higher affinity to $Fc\gamma RIII A$ over HM IgG4-Fc. For $GlcNAc_1$, k_{on} reveals a 2- to 4-fold reduction compared to HM and Man_5 , while k_{off} shows a 7.7-fold increase over HM and Man_5 IgG4-Fc. Hence, $GlcNAc_1$ presents a 14.7-fold reduction of binding affinity to $Fc\gamma RIII A$ as compared to HM and Man_5 . For N297Q IgG4-Fc, the binding response merely reached $\Delta nm = 0.03$ at concentrations $[P_0]$ of 11.35 μM and 16.27 μM (Fig. 5 and 6). In addition, no reasonable curve fits were obtained, indicating no significant binding with $Fc\gamma RIII A$ at the high concentration tested as a result of the lack of glycans.

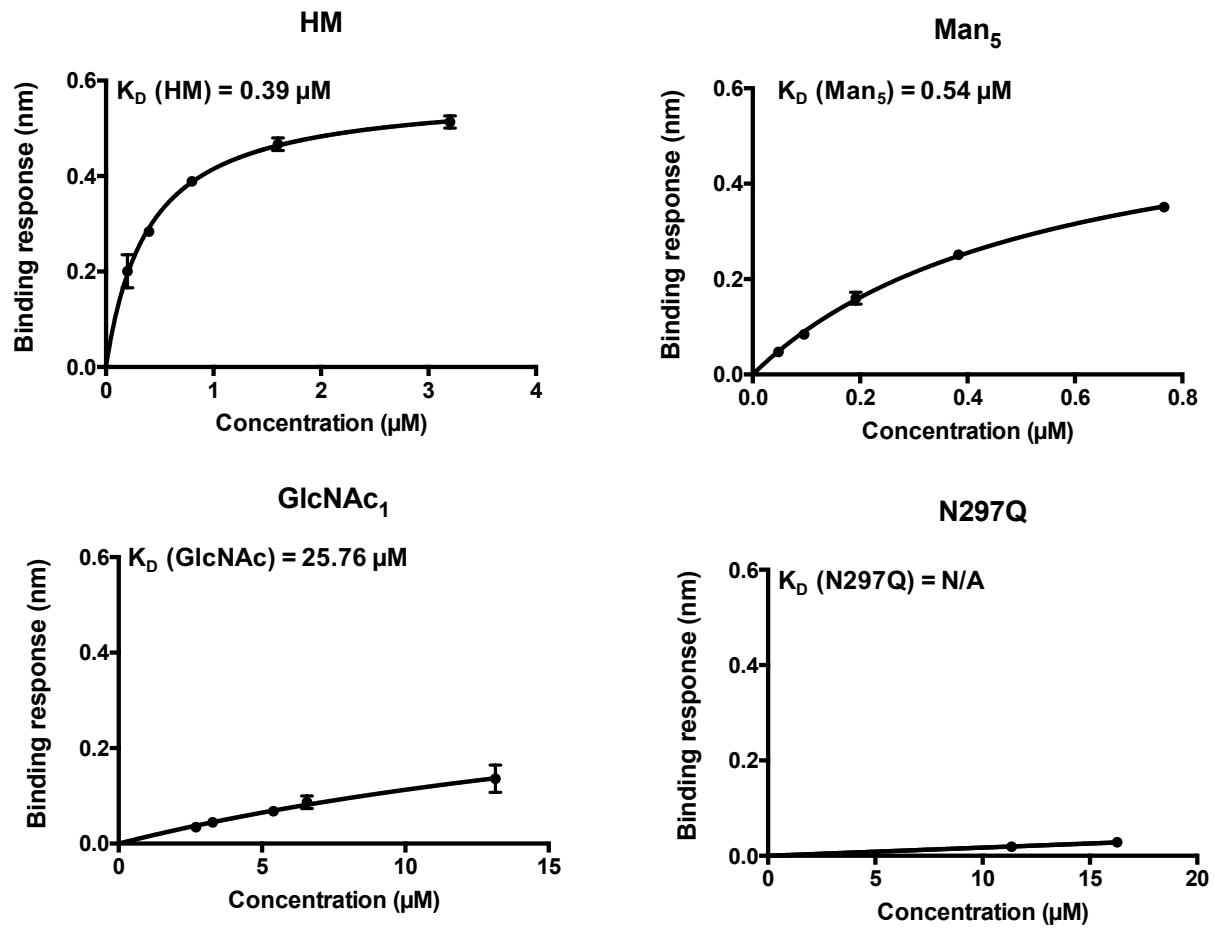
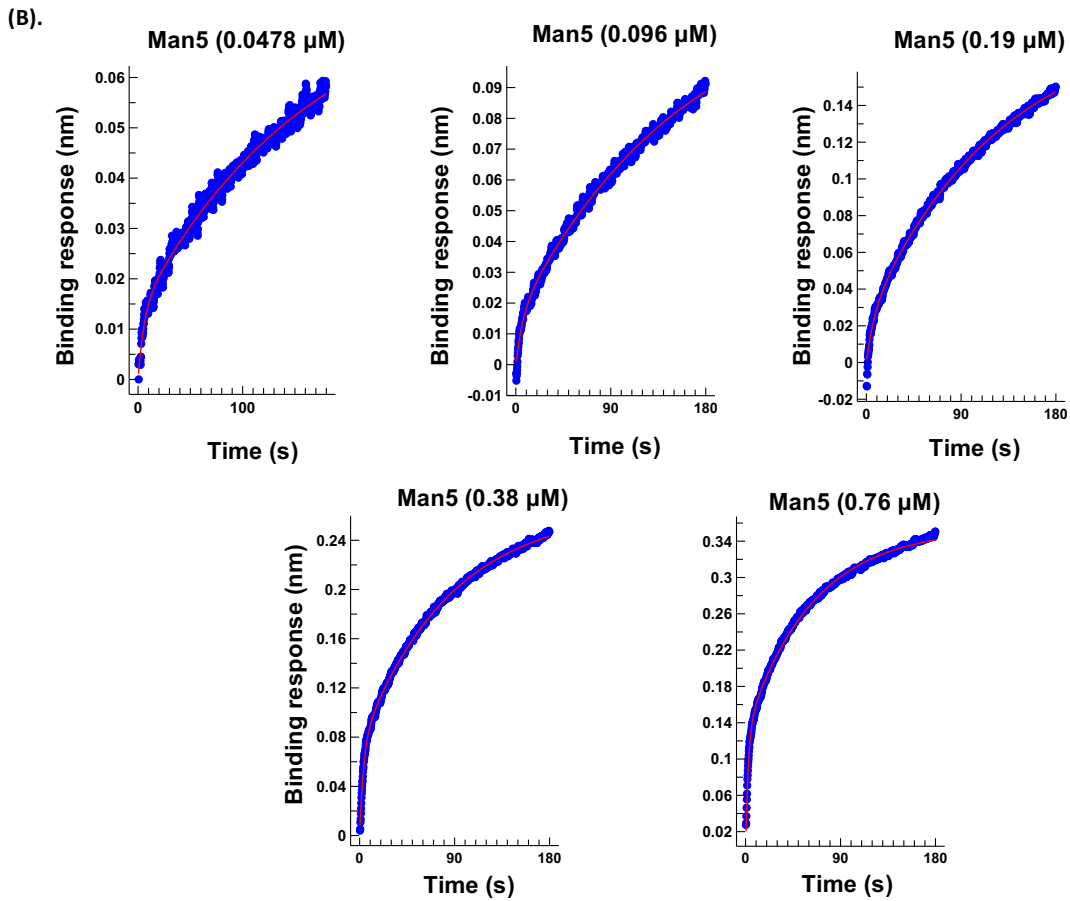
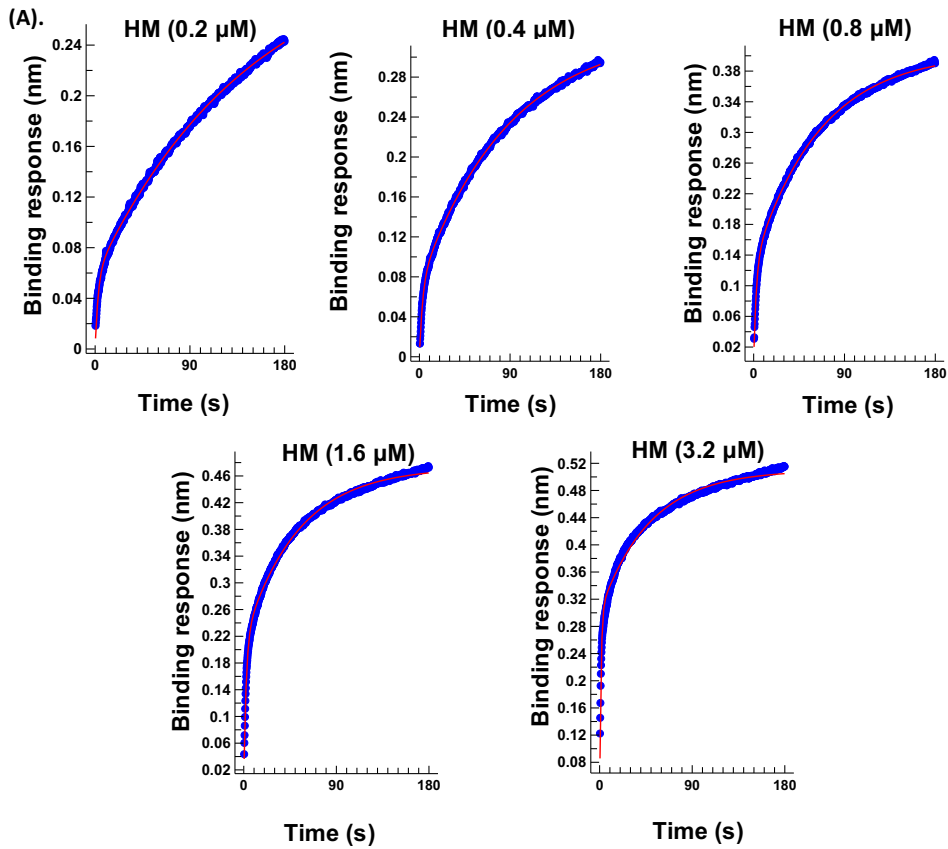
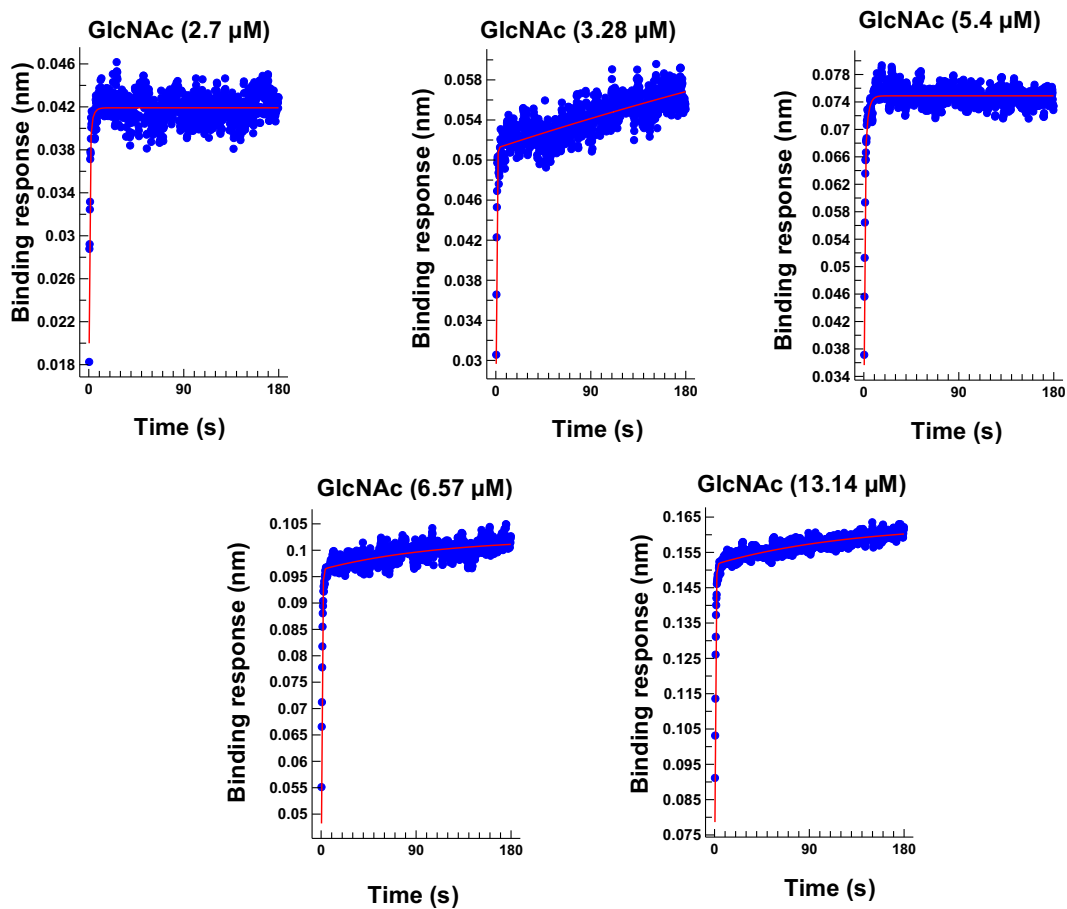


Fig. 5. Equilibrium dissociation constant, K_D , obtained with non-linear regression, using equation equivalent to the Langmuir isotherm. Respective K_D constants are displayed. Not applicable (NA) of N297Q indicates there is no measurable binding for the non-glycosylated IgG4-Fc.



(C).



(D).

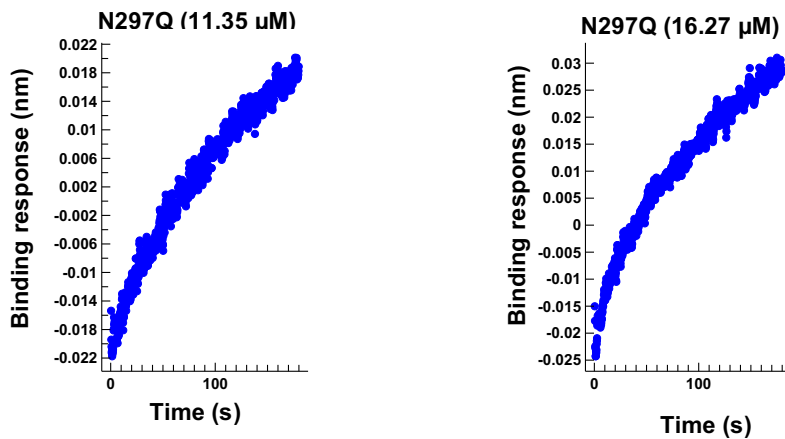


Fig. 6. BLI sensorgrams of (A) HM (B) Man₅ (C) GlcNAc₁, and (D) N297Q IgG4-Fc, where the red line is curve fit, and the blue dots are experimental data. The curve fitting is not applicable for N297Q IgG4-Fc.

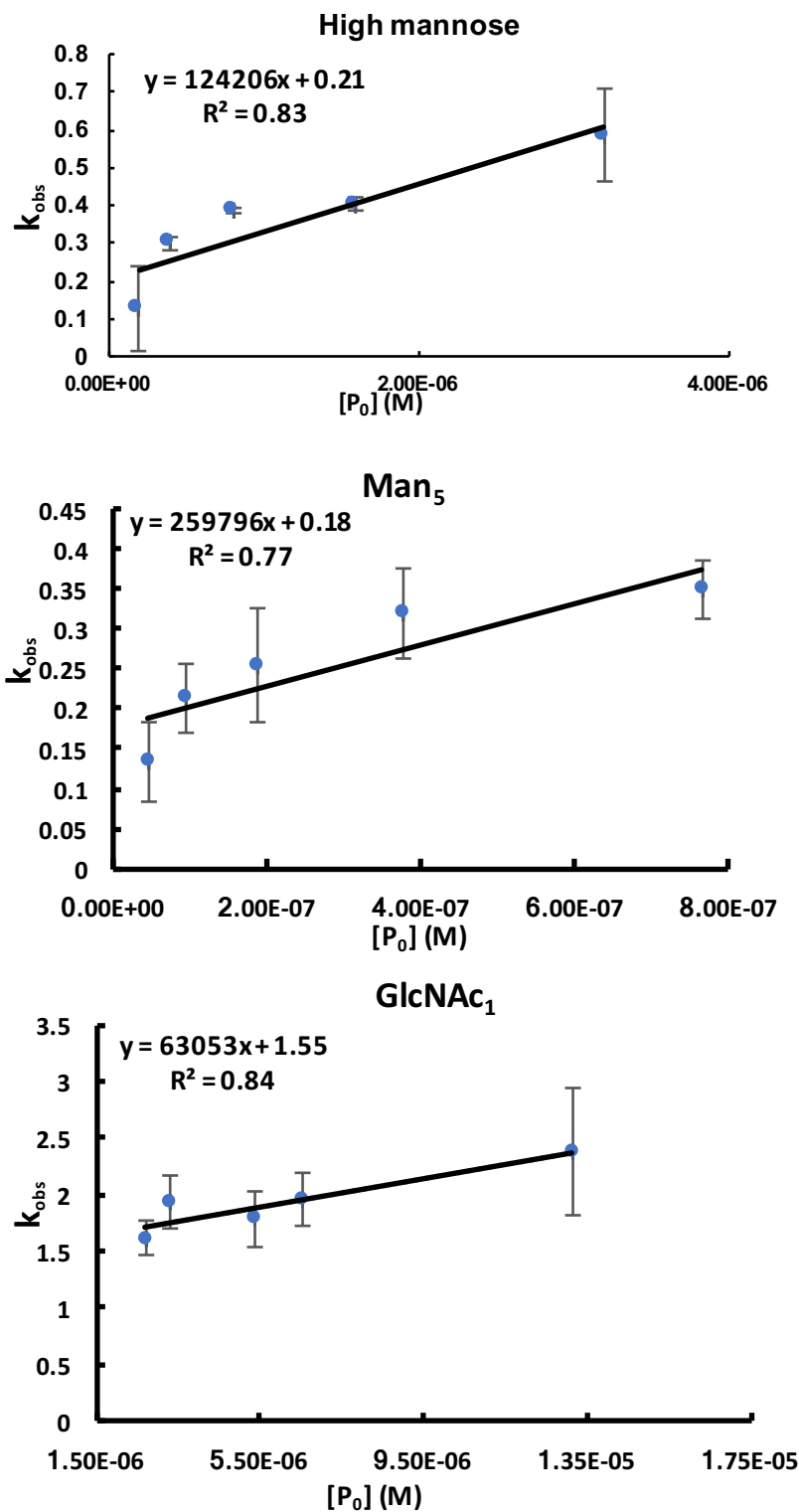


Fig. 7. Plots of k_{obs} (s^{-1}) as a function of IgG4-Fc concentration (M) for (A) HM, (B) Man₅ and (C) GlcNAc₁.

4. Discussion.

The aim of this work was to evaluate the effect of glycan structure (HM, Man₅, GlcNAc₁ and non-glycosylated) at Asn²⁹⁷ IgG4-Fc on the physicochemical stability (pH 7.1, 20 mM sodium phosphate, 0.22 mg/mL), photostability, and receptor binding. The four IgG4-Fc variants were initially characterized by HPLC-MS, indicating that the glycoforms display > 95% (HM and GlcNAc₁), 86% (Man₅), and 100% (N297Q) homogeneity.

The nature of these glycans was previously shown to affect IgG1-Fc conformation, which is essential for mAb stability, safety and efficacy (11). A similar effect of glycans was observed here on the thermal stability of IgG4-Fc. Based on the values for T_{m1} derived by DSC, HM, Man₅ and GlcNAc₁ IgG4-Fc display similar thermal stability, while N297Q IgG4-Fc shows lower thermal stability (Table 1). The T_{m1} value, corresponding to the melting temperature of the C_{H2} domain, is a measure of conformational stability, involving the unfolding of C_{H2} domains, C_{H2} glycan contacts, and C_{H2}/C_{H3} inter-domain interactions (49). The decreased T_{m1} value of N297Q can, therefore, be attributed to the lack of a glycan, which prevents glycan-glycan or glycan-protein interactions (50). For all four IgG4-Fc variants, more than two thermal transitions were observed by DSC (Fig. 1). Interestingly, a previous report showed that homogeneous G0 and G2 glycoforms of IgG4-Fc reveal only one thermal transition with a melting temperature of 64°C(51). It was also reported that deglycosylated IgG4-Fc reveals two transitions, where T_{m1}= 60 °C, and T_{m2}= 68 °C(51). In this work, the DSC thermograms of IgG4-Fc with different truncated glycans present a similar phenomenon: two thermal transitions are resolved better for the smaller sized glycans

(Fig. 1). All four IgG4-Fc variants reveal a 10°C reduction of T_m2 as compared to IgG1-Fc, where the T_m2 of IgG4-Fc is approximately 70°C while the T_m2 of IgG1-Fc is approximately 78 -80°C, reported elsewhere(11). This difference can be attributed to the weakened hydrophobic interactions between the C_H3 domains in IgG4-Fc homodimers compared to IgG1-Fc (22, 24).

During the process of pharmaceutical development, light exposure needs to be strictly controlled, due to the fact that mAb-based therapeutics are prone to photo-degradation(52, 53) (54, 55). Upon exposure to UV light, photo-sensitive amino acids (Tyr, Trp, Cys, cystine, and Phe) can directly absorb light leading to several pathways of photo-transformation(52). Upon exposure to visible light, proteins are potentially damaged by reactive oxygen species(54, 56). Here, we investigated the effects of glycan structure on IgG4-Fc photo-stability during photo-irradiation at $\lambda_{max}=305$ nm (between 295 nm and 340 nm). The relative yields of photo-degradation products resulting from Tyr (Tyr³⁷³ and Tyr⁴³⁶), Met (Met²⁵², Met³⁵⁸, and Met⁴²⁶), and Cys (Cys³²¹, Cys³⁶⁷, and Cys⁴²⁵) were quantified.

We previously discovered and characterized a photo-induced Tyr side chain fragmentation, initiated by electron transfer from Tyr to an intermediary Trp radical cation (Trp⁺)(32). The distance between Tyr and Trp can affect the efficiency of photo-induced Tyr side chain fragmentation(32). Products **1-5**, resulting from photo-induced Tyr side chain fragmentation reveal relatively higher yields in IgG4-Fc with smaller sizes of Asn²⁹⁷ glycans (e.g., in N297Q and GlcNAc₁). The smaller size glycans may allow for a more dynamic protein conformation (57)

resulting a closer approach between Tyr and Trp⁺.

FcγRIIIA is the most important Fc receptor for natural killer cells since it is the only one present for ca. 80% of people(58, 59). In addition, binding affinities between IgGs and FcγRIIIA depend on the patterns of Asn²⁹⁷ glycans in IgGs (27, 60). Therefore, FcγRIIIA was selected in the present work. We utilized biotinylated FcγRIIIA (Val¹⁵⁸) and streptavidin (SA) to immobilize FcγRIIIA on SA biosensor tips(13), to measure its affinities to the IgG4-Fc variants. The association rate of Man₅ IgG4-Fc ($2.60 \times 10^5 \text{ M}^{-1}\text{s}^{-1}$) reveals a somewhat higher k_{on} value compared to HM ($1.24 \times 10^5 \text{ M}^{-1}\text{s}^{-1}$), and both present rather similar k_{off} values. The truncated GlcNAc₁ glycoform revealed an approximate two-fold reduction of k_{on} , and a seven-fold increase of k_{off} , as compared to Man₅ and HM. N297Q does not reveal any significant binding to FcγRIIIA at the highest concentration tested (16 μM). The reduction of N297 glycan size in IgG4-Fc has a smaller effect on k_{on} but a larger effect on k_{off} . The effect of glycan nature on IgG4-Fc affinities to FcγRIIIA is similar to that reported for similar glycoforms of IgG1-Fc in that both HM and Man₅ glycoforms bind tightly, the GlcNAc₁ glycoform retains weak affinity, and the non-glycosylated IgG4-Fc mutant does not show significant affinity (13).

The equilibrium constant (K_{D}) between a serum-derived IgG4 and FcγRIIIA was reported to be ca. 4 μM (6). This K_{D} value was obtained via analysis of the binding response at equilibrium as a function of protein concentration, where the corresponding steady-state K_{D} can be derived (6). For comparison, we applied a similar analysis of our data, rendering steady-state K_{D} values of 0.39

μM , $0.54 \mu\text{M}$, and $25.76 \mu\text{M}$ for HM, Man_5 and GlcNAc_1 , respectively (Fig. S3). The K_D of HM and Man_5 IgG4-Fc reveal a 10- and 8-fold reduction as compared to the serum-derived IgG4, suggesting an 8-10-fold increase of the affinities to $\text{Fc}\gamma\text{RIIIA}$. These increased affinities of our IgG4-Fc glycoforms can be rationalized by the absence of fucose in the high mannose glycoforms tested in this study and the likelihood of high levels of core-linked fucose in serum derived IgG4 (60-62). As mentioned previously, fucosylation of IgG1-Fc and differential glycosylation of N162 of $\text{Fc}\gamma\text{RIIIA}$ has proven to modulate the interactions between the two proteins (60-62). Given that the dissociation constants measured in this study for HM and Man_5 IgG4-Fc, 0.39 and $0.54 \mu\text{M}$ respectively, are similar to dissociation constants that have been measured for fucosylated IgG1 Fc glycoforms (ranging from 0.095 - $0.5 \mu\text{M}$)(6, 27) high mannose IgG4 glycoforms may elicit ADCC similar to fucosylated IgG1. Based on this, in addition to monitoring levels of afucosylated IgG4 (63), it would be prudent to monitor levels of high mannose IgG4 glycoforms as well for IgG4 based mAb therapeutics.

5. Acknowledgements.

We gratefully acknowledge financial support by a Genentech Foundation Fellowship.

References.

1. Slamon DJ, Leyland-Jones B, Shak S, Fuchs H, Paton V, Bajamonde A, et al. Use of chemotherapy plus a monoclonal antibody against HER2 for metastatic breast cancer that overexpresses HER2. *N Engl J Med*. 2001; 344:783-92.
2. Trauth BC, Klas C, Peters AM, Matzku S, Moller P, Falk W, et al. Monoclonal antibody-mediated tumor regression by induction of apoptosis. *Science*. 1989; 245:301-5.
3. Peyrin-Biroulet L, Demarest S, Nirula A. Bispecific antibodies: The next generation of targeted

- inflammatory bowel disease therapies. *Autoimmun Rev*. 2018.
4. Shah IS, Lovell S, Mehzabeen N, Battaile KP, Tolbert TJ. Structural characterization of the Man5 glycoform of human IgG3 Fc. *Mol Immunol*. 2017; 92:28-37.
 5. Vidarsson G, Dekkers G, Rispens T. IgG subclasses and allotypes: from structure to effector functions. *Front Immunol*. 2014; 5:520.
 6. Bruhns P, Iannascoli B, England P, Mancardi DA, Fernandez N, Jorieux S, et al. Specificity and affinity of human Fcγ receptors and their polymorphic variants for human IgG subclasses. *Blood*. 2009; 113:3716-25.
 7. Scapin G, Yang X, Prosser WW, McCoy M, Reichert P, Johnston JM, et al. Structure of full-length human anti-PD1 therapeutic IgG4 antibody pembrolizumab. *Nat Struct Mol Biol*. 2015; 22:953-8.
 8. Kaplon H, Reichert JM. Antibodies to watch in 2019. *MAbs*. 2019; 11:219-38.
 9. Ecker DM, Jones SD, Levine HL. The therapeutic monoclonal antibody market. *MAbs*. 2015; 7:9-14.
 10. Edelman GM, Cunningham BA, Gall WE, Gottlieb PD, Rutishauser U, Waxdal MJ. The covalent structure of an entire gammaG immunoglobulin molecule. *Proc Natl Acad Sci U S A*. 1969; 63:78-85.
 11. More AS, Toprani VM, Okbazghi SZ, Kim JH, Joshi SB, Middaugh CR, et al. Correlating the Impact of Well-Defined Oligosaccharide Structures on Physical Stability Profiles of IgG1-Fc Glycoforms. *J Pharm Sci*. 2016; 105:588-601.
 12. Mozziconacci O, Okbazghi S, More AS, Volkin DB, Tolbert T, Schoneich C. Comparative Evaluation of the Chemical Stability of 4 Well-Defined Immunoglobulin G1-Fc Glycoforms. *J Pharm Sci*. 2016; 105:575-87.
 13. Okbazghi SZ, More AS, White DR, Duan S, Shah IS, Joshi SB, et al. Production, Characterization, and Biological Evaluation of Well-Defined IgG1 Fc Glycoforms as a Model System for Biosimilarity Analysis. *J Pharm Sci*. 2016; 105:559-74.
 14. Seo N, Polozova A, Zhang M, Yates Z, Cao S, Li H, et al. Analytical and functional similarity of Amgen biosimilar ABP 215 to bevacizumab. *MAbs*. 2018; 10:678-91.
 15. Kim S, Song J, Park S, Ham S, Paek K, Kang M, et al. Drifts in ADCC-related quality attributes of Herceptin(R): Impact on development of a trastuzumab biosimilar. *MAbs*. 2017; 9:704-14.
 16. Reusch D, Tejada ML. Fc glycans of therapeutic antibodies as critical quality attributes. *Glycobiology*. 2015; 25:1325-34.
 17. Lee C, Jeong M, Lee JJ, Seo S, Cho SC, Zhang W, et al. Glycosylation profile and biological activity of Remicade(R) compared with Flixabi(R) and Remsima(R). *MAbs*. 2017; 9:968-77.
 18. Lee KH, Lee J, Bae JS, Kim YJ, Kang HA, Kim SH, et al. Analytical similarity assessment of rituximab biosimilar CT-P10 to reference medicinal product. *MAbs*. 2018; 10:380-96.
 19. Hong J, Lee Y, Lee C, Eo S, Kim S, Lee N, et al. Physicochemical and biological characterization of SB2, a biosimilar of Remicade(R) (infliximab). *MAbs*. 2017; 9:364-82.
 20. Zheng K, Bantog C, Bayer R. The impact of glycosylation on monoclonal antibody conformation and stability. *MAbs*. 2011; 3:568-76.
 21. Mimura Y, Church S, Ghirlando R, Ashton PR, Dong S, Goodall M, et al. The influence of

- glycosylation on the thermal stability and effector function expression of human IgG1-Fc: properties of a series of truncated glycoforms. *Molecular Immunology*. 2000; 37:697-706.
22. Rispens T, Ooijevaar-de Heer P, Bende O, Aalberse RC. Mechanism of immunoglobulin G4 Fab-arm exchange. *J Am Chem Soc*. 2011; 133:10302-11.
 23. Davies AM, Rispens T, Ooijevaar-de Heer P, Gould HJ, Jefferis R, Aalberse RC, et al. Structural determinants of unique properties of human IgG4-Fc. *J Mol Biol*. 2014; 426:630-44.
 24. Labrijn AF, Rispens T, Meesters J, Rose RJ, den Bleker TH, Loverix S, et al. Species-specific determinants in the IgG CH3 domain enable Fab-arm exchange by affecting the noncovalent CH3-CH3 interaction strength. *J Immunol*. 2011; 187:3238-46.
 25. Labrijn AF, Buijsse AO, van den Bremer ET, Verwilligen AY, Bleeker WK, Thorpe SJ, et al. Therapeutic IgG4 antibodies engage in Fab-arm exchange with endogenous human IgG4 in vivo. *Nat Biotechnol*. 2009; 27:767-71.
 26. Shields RL, Lai J, Keck R, O'Connell LY, Hong K, Meng YG, et al. Lack of fucose on human IgG1 N-linked oligosaccharide improves binding to human FcγRIII and antibody-dependent cellular toxicity. *J Biol Chem*. 2002; 277:26733-40.
 27. Li T, DiLillo DJ, Bournazos S, Giddens JP, Ravetch JV, Wang LX. Modulating IgG effector function by Fc glycan engineering. *Proc Natl Acad Sci U S A*. 2017; 114:3485-90.
 28. Subedi GP, Barb AW. CD16a with oligomannose-type N-glycans is the only "low-affinity" Fc γ receptor that binds the IgG crystallizable fragment with high affinity in vitro. *J Biol Chem*. 2018; 293:16842-50.
 29. Falconer DJ, Subedi GP, Marcella AM, Barb AW. Antibody Fucosylation Lowers the FcγRIIIa/CD16a Affinity by Limiting the Conformations Sampled by the N162-Glycan. *ACS Chem Biol*. 2018; 13:2179-89.
 30. Mizushima T, Yagi H, Takemoto E, Shibata-Koyama M, Isoda Y, Iida S, et al. Structural basis for improved efficacy of therapeutic antibodies on defucosylation of their Fc glycans. *Genes Cells*. 2011; 16:1071-80.
 31. Ferrara C, Grau S, Jager C, Sondermann P, Brunker P, Waldhauer I, et al. Unique carbohydrate-carbohydrate interactions are required for high affinity binding between FcγRIII and antibodies lacking core fucose. *Proc Natl Acad Sci U S A*. 2011; 108:12669-74.
 32. Kang H, Tolbert TJ, Schoneich C. Photoinduced Tyrosine Side Chain Fragmentation in IgG4-Fc: Mechanisms and Solvent Isotope Effects. *Mol Pharm*. 2019; 16:258-72.
 33. Varalakshmi KN, Kumudini BS, Nandini BN, Solomon J, Suhas R, Mahesh B, et al. Production and characterization of alpha-amylase from *Aspergillus niger* JGI 24 isolated in Bangalore. *Pol J Microbiol*. 2009; 58:29-36.
 34. Wu S, Letchworth GJ. High efficiency transformation by electroporation of *Pichia pastoris* pretreated with lithium acetate and dithiothreitol. *Biotechniques*. 2004; 36:152-4.
 35. Zhu Y, Suits MD, Thompson AJ, Chavan S, Dinev Z, Dumon C, et al. Mechanistic insights into a Ca²⁺-dependent family of alpha-mannosidases in a human gut symbiont. *Nat Chem Biol*. 2010; 6:125-32.
 36. Cuskin F, Lowe EC, Temple MJ, Zhu Y, Cameron E, Pudlo NA, et al. Human gut Bacteroidetes



- can utilize yeast mannan through a selfish mechanism. *Nature*. 2015; 517:165-9.
37. Choi BK, Bobrowicz P, Davidson RC, Hamilton SR, Kung DH, Li H, et al. Use of combinatorial genetic libraries to humanize N-linked glycosylation in the yeast *Pichia pastoris*. *Proc Natl Acad Sci U S A*. 2003; 100:5022-7.
 38. Lee J, Seliger HH. Quantum Yield of Ferrioxalate Actinometer. *J Chem Phys*. 1964; 40:519-&.
 39. Hatchard CG, Parker CA. A New Sensitive Chemical Actinometer .2. Potassium Ferrioxalate as a Standard Chemical Actinometer. *Proc R Soc Lon Ser-A*. 1956; 235:518-36.
 40. Baertschi SW, Alsante KM, Tonnesen HH. A critical assessment of the ICH guideline on photostability testing of new drug substances and products (Q1B): Recommendation for revision. *J Pharm Sci*. 2010; 99:2934-40.
 41. Bruylants G, Wouters J, Michaux C. Differential scanning calorimetry in life science: thermodynamics, stability, molecular recognition and application in drug design. *Curr Med Chem*. 2005; 12:2011-20.
 42. Dorion-Thibaudeau J, Raymond C, Lattova E, Perreault H, Durocher Y, De Crescenzo G. Towards the development of a surface plasmon resonance assay to evaluate the glycosylation pattern of monoclonal antibodies using the extracellular domains of CD16a and CD64. *J Immunol Methods*. 2014; 408:24-34.
 43. Grunwald C, Kuhlmann J, Woll C. In deuterated water the unspecific adsorption of proteins is significantly slowed down: results of an SPR study using model organic surfaces. *Langmuir*. 2005; 21:9017-9.
 44. Robelek R, Wegener J. Label-free and time-resolved measurements of cell volume changes by surface plasmon resonance (SPR) spectroscopy. *Biosens Bioelectron*. 2010; 25:1221-4.
 45. Derebe MG, Nanjunda RK, Gilliland GL, Lacy ER, Chiu ML. Human IgG subclass cross-species reactivity to mouse and cynomolgus monkey Fcγ receptors. *Immunol Lett*. 2018; 197:1-8.
 46. Ferrara C, Stuart F, Sondermann P, Brunker P, Umana P. The carbohydrate at FcγRIIIa Asn-162. An element required for high affinity binding to non-fucosylated IgG glycoforms. *J Biol Chem*. 2006; 281:5032-6.
 47. Shibata-Koyama M, Iida S, Okazaki A, Mori K, Kitajima-Miyama K, Saitou S, et al. The N-linked oligosaccharide at Fc γ RIIIa Asn-45: an inhibitory element for high Fc γ RIIIa binding affinity to IgG glycoforms lacking core fucosylation. *Glycobiology*. 2009; 19:126-34.
 48. Khor HK, Jacoby ME, Squier TC, Chu GC, Chelius D. Identification of methionine sulfoxide diastereomers in immunoglobulin gamma antibodies using methionine sulfoxide reductase enzymes. *MAbs*. 2010; 2:299-308.
 49. Mimura Y, Church S, Ghirlando R, Ashton PR, Dong S, Goodall M, et al. The influence of glycosylation on the thermal stability and effector function expression of human IgG1-Fc: properties of a series of truncated glycoforms. *Mol Immunol*. 2000; 37:697-706.
 50. Feige MJ, Walter S, Buchner J. Folding mechanism of the CH2 antibody domain. *J Mol Biol*. 2004; 344:107-18.

51. Ghirlando R, Lund J, Goodall M, Jefferis R. Glycosylation of human IgG-Fc: influences on structure revealed by differential scanning micro-calorimetry. *Immunol Lett.* 1999; 68:47-52.
52. Kerwin BA, Remmele RL, Jr. Protect from light: photodegradation and protein biologics. *J Pharm Sci.* 2007; 96:1468-79.
53. Qi P, Volkin DB, Zhao H, Nedved ML, Hughes R, Bass R, et al. Characterization of the photodegradation of a human IgG1 monoclonal antibody formulated as a high-concentration liquid dosage form. *J Pharm Sci.* 2009; 98:3117-30.
54. Mallaney M, Wang SH, Sreedhara A. Effect of ambient light on monoclonal antibody product quality during small-scale mammalian cell culture process in clear glass bioreactors. *Biotechnol Prog.* 2014; 30:562-70.
55. Sreedhara A, Yin J, Joyce M, Lau K, Wecksler AT, Deperalta G, et al. Effect of ambient light on IgG1 monoclonal antibodies during drug product processing and development. *Eur J Pharm Biopharm.* 2016; 100:38-46.
56. Stroop SD, Conca DM, Lundgard RP, Renz ME, Peabody LM, Leigh SD. Photosensitizers form in histidine buffer and mediate the photodegradation of a monoclonal antibody. *J Pharm Sci.* 2011; 100:5142-55.
57. More AS, Toth RTt, Okbazghi SZ, Middaugh CR, Joshi SB, Tolbert TJ, et al. Impact of Glycosylation on the Local Backbone Flexibility of Well-Defined IgG1-Fc Glycoforms Using Hydrogen Exchange-Mass Spectrometry. *J Pharm Sci.* 2018; 107:2315-24.
58. Gillis C, Gouel-Cheron A, Jonsson F, Bruhns P. Contribution of Human FcγR3s to Disease with Evidence from Human Polymorphisms and Transgenic Animal Studies. *Front Immunol.* 2014; 5:254.
59. van der Heijden J, Breunis WB, Geissler J, de Boer M, van den Berg TK, Kuijpers TW. Phenotypic variation in IgG receptors by nonclassical FCGR2C alleles. *J Immunol.* 2012; 188:1318-24.
60. Subedi GP, Barb AW. The immunoglobulin G1 N-glycan composition affects binding to each low affinity Fc gamma receptor. *MAbs.* 2016; 8:1512-24.
61. Hayes JM, Frostell A, Cosgrave EF, Struwe WB, Potter O, Davey GP, et al. Fc gamma receptor glycosylation modulates the binding of IgG glycoforms: a requirement for stable antibody interactions. *J Proteome Res.* 2014; 13:5471-85.
62. Patel KR, Roberts JT, Subedi GP, Barb AW. Restricted processing of CD16a/Fc gamma receptor IIIa N-glycans from primary human NK cells impacts structure and function. *J Biol Chem.* 2018; 293:3477-89.
63. Gong Q, Hazen M, Marshall B, Crowell SR, Ou Q, Wong AW, et al. Increased in vivo effector function of human IgG4 isotype antibodies through afucosylation. *MAbs.* 2016; 8:1098-106.

Table 1. T_m values of HM, Man₅, GlcNAc₁, and N297Q IgG4-Fc from DSC and intrinsic fluorescence analysis. The average T_m and the range from two independent measurements are presented.

	T_{m1} (°C) (DSC)	T_{m2} (°C) (DSC)	T_m (°C) (Fluorescence)
HM	64.5 ± 0.0071	71.7 ± 0.11	61.97 ± 0.14
Man ₅	65.3 ± 0.25	71.3 ± 0.099	62.69 ± 0.16
GlcNAc ₁	64.6 ± 0.014	70.8 ± 0.078	61.24 ± 0.23
N297Q	61.5 ± 0.028	70.5 ± 0.035	59.86 ± 0.08

Table 2. A list of eleven photoproducts were identified and quantified from photoirradiation of HM, Man₅, GlcNAc₁, and N297Q IgG4-Fc at λ_{\max} = 305 nm for 30 min. Corresponding product sequences and modified residues are listed.

Product	Photoproducts	Position	m/z	z
1	MTKNQVSLTC(+57)LVKGF-NH ₂	Tyr ³⁷³	575.61	3
2	M(+16)TKNQVSLTC(+57)LVKGF-NH ₂	Tyr ³⁷³	580.96	3
3	 TQKSLSLSLGK	Tyr ⁴³⁶	609.30	2
4	 [Tyr ⁴³⁶]+18	Tyr ⁴³⁶	618.30	2
5	TQKSLSLSLGK	Tyr ⁴³⁶	387.89	3
6	FLGGPSVFLFPPKPKDTLM(+16)ISRTPE	Met ²⁵²	698.38	4
7	M(+16)TKNQVSLTC(+57)LVKGFYPSDI AVE	Met ³⁵⁸	872.76	3
8	GNVFSC(+57)SVM(+16)HE	Met ⁴²⁶	641.75	2
9	YKC(+55)KVSNGKLPSSIE ^a	Cys ³²¹	569.96	3
10	MTKNQVSLTC(+55)LVKGFYPSDIAVE	Cys ³⁶⁷	866.76	3
11	GNVFSC(+55)SVMHE	Cys ⁴²⁵	632.75	2

^aThe product Cys(+55) indicates an amidomethyl adduct of vinyl Cys

Table 3. Binding parameters, k_{on} , k_{off} and K_D of HM, Man₅, GlcNAc₁, and N297Q IgG4-Fc, representative of binding affinities to FcγRIIIA. k_{on} , k_{off} and K_D (kinetic) were obtained from kinetic binding analysis. K_D (kinetic) was obtained from the ratio of k_{off} to k_{on} . K_D (equilibrium) was obtained from equilibrium binding analysis with non-linear regression fit. These data are averaged from 2 or 3 independent measurements.

	k_{on} (M ⁻¹ s ⁻¹)	k_{off} (s ⁻¹)	K_D (μM): kinetic	K_D (μM): equilibrium
HM	(1.24±0.3) x10 ⁵	0.207 ± 0.052	1.66	0.39
Man ₅	(2.60±0.9) x10 ⁵	0.177 ± 0.035	0.68	0.54
GlcNAc ₁	(6.30±3) x10 ⁴	1.546 ± 0.238	24.52	25.76
N297Q	NA	NA	NA	NA

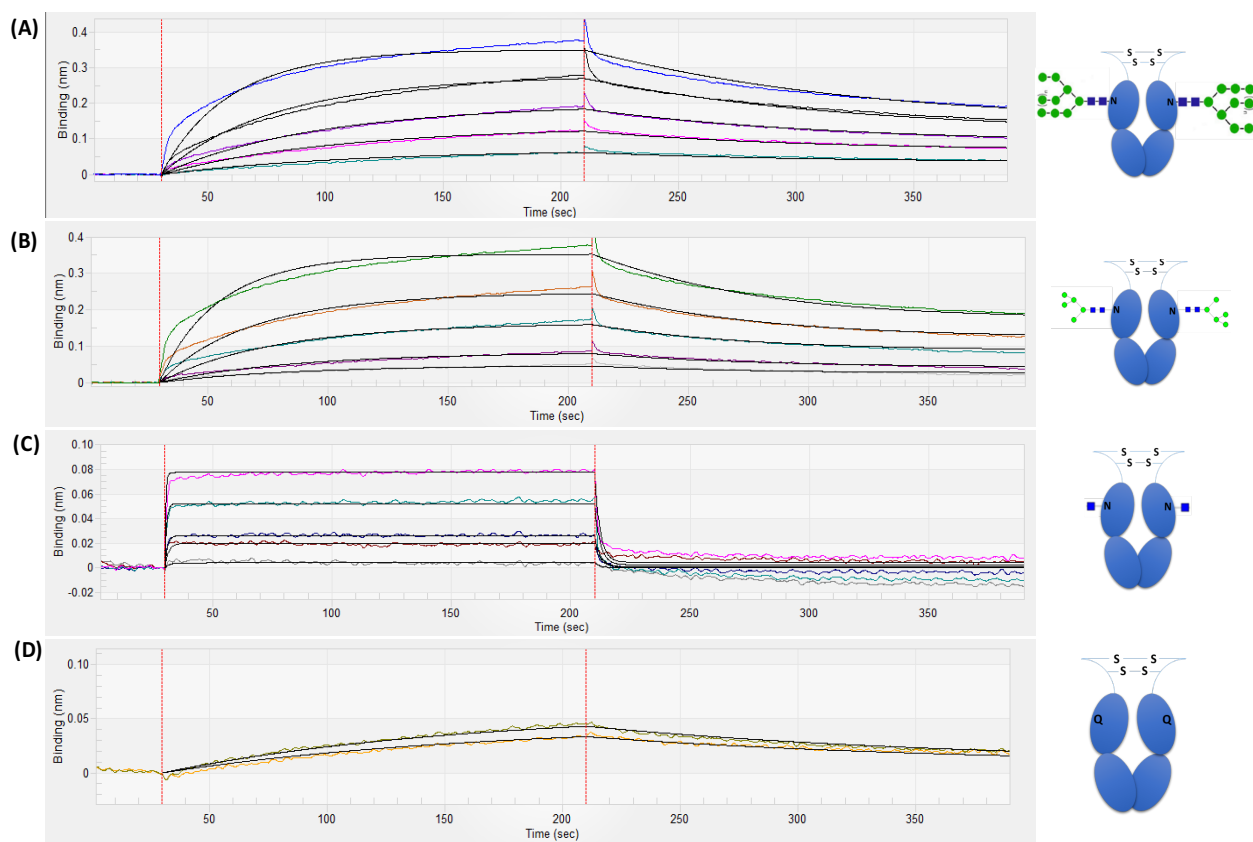


Fig. S1. Binding analysis of IgG4-Fc glycoforms and FcγRIIIA. Fitted curve is displayed in black with corresponding glycoform structure (A) HM-IgG4-Fc (B) Man5-IgG4-Fc (C) GlcNAc1 IgG4-Fc (D) N297Q IgG4-Fc.

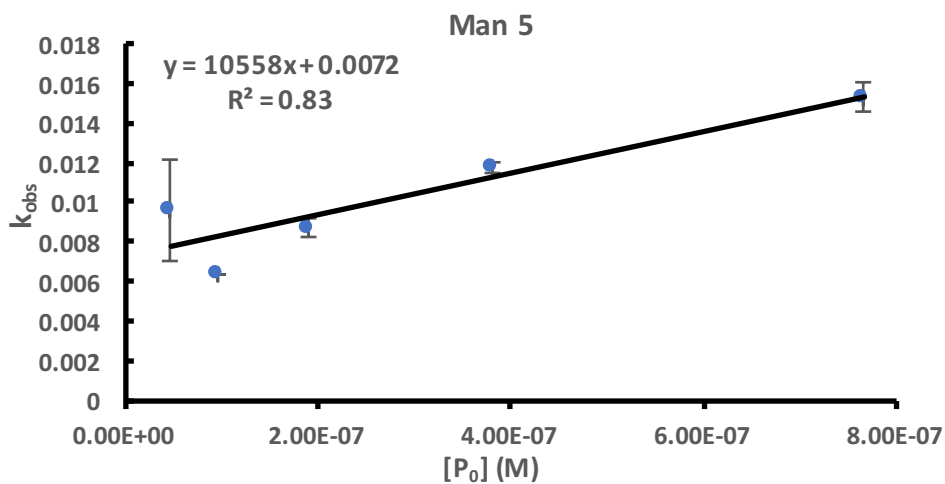
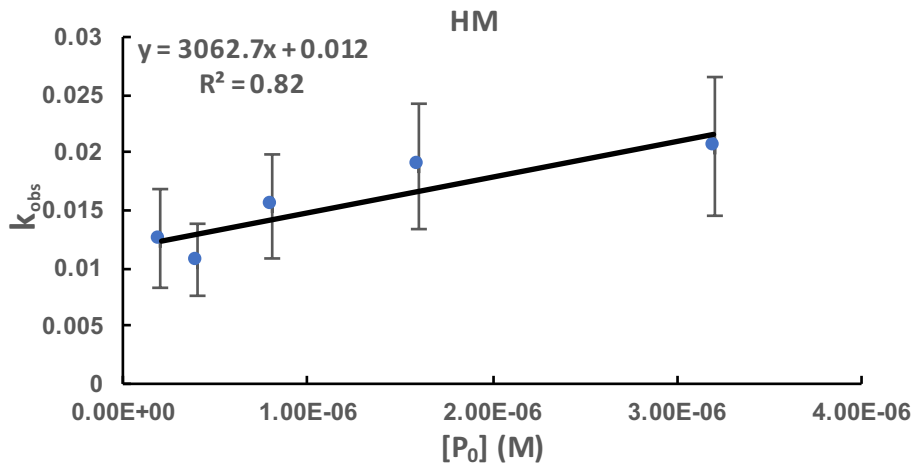


Fig. S2. Plots of k_{obs} of the slow phase as a function of $[P_0]$ for HM and Man₅ IgG4-Fc. The error bars represent the standard error from two or three independent measurements. GlcNAc₁ IgG4-Fc is not displayed due to the lack of linear relationship between k_{obs} and protein concentration. N297Q is not displayed due to no obvious binding with Fc γ RIIIA.

Chapter 5. The reaction of acetonitrile with N-terminal Cys of IgG4-Fc

5.1 Introduction.

Antibody-drug conjugates (ADCs) are rapidly evolving due to their high potency and specificity. So far, two ADCs have been marketed in the US and approximately 60 ADCs are in the clinical development¹. ADCs refer to the chemical conjugation of a humanized antibody to small cytotoxic molecules (e.g., antimetabolic agents) through a chemical linker. Thus, ADCs combine the specificity of an antibody for its target antigen and the potency of a small molecule drug². In ADCs, the antibody reacts as a cell-targeting molecule and its conjugation with cytotoxic drugs, enabling the selective delivery of the toxic agents, leading to death of the targeted cells.

The selection of the linker chemistry is critical for the successful development of ADCs. An optimal linker needs to meet the potential criteria as follows¹. First, the linker needs to present sufficient stability before reaching target cells. Second, the linker is readily to be cleaved after endocytosis. Third, the linker should not induce instability of the conjugated molecule. Conjugation is typically achieved via two major methods, e.g., chemical and enzymatic conjugation, where chemical conjugation potentially involves coupling with Lys amine or Cys thiol. Overall, Cys-based conjugation is superior to Lys attributed to Cys low abundance in proteins, leading to more controlled drug-to-antibody ratio (DAR)³, reduced heterogeneity, high efficacy and improved therapeutic window⁴. The most common approach of Cys coupling is to utilize maleimide-based conjugation, e.g., in brentuximab vedotin, an FDA approved ADC⁵, where such process requires reduction and re-oxidation of disulfides. These processes normally introduce

difficulties to control the extent of the reactions and lead to undesired polymerization⁶. For example, the partial reduction process may result in the loss of the light chain, impairing binding affinity of mAbs to antigens, and additionally lead to reduced stability⁷. Therefore, in this work, a specific chemical modification at the N-terminal Cys of an IgG4-Fc was investigated via reaction with acetonitrile, which results in a cyclic product at the N-terminus of the IgG4-Fc. An Fc domain was utilized due to its simplicity for deriving reactions, as compared to a full IgG. Conjugation to an Fc fragment prolongs the half-life of the conjugated molecule⁸, and potentially improves solubility and stability of the partner molecule in vivo and in vitro⁹. The IgG4-Fc was expressed from yeast strain *Pichia pastoris*, presenting predominantly high mannose (HM) glycoforms at Asn²⁹⁷ containing GlcNAc₂Man_(8+n) (n = 0-4).

5.2 Experimental section.

5.2.1 Materials.

GluC was purchased from Promega Corporation (Madison, WI). Iodoacetamide (IAA), iodoacetic acid (IAC), ammonium bicarbonate, tris (2-carboxyethyl)phosphine hydrochloride (TCEP), 4-cyano-1-butyn (HCCCH₂CH₂CN) and guanidine hydrochloride (GdnHCl) were bought from Sigma-Aldrich (Saint Louis, MO). Bis(2-mercaptoethyl)sulfone (BMS) was purchased from EMD Millipore Corp. (Billerica, MA). Acetonitrile (CH₃CN) was bought from Fisher (Fair Lawn, NJ). Deuterium-labeled acetonitrile (CD₃CN) was purchased from Cambridge Isotope Laboratories, Inc. (Andover, MA).

5.2.2 Reaction of acetonitrile with intact WT IgG4-Fc under reducing conditions.

An aliquot of 150 μ L of IgG4-Fc (0.2 mg/mL) in 20 mM sodium phosphate, pH 7.0, was mixed with 8 μ L of 100 mM BMS (dissolved in CH₃CN). 100 mM BMS was prepared by dissolving 93.1 mg of BMS in 5 mL of CH₃CN. The mixture was incubated at 37°C for different time points: 1 hr, 2 hr, 3 hr, 6 hr, 12 hr, and 24 hr. At each time point, the reaction mixtures were collected and stored at -80°C for future analysis.

5.2.3 Reaction of 4-cyano-1-butyne (HCCCH₂CH₂CN) and intact N297Q IgG4-Fc under reducing conditions.

An aliquot of 150 μ L of N297Q IgG4-Fc (0.2 mg/mL) in 20 mM sodium phosphate, pH 7.0, was mixed with 4 μ L of 200 mM tris (2-carboxyethyl)phosphine hydrochloride (TCEP) and 8 μ L of HCCCH₂CH₂CN. 200 mM TCEP was prepared by dissolving 57.3 mg of TCEP in 1 mL of sodium phosphate, pH 7.0. The mixture was incubated at 37°C for 90 min, followed by analyzed with HPLC-MS.

5.2.4 HPLC-MS of intact IgG4-Fc

Wild type and nonglycoform N297Q IgG4-Fc were prepared in the same manner as described in Sections 2.2.2 and 2.2.4 in Chapter 2. The reaction mixtures of IgG4-Fc (0.2 mg/mL in 20 mM sodium phosphate, pH 7.5) and acetonitrile in the presence of reducing agents were collected at different time points and analyzed on an HPLC-MS system. Aliquots of 95 μ L of the reaction

mixtures were injected onto a C4 column (50 mm, 4.6 mm i.d.; 300-Å pore size, 5 µm particle size, Vydac 214 MS, Grace, Deerfield, IL) operated by an HPLC system coupled with ESI-MS. The analysis was performed in the same way as described Section 3.2.5 in Chapter 3.

5.2.5 Peptide mapping of IgG4-Fc.

An aliquot of 250 µL IgG4-Fc in 20 mM sodium phosphate (pH 7.0) was denatured and reduced by addition of 250 µL 6 M GdnHCl and 25 µL of 100 mM BMS, followed by incubation at 37°C for 1 hr. 6 M GdnHCl was prepared by dissolving 5.73 g in 10 mL of 50 mM ammonium bicarbonate. 100 mM BMS was prepared by dissolving 93.1 mg of BMS in 5 mL of CH₃CN or CD₃CN. After reduction, 41.6 µL of 500 mM IAA (in NH₄HCO₃) were added, and the protein solution was incubated at 37°C for 1hr. Excess quantities of GdnHCl, BMS and IAA were exchanged to 5 mM NH₄HCO₃ through a 10 kDa filter unit (Amicon, Ultra Centrifugal Filter, County Cork, Ireland) via centrifugation at 16,900 g for 15 min at 4°C. The protein solution was reverse-flip collected via centrifugation at 300g for 4 min at 4°C. The collected IgG4-Fc (ca. 50 µg) was digested with 5 µg of GluC for 6 hr. GluC was prepared by dissolving in 5 mM NH₄HCO₃ at 0.2 mg/mL. Two shots of GluC were applied, with 12.5 µL in each shot, and added at 0 hr and 3 hr, respectively. The GluC-digested peptides were analysed by HPLC-MS/MS.

5.2.6 HPLC-MS/MS. A detailed approach was described in Section 2.2.8 in Chapter 2.

5.3 Results.

5.3.1 Identification of an N-terminal peptide derivative resulting from reaction with acetonitrile.

IgG4-Fc was reduced with BMS (dissolved in acetonitrile), alkylated with IAA, digested with GluC, and analyzed by HPLC-MS/MS. A new peak with an m/z value of 884.34 ($z=1$) was observed. The MS/MS spectrum of this peak is displayed in Fig. 1, bottom. The presence of a series of b ions, including b2, b3, b4 and b6, indicates that the N-terminal Cys reveals a mass addition of 24 Da. Overall, the peak was identified as an N-terminal peptide derivative with the following sequence: C²²⁵(+24)PSC²²⁸(+57)PAPE, where +24 indicates that Cys²²⁵ is modified, +57 indicates that Cys²²⁸ is alkylated by IAA. The product is proposed to result from the reaction of the N-terminal Cys with acetonitrile, which was utilized to dissolve the reducing agent, BMS. Therefore, a deuterium-labeled acetonitrile (CD₃CN) was subsequently applied. The MS/MS spectrum of the product from CD₃CN corresponds to C²²⁵(+27)PSC²²⁸(+57)PAPE, indicating that the product results from reaction with acetonitrile, and that the three hydrogens in acetonitrile are all incorporated in the product at the N-terminal Cys residue, revealed by the mass addition of 27 Da at Cys²²⁵.

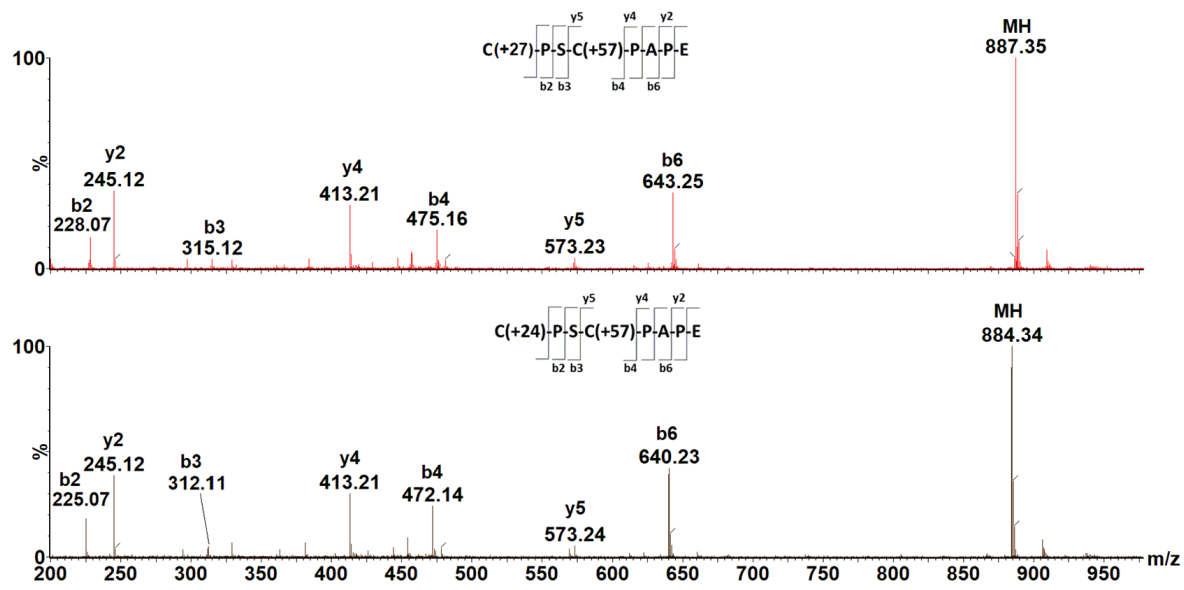


Fig. 1. MS/MS identification of N-terminal cyclic product, top: C(+27)PSC(+57)PAPE, formed in CD₃CN; and bottom: C(+24)PSC(+57)PAPE, formed in CH₃CN.

5.3.2 Characterization of reaction of intact IgG4-Fc with acetonitrile: identification of reaction intermediates, products and effect of incubation time

To further characterize the reaction of IgG4-Fc and acetonitrile, 150 μ L HM IgG4-Fc (0.2 mg/mL, pH 7.1) was incubated with 8 μ L acetonitrile under reducing conditions at 37°C for different times, e.g., 1 hr, 2 hr, 3 hr, 6 hr, 12 hr, and 24 hr. At each time point, the solution was collected and subsequently analyzed by HPLC-MS, where the de-convoluted mass spectra are shown in Fig. 2. The top two abundant species of IgG4-Fc, GlcNAc₂Man₈ IgG4-Fc (theoretical mass: 26708.6 Da) and GlcNAc₂Man₉ IgG4-Fc (theoretical mass: 26870.16 Da) were monitored for potential chemical modifications, displayed in Fig. 2. After 1 hr incubation, two new peaks were observed, derived from native GlcNAc₂Man₈ IgG4-Fc (experimental mass: 26708.2 Da) (Fig. 2A), revealing the mass addition of 24 Da and 41 Da, referred to as peak 1 and peak 2, respectively. The mass of peak 1 is consistent with the modification at N-terminal Cys²²⁵, as described in Section 5.3.1. We propose that peak 2 corresponds to a potential intermediate. A reaction scheme will be discussed in Section 5.4.1. Meanwhile, similar products were observed for GlcNAc₂Man₉ IgG4-Fc, referred to as peak 1' and peak 2' (Fig. 2A). Approximately 30% of non-modified IgG4-Fc is present after 1 hr incubation (Fig. 2A). After 2 hr (Fig. 2B) and 3 hr (Fig. 2C) incubation, the quantity of native proteins decreased significantly, yielding higher intensities of peak 1, 2, 1' and 2' (Fig. 2B). It needs to be noted that there is not much of an effect of incubation time on the relative difference in intensities between peak 1 and peak 2, or peak 1' and peak 2'. When the incubation time was longer than 12 hr, more peaks are observed, referred to as peaks 3, 4, 3', and 4' in Fig. 2E and 2F. We propose that these correspond to the products resulting from side reactions occurring during

elongated incubation time. A proposed mechanism is discussed in Section 5.4.2.

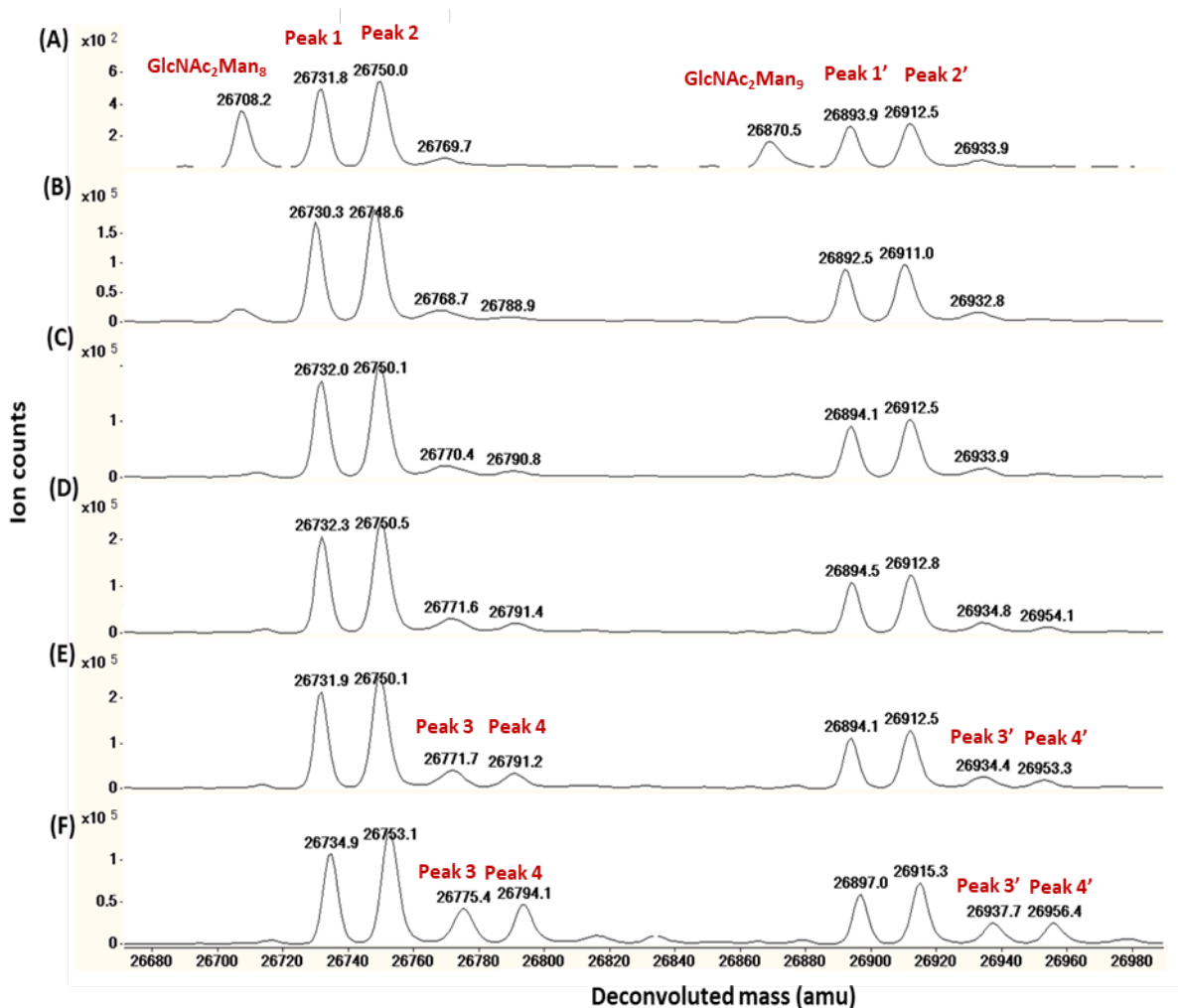


Fig. 2. Characterization of reaction of CH_3CN and WT IgG4-Fc in the presence of 5 mM BMS after incubation at (A) 1 hr (B) 2 hr (C) 3 hr (D) 6 hr (E) 12 hr, and (F) 24 hr at 37°C . Theoretical mass of IgG4-Fc- $\text{GlcNAc}_2\text{Man}_8$ is 26708.06 Da, observed mass of IgG4-Fc- $\text{GlcNAc}_2\text{Man}_8$ is 26708.02 Da, theoretical mass of IgG4-Fc- $\text{GlcNAc}_2\text{Man}_9$ is 26870.16 Da, observed mass of IgG4-Fc- $\text{GlcNAc}_2\text{Man}_9$ is 26870.5 Da. Corresponding $\text{GlcNAc}_2\text{Man}_8$ -IgG4-Fc and $\text{GlcNAc}_2\text{Man}_9$ -IgG4-Fc species are labeled in Fig. 2A. The labeled Peak 1, 2, 3, 4, 1', 2', 3', and 4' represent the IgG4-Fc species derived from reaction with acetonitrile.

5.3.3 Characterization of the reaction of IgG4-Fc with 4-cyano-1-butyne.

We designed to utilize the reactions between N-terminal Cys of IgG4-Fc and acetonitrile as potential linker chemistry for molecules of interests to proteins 4-cyano-1-butyne was selected, because of the presence of two functional groups, a terminal nitrile and alkyne, where the nitrile can selectively react with the N-terminal Cys of a protein and the alkyne can react with azide in a process known as “click” reaction¹⁰. Additionally, we incorporated two methyl groups between the two functional groups to allow increased flexibility.

To characterize the reaction of IgG4-Fc and 4-cyano-1-butyne, 150 μ L of nonglycosylated N297Q IgG4-Fc (0.2 mg/mL, pH 7.1) was incubated with 8 μ L of 4-cyano-1-butyne at 37°C for 90 min, followed by analysis with HPLC-MS. Unexpectedly, the presence of alkyne induces polymerization of N297Q IgG4-Fc (Fig. 3), under reducing (Fig. 3B) and non-reducing (Fig. 3C) conditions. In particular, under reducing conditions, there is a new peak presenting a mass value of 25313 Da, indicating the potential reaction of 4-cyano-1-butyne with the free thiol (RSH). In the absence of the reducing agent, TCEP, a series of potential protein polymerization products were observed as well (Fig. 3C), suggesting that other functional groups of N297Q can potentially react with the alkyne and induce polymerization.

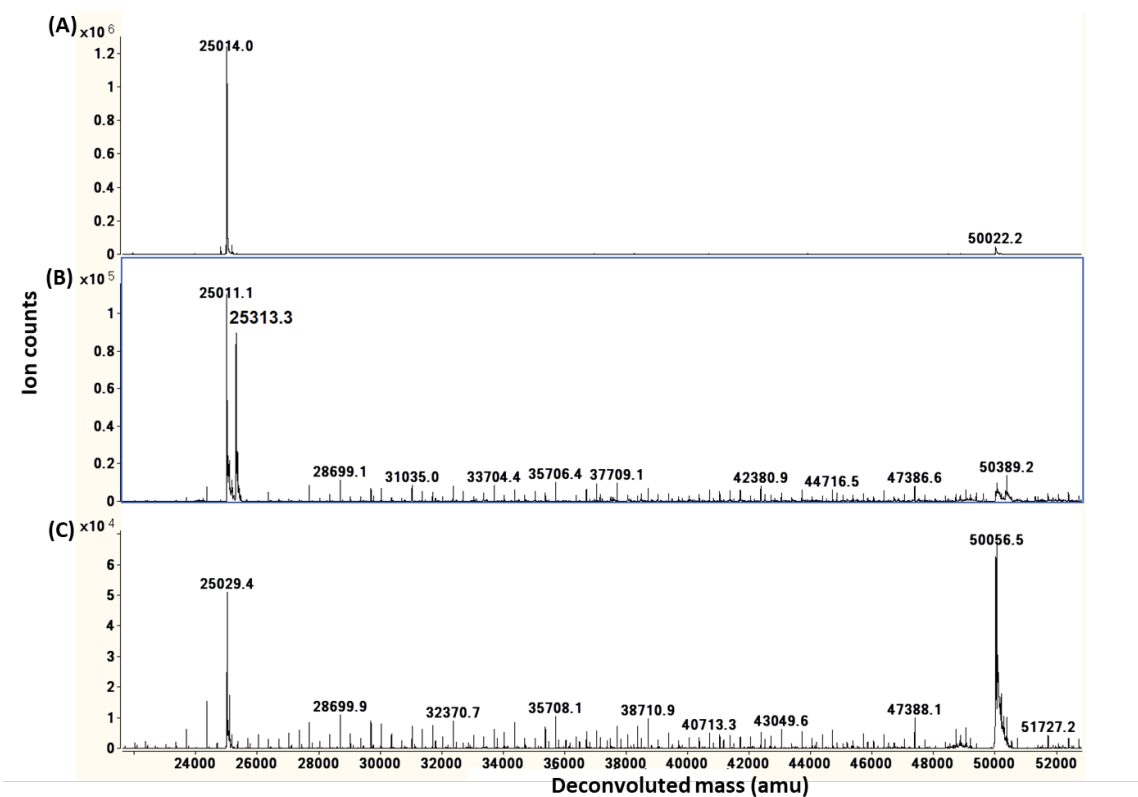


Fig. 3. Characterization of reaction of (A) N297Q IgG4-Fc and TCEP at 37°C for 90 min, pH 7.0 (B) N297Q, HCCCH₂CH₂CN and TCEP at 37°C for 90 min, pH 7.0; (C) N297Q and HCCCH₂CH₂CN at 37°C for 90 min, pH 7.0.

5.4 Discussion

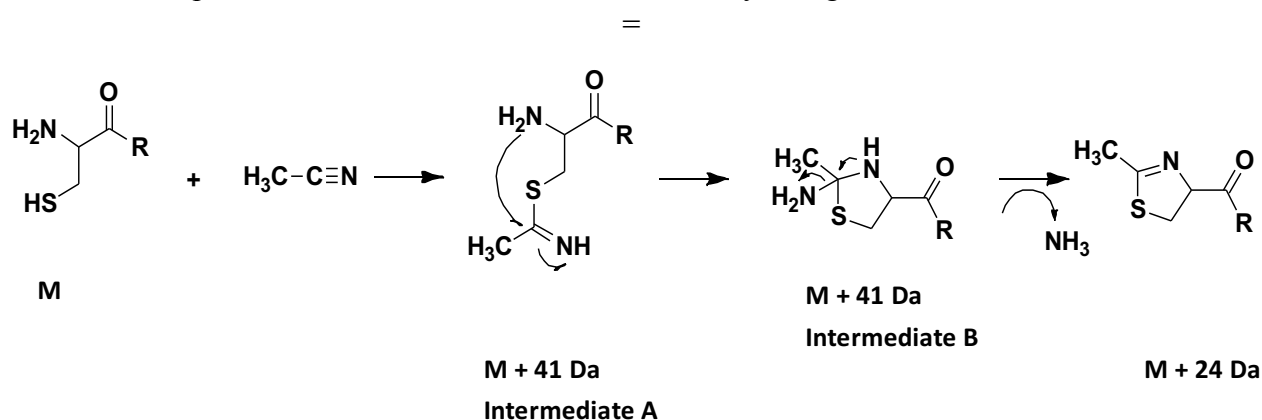
5.4.1 Proposed mechanism of N-terminal Cys of IgG4-Fc with acetonitrile.

A chemical modification at the N-terminal Cys of IgG4-Fc was observed, likely resulting from the presence of a co-solvent (CH_3CN) during the process of reduction. Particularly, we examined the role of acetonitrile with a deuterium-labeled acetonitrile (CD_3CN), where the modification at the N-terminal Cys presented an additional mass of 3 Da (Fig. 1). Based on these observations, we propose the mechanism displayed in Scheme 1. Under reducing conditions, the thiol group (RSH) attacks the nitrile carbon and forms a thioether intermediate A, where the nitrile carbon can be subsequently attacked by the N-terminal primary amine, forming cyclic intermediate B. Intermediates A and B present same mass (Fig.2, peak 2 and/or peak 2'), and the mass corresponding to intermediates A and B is detected by HPLC-MS (Fig. 2). The primary amine formed on the 5-membered ring eliminates ammonia, resulting in the cyclic product with a mass addition of +24 Da (Fig.2, peak 1 and/or peak 1'). The cyclic product was observed with a mass addition of +27 Da during reaction with CD_3CN , confirming that the methyl group from acetonitrile is incorporated (Fig. 1).

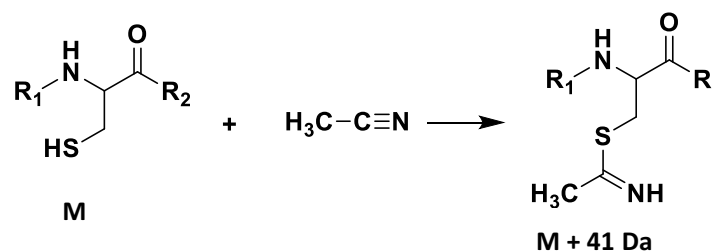
We further investigated the effects of incubation time on the yields of the product (Fig. 2), where the duration of 3 hr reveals potentially the optimal incubation time, due to the fact that the native IgG4-Fc was predominantly reacted. A longer incubation, on the other hand, results in increased formation of side products, indicated by the increased intensities of additional peaks, peak 3, 4, 3'

and 4' in Fig. 2E and 2F. We propose that this results from the reaction of other Cys residues with acetonitrile (Scheme 2), considering that the protein:CH₃CN ratio is 1:2.5x10⁵ (concentration:concentration). The major products reveal the addition of acetonitrile to other Cys residues, e.g., peak 3 derived from peak 1, peak 4 derived from peak 2. These observations indicate that the other Cys residues in IgG4-Fc react at a significant slower rate with acetonitrile, as compared to the N-terminal Cys. These side reactions can be potentially minimized through dialysis of the excess quantity of CH₃CN and shortened reaction time.

Scheme 1. Proposed mechanism of reduced N-terminal Cys of IgG4-Fc with acetonitrile.



Scheme 2. Proposed mechanism of reduced non-N-terminal Cys residues of IgG4-Fc with acetonitrile.



5.5 References.

1. Tsuchikama, K.; An, Z., Antibody-drug conjugates: recent advances in conjugation and linker chemistries. *Protein Cell* **2018**, *9* (1), 33-46.
2. Singh, S. K.; Luisi, D. L.; Pak, R. H., Antibody-Drug Conjugates: Design, Formulation and Physicochemical Stability. *Pharm Res* **2015**, *32* (11), 3541-71.
3. McDonagh, C. F.; Turcott, E.; Westendorf, L.; Webster, J. B.; Alley, S. C.; Kim, K.; Andreyka, J.; Stone, I.; Hamblett, K. J.; Francisco, J. A.; Carter, P., Engineered antibody-drug conjugates with defined sites and stoichiometries of drug attachment. *Protein Eng Des Sel* **2006**, *19* (7), 299-307.
4. Akkapeddi, P.; Azizi, S. A.; Freedy, A. M.; Cal, P.; Gois, P. M. P.; Bernardes, G. J. L., Construction of homogeneous antibody-drug conjugates using site-selective protein chemistry. *Chem Sci* **2016**, *7* (5), 2954-2963.
5. Senter, P. D.; Sievers, E. L., The discovery and development of brentuximab vedotin for use in relapsed Hodgkin lymphoma and systemic anaplastic large cell lymphoma. *Nat Biotechnol* **2012**, *30* (7), 631-7.
6. Yao, H.; Jiang, F.; Lu, A.; Zhang, G., Methods to Design and Synthesize Antibody-Drug Conjugates (ADCs). *Int J Mol Sci* **2016**, *17* (2).
7. Hoffmann, R. M.; Coumbe, B. G. T.; Josephs, D. H.; Mele, S.; Ilieva, K. M.; Cheung, A.; Tutt, A. N.; Spicer, J. F.; Thurston, D. E.; Crescioli, S.; Karagiannis, S. N., Antibody structure and engineering considerations for the design and function of Antibody Drug Conjugates (ADCs). *Oncoimmunology* **2018**, *7* (3), e1395127.
8. Beck, A.; Reichert, J. M., Therapeutic Fc-fusion proteins and peptides as successful alternatives to antibodies. *MAbs* **2011**, *3* (5), 415-6.
9. Czajkowsky, D. M.; Hu, J.; Shao, Z.; Pleass, R. J., Fc-fusion proteins: new developments and future perspectives. *EMBO Mol Med* **2012**, *4* (10), 1015-28.
10. Presolski, S. I.; Hong, V. P.; Finn, M. G., Copper-Catalyzed Azide-Alkyne Click Chemistry for Bioconjugation. *Curr Protoc Chem Biol* **2011**, *3* (4), 153-162.

Chapter 6. The role of ultrafiltration device bias hydrolysis products during peptide map

6.1 Introduction

Peptide mapping refers to selective fragmentation of a protein into well-defined peptides using suitable enzymes or chemicals¹. Through peptide mapping of a protein product, primary structures and corresponding covalent modifications (e.g., site-specific glycosylation, oxidation, and amino acid substitution) can be identified. A typical peptide mapping contains a denaturation step to unfold the protein to be accessible for the following reduction and alkylation². The reduction step serves to break covalently linked disulfide bonds, and the alkylation step serves to protect reduced thiol with alkylating agents, due to the fact that the reduced thiol (RSH) is highly reactive³. Typical reducing agents are dithiothreitol (DTT) and bis(2-mercaptoethyl)sulfone (BMS), and typical alkylating agents are iodoacetic amide (IAA), iodoacetic acid (IAC), and N-ethylmaleimide (NEM)⁴. After denaturation, reduction and alkylation, proteins are accessible for enzymatic or chemical treatment. Peptide map is a powerful and universal analytical technique to characterize primary structures of proteins. Hence, the International Council for Harmonization (ICH) Q6B guideline recommends the utilization of peptide mapping for structural characterization and confirmation of biotherapeutics⁵.

Sufficient quantities of denaturing, reducing and alkylating agents are introduced during peptide mapping to ensure the completion of each step. The subsequent depletion of these components is necessary for reducing side reactions⁶, minimizing matrix effects (generating good signals in analytical detection)⁷, and sustaining an efficient enzymatic digestion. Enzymes are recommended

to be in a buffer system, where they maintain their optimal activity⁸. Ultra-centrifugal filters, spin column, and dialysis are the common approaches to remove the salts. Among these, centrifugal filter device represents a relatively convenient and efficient tool, and has been extensively utilized⁹. In the present work, we observed a hydrolysis reaction between Cys⁴²⁵ and Ser⁴²⁶ (Eu numbering¹⁰) in an IgG4-Fc during peptide mapping, where the hydrolysis products were identified by HPLC-MS/MS. Notably, the measured relative yields of the hydrolysis products are dependent on the steps selected for sample preparation, e.g., the usage of distinct alkylating agents and filtration devices.

6.2 Materials and Methods

6.2.1 Materials. Sodium phosphate, guanidine hydrochloride (GdnHCl), IAA, IAC, ammonium bicarbonate, and Trypsin/LysC were purchased from the same sources as described in Chapter 2.2.1. ¹⁸O-labeled water (95–98% atom pure ¹⁸O) was purchased from Cambridge Isotope Laboratories, Inc. (Andover, MA).

6.2.2 Peptide mapping of IgG4-Fc. An aliquot of 500 μ L IgG4-Fc (0.22 mg/mL, pH 7.1) in 20 mM sodium phosphate was mixed with 500 μ L of 6 M GdnHCl, 5 μ L of 1 M DTT, and incubated at 37°C for 1 hr. IgG4-Fc was alkylated by the addition of 20 μ L 1 M IAA, and incubated at 37°C for 1 hr. The excess quantity of denaturing, reducing and alkylating agents was filtered with a 10 kDa filter unit (Amicon Ultra Centrifugal Filter, County Cork, Ireland), and exchanged with 300

μL of 5 mM ammonium bicarbonate twice via centrifugation at 16,900 g. For the last centrifugation step, the protein solution was concentrated to approximately 200 μL . The protein solution was collected by reverse-flip of the filters, and centrifuged at 300g for 4 min. The stock solutions of GdnHCl, DTT, and IAA were prepared in 50 mM ammonium bicarbonate. Collected protein was digested with trypsin/LysC at a protein:enzyme ratio of 30:1 (w:w). 20 μg of trypsin/LysC was dissolved in 100 μL of 5 mM ammonium bicarbonate, where 16.6 μL of trypsin/LysC solution were added to the protein solution. The digestion was performed at 37°C for 6 hr prior to analysis by HPLC-MS/MS.

6.2.3 HPLC-MS analysis. A similar approach was described in Section 3.2.8.

6.3 Results

6.3.1 Identification of hydrolysis products.

IgG4-Fc was denatured with GdnHCl, reduced with DTT, alkylated with IAA, and digested with trypsin/LysC, followed by analysis with HPLC-MS. Two hydrolysis products, WQEGNVFSC(+57) and SVMHEALHNHYTQK, were observed, originating from the tryptic peptide WQEGNVFSC(+57)SVMHEALHNHYTQK, where +57 indicates that Cys has been chemically alkylated by IAA. The collision-induced dissociation (CID) MS/MS spectra of WQEGNVFSC(+57) ($m/z=563.7$, $z=2$) are displayed in Fig. 1. The presence of y3, y7, and b7 ions identifies the peptide as a hydrolysis product with the C-terminal sequence SC(+57). The CID

MS/MS spectra of SVMHEALHNHYTQK ($m/z=424.4$, $z=4$) are displayed in Fig. 2. The identification of the b7 ion, and a series of the y ions (e.g., y3, y4, y7, y10, y11, and y12 ions) confirms the amino acid sequence of the product.

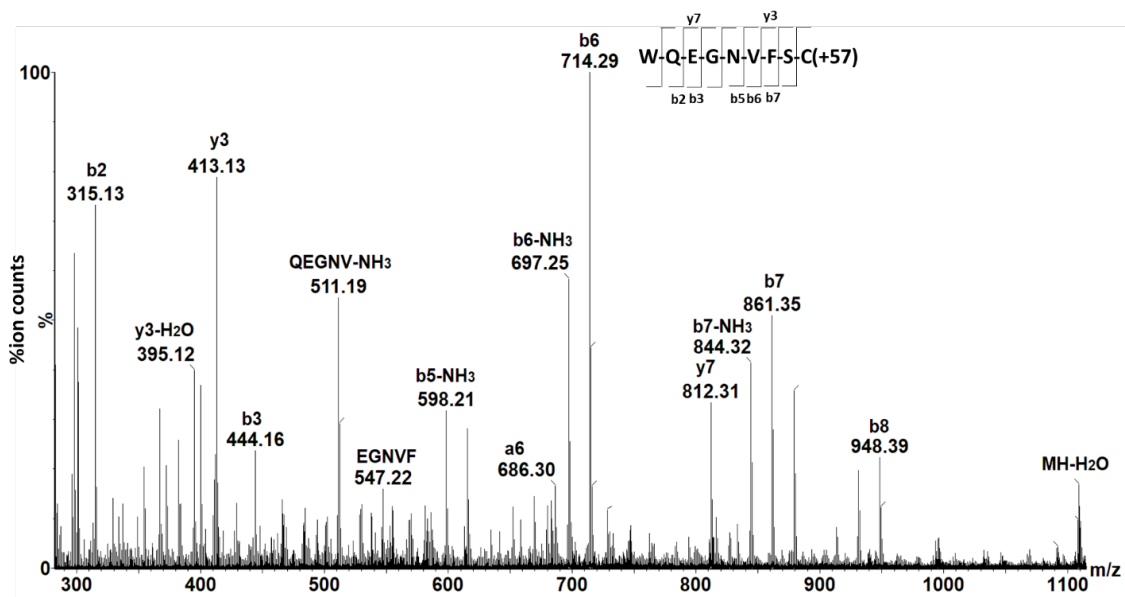


Fig. 1. CID spectra of hydrolysis product WQEGNVFSC(+57) (m/z 563.71; $z=2$).

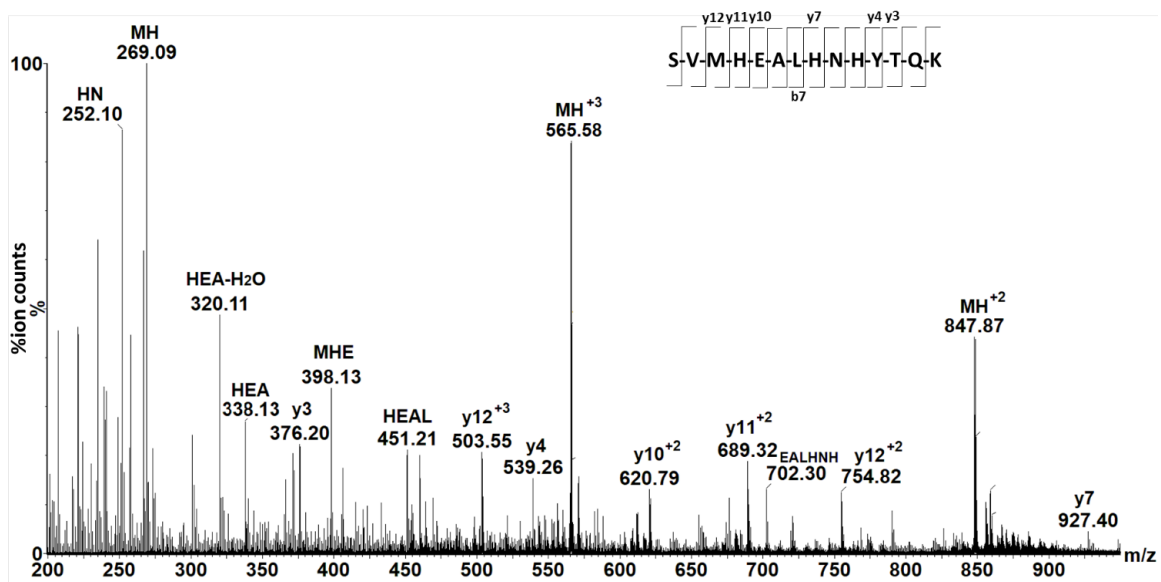


Fig. 2. CID spectra of hydrolysis product SVMHEALHNHYTQK (m/z 424.4; $z=4$).

6.3.2 The origin of oxygen in hydrolysis products.

Two fragment products, WQEGNVFSC(+57) and SVMHEALHNHYTQK, were observed originating from the tryptic peptide WQEGNVFSC(+57)SVMHEALHNHYTQK. A carboxylic acid was formed at the C-terminus of WQEGNVFSC(+57), indicating the incorporation of one oxygen. Hence, we investigated the origin of the oxygen utilizing ^{18}O -labeled water during tryptic digestion. Aliquots of IgG4-Fc were denatured, reduced and alkylated as described in Section 6.2.2 in H_2^{16}O prior to tryptic digestion. The excess denaturing, reducing and alkylating agents were exchanged into 5 mM ammonium bicarbonate in H_2^{18}O using 10 kDa Amicon Ultracentrifuge filters. The digestion was performed in 5 mM ammonium bicarbonate in H_2^{18}O with trypsin/LysC for 8 hrs at 37°C , followed by analysis with HPLC-MS. The incorporation of ^{18}O was monitored for the two products, WQEGNVFSC(+57) and SVMHEALHNHYTQK, displayed in Fig. 3 and 4, respectively. WQEGNVFSC(+57) reveals the incorporation of one ^{18}O indicated by the mass addition of 2 Da. SVMHEALHNHYTQK reveals the incorporation of one and two oxygens, respectively, indicated by the mass additions of 2 Da and 4 Da, respectively.

Prior to digestion, IgG4-Fc was buffer-exchanged to ^{18}O -labeled water through filtration, indicating the presence residual H_2^{16}O . Therefore, the highest mass shift of each product is taken into consideration. The mass shift in product WQEGNVFSC(+57) corresponds to a hydrolysis reaction. The mass shift in product SVMHEALHNHYTQK corresponds to a tryptic cleavage¹¹.

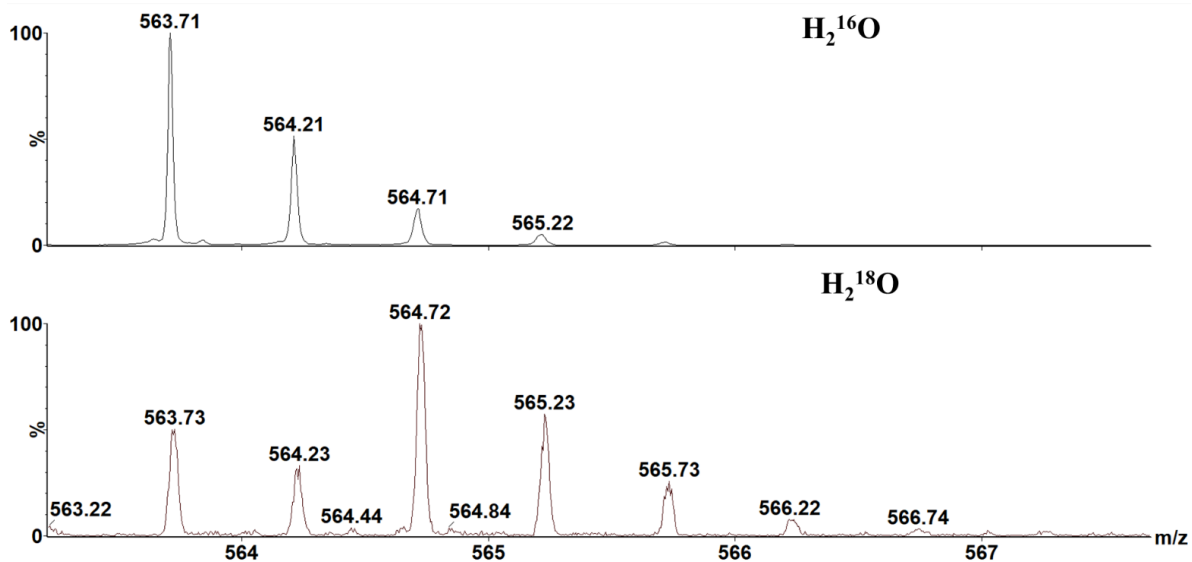


Fig. 3. Incorporation of ^{18}O in peptides WQEGNVFSC(+57) due to hydrolysis from WQEGNVFSC(+57)SVMHEALHNHYTQK. Spectra displayed in front correspond to digestion performed in $H_2^{16}O$, spectra displayed in bottom indicate digestion performed in $H_2^{18}O$.

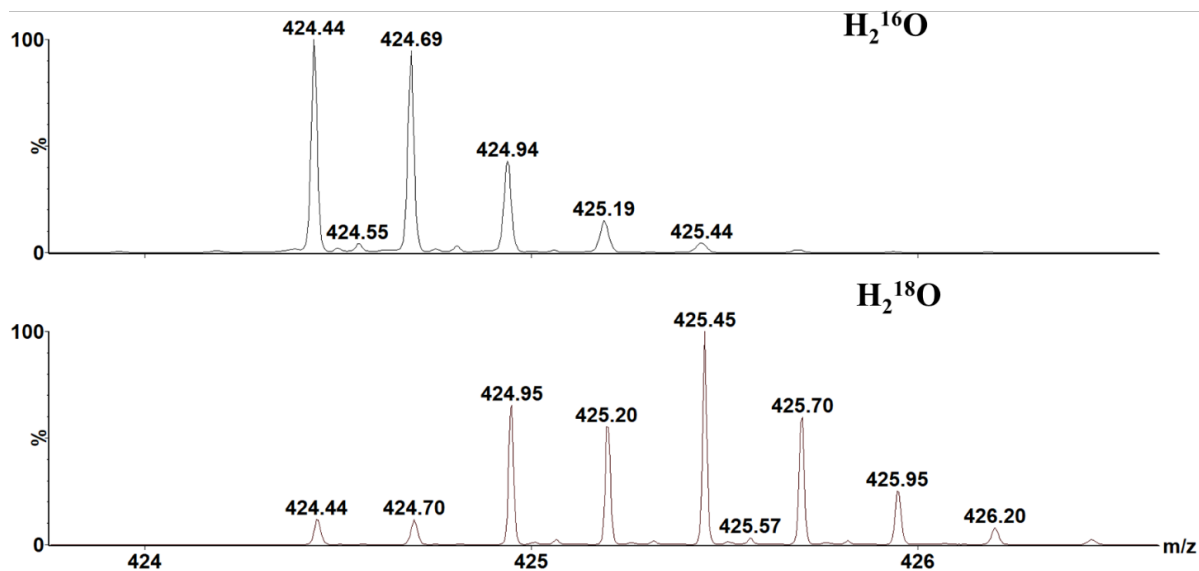


Fig. 4. Incorporation of ^{18}O in peptides SVMHEALHNHYTQK due to digestion. Spectra displayed in front correspond to digestion performed in $H_2^{16}O$, spectra displayed in bottom indicates digestion performed in $H_2^{18}O$.

6.3.3 The effects of the usage of Amicon filter on the quantity of products.

Prior to enzymatic digestion, a filtration step was introduced in the sample preparation as described in section 6.2.2. We, therefore, evaluated the potential role of this step on the relative quantity of the hydrolysis products. The quantification of each peptide was obtained by extracting the intensity of each peak using MassLynx (Waters Inc., Milford, CA). The relative hydrolysis products are quantified by the means of taking the ratio of the quantity of the product to the total ion count of the full chromatography. The equation is shown as follows.

$$\text{yield (\% of hydrolysis products)} = \frac{\text{area of hydrolysis product} \times 100}{\text{total ion count}} \quad \text{Equation 1}$$

Interestingly, the introduction of the filtration step results in a 1000- to 2000- fold enrichment of products 1 and 2, as compared to sample preparation without usage of the filter (Fig. 5).

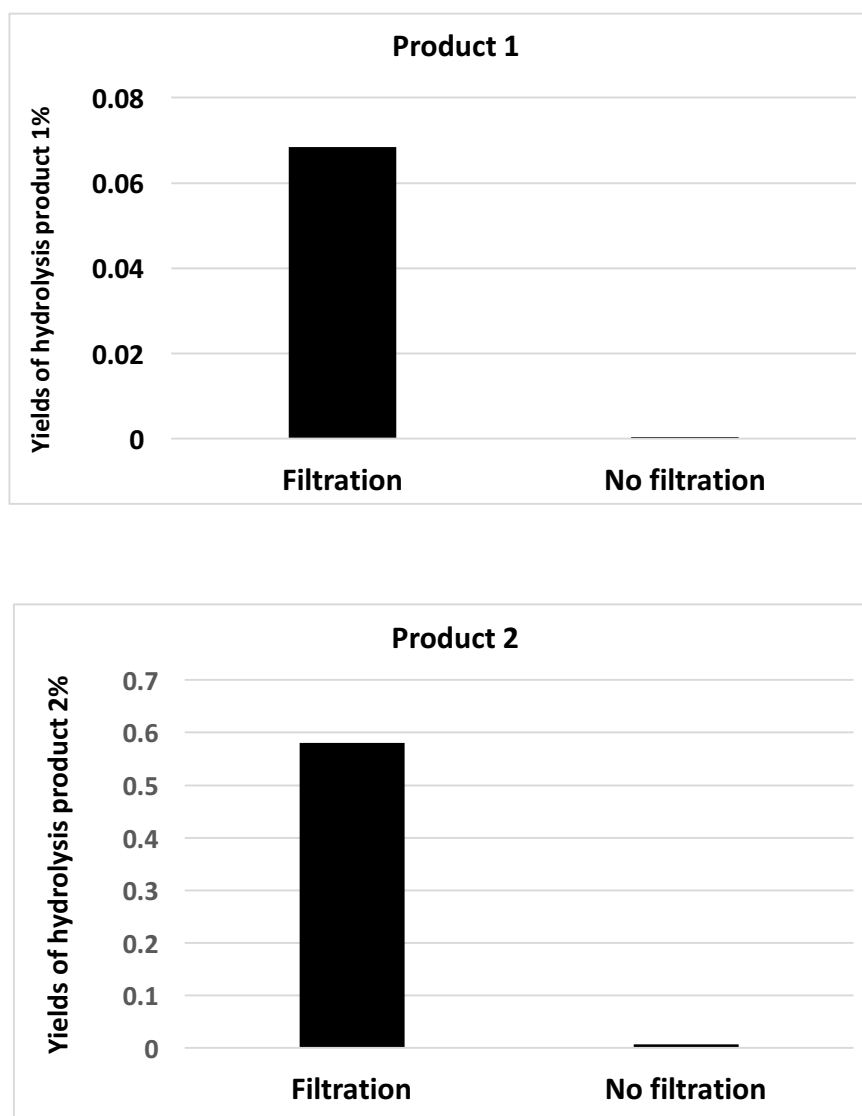


Fig. 5. The yields of hydrolysis products (%) formed during peptide map of IgG4-Fc after denaturation with GdnHCl, reduction with DTT and alkylation with IAA, with or without filtration, where product 1 corresponds to WQEGNVSC(+57), and product 2 corresponds to

SVMHEALHNHYTQK.

6.4 Discussion

In this chapter, a hydrolysis reaction was observed between Cys⁴²⁵ and Ser⁴²⁶ in an IgG4-Fc during the process of peptide mapping. Two hydrolysis fragments, WQEGNVSC(+57) and SVMHEALHNHYTQK, were identified by HPLC-MS/MS (Fig. 1 and Fig. 2) originating from the native peptide, WQEGNVSC(+57)SVMHEALHNHYTQK. To rule out the potential effects of digestion from Trypsin/LysC leading to the formation of these products, digestion was performed in ¹⁸O-labeled H₂O. As displayed in Fig. 3, WQEGNVFSC(+57) (m/z 563.71, z=2) reveals the presence of no mass shift and an additional mass of 2 Da, indicating there is 0 to 1 ¹⁸O incorporation. On the other hand, SVMHEALHNHYTQK (m/z 424.4, z =4) reveals the presence of no mass shift, an additional mass of 2 Da and 4 Da, indicating there is 0, 1 and 2 ¹⁸O incorporation. We prepared the digestion solution in H₂¹⁸O with Amicon filtration via exchange H₂¹⁶O to H₂¹⁸O through centrifugation, suggesting that residual amounts of H₂¹⁶O were present during trypsin/LysC digestion, which explains the additional presence of no mass shift in products 1 and 2. We conclude the +2 Da mass addition of WQEGNVFSC(+57) is due to the hydrolysis from the parent peptide, with one oxygen from H₂¹⁸O incorporated at the C-terminus of the peptide. The +2 Da and +4 Da mass additions for the other hydrolysis product, SVMHEALHNHYTQK, are due to trypsin/LysC digestion. Therefore, these observations confirm that the two fragments originated from hydrolysis. It needs to be noted that the hydrolysis reaction can occur during the

process of reduction, alkylation and digestion.

The yields of the hydrolysis products are higher when IAA was used as the alkylating agent as compared to IAC (Fig. 6). The proposed mechanisms are displayed in Scheme 1 (with IAA) and Scheme 2 (with IAC), respectively, involving the side chain (OH group) of Ser⁴²⁶ adding to the neighboring N-terminal peptide bond, resulting in the fragmentation of the backbone at Cys⁴²⁵-Ser⁴²⁶. In addition, our rationale that alkylation of Cys with IAA results in higher yields is due to inductive effects of the amide group of IAA, as compared to IAC, facilitating the addition of OH group of Ser⁴²⁶ to carbonyl group of peptide bond. (Scheme 1 and Scheme 2)

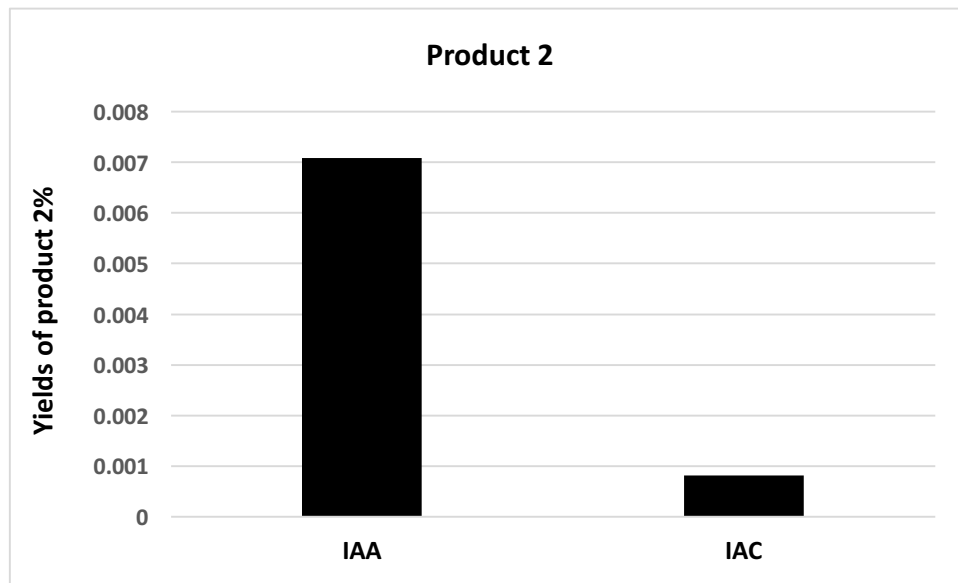
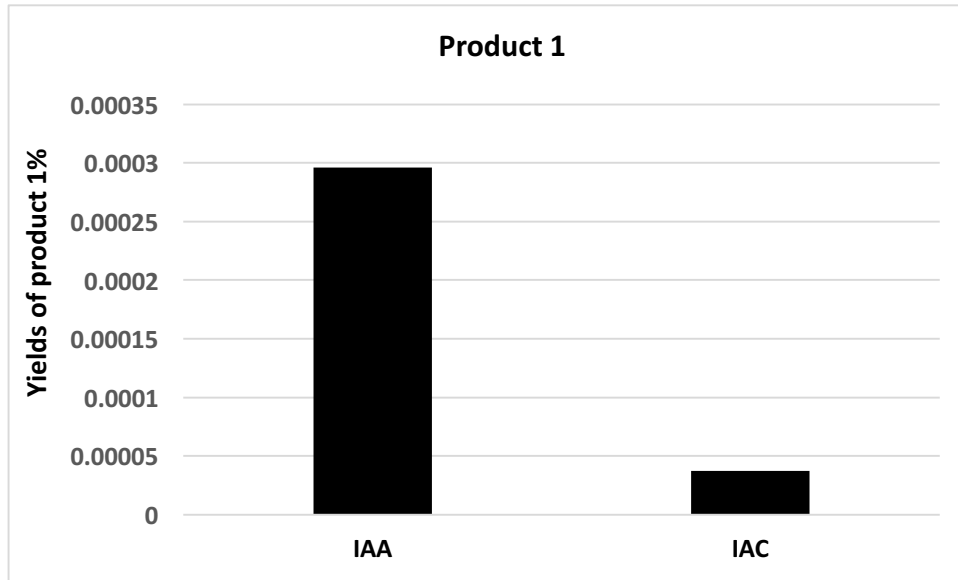


Fig. 6. The yields of hydrolysis products (%) formed during peptide map of IgG4-Fc after denaturation with GdnHCl, reduction with DTT and alkylation with IAA and IAC, respectively, where product 1 corresponds to WQEGNVSC(+57), and product 2 corresponds to SVMHEALHNHYTQK. No filtration step was applied.

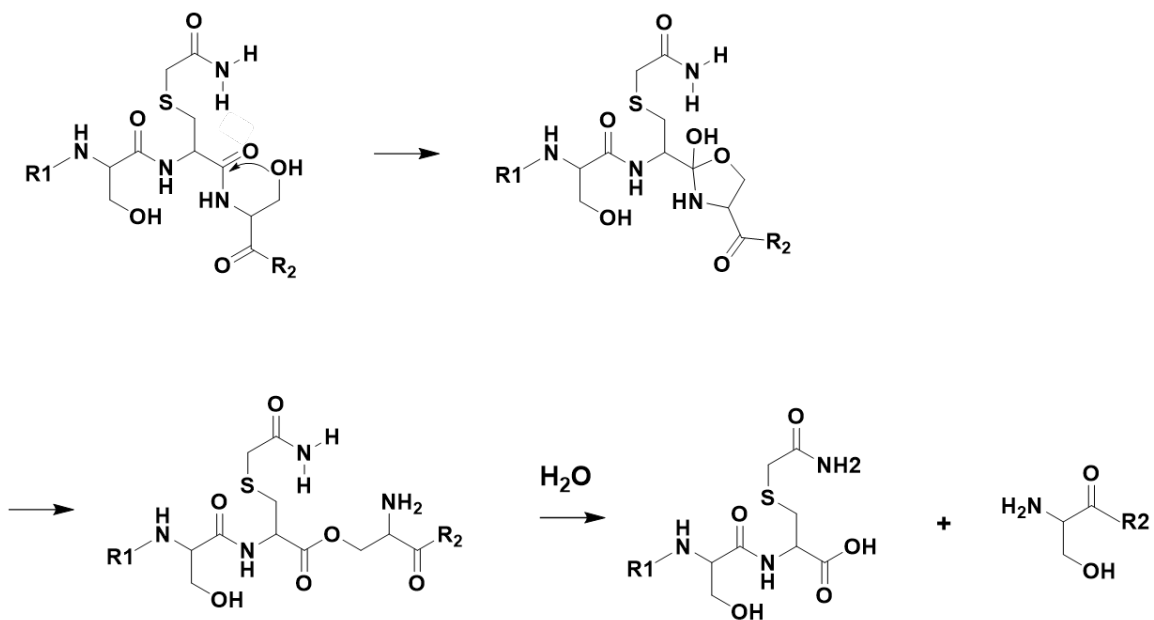
Moreover, we observed the utilization of Amicon filters played significant roles in the quantity of

the fragmentation products (Fig. 5), where the application of filter step enriched the fragmentation products. Our rationale for this observation is that a filtration step potentially enriches the shorter protein resulted from the hydrolysis, where the relatively long unfolded proteins may preferably attach to the filter units.

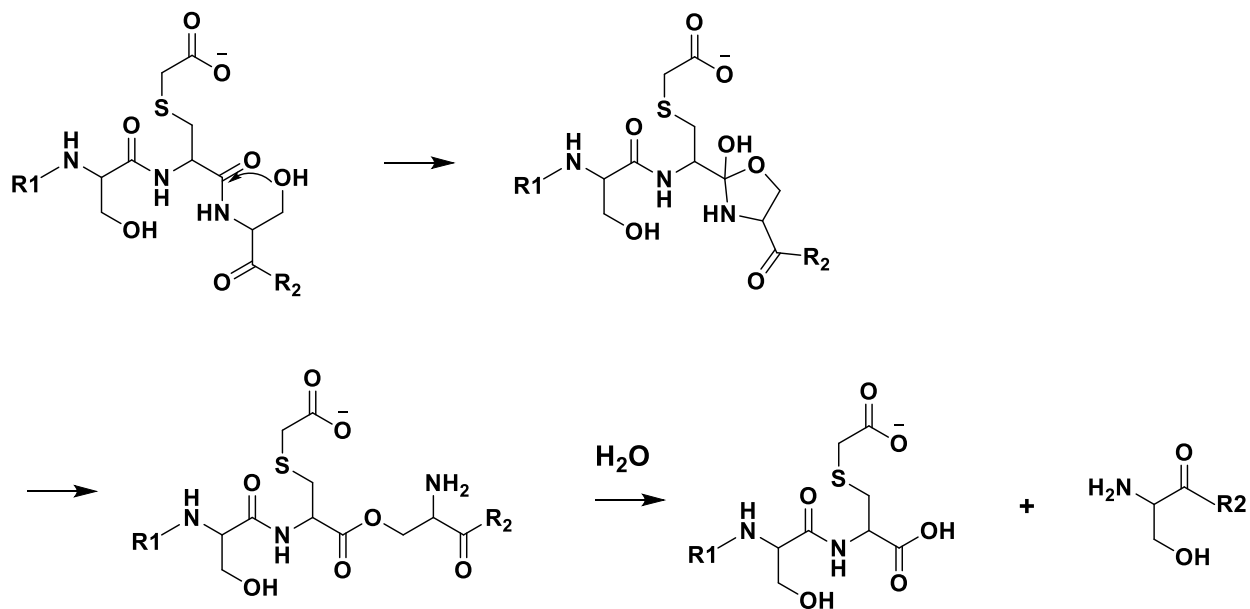
6.5 References

1. Yates, J. R., 3rd; Speicher, S.; Griffin, P. R.; Hunkapiller, T., Peptide mass maps: a highly informative approach to protein identification. *Anal Biochem* **1993**, *214* (2), 397-408.
2. Janin-Bussat, M. C.; Dillenburg, M.; Corvaia, N.; Beck, A.; Klinguer-Hamour, C., Characterization of antibody drug conjugate positional isomers at cysteine residues by peptide mapping LC-MS analysis. *J Chromatogr B Analyt Technol Biomed Life Sci* **2015**, *981-982*, 9-13.
3. Lundell, N.; Schreitmuller, T., Sample preparation for peptide mapping--A pharmaceutical quality-control perspective. *Anal Biochem* **1999**, *266* (1), 31-47.
4. Sechi, S.; Chait, B. T., Modification of cysteine residues by alkylation. A tool in peptide mapping and protein identification. *Anal Chem* **1998**, *70* (24), 5150-8.
5. International Conference on Harmonisation; guidance on specifications: test procedures and acceptance criteria for biotechnological/biological products. Notice. Food and Drug Administration, HHS. *Fed Regist* **1999**, *64* (159), 44928-35.
6. Boja, E. S.; Fales, H. M., Overalkylation of a protein digest with iodoacetamide. *Anal Chem* **2001**, *73* (15), 3576-82.
7. Piwowar, A. M.; Lockyer, N. P.; Vickerman, J. C., Salt effects on ion formation in desorption mass spectrometry: an investigation into the role of alkali chlorides on peak suppression in time-of-flight-secondary ion mass spectrometry. *Anal Chem* **2009**, *81* (3), 1040-8.
8. Proc, J. L.; Kuzyk, M. A.; Hardie, D. B.; Yang, J.; Smith, D. S.; Jackson, A. M.; Parker, C. E.; Borchers, C. H., A quantitative study of the effects of chaotropic agents, surfactants, and solvents on the digestion efficiency of human plasma proteins by trypsin. *J Proteome Res* **2010**, *9* (10), 5422-37.
9. Wisniewski, J. R.; Zougman, A.; Nagaraj, N.; Mann, M., Universal sample preparation method for proteome analysis. *Nat Methods* **2009**, *6* (5), 359-62.
10. Edelman, G. M.; Cunningham, B. A.; Gall, W. E.; Gottlieb, P. D.; Rutishauser, U.; Waxdal, M. J., The covalent structure of an entire gammaG immunoglobulin molecule. *Proc Natl Acad Sci U S A* **1969**, *63* (1), 78-85.
11. Ye, X.; Luke, B.; Andresson, T.; Blonder, J., 18O stable isotope labeling in MS-based proteomics. *Brief Funct Genomic Proteomic* **2009**, *8* (2), 136-44.

Scheme 1. Proposed mechanism for hydrolysis between Cys⁴²⁵ and Ser⁴²⁶ in an IgG4-Fc, where Cys⁴²⁵ is chemically alkylated by IAA.



Scheme 2. Proposed mechanism for hydrolysis between Cys⁴²⁵ and Ser⁴²⁶ in an IgG4-Fc, where Cys⁴²⁵ is chemically alkylated by IAC.



Chapter 7. Conclusions and future perspectives

7.1 Summary and conclusions

IgG mAbs are glycoproteins that have emerged as powerful and promising protein therapeutics. IgGs are marginally stable¹ and sensitive to intrinsic (e.g., glycosylation, primary sequences) and extrinsic factors (e.g., light, temperature)². Photodegradation in IgGs alters their primary structures, associated with chemical and physical instability³. More recent studies have recognized an additional, critical role of light-induced oxidative, chemical protein modifications for immunogenicity⁴⁻⁶. Importantly, when Boll et al.⁷ analyzed immunogenic samples of an oxidized monoclonal antibody (mAb) for common oxidation products of Met and Trp, they concluded that these did not contribute significantly to immunogenicity. Hence, the initial aim of the thesis was to identify photo-induced chemical modifications other than conventional oxidation products, using IgG4-Fc as a model protein. Furthermore, we elucidated the consequences of these chemical modifications on the quality and function of IgG4-Fc, in combination with the effects of glycosylation. During the method development processes, the reaction of N-terminal Cys of IgG4-Fc with acetonitrile under reducing conditions was observed and investigated. These reactions can likely be utilized as linker chemistry in molecules of interest to proteins. In addition, an ultrafiltration device was observed to bias towards the detection of two hydrolysis products from peptide backbone cleavage between Cys⁴²⁵ and Ser⁴²⁶.

Chapter 2 details a mechanism for the photolytic Tyr side chain fragmentation at Tyr³⁰⁰, Tyr³⁷³ and Tyr⁴³⁶ in IgG4-Fc upon irradiation at UVC light at $\lambda = 254$ nm and UVB light with $\lambda_{\text{max}} = 305$ nm. Tyr side chain fragmentation yielded either Gly or various backbone cleavage products,

including glyoxal amide derivatives. A mechanism is proposed involving intermediate Tyr radical cation formation, either through direct light absorption of Tyr or through electron transfer to an initial Trp radical cation, followed by elimination of quinone methide. To our knowledge, this is the first observation of a photo-induced Tyr side chain reaction in a protein.

Chapter 3 elucidates the impact of photo-induced side chain fragmentation at Tyr³⁰⁰, Tyr³⁷³, Tyr⁴³⁶ and Trp³⁸¹ on physicochemical stability and receptor binding of IgG4-Fc. Trp and Tyr are the two major light-sensitive amino acids and are critical to maintain the conformational structures of proteins. Photo-induced side chain fragmentation at these amino acids typically leads to their transformation to Gly^{8, 9}. To evaluate the impact of these photodegradation products, Y300G, Y373G, Y436G, W381G and W381A IgG4-Fc were representatively prepared. Y373G and Y436G reveal significantly reduced thermal stability, as compared to WT. W381A and W381G reveal an overall conformational structure perturbation, indicated by no detectable thermal transition on DSC. W381A, Y300G, and Y436G present a ca. 10-fold reduction in binding affinity to FcγRIIIA, as compared to WT. Nearly two thirds of an adjacent Ser³⁷⁵ was O-mannosylated in W381A and W381G IgG4-Fc. Results from this study demonstrate that photo-induced conversion of Trp and Tyr to Gly (e.g., at Trp³⁸¹, Tyr³⁷³, Tyr³⁰⁰) notably modifies the physico-chemical properties and biological functions of IgG4-Fc.

Chapter 4 characterizes the impact of N-glycan structures on physico-chemical stability, photostability, and receptor binding of IgG4-Fc. N297Q reveals the lowest thermal stability in the C_H2 domain, as compared to HM, Man₅, and GlcNAc₁. Man₅ presents two-fold higher in binding affinity to FcγRIIIA than HM, and ca. 36-fold higher as compared to GlcNAc₁. N297Q does not

present measurable binding affinity to FcγRIIIA. Moreover, N-glycan structures at Asn²⁹⁷ were revealed to play a role in the yield of photoproduct formation including vinyl Cys and backbone cleavage products from Tyr side chain fragmentation.

Chapter 5 investigates a reaction between N-terminal Cys of IgG4-Fc and a co-solvent (acetonitrile) under reducing conditions, where a five-membered cyclic product was formed at the N-terminal Cys.

Chapter 6 discovers two hydrolysis products resulting from a hydrolysis reaction of IgG4-Fc during peptide mapping. Two factors were demonstrated to impact the relative quantity of the hydrolysis products analyzed by HPLC-MS, including the selection of alkylating agents and the application of a filtration device during sample preparation.

7.2 Future directions

Currently, several specific glycan patterns^{10, 11} and oxidation products¹² of mAbs, known to impact their half-life, efficacy, and shelf-life, are listed as critical quality attributes, and need to be strictly controlled and monitored. The findings of this thesis elucidate the consequences of photo-induced Trp and Tyr side chain fragmentation and glycan structures of IgG4-Fc to its physicochemical properties, receptor binding, and photostability. Studying these characteristics of IgGs can advance our knowledge to maintain IgGs stability and functions, aid in the development of a better drug substance and product.

7.3 References

1. Taverna, D. M.; Goldstein, R. A., Why are proteins marginally stable? *Proteins* **2002**, *46* (1), 105-9.
2. Hawe, A.; Wiggenhorn, M.; van de Weert, M.; Garbe, J. H.; Mahler, H. C.; Jiskoot, W., Forced degradation of therapeutic proteins. *J Pharm Sci* **2012**, *101* (3), 895-913.
3. Shah, D. D.; Zhang, J.; Maity, H.; Mallela, K. M. G., Effect of photo-degradation on the structure, stability, aggregation, and function of an IgG1 monoclonal antibody. *Int J Pharm* **2018**, *547* (1-2), 438-449.
4. Bessa, J.; Boeckle, S.; Beck, H.; Buckel, T.; Schlicht, S.; Ebeling, M.; Kiialainen, A.; Koulov, A.; Boll, B.; Weiser, T.; Singer, T.; Rolink, A. G.; Iglesias, A., The immunogenicity of antibody aggregates in a novel transgenic mouse model. *Pharm Res* **2015**, *32* (7), 2344-59.
5. Luo, Q.; Joubert, M. K.; Stevenson, R.; Ketchum, R. R.; Narhi, L. O.; Wypych, J., Chemical modifications in therapeutic protein aggregates generated under different stress conditions. *J Biol Chem* **2011**, *286* (28), 25134-44.
6. Fradkin, A. H.; Mozziconacci, O.; Schöneich, C.; Carpenter, J. F.; Randolph, T. W., UV photodegradation of murine growth hormone: chemical analysis and immunogenicity consequences. *Eur J Pharm Biopharm* **2014**, *87* (2), 395-402.
7. Boll, B.; Bessa, J.; Folzer, E.; Rios Quiroz, A.; Schmidt, R.; Bulau, P.; Finkler, C.; Mahler, H. C.; Huwyler, J.; Iglesias, A.; Koulov, A. V., Extensive Chemical Modifications in the Primary Protein Structure of IgG1 Subvisible Particles Are Necessary for Breaking Immune Tolerance. *Mol Pharm* **2017**, *14* (4), 1292-1299.
8. Haywood, J.; Mozziconacci, O.; Allegre, K. M.; Kerwin, B. A.; Schöneich, C., Light-induced conversion of Trp to Gly and Gly hydroperoxide in IgG1. *Mol Pharm* **2013**, *10* (3), 1146-50.
9. Kang, H.; Tolbert, T. J.; Schöneich, C., Photoinduced Tyrosine Side Chain Fragmentation in IgG4-Fc: Mechanisms and Solvent Isotope Effects. *Mol Pharm* **2019**, *16* (1), 258-272.
10. Reusch, D.; Tejada, M. L., Fc glycans of therapeutic antibodies as critical quality attributes. *Glycobiology* **2015**, *25* (12), 1325-34.
11. Goetze, A. M.; Liu, Y. D.; Zhang, Z.; Shah, B.; Lee, E.; Bondarenko, P. V.; Flynn, G. C., High-mannose glycans on the Fc region of therapeutic IgG antibodies increase serum clearance in humans. *Glycobiology* **2011**, *21* (7), 949-59.
12. Goetze, A. M.; Schenauer, M. R.; Flynn, G. C., Assessing monoclonal antibody product quality attribute criticality through clinical studies. *MAbs* **2010**, *2* (5), 500-7.